JRA

JOURNAL OF RESEARCH AND APPLICATIONS

Organized by
University of Computer Studies
(Meiktila)

Volume - 02, Issue - 01

2020

Preface

Today, Higher Education is a new experience-based education system that uses digital technologies instead of the rote-based system and responds to the needs of the new world through personalised education. This system brings together technology, individuality and discovery-based learning. Therefore, Journal of Research and Applications (JRA), UCSMTLA, 2020 is published as the second time in order to doing research in their respective educational fields. Now, I would like to express my sincere and special gratitude to everyone who had collaborated for the sake of publishing this journal successfully. Finally, I would like to thank all the authors who had submitted their research papers by putting their great efforts in the Journal of Research and Applications (JRA), UCSMTLA, 2020, Volume-02, Issue-01.

Dr. Mie Mie Khin

Rector

University of Computer Studies (Meiktila)

Journal of Research & Applications (JRA), UCSMTLA, 2020 Committees

Committee Chair: *Rector Dr. Mie Mie Khin*

Technical Program Committee Members:

- Dr. Pyke Tin
- Dr. Thi Thi Zin
- Dr. Hlaing Phyu Phyu Mon
- Dr. Thida Win
- Dr. Thin Thin Hlaing
- Dr. Khin Khin Sein
- Dr. Hmway Hmway Tar
- Dr. Khin Myo Aye
- Dr. Thein Than Thwin
- Dr. Myint Myint Hlaing
- Dr. NiLar Winn
- Dr. Sanda Moe
- Dr. Shwe Shwe

Organizing Committee Members:

- Dr. Thein Than Thwin
- Dr. Win Lai Hnin
- Daw Myint Myint Toe
- Daw Thida Lwin
- Daw Aye Nyein San
- Daw Su Mon Ko
- Daw Hnin Yu Hlaing
- Daw Khin Phyu Thant

Acknowledgement for Reviewers of Journal of Research & Applications (JRA), 2020

The Journal of Research & Applications (JRA), UCSMTLA, 2020 technical program committee would like to express the deepest gratitude to the external reviewers for supporting opinions about the submitted papers. The following individuals would be expressed as deeply indebted supporters for the Journal of Research & Applications (JRA).

- Dr. Mie Mie Khin
- Dr. Soe Soe Khaing
- Dr. Kyaw Nyunt
- Dr. Kyaing Kyaing Thet
- Dr. San San Mon
- Dr. Mi Mi Nge
- Dr. Nyein Aye
- Dr. Myat Myat Min
- Dr. Win Htay
- Dr. Nang Sai Moon Kham
- Dr. Thi Thi Zin
- Dr. Than Naing Soe
- Dr. Aung Htein Maw
- Dr. Khin Phyo Thant
- Dr. Su Thawda Win
- Dr. Khin Myo Aye
- Dr. Nyein Nyein Myo
- Dr. Zin May Aye
- Dr. Thin Thin Hlaing
- Dr. Khin Khin Sein
- Dr. Thida Win
- Dr. Mie Mie Thaw
- Dr. Thuzar Aung
- Dr. Hlaing Phyu Phyu Mon
- Dr. Chaw Yupar Soe
- Dr. Thein Than Thwin
- Dr. Myint Myint Hlaing
- Dr. Darli Myint Aung
- Dr. Nilar Winn
- Dr. Than Htut Swe
- Dr. Kyaw Thu Aung
- Dr. Lin Lin Naing
- Dr. Myat Myat Mon
- Dr. Win Win Khaing
- Dr. Kay Thwe Kywe Aye
- Dr. Cho Cho Thein
- Dr. Sanda Moe
- Dr. Aung Kyaw Min
- Dr. Shwe Shwe
- Dr. Phyu Phyu Win
- Dr. Ni Ni Aung
- Dr. Zin Maung Maung
- Dr. Aye Min
- Dr. Thin Htet Htet San
- Dr. Zin Mar Yin
- Dr. Win Pa Pa San
- Dr. Thi Thi Soe
- Dr. Mg Mg
- Dr. Khin Myo Htun
- Dr. Win Lai Hnin

CONTENTS

Pages

Article ID – JRA6006120

Predicting Student Results Data using Direct Vertical Algorithm

Khin Phyu Thant
Faculty of Computer Science
University of Computer Studies
(Meiktila)
khinphyuthant31@gmail.com

Win Lai Hnin
Faculty of Computer Science
University of Computer Studies
(Meiktila)
winlaihnin.84@gmail.com

Thein Than Thwin
Faculty of Computer Science
University of Computer Studies
(Meiktila)
theinthanthwin@gmail.com

***Abstract*— Information and Communications Technology (ICT) is changing the face of education. ICT can improve the quality of education in several ways: by increasing student motivation and by enhancing teacher training. The study involves a sample of students collected from University of Computer Studies, Meiktila. The data was collected and arranged with the Microsoft excel. Direct vertical algorithm is used to mine frequent patterns from the data without generating candidate itemsets and subsets. It makes only one scan of the data to mine the complete set of frequent itemsets. We used support value and confidence level to measure the performance of the proposed work. This system analyzes the performance of students in their examinations and predicts the outcome of the upcoming examination. This prediction allows student and teacher to define the subjects which need more attention before the second semester.**

Keywords—ICT, education, frequent patterns, direct vertical algorithm, students' performance

I. INTRODUCTION

Association rule mining is one of the most popular data mining techniques which mines the transactions to produce association rules. It is a procedure which aims to observe frequently occurring patterns, correlations, or associations from datasets found in various kinds of databases such as relational databases, transactional databases and other forms of repositories [2]. Many researchers have focused on the mining of educational data stored in databases of educational software and learning management systems. The goal is the knowledge discovery that can help educators to support their students by managing effectively educational units, redesigning student's activities and finally improving the learning outcome.

Students result data prediction is one of the fully personalized learning environments and also an important factor of the quality education [7]. There are many data mining method for prediction. This system applied direct vertical association rule mining algorithm to predict the students' examination data. This algorithm mines the frequent patterns by doing combinations of itemsets. While the transaction is read from the input database, it generates a complete set of frequent itemsets up to the current transaction and automatically discards all the infrequent itemsets on the fly. At the end of reading the input database, it extracts final set of all frequent itemsets. This algorithm is efficient to be applied on dynamic databases, in which the records are appended at a regular interval. It is not needed to repeat the execution of the algorithm on the whole new dataset again instead it is enough to execute the algorithm on the newly records alone. The direct vertical algorithm has been compared with some of the existing algorithms. This algorithm can be reduced the number of intersections when compared with other algorithms. It is efficient than existing algorithms in terms of execution time and generation of candidate and subsets [4].

The objective of the proposed system is to find out if there are frequent patterns in the data that could be useful for predicting students' exam results. If we know this frequent pattern, then this knowledge can be used to inform teachers and students to improve their performance.

The rest of the paper is organized as follows. Section 2 reviews the related works. Sections 3 describes the data collection and presents the preprocessing on the data. In section 4, we briefly describe the process step of the direct vertical algorithm. Section 5 presents the experimental result of this proposed system. Finally, in section 6, we conclude the proposed system.

II. RELATED WORK

In the modern era, many students can't concentrate on their study because of the various factors surrounding them [1]. So, they tried to find out the most significant factors harmful for a student. Various innovative techniques and technologies, especially ICT in teaching learning processing is developing day by day [5]. This system used every data regarding a student, right from their enrollment into a course to graduation and placement. This prediction identified the subjects which need more attention for students and teacher before the second semester.

In recent years, many studies have emerged about regarding the topic of school failure, showing a growing interest in determining the multiple factors that may influence it [2]. This system proposed the data mining techniques to produce the factors that influence the failure or dropout of the high school students. One of the educational data mining tasks is student performance prediction that has received great deal of attentions [3].

This paper focus on developing a performance prediction models in information-lacking environment for identifying at-risk students who have tendency to receive low grades.

The data mining prediction has allowed a decision-making tool which can facilitate better resource utilization in terms of student's performance [6]. This paper aims to develop a trust model using data mining techniques which mines required information, so that the present education system may adopt this as a strategic management tool. There is a perpetual elevation in demand for higher education in the last decade all over the world; therefore, the need for improving the education system is imminent. Educational data mining is a newly-visible area in the field of data mining and it can be applied to better understanding the educational systems in Bangladesh [7]. This paper presents how data can be preprocessed using a discretization method called the Optimal Equal Width Binning and an over-sampling technique known as the Synthetic Minority Over-Sampling (SMOTE) to improve the accuracy of the students' final grade prediction model for a particular course.

III. METHOD

Two different approaches have been used to predict the performance of students in examination. These approaches have been given below:

(1) Data Collection
(2) Data Preprocessing

A. Data Collection

In this study, we collected the data from the Student Affair Department of Computer University (Meiktila). Computer Science and Computer Technology is main major in this university. In an academic year, it has semester 1 and 2. In each semester, students studied 7 subjects. This subject can be used as attributes. In this analysis, we used third year students' marks. The dataset contains 115 records including with CS and CT students.

B. Data Preprocessing

We can reduce the missing values because of using the real dataset. The data can be divided into two groups based on pass with distinction and fail. Then, we convert the data that will effectively processed by the algorithms. And, we make the transactions with suitable data. This data is available in Excel. Sample transactions dataset can be shown in Table 1and Table 2.

IV. DIRECT VERTICAL ALGORITHM

Association rule mining can define the dependency between any two itemsets. In this study, we use direct vertical algorithm. Direct vertical method is the new association rule mining algorithm and it can calculate the transactions only once. It uses combinatorial method. These combinations have verified for minimum support by using intersection method. All combinations that satisfy support count are implemented as frequent itemsets and are stored in frequent itemset table. So, this algorithm read one transaction at a time and generates the set of all frequent itemsets without generating any candidate sets and subsets. All infrequent itemsets will be filtered on the fly. Other association rule mining algorithm generates too may candidate sets and subsets which takes much time to complete the process and occupies more memory. This algorithm generates the frequent itemsets which are greater than the predefined support count. It can be used to improve the efficiency and reduce the complexity using the divide-and-conquer technique. Figure 1 shows the system design of the proposed system [4].

TABLE 1: SAMPLE DATASET FOR PASS/DISTINCTION

Transactions	List of Item-IDs
T001	I1, I2, I5, I6
T002	I1, I2, I3, I4, I5, I6
T003	I1, I6
T004	I5
T005	I6
T006	I1, I5, I6
. . .	
T025	I5
T026	I5
T027	I4

TABLE 2: SAMPLE DATASET FOR FAIL

Transactions	List of Item-IDs
T001	I5
T002	I2
T003	I2
T004	I2
T005	I2
T006	I2, I5
. . .	
T037	I7
T038	I2
T039	I2, I5, I6

V. EXPERIMENTAL RESULT

In this work, we focus on subjects of third year computer science and technology. In computer science, that are English, Mathematics in Computing III, Computer Organizations, Data and Computer Communications(I), Software Engineering, Computer Application Techniques III and Advanced Programming Techniques. In computer technology, that are English, Mathematics in Computing III Data and Computer Communications(I), Electronics, Linear Control System and Electrical Circuits (II). In this system, direct vertical algorithm generates frequent itemsets. These transactions are equal to or greater than the minimum support count. This system uses the minimum support count whose value is 3. It generates 3 frequent itemsets for pass/distinction and 4 frequent itemsets for fail. These results can be shown in Table 3.

As an example, if the students pass in I2, we recommend the subjects I5 and I6 will pass. This system compared the generated transaction and previous transactions. So, this system can predict which type of

subject is likely to pass. It can be seen in Table 4 and Table 5.

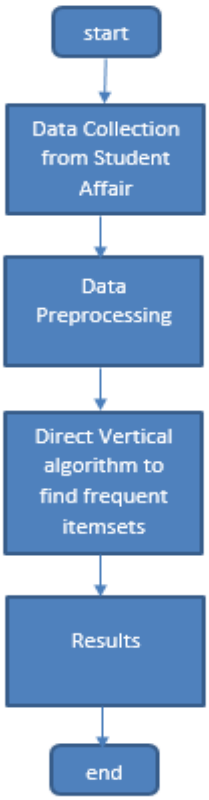

Fig. 1. System Design of the proposed system

TABLE 3: RESULTS FOR PASS/DISTINCTION AND FAIL

No	List of Item-IDs
1	I1, I5, I6
2	I2, I5, I6
3	I4, I5
4	I2, I5, I6
5	I2, I4, I6
6	I2, I4, I5
7	I2, I4, I6

TABLE 4: COMPARING CURRENT SUBJECT AND RECOMMEND SUBJECT

	Current pass/distinction subject	Recommend subject	
Subject ID	I2	I5	I6
	Mathematics in Computing III	Computer Application Techniques III	Advanced Programming Techniques

TABLE 5: COMPARING CURRENT SUBJECT AND RECOMMEND SUBJECT

	Current pass/distinction subject	Recommend subject
Subject ID	I4	I5
	Electronics	Linear Control System

As an example, if the students fail in I2, we recommend the subjects I4 and I5 will fail. This system compared the generated transaction and previous transactions. So, this system can predict which type of subject is likely to fail. It can be seen in Table 6 and Table 7.

TABLE 6: COMPARING CURRENT SUBJECT AND RECOMMEND SUBJECT

	Current fail subject	Recommend subject	
Subject ID	I2	I4	I5
	Mathematics in Computing III	Software Engineering	Computer Application Techniques III

TABLE 7: COMPARING CURRENT SUBJECT AND RECOMMEND SUBJECT

	Current fail subject	Recommend subject	
Subject ID	I2	I4	I6
	Mathematics in Computing III	Electronics	Electrical Circuits (II)

Association rule mining recognizes frequent if-then associations which are known as association rules. It has two segments namely, antecedent that is known as 'if' and consequent which is known as 'then'. Generally, an antecedent is a thing identified within the data, whereas consequent discovered in blend with the antecedent. Association rules are made via scanning information for successive if-then forms and utilizing the criteria support and confidence to distinguish the most significant connections. In this analysis, we used support and confidence to measure. Support means how much of the time the items show up in the information. Confidence shows the occasions the if-then statements are discovered trued. In this system, we have 50 % and 60 % for support and confidence respectively.

VI. CONCLUSION

This paper proposed the system of data mining in education. Association rule mining is widely used in education system. Among association rule mining algorithm, direct vertical algorithm is used to analyze the performance of students' examination results. The proposed rules are used to predict the outcome of the upcoming examination. The result of this system is notified the subjects which need more attention before the semester for the students. For teachers, they can know the conditions

of the students and guide the students to improve their performance on different subjects.

REFERENCES

[1] M. Raihan, Md. T. Islam, P. Ghosh, J. H. Angon, Md. M. Hassan, and F. Farzana, "A Machine Learning Approach to Identify the Correlation and Association among the Students' Educational Behavior," in *Proceedings of the International Conference on Computing Advancements*, Dhaka, Bangladesh, Jan. 2020, pp. 1–6.

[2] A. Viloria, J. G. Guliany, W. N. Núñez, H. H. Palma, and L. N. Núñez, "Data Mining Applied in School Dropout Prediction," *J. Phys. Conf. Ser.*, vol. 1432, p. 012092, Jan. 2020.

[3] H. Chanlekha and J. Niramitranon, "Student performance prediction model for early-identification of at-risk students in traditional classroom settings," in *Proceedings of the 10th International Conference on Management of Digital EcoSystems*, Tokyo, Japan, Sep. 2018, pp. 239–245.

[4] Devi, "A COMBINTORIAL TREE BASED FREQUENT PATTERN MINING," *J. Comput. Sci.*, vol. 10, no. 9, pp. 1881–1889, Sep. 2014.

[5] Omprakash Chandrakar and Jatinderkumar R. Saini, " Predicting Examination Results using Association Rule Minin", in Proceedings of the International Journal of Computer Applications, India, vol. 116, pp 7-10, Apr 2015.

[6] M. Durairaj,C. Vijitha, "Educational Data Mining for Prediction of Student Performance Using Clustering Algorithms", in International Journal of Computer Science and Information Technologies, India, vol.5, pp5987-5991,2014.

[7] S. Tanveer Jishan, R. Islam Rashu, N. Haque, M. Rashedu Rahman, "Improving accuracy of students' final grade predicition model using optimal equal width binning and synthetic minority over-sampling technique", in SpringerOpen Journal, Decision Analytics (2015).

Article ID – JRA6008920

Performance of Improved FP-Growth Algorithm based Association Graph using Frequent Pattern Mining

Aye Aye Cho
Faculty of computer Science
University of Computer Studies Hinthada
Myanmar
ayeayecho@ucsh.edu.mm

Myo Myo Khin
Information Technology Supporting and Maintenance Department
University of Computer Studies, Hinthada
Myanmar
myomyokhin@ucsh.edu.mm

Moe Moe Tha
Information Technology Supporting and Maintenance Department
University of Computer Studies Hinthada
Myanmar
moemoetha@ucsh.edu.mm

***Abstract*— Frequent pattern mining is the repeated items in the database, it is useful in the basket market analysis of the data mining task. Many efficient pattern mining techniques have been discovered in the last period. Among these techniques, we analyzed the FP-Growth algorithm. Data mining techniques are used for classification, clustering, and prediction. In the research, we predict the performance for Improved FP-Growth based Association Graph and then compare it to the FP-Growth algorithm. Improved FP-Growth algorithm reduces the algorithm's time because it uses an association graph and adjacency table instead of the FP tree.**

Keywords*— Improved FP-Growth algorithm, FP-Growth algorithm, dataset, association graph, FP-tree, performance

I. INTRODUCTION

Frequent pattern mining is active with the decision support problem faced by most large retail organizations. Several organizations are organized and stored a large amount of sales data, referred to as the basket market data. A record consists of the transaction date and the items bought with the transaction. Sale records consist of customer-id, particularly when the purchase has been made using a credit card or a frequent buyer card for their products. Companies or a business organization are collected data using by custom orders. From the customer receive voucher, we got transactional datasets.

Information system assistant to a business organization for decision-making activities. Decisions are made based on sale records. Economical organization to be able to change frequently to the reacting demands of the customers must utilize sophisticated information technology to transform vast resources of raw data into an actionable business plan. Organizations collect and store a massive amount of sales data referred to as the basket market. There are frequent itemsets algorithms. They are Apriori, Eclat, and FP-growth, and so on. Among these methods, we represent the FP-Growth algorithm and the Improved FP-Growth algorithm.These presents have the same input dataset and different output processing time. As an FP-Growth algorithm, the input is a transaction database using the tree method and a minimum support threshold. A minimum support threshold is applied to find all frequent itemsets in the database. From the support count, we will find strong rules of the frequent patterns. Finally, the manager is decision using strongly rules with decision tree method or FP-tree. Finally, Improved FP-Growth algorithm, the transaction database using the association graph and then, create the adjacency table. And unrelated items are removed using minimum support count. found an Improved FP-Growth algorithm faster than the FP-Growth algorithm.

The FP-Growth algorithm is based on frequent pattern tree (FP-Tree), which doesn't generate a large number of candidates itemsets. However, FP-Tree requires two steps for the generation of frequent pattern mining by recursive mining procedures. This paper proposes an improved algorithm based on the adjacency table. FP-Growth algorithm is based on the adjacency table which the idea of graphs. Improved FP-Growth algorithm is using data structures concept for faster running speed. After scanning the itemsets in the transaction database, we adopt a storage method combing the adjacency table, which can remove itemsets that are less than minimum support. The algorithm makes full use of the established adjacency table and only needs to scan the original transaction database once.

II. RELATED WORK

We can test the future work these algorithms using different database. We can test new minimum confidence by multiple support algorithms. From the experiment, we can test the reliability of the data mining technique in terms of accuracy and efficiency. And then, experimental result is more accurate for various algorithms. The future work will run using FP-Growth algorithm and study the improvement in parallelization. Accuracy and efficiency depend on various algorithms.

The Graph is introduced to Ming Yin, Wenjie, Yang Lie, and Jiang Dan, "An improvement of FP-Growth association rule mining algorithm based on adjacency table" 2018(In MATEC Web of Conferences).

Multiple Minimum Supports based maximum constraints in Improved FP-Growth algorithm [3] is proposed for efficient FP-Growth algorithm by making in related node pruning stage that the size of MIS-Tree result less than or equivalent to the FP-Tree structure.

Association Graph based on adjacency table [5] to solve the problems of large memory usage and low time effectiveness FP-Growth algorithm. In this algorithm, the adjacency table which draws on the idea of the graph is used. After scanning the itemsets in the transactional database, a storage method combing the adjacency table with the hash table is adopted. This method can remove itemsets that are less than support count as well as avoid generating all nonempty subsets of the largest itemsets. The algorithm uses full of the constructed adjacency table and only needs to scan the original transactional database once.

In[6], the Proposed of the Improved FP-Growth algorithm is introduced using a tree structure. It provides to search faster than other frequent pattern mining. FP-Growth algorithm traverses the tree structure quickly. Improved FP-Growth algorithm reduces runtime and memory. Improved FP-Growth algorithm is a divide and conquers algorithm using two steps. In comparison to the Apriori algorithm, candidate patterns are not searched and the database is scanned only twice.

FP-Growth algorithm is based using a top-down procedure to generate frequent itemsets [7]. It provides the problem of running time-efficient for frequent itemsets. The top-down of the Improved FP-Growth algorithm overcomes the problem of the existing FP-Growth algorithm reverse procedure. Using a top-down procedure, Top-Down Improved FP-Growth algorithm slower amount of time and memory, it is not processed conditional pattern based and sub-FP-Tree.

III. BACKGROUND THEORY

We will use methods for mining form frequent patterns such as "basket market data analysis". We are generating association rules from frequent itemsets.

A. Frequent Itemset mining methods

Generate association rules from the frequent items. To do consider all partitioning of the item set into rule left-hand and right-hand sides. Confidence of a candidate rule X and Y is calculated as support (XY) / support (X). All rules that meet the confidence threshold are reported as the discovery of these algorithms.

B. FP-Growth Algorithm

- Step 1: Built an FP-tree. FP-tree is constructed using two passes over the dataset.

  Pass1- Read data and find support for each item. Delete infrequent items. Arrange frequent items in decreasing order based on their support.

  Pass2 - Nodes matched to items and have a counter.

  FP-growth reads one transaction at a time and copies it to a path. Fixed order is done, so paths can overlap when transactions share items. Pointers are kept between nodes containing the same item, creating linked lists. The more paths overlap, the higher the compression. FP-tree will fit in memory. Frequent itemset extracted from the FP-tree.

- Step 2: Frequent itemset Generation, FP-Growth runs frequent items from the FP-tree. A bottom-down algorithm from the leaves backward the root. Partition the conquer first look for frequent itemsets ending in ..... then ....., etc. First, extract prefix path sub-trees halt in an item (set).We consider the following example of transaction database.

TABLE I. TRANSACTION DATASETS

Transaction ID	Item Bought
T1	{PPencil, Compact Disc, Correction Pen, Book, Ruler, Refill Ink}
T2	{Note Book, Compact Disc, Correction Pen, Book, Ruler, Refill Ink}
T3	{Pencil, File, Book, Ruler}
T4	{Pencil, Stapler, Tape, Book, Refill Ink}
T5	{Tape, Compact Disc, Book, Eraser, Ruler}

TABLE II. PASS1 STEP OF FP-GROWTH ALGORITHM

Item	Number of Transactions
Pencil	3
Compact Disc	3
Correction Pen	2
Book	5
Ruler	4
Refill Ink	3
NoteBook	1
File	1
Stapler	1
Tape	2
Eraser	1

TABLE III. SORT OF FREQUENT ITEMSET

Item	Number of Transactions
Book	5
Ruler	4
Pencil	3
Compact Disc	3
Refill Ink	3

TABLE IV. PASS2 STEP OF FP-GROWTH ALGORITHM

Transaction ID	Item sets	Item Bought
T1	{Pencil, Compact, Disc, Correction, Pen, Book, Ruler, Refill Ink}	{Book, Ruler, Compact Disc, Pencil, Refill Ink}
T2	{Note Book, Compact, Disc, Correction, Pen, Book, Ruler, Refill Ink}	{Book, Ruler, Compact Disc, Pencil, Refill Ink}
T3	{Pencil, File, Book, Ruler}	{Book, Ruler, Pencil}
T4	{Pencil, Stapler, Tape, Book, Refill Ink}	{Book, Pencil, Refill Ink}
T5	{Tape, Compact, Disc, Book, Eraser Ruler,}	{Book, Ruler, Compact Disc}

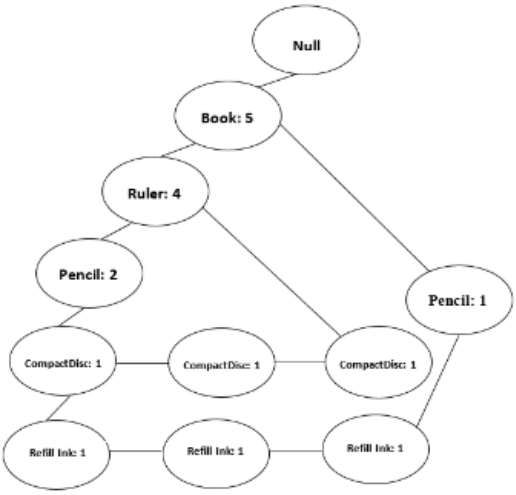

Fig 1. FP-Tree structure from conditional pattern base.

TABLE V. CONDITIONAL DATABASE PATTERN

Item	Conditional pattern base
Refill Ink	{Book, Ruler, Pencil, Compact Disc:1}, {Book, Ruler, Compact Disc:1} {Book, Pencil:1}
Compact Disc	{Book, Ruler, Pencil:1}, {Book, Ruler:2}
Pencil	{Book, Ruler:2}, {Book:1}
Ruler	{Book:4}
Book	null

Therefore, association rules are generated from the frequent pattern using support count. There are two association rules ie: either Book implies Book. If the minimum support is provided in the question then we find strong rules from association rules. There are various types of decision tree algorithms are available in the field of data mining but the major drawback of decision trees technique is that if behave differently with distinct types of datasets.

TABLE VI. CONDITIONAL FP-TREE

Item	Conditional pattern base
Refill Ink	Book-3
Compact Disc	Book, Ruler-3
Pencil	Book-3
Ruler	Book-4
Book	-

Generate Frequent Pattern from Refill Ink, Compact Disc, Ruler, Pencil.

Refill Ink - {Book, Refill Ink: 3}
Compact Disc - {Book, Compact Disc:3}, {Ruler, Compact Disc:3}, {Compact Disc, Ruler, Book:3}
Pencil - {Pencil, Book:3}
Ruler - {Ruler, Book:4}

C. Improved FP-Growth Algorithm

Improved FP-Growth algorithm terminates the disadvantage of the FP-Growth algorithm by using the association graph Improved FP-Growth algorithm works as follows:

- For each transaction, itemsets can be considered related to each other and form a complete graph. The items in each transaction are considered to be related to each other. And the weight of the edge connecting the related items is incremented by one. The graph of the weight is the association frequency. Therefore, after the first scan of the database, the association graph is obtained.
- Using the association graph, the adjacency table is created. And unrelated items are removed using minimum support count. By the subset to mine adjacency table, frequent itemsets are obtained.

D. Example of Improved FP-Growth Algorithm

Input: Transactional Database(D), minimum support count (Min)
Output: Frequent itemsets (F)
for each transaction T in D
for i=1 to T. size-1
for j=i+1 to T. size
w (l_I, lj) = w (li, lj) +1
createEdge w (l_I, lj)
endfor
endfor
for each item l_i, in the association graph
for each item l_j where w (l_I, lj) > Min
l.link=createnode w (l_I, lj)
end for
endfor

By the subset to mine adjacency table, frequent itemsets are obtained.

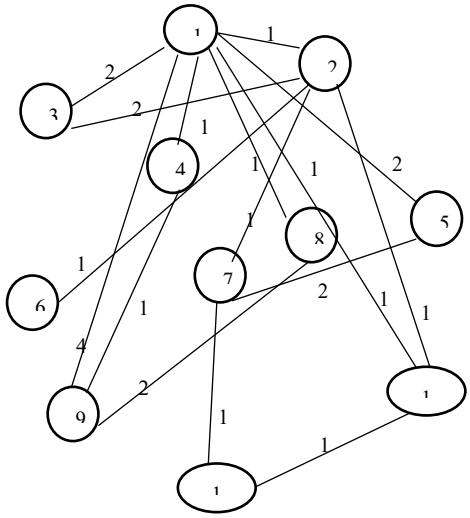

Fig 2. Association graph using table 1 datasets.

The above graph, Node1 is Book, Node2 = Compact Disc, Node3= Correction Pen, Node4= Eraser, Node5= File, Node 6= NodeBook, Node7= Pencil, Node8= Refill Ink, Node 9 = Ruler, Node10= Stapler and Node11= Tape.

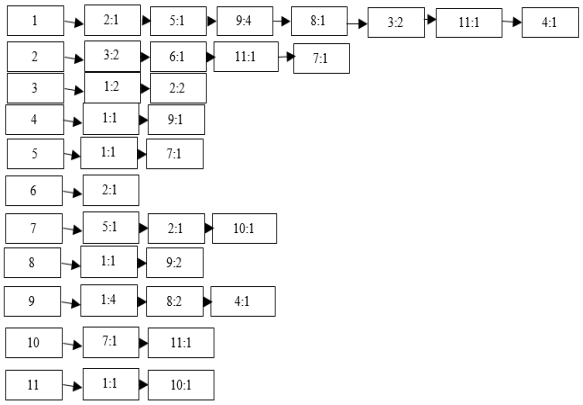

Fig 3. Adjacency table from the association graph

The adjacency table gets from the above graph. We generate the count of itemsets from the adjacency table.

TABLE VII. FOUR FREQUENT ITEMSETS FROM ADJACENCY TABLE

Frequent itemsets	Count
1,9	4
2,3	2
3,1	2
8,9	2

IV. ANALYSIS OF TIME COMPLEXITY

This paper is to analyze the time complexity between FP-Growth and Improved FP-Growth algorithms.

We are analyzed the following procedure:

Number of transactions in the original database =n

Number of itemsets in the FP-tree = N_1

Average number of items per item I= N_2

Time required to read transaction i from the original database = T_i

Time for counting frequency of each item in database using FP-Growth =T_{fp}

Time for counting frequency of each item in database using Improved FP-Growth =T_{ifp}

Time for sorting each itemset =T_{sort}

Time required to insert each item into FP-tree=$T_{in(FP)}$

Time required to insert each item into adjacency table = $T_{in(IFP)}$

Time to get frequent itemsets from original database using FP-Growth algorithm=T_{if}

Time to get frequent itemsets form original database using

I FP-Growth algorithm= T_{gi}

Time to find all frequent itemsets using FP-Growth algorithm=$T_{FP\text{-}Growth}$

Time to find all frequent itemsets using IFP-Growth algorithm=$T_{IFP\text{-}Growth}$

$$T_{(FP-Growth)} = \sum_{i=1}^{n}\left(T_i + T_{fp} + T_{sort} + T_{in(FP)} + T_{if}\right) \quad \ldots.(1)$$

$$T_{(FP-Growth)} = \sum_{i=1}^{n}\left(T_i + T_{fp} + T_{sort}\right) + \sum_{i=1}^{n} log_2(i) + N_1 log_2(N_1) \quad \ldots\ldots(2)$$

$$T_{(IFP-Growth)} = \sum_{i=1}^{n}\left(T_i + T_{ifp} + T_{in(IFP)} + T_{gi}\right) \quad \ldots\ldots(3)$$

$$T_{(IFP-Growth)} = \sum_{i=1}^{n}\left(T_i + T_{ifp}\right) + O(n) + N_2 O(N_2) \quad \ldots..(4)$$

Therefore,

$$\sum_{i=1}^{n}\left(T_i + T_{fp} + T_{sort}\right) > \sum_{i=1}^{n}\left(T_i + T_{ifp}\right) \quad \ldots.(5)$$

$$\sum_{i=1}^{n} log_2(i) = log_2\, n! \quad \ldots.(6)$$

Equation (7) can be obtained the following

$$O(n) + N_2 O(N_2) < \sum_{i=1}^{n} log_2\,(i) + N_1 log_2(N_1) \ldots\ldots (7)$$

Therefore,

$$T_{(FP-Growth)} > T_{(IFP-Growth)}$$

V. PROPOSED SYSTEM

The overall system of the FP-Growth algorithm is discussed in this section "Item Name" "Unit Price" and "Description" for new items are entered as input to become a traditional dataset. The overview of the system of the following figure. Customers bought frequent itemsets of the stationary store is stored the database of the proposed system as a form of "Sales Vouchers" with Voucher numbers.

There are three main parts: show transactional datasets, generate frequent itemsets by using FP-Growth and Improved FP-Growth algorithms, and then the prediction of these algorithm complexity. In general, frequent itemsets and strong rules by using the FP-Growth algorithm process, firstly frequent itemsets are collected from the transactional database according to the minimum support count value. Frequent itemsets are arranged according to descending order.

Frequent pattern tree is constructed and frequent pattern-based are created from FP-tree. Conditional frequent pattern based is generated depends on the frequent pattern base. Strong rules are based on the frequent pattern using minimum support count value. The Improved FP-Growth algorithm is to create an association graph and then using the adjacency table. From this table, we found suppose count value, confidence, and strong rules from frequent itemsets. Finally, two algorithms are compared to output the runtime.

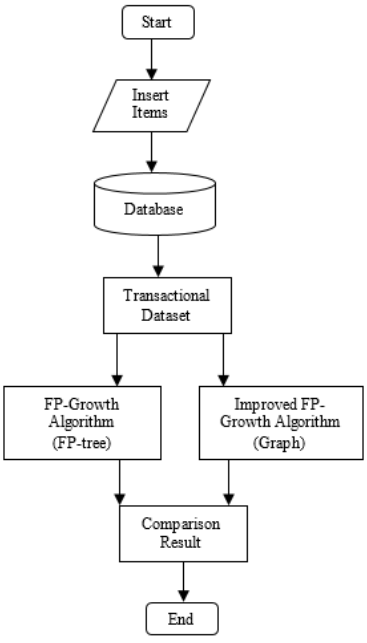

Fig.4 Overview of the system design

VI. IMPLEMENTATION

For the experimental results, we use the two datasets on Intel® Core™ i7, CPU 4.80 GHz, and 16 GB of RAM computer. There is a Supermarket Sales dataset used to test with two algorithms. The dataset was generated from the Kaggle repository of machine learning database. The Supermarket Sales dataset averages 8 items per transaction sets and the number of transaction sets is 1001. And another dataset is Online Shoppers Purchasing Intention Dataset is generated from the UCI Machine Learning Repository. The Online Shoppers Purchasing Intention Dataset averages 10 items per transaction sets and the number of transaction sets is 12330.

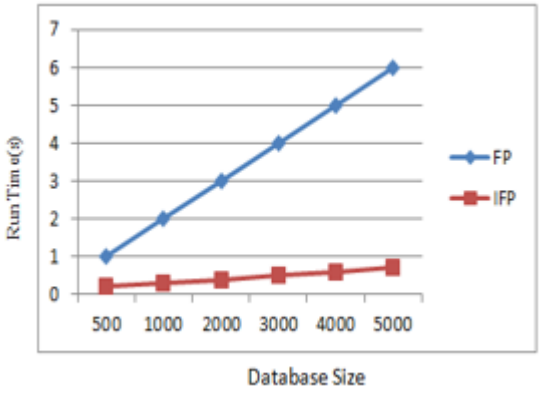

Fig 5. Comparison of different numbers for Online Shopper Purchasing Intention transaction items

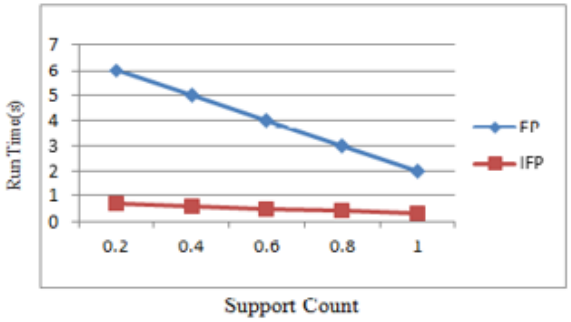

Fig 6. Comparison of different support counting for Online Shopper Purchasing Intention transaction items

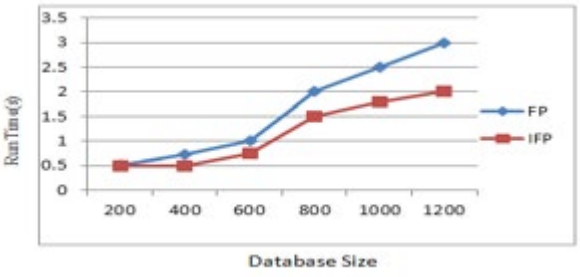

Fig 7. Comparison of different numbers for Supermarket Sales transaction items

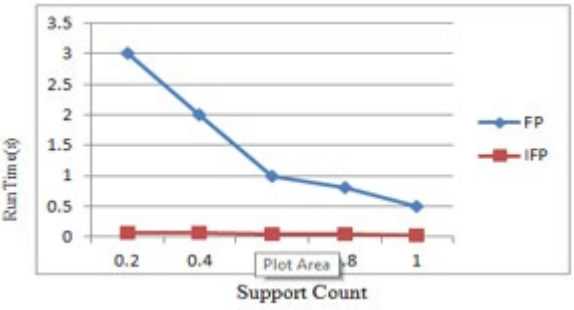

Fig 8. Comparison of different support for Supermarket Sales transaction items

From the experimental results, it can be concluded that the efficiency of mining frequent itemsets using the IFP-Growth algorithm is faster than the FP-Growth algorithm. IFP-Growth algorithm needs to scan time in the transaction database once, and doesn't have to sort many itemsets by support count. IFP-Growth algorithms avoid the recursive procedure time.

VII. CONCLUSION

Using frequent pattern mining methods, customer buying behavior or pattern is mined to help not only the customers but also managers who make marketing strategies. The FP-Growth algorithm considerably reduced the algorithm's time because it uses an association graph and adjacency table instead of a FP-tree. We compare the FP-Growth algorithm using FP-tree and Association Graph methods. From the result, the processing time is faster than the FP-tree algorithm. In the future, we can test the two algorithms with a different database. These features test the data mining technique in terms of accuracy and efficiency, which is more accurate than other methods. We are found FP-tree may not fit in memory and be expensive to build. FP-tree method is slower than the association graph because FP-tree is a recursive procedure.

ACKNOWLEDGMENT

I would like to express my gratitude to all my teachers at the University of Computer Studies, Yangon in Myanmar for providing necessary technical knowledge. Thanks to all of the teachers in Lab2 who helped the preprocessing database with the necessary assistance to prepare this paper.

REFERENCES

[1] R. O. Dude, P. E. Hart, and D. G. Stork., *Pattern Classification* (2nd. ed.). John Wiley and Sons, 2001.

[2] R. Feldman and H. Hirsh. Finding associations in collections of text. In R. S. Michal ski, I. Bartok, and M. Kuban, *Machine Learning and Data Mining: Methods and Applications*, pages 223–240. John Wiley & Sons, 1998.

[3] Elsayed M. Elgaml, Dina M. Ibrahim, Essayed A. Sallam "Improved FP-Growth Algorithm with Multiple Minimum Supports Using Maximum Constraints", International Journal of Computer and Information Engineering Vol-9, No-5, 2015.

[4] M. S. Mythili, A. R. MohamedShanavas, "Performance Evaluation of Apriori and FP-Growth Algorithms" International Journal of Computer Applications (0975-8887), Volume79-No 10, October 2013.

[5] Ming Yin, Wenjie, Yang Lie, and Dan Jiang, "An improvement of FP-Growth association rule mining algorithm based on adjacency table", MATEC Web of Conferences 189,10012(2018).

[6] M. Sinthuji, Dr.N. Puviarasan, Dr.P. Aruna, "Research of Improved FP-Growth (IFP)Algorithm in Association Rules Mining", International Journal of Engineering Science Invention (IJESI), ISSN:2319-6726, www.ijesi.org\\PP.24-31.

[7] M. Sinthuji, Dr.N. Puviarasan, Dr.P. Aruna, "Improved FP-Growth Algorithm Based on Top-Down Approach in Mining Frequent Itemsets", International Journal for Research in Engineering Application &Management (IJRE)ISSN:2454-9150 Vol-04, Issue-02, May 2018.

[8] Gayathri.GS, "Performance Comparison of Apriori, Eclat and FP-Growth Algorithm for Association Rule Learning", International Journal of Computer Science and Mobile Computing, Vol-6 Issue-2, February-2017, pg.81-89.

[9] Siddhrajsinh Solanki, Neha Soni, "A Servey on Frequent Pattern Mining Methods Apriori, Eclat, FP growth", International Journal of Computer Techniques"—Volume X Issue X, Year.

[10] R. Agrawal, R. Spirant" Mining sequential patterns including time intervals" Orlando, USA, Volume 4057, pg.213-220,2000.

[11] R. Agrawal, R. Spirant" Mining sequential patterns", Conference of Data Engineering Vol-95, page 3-14, 1995.

[12] C. Krauss, A. Mercer on, S. Arbanowski" The novel approach to evaluate educational recommender systems for closed-courses ", 9th International conferences, USA, Page-195-204, 2019.

[13] Mahajan, A. Reshamwala" An approach to optimized fuzzy time interval sequential pattern using multi-objective genetic algorithm", page.115-120, Springer, 2011.

[14] I. Sato, Y. Hirate and H. Yamana, "Text mining using prefix span constrained by item interval and item attribute", 22th ICDC, Atlanta, USA, page. 118,2006.

[15] Sumalatha and R. Subramanyam," Distributed mining of high utility time interval sequential patterns using mapreduce approach",141:112967, 2020.

Article ID – JRA6007320

Trimming And Optimizing Of Frequent Itemset Using Mining Technique In Sparse Big Data

Aye Aye Thein
Faculty of Information Science
University of Computer Studies(Meiktila)
Meiktila, Myanmar
ayeayethein@ucsmtla.edu.mm

Thein Than Twin
Research and Development Department
University of Computer Studies(Meiktila)
Meiktila, Myanmar
theinthantwin@ucsmtla.edu.mm

***Abstract*— The processes of mining frequent itemsets for big data have attracted in data mining research area by applying various algorithms. Big data involve irrelevant and infrequent different data. The correlation pattern of hidden itemsets evolve into more time consuming to be mined when the data quantity is increases over the time. Besides, memory consumption is required in finding hidden frequent itemsets due to a computation by the algorithm. So, an efficient algorithm is required to mine the itemsets frequency within a shorter run time and optimized the use of memory assessment while the huge of data increases over the time period. This paper presents and reviews a comparison of different algorithms for mining frequent itemsets attempt to more efficient itemsets mining algorithm can be developed. The algorithm of different computational turned over inexpensive by trimmed scanning on sparse data set because transaction query length is longer to database. This is the reason why applied TRICE algorithm. This paper highlights a review of frequent itemsets mining algorithms with comparable performance in sparse big data.**

***Keywords*— Algorithm, Big data, Data Mining, Frequent, Itemsets**

I. INTRODUCTION

Itemset mining is a process focused on interesting items with and discovering of correlation**.** Itemset mining is also a key factor in data item frequency motivation as well as in itemset feature retention. Extracting of frequent itemsets is leading and mining task of association rule. Fining frequent itemsets from large datasets to reveal unclear in big data becomes more desirable task for extract of association rules in data mining. The challenges of two step faced that run time for query length is longer and large consumption of memory space in computing the algorithm to mine all the frequent itemsets. So, the aim of this review paper is to construct an algorithm that is able to mine all the significant frequent itemsets within a dataset. The highlight of this paper is to review comparable performance of some significant and frequent itemset mining algorithms. The objective of this study is to review the strengths of the recent algorithms if itemset mining is sparse big data so that an efficiently itemset mines algorithm can be developed. Many data mining techniques are on available that it can be workable to sparse big data. Sparseness is on occasion in big data from various fields of ubiquitous computing, IoT, business activity, behavioral data. Even so, methods of extracting for frequent itemset are minimal prospected for sparse data of comparable performance. HARPP, SaM, RElim have been considered in each of the mining techniques and these applies to sparse big data. One such thoroughly pointed out method that is executed is frequent itemset query to sparse big data The collected data in sparse real-world applications can have unclear. Although many attempts to explore this relationship of techniques to dense data have been validated, sparse such kind of data make it calm a big challenge. Thus, there is a need to assess these techniques in addition to implementing new method for large sparse real-world datasets. Different algorithms of frequent itemsets mining by (TRICE) Iterative Trimmed Transaction lattice is compared. To solve performance gap of occurrence frequencies of itemsets on minimum threshold value of transaction, TRICE maintains a substantial this condition for all sparse datasets on thresholds. The results enlighten that algorithm TRICE outperforms all these HARPP, FP-growth, optimized SaM and Recursive Elimination algorithms both execution time and memory usage with Table II and Table III. TRICE iteratively generates combinations of transaction lattice sized trimmed subsets of distant items in a transactional database list.

Primarily business of association rule mining determines frequent itemsets. The first time of data items are decomposed frequent if satisfy the predefined in a higher number of transactions than the minimum support and threshold value defined in foremost. The next time is to generate association rule from these high frequency item sets. This trend is a way that heavily process. In variance to the previous one, this trend in a computing which process do not expensive. Consequently, the performance of mining association rule is decided on the first time. The attainment of assess time and memory consumption in an effective strategy through optimizing, conserving transactional lattice by TRICE on six sparse datasets. It's compared with HRAP, FP-Growth, Optimized SaM and RElim algorithm [1].

II. RELATED WORKS AND BACKGROUND

An itemset frequency solving on sparse big data is the significant problem in mining task with an intention of finding knowledge information. Itemset mining is the in

the form of iterative itemsets. For elementary reference Table 1 lists the specific of existing methods and their support suitability for real world sparse datasets [1].

A. Contribution of Frequent Itemset Mining

The several real life datasets are sparse, impure and high volume of variety of data. In such condition, extracting interesting on the results using itemset mining by identifying an input threshold minimum key specify. The itemset mining is the attractive significant issue of a process used to extract actionable key, value pairs from a larger set sparse big data. With the development of knowledge extraction from data and the growing intenseness of correlation between attribute, it is needed to optimize the time consuming and memory efficiency. One beneficiation undertaking, frequent itemset mining, has already directed data mining for its leading performance of executing run time and memory consuming [1][2]. Mining effective algorithm finds out occurrence frequencies of item and correlations, hidden pattern in data and make use of these itemsets to predict for future manner of decision making. The task of Itemset mining is to extract the types of most frequently correlations among the variables of characteristics in large transaction databases in data indexing with frequency no less than a specified threshold values. The combinations of distinct itemsets in a transactional database are large. The number of generated itemsets for small threshold can be very large. Thus, it is a great problem to construct model algorithms for mining frequent itemset. The present work on sparse database of this paper targets 1:)to preprocessing step for reduce the number of accesses to the transactional database, 2:) to optimizing for reduce of I/O cost.

B. Chellgences of Frequent Itemset Mining

In this section, the tasks are going to mention some related research in real world big data of sparse. Tremendous tasks in related with frequent itemsets using mining algorithms have motivated this paper work. Many researchers have been proposing to dig out frequent itemsets from transactional table base of sparse big data and to construct the corresponding power set the memory requirement computing for frequency item in data. The author in [1] proposed iterative trimmed algorithm have been derived by trimming its memory through for the dataset having longer transaction length. This function based on HARPP algorithm of iterative transaction lattice which can reduce memory as the power sets exclude empty set will be smaller subset transaction in size. Item lattice is an immenseness power sets containing two small subsets of itemset lattice that to find frequent itemsets. This method is able to achieve both execution times and conserves memory. At the starting, the operation scans for all transaction and iteratively execute an itemset whose support is equal or greater than min support count is filtered. In [2], a pre-computation based frequent itemset mining algorithm is proposed. This procedure is to compute the frequent itemsets rapidly on massive data. First, this algorithm pre-computes the specified a lower bound for min support threshold value. It set up the quasi frequent itemsets on the large old dataset and relatively small new dataset. In [3], the author also exploits to mining closed frequent itemset and extracting shorter frequent sub item in long dataset based on IoT. This paper analyzes hidden track in IoT to extract beneficial information in big data. Author in this paper carried out the frame work of an online pattern mining on IoT and reduce the size of the closed pattern sets. Authors in [4, 5] published projected database reduce the scanning time of the transaction implemented more efficient. The HUIM is to mine a set of patterns which give high profit measure. The authors implemented efficient procedures to significantly prune the search space and reduce database scan.

III. METHODOLOGY

Itemset mining involves the following steps shown in Figure1, which can be executed in transactional sequence of frequentitem1 and frequent itemset. Primarily the techniques have been computed on dense dataset, a significant different support in their performance. Even so, for large sparse real-world dataset, there is no valid dissimilarity among their performance. Trimmed algorithm optimizes by eliminating it memory exhaustiveness and efficiently finds itemset frequency from several sparse datasets.

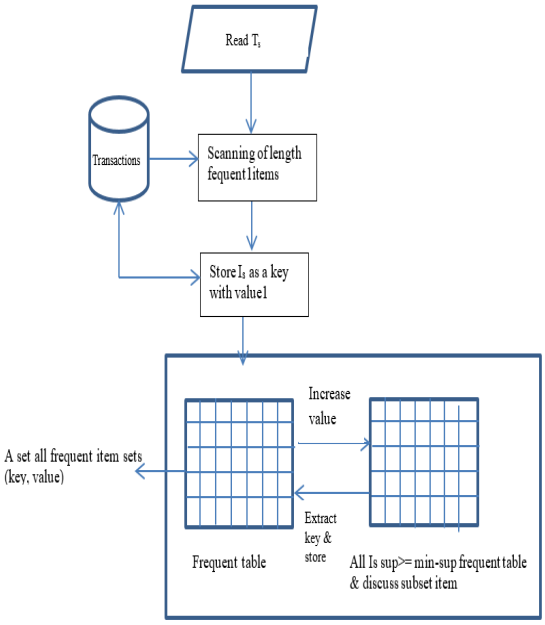

Fig. 1. Working chart of mining itemsets

A. APRIORI Algorithm

According to the concept of hierarchical monotonicity, the supersets of candidate itemset will be infrequent. So, apriori algorithm carries improvement in the brute-force algorithm by pruning the itemset lattice. It uses an iterative level-wise search technique to discover (k+1)-itemsets from k-itemsets and compute their support in the database. In frequent cases, the apriori algorithm compress the candidate itemsets size. However, it is challenge of a large number of candidate itemsets may still necessary to be generated if the total count of a frequent k-itemsets increases. Then, the hold database is required to be scanned and a huge itemset set of candidate set are required to be supported using the pattern matching [1].

B. FP-Growth Algorithm

FP-algorithm working with set of frequent items without a costly candidate generation process. It is to compress the frequent items extended prefix tree structure. This tree is split up into a set of conditional FP tree. An algorithm finds out the identifying long itemset frequency by observing through conditional FP-trees iteratively. The conditional sub pattern base consists of every prefix path in the FP-tree which co-occurrences with every frequent length-1 item. This made use of to construct the conditional tree and generate all frequent patterns linked to all frequent item length-1. Hence, the searching cost for frequent itemsets is reduced substantially. Although, creating the FP tree is time consuming if the dataset is large [1], [3].

C. RElim Algorithm

The algorithm CBAR follows apriori. This algorithm action a dataset scan and construct cluster records. The whole time this procedure, CBAR maintains a transaction table of k length to k-th cluster record. This makes candidate-2 itemsets with the way used by apriori algorithm. After this, procedure of CBAR contrasts with candidate 2-itemsets in second cluster. If its support becomes equal to the threshold value, an itemset is true to be frequent and checking in larger clusters is paused. In the same way, candidate 3-itemsets are checked in the third cluster and so on. This algorithm executes in a fast procedure because it brings contrasting partial cluster records over the hold database. CBAR performs two optimizations as structure table trimming by ignoring all infrequent items before constructing clusters. It optimizes CBAR by applying a counter for all transaction [1].

D. HARPP Algorithm

Frequent itemset mining in transaction database is a data analysis task. This procedure is to be one of the elemental data mining problems which intend to find groups of interesting items that frequently within a transaction. In this work, HARPP technique is Power set based algorithm. Key and value pair that the frequency of occurrence of each sub itemset and its support count is stored in a database dictionary. Longer transaction itemset trims combinations of transaction by power set. For sparse datasets, algorithm named as HARnessing the Power of Power sets for mining frequent itemset solve when min-sup is decrease. This algorithm works a single pass over the database and discovers frequent itemsets on the move. The frequent itemsets is efficiently discovered at lower min_sup thresholds value from real sparse datasets by procedure of this algorithm [1].

E. SaM Algorithm

SaM algorithm for frequent itemset mining which uses an unmix horizontal transaction demonstration. Customarily, the undertaking of frequent itemset mining can be constructed the set of items, and transactions database. Each, any subset of item base refers to the set of all item offered by an external storage. This algorithm performs in two steps. The split step is the first process in data structure. The first item of the first transaction is reproduced into a new processing scheme and that first item is eliminated. This work is recursively trpeated to find all frequent itemsets for the first round. The consequence another step is merging. This step is performed with the trimmed dataset that eliminated item from first step to construct the conditional pattern based [1].

F. RElim Algorithm

This is one patterned for extraction of frequent itemsets by the recursive eliminating. It does without prefix paths tree structures, directly transaction considering. The accessibility of its tree part is the advantage of this algorithm. This algorithm based on FP- growth but instead using FP-tree, it does recursion for eliminate items. FP-Growth algorithm that scans the database hire prefic/suffic parth of array structure. Node-link is supported by each itemset. Each node keeps a counter to transactions track that link the the sub-node all the way through one. It tasks by selecting the least frequent item. As a result, the smaller trimmed dataset is obtained. RELim procedure the found item during the recursively iterate process and execute all frequent itemsets related to remove it. And then, this task again by splitting the next least frequent item and so on. RElim access an item set to be supported by transactions item part only [1].

G. TRICE Algorithm

Data generation of big data has enlarged incessantly, it is expensive to conduct, acquire or extract and operate data applying existing algorithms. One such attractive appropriate algorithm is implemented is an itemset frequency mining in sparse big data as TRICE algorithm. With data size increasing in transaction it is expensive to perform data scan. Recently an algorithm of finding interesting itemset frequency presented because memory consumption is required in mining the frequent item. Thus an efficient algorithm is needed to extract the itemset of frequency within a shorter run time. There is involving frequent and infrequent items in a database transaction Therefore, TRICE algorithm can solve this condition in transaction database from sparse to find interesting frequent itemsets. In a transaction dataset, it has longer average length transaction. Memory intensive for that length cut out by performance of this algorithm. Suppose I= {i1, i2…., im} be the all itemsets and D be the transaction structure belonging to I. Is point to an itemset if Is is set of items. Ts is a transaction includes Is if and only if Is ⊆ Ts. Support of Is ϵ D. Is means frequent if if Sup (Is) ≥ minsup X|D|) [1]. An itemset frequency hold k items call frequent k-itemset. It can be expressed holds all data itemset having support greater than min_sup x |D|. The power set contain all subsets include the set itself but removing the empty subset. This algorithm performs the iterative trimmed transaction lattice by making power sets. This processing event is including in sparse dataset. Previously does iterative trimmed transaction lattice, trimming removes infrequent items from record. Trimmed Lattice transaction is built once if TRICE trims and saves only once. This procedure bypasses redundant process in next step and memory efficiency. This TRICE can better performance of HARPP, FP-growth, optimized SaM and RElim. The following are description of this algorithm [1].

The outcomes of presented review are effectiveness and maintain memory due to its transaction trimming

structure as well as handling identical transactions. An optimization factor provides reducing the runtime for large transactional databases. This algorithm making repetition generates transaction lattice by doing power sets of each transaction in an attribute-value pairs. The idea of these issues cut-out the infrequent set of a transaction first. It is used on storage data structure changing. The storage space is constricted to reduce the number of scans and trims similarly transactions only once, so the corresponding iterative trimmed transaction lattice structure is also constructed once. This structure eliminates redundant processing in later stage. It is also support in getting efficiency and preserving memory. This algorithm sufficiently supported for sparse data set and it generates attribute pairs of trimmed subsets of the distinct itemsets in a data structure. Insight from this algorithm preserves a performance gap on all min_sup for sparse datasets. After that, memory assessment uses of optimized SaM and RElim algorithm has been worked for the initiative.

IV. Result and Discussion

This following table is describing the main point of dataset features that can be described in SPMF [11,12]. PowerC, Kddcup99, OnlineRetail, Record Link, FoodMart datasets are got from [11]. Extended Backery dataset is take from [12]. The review of this paper studied based on many papers related to this process. The start by presenting the thought related to implement algorithm. The environmental set up for evaluation results, a computer carrying Windows 8 Pro x 64 bit, and 8G memory, 2.0 GHz Processor, Intel Corei7-3667U has been worked in [1].

TABLE 1. Datasets Feature of Frequent Itemset Mining Algorithm

No	Dataset name	Transaction count	Item count	Average item Count/ transaction
1	PowerC	1040000	140	7
2	Kddcup99	1000000	135	16
3	OnlineRetail	541909	2603	477
4	Record Link	574913	29	10
5	ExtendedBackery	75000	50	124
6	FoodMart	4141	1559	442

The different computational evaluation on six sparse datasets, that found the efficiency of mining itemsets with support value depends on frequency count, conditional structure node [1]. The algorithm has help optimizes the itemset frequency counting cost.

From table, for kddcup99, TRICE is faster than FP-growth for minsup=70% and memory assessment less than other minsup limit. For PowerC, TRICE and HARPP do equally time at min_sup0.001% and momery consumption is 37 times less at minsup1%. For OnlineRetail, a comparable performance by TRICE give at min_sup=0.03% and memory use 15 times memory. For RecordLink, TRICE is faster than other algorithm and memory use 33 times less than another algorithm at minsup70%. For ExtendedBackery, TRICE describes a comparable performance all min_sup value and it consumes the least memory at minsup2%. For FoodMark, TRICE is quickly than SaM and RElim. But it is giving a comparable performance of HARPP. For all threshold value, TRICE memory consumption is min on dataset. For the kddcup99 dataset, utilized memory is far less than of the others on all min-sup. For Food Mart dataset, TRICE consumes the least memory whereas, SaM consumes the least memory on lower min-sup values [1].

TABLE II. RUNTIME ASSESSMENT

Dataset	FP-growth (seconds)	SaM (seconds)	RElim (seconds)	HARPP (seconds)
Kddcup99				
min_sup=30%	3	2	2	
min_sup=70%	4	3	3	exceed 1000sec
PowerC				
(all min_sup)	4	4	3	equally
OnlineRetail				
min_sup=3%	4	4	5	
min_sup=0.01 %	2	2	5	10
RecordLink				
min_sup=70%	4	3	3.5	exceed 600sec
Extende dBakery				
min_sup= 0.01%	5	3	3	consistent
FoodMart				
min_sup= 0.04%	47	11	8	

TABLE III. MEMORY ASSESSMENT

Dataset	FP-growth times	SaM	RElim	HARPP
Kddcup99				
min-sup=70%	75	higher	higher	higher
min-sup=30%	40	less	less	less
PoewrC				
min-sup=40%	42	less	less	less
min-sup=1%	37	less	les	les
Online Retail				
min-sup=3%	<15	<15	<16	<16
Record Link				
min-sup=70%	33	less	less	less
min-sup=0.01%	27			
Extended Bakery				
min-sup=2%	higher	less	less	less
Food Mart				
higher min-sup	higher	less	less	less

V. Further Research Consideraton

Sparse big data are having two challenges. The first challenge is the scalability memory for dataset sizes have too large faster than the accessible of a memory workplace. The second is the execution time needed to obtain a solution. As described above, sparse data may involve different type and approximate zero, empty. This paper has reviewed obtainable itemset mining methods have to do with sparse data. A few possible future ways will be considered in this section.

Data model: The itemset transaction will be updated so that the hidden itemset of data can be sought within a reduce run time using less memory using when the amount of data increases over the time. In the looking at outcomes and the impacted data item, data analytics is an important research section. The hidden structure of the frequent iemset is made increase time consuming to be mined. Besides, memory consuming is required because weighty execution by the algorithm. Thus, a preprocessing model is needed to mine the hidden itemset of frequency inside a shorter run time and using less memory consumption. This operating step is cleaning refers to removal of irrelevant pair from transaction.

TABLE IV. DESCRIPTION AND NOTATIONS

Notations	Description
D	A transactional datbase
I_s	An itemset
T_s	A set ADT representation of D
ADT	A dictionary as a pair of key and value
|D|	Total number of tractions in D
min-sup	Given threshold
Dict1	A dictionary ADT that keeps T_s and pair of key and value
F	All frequent itemsets

Preprocessing clean algorithm
D: DB
Is: a itemset
Ts: A set ADT representation of D include Is
Input:(key: transaction D; total number of transactin |D| value: min_sup)
Output:(key: transaction, value: combination of a pair in Dict1)
begin
1. **for** each value;
2. read all transaction D;
3. F_i,F_I=ϕ(key, value);
4. for i=1…..m, m is the number of Ts then// compute frequency
5. for j=1…n, nis the number of Is then
6. F_I=F_I . indexof (I_i)
7. F_I ++;
8. end for j
9. end for i
10. if extract all key-value pairs ≥min_sup, by value then
11. release(key', value')
12. endif
13. return (key', value')
14. end algorithm

Data structure: After behavior an evaluation to compare the different algorithms for quarrying itemset frequency, the next step of research is to build a more efficient algorithm for mining itemset. The algorithm will be organized to mine the data from a transactional structure table in order to achieve the sequence items and hidden structures. All the frequent items have been found from the transactional table will be stored in a frequent itemsets database using the method of NoSQL.

VI. CONCLUSION

The collected and generated data in sparse real-world applications can have uncertain, such as mining of data stream, IoT services device, recommender system. In sparse dataset may involve values that are indefinite zero that makes the decidedness of correlation ship degree, type of attribute formats. The increasing of data emanating while existing computation and assessment are something required sparse big data, there is an increasing insufficient for efficient frequent itemsets mining methods for sparse big data in this case. Itemset mining from sparse dataset is indeed heavy and challenging. Itemset mining source data may not fit on hard drive in its violate memory. The exponential space combinations this problem. For this problem, another thing more work is needful, some strategies have specific to a framework, which are reviewed in this paper. It will be beholden if this review task provides s a reference for big data via itemsets mining.

As a basic operation of data mining, finding frequent pattern can widely improve the efficiency of big data in Internet of Things data. This paper review mining frequent itemsets for sparseness on big data emerging from a various source, involving IoT, pervasive computing, and behavioral data, firstly. The information retrieves on this paper work were reviewed which mining algorithms are evaluated to customize. There is some operation and technique is applied to solve specific problem. That are reviewed in this paper. The advent of the information - based big data, various portable devices, AI must solve in these processes. These challenges of frequent mining are expected to be a for next future need research.

ACKNOWLEDGMENT

I would like to thank all members of the Research Journal and Paper group in CU(Meiktila) FIS, FCS, Natural Language (English), Natural Language (Myanmar), FCST, ITSM. I also would like to thank the Professor Dr. Thein Than Thwin for his help and support. Finally, I would like to express my special respect and thank to organizing committee of "Journal of Research & Applications" (JRA)2020, UCSMTLA.

REFERENCES

[1] M. Yasir *et al.*, "TRICE: Mining Frequent Itemsets by Iterative TRimmed Transaction LattICE in Sparse Big Data," *IEEE Access*, vol. 7, pp. 181688–181705, 2019.
[2] X. Han, X. Liu, J. Chen, G. Lai, H. Gao, and J. Li, "Efficiently Mining Frequent Itemsets on Massive Data," *IEEE Access*, vol. 7, pp. 31409–31421, 2019.
[3] Z. Tianrui, W. Mingqi, and L. Bin, "An Efficient Parallel Mining Algorithm Representative Pattern Set of Large-Scale Itemsets in IoT," *IEEE Access*, vol. 6, pp. 79162–79173, 2018.
[4] A. Bai, P. S. Deshpande, and M. Dhabu, "Selective Database Projections Based Approach for Mining High-Utility Itemsets," *IEEE Access*, vol. 6, pp. 14389–14409, 2018.
[5] A. Podaras, "Measuring the Accuracy Levels Regarding the Dual Business Function Criticality Classifier," *IEEE Access*, vol. 6, pp. 41598–41606, 2018.
[6] B. Vo, L. T. T. Nguyen, N. Bui, T. D. D. Nguyen, V.-N. Huynh, and T.-P. Hong, "An Efficient Method for Mining Closed Potential High-Utility Itemsets," *IEEE Access*, vol. 8, pp. 31813–31822, 2020.
[7] I. M. El-Hasnony, S. I. Barakat, M. Elhoseny, and R. R. Mostafa, "Improved Feature Selection Model for Big Data Analytics," *IEEE Access*, vol. 8, pp. 66989–67004, 2020.
[8] B. Vo *et al.*, "Mining Correlated High Utility Itemsets in One Phase," *IEEE Access*, vol. 8, pp. 90465–90477, 2020.
[9] Q. Zhang, W. Fang, J. Sun, and Q. Wang, "Improved Genetic Algorithm for High-Utility Itemset Mining," *IEEE Access*, vol. 7, pp. 176799–176813, 2019.
[10] P. Su, D. Zeng, and H. Zhao, "Behavior Action Mining," *IEEE Access*, vol. 7, pp. 19954–19964, 2019.
[11] http://www.philippe-fouinier-viger.com/spmf
[12] https://wiki.csc.calpoly.edu/datasets/wiki/Extended.

Article ID – JRA6005920

Movie Recommender System using Collaborative Filtering Method

Pa Pa Win
Faculty of Information Science
University of Computer Studies (Meiktila)
Meiktila, Myanmar
papawin@ucsmtla.edu.mm

Seint Wint Thu
Faculty of Information Science
University of Computer Studies (Meiktila)
Meiktila, Myanmar
seintwintthu@ucsmtla.edu.mm

Zin Mar Naing
Faculty of Information Science
University of Computer Studies (Meiktila)
Meiktila, Myanmar
zinmarnaing@ucsmtla.edu.mm

***Abstract*—Recommender system is information filtering tool to recommend users for finding relevant items of interest from big data. Nowadays, recommender system plays a critical role in e-commerce applications and social networks. Model-based collaborative filtering utilized the ratings of the user-item matrix dataset to generate a prediction. This paper presents the comparison of the two widely used efficient techniques such as Biased Matrix Factorization and a regular Matrix Factorization, both using Stochastic Gradient Descent (SGD). This system especially uses the real-world public dataset: Movie Lens 100 K for predicting item ratings of users and evaluate by two metrics such as Root Mean Square Error (RMSE) and Mean Absolute Error (MAE). And then, the system demonstrates that the results of Biased Matrix Factorization used SGD techniques more accurate for rating prediction in experimental on Movie Lens 100 K dataset. The computation of a regular Matrix Factorization techniques and Biased Matrix Factorization produced the reduction of the RMSE by 19.69% and MAE by 14.08% for Movie Lens 100 K dataset.**

***Keywords*—Model-based Collaborative filtering, MovieLens, RMSE, MAE**

I. INTRODUCTION

The amount of movie has increased to become a lot of congested; so, to search out a movie what users are searching for through the present technologies are very hard. For this reason, the users desire a system that may recommend the movie show demand to them and therefore the best technology concerning these is that the recommendation system. Therefore, the most recommendation system is mistreatment cooperative filtering strategies to predict the requirements because of this technique offers the foremost correct prediction.

Recommendation systems are computer-based tools and techniques providing suggestions for helpful items to a user. Nowadays, recommendation systems are widely utilized in soft of areas as well as movies, news, books, analysis articles restaurants, garments, financial services, insurance, social tags and products generally. Recommendation system currently plays a central role for smart mechanisms in e-commercial services and various online applications and purchasing products recommendation based on a rapidly growing amount of information [1]. a variety of fields are employing collaborative filtering (CF) which is most popular and well-known approach associated with recommendation system, moreover this technique can recommend products that are likely to fit customer needs efficiently. It is well known; CF predicts the interest of products for an active customer based on the aggregated rating information of similar users.

Recommendation systems will be classified into two categories: memory-based filtering and model-based filtering. Memory-based recommendation systems are content oriented, which implies the content of users interests and the content of the features of items play a necessary role within the recommendation process[2].Recommendation systems using memory-based filtering approach base their evaluations on ratings given by a user on a group of items. Content-based filtering determines which items are likely to be useful or interesting to a given user by analyzing the content or the descriptions of items[3].

On the other hand, model-based approaches learn the parameters of a model and store only those parameters. Model-based CF has been researched to solve the problem for prediction of user's rating applying different data mining, machine learning algorithms [4]. Hence, in this system, we investigate Matrix Factorization which has been widely and effectively used in the model-based recommendation. Collaborative filtering recommendation systems verify the units of associated item supported the feedback of comparable users [5]. In our system, we will focus on understanding Matrix Factorization- a collaborative filtering solution for recommendations, using Movie Lens 100 K dataset. This system will compare two implementations of matrix factorization using stochastic gradient descent. The utilization of recommendation systems may facilitate users to save lot of time and energy whereas looking for movie that match their preferences and interests.

The structure of this paper is organized as follows. The first section provides the introduction. The second section briefly introduces some related works. The third section presents proposed method and the experimental workflow of the system. The section 4 describes data set and the

experimental result for the evaluation the system. Finally, the section 5 demonstrates conclusion of this system.

II. Related works

Recommender system is supported a spread of approaches like content based[6], collaborative approach[7], hybrid[8]. Furthermost movie recommendation system is focused on collaborative filtering and clustering. In movie recommender systems the users are asked to rate the movies which users have already seen then these ratings are applied to recommend alternative movies to the user that user has not perceived by utilizing collaborative filtering that is supported similar ratings. Collaborative filtering[9] [10] is enormously spreading in such how that this approach influences most of the recommender systems. Collaborative filtering majorly is classified into two principal categories like memory-based collaborative filtering and model-based collaborative filtering. Memory-based collaborative filtering explores for nearest neighbors within the user space for a full of life user and dynamically recommend the movies. The shortcomings associated with this methodology are computation complexness and information sparsely. Several authors tried to cut back this procedure complexness and memory bottle neck problems like in item based mostly collaborative filtering technique, during which relations between items were computed for neighborhood region around a target object. They showed in their empirical studies that item-based methodology might decrease the time of computation similarity as deliver rationally correct prediction and accurateness. Model-based collaborative technique produces a pre-built model to gather rating patterns supported the information of users and ratings which will treat the problem of information sparsely and model-based collaborative filtering is long and its off-line in nature[11] [12].

Movie recommendations exploitation many techniques are extensively studied within the past decades. Examples embraces a recommendation system exploitation the ALS algorithm, a recommendation supported the weight technique, item similarity-based collaborative filtering. These techniques need previous information concerning the ratings for the movies that square measure generated by the user. These techniques majorly use movie lens datasets for evaluation purposes. These systems square measure a small amount correct, and analysis is progress to boost the period of time performance of those systems. Movie Recommender System Exploitation Collaborative Filtering Technique.

Some of the most successful realizations of latent factor models are based on matrix factorization. In its basic form, matrix factorization characterizes both items and users by vectors of factors inferred from item rating patterns. High correspondence between item and user factors leads to a recommendation. These methods have become popular in recent years by combining good scalability with predictive accuracy. In this paper we use matrix factorization technique to build a sophisticated recommender system.

III. Proposed method

A recommender system is a system that recommends items for a user. Recommend can mean different things in different contexts. In the general case given an item in the system and/or a user of the system give a prediction of how much the user will enjoy the particular item. The general recommender systems' data include users, items that the users can interact with, item features, and user-item interactions. Example of items can be movies, songs, and products in an online shop such as clothes or electronics. The user-item interactions can consist of either unary data such as a view or purchase, binary data such as like or dislike, a numerical value such as a 1-5 rating or time viewed. Recommender systems are particularly useful in cases where there is an abundance of content that is not relevant to the user. The goal of a recommender system is often to increase the number of items sold or time spent interacting with the system, sell more diverse items and increase user satisfaction. A number of different approaches for predicting user preference and item similarity has been developed.

A. Collaborative Filtering

Collaborative filtering uses user-item relations to make predictions for a user. This is a powerful approach as the system does not need to know anything about the items inherent attributes. Collaborative filtering methods can be divided into two categories; memory-based and model based. Memory-based approaches is usually simple to implement and can provide very good prediction scores. However, memory-based techniques have been proven to be inefficient and difficult to scale with large datasets that is common in many real-world applications. Model-based collaborative filtering uses machine learning algorithms to create a model based on training data and then use the model to make predictions. In this paper, we use of matrix factorization which is known to be one of the most successful methods for rating prediction, outperforming other state-of-the-art methods. An effective latent factor method for recommender systems is called matrix factorization which we will focus on in this paper.

B. Matrix Factorization

Matrix factorization techniques have become a dominant methodology within collaborative filtering recommenders. Matrix Factorization has many benefits for overcoming problems in recommendation system. Matrix Factorization technique computes users and items in lower dimensional latent factor.

These user–item interactions can be represented as a matrix with users on one axis and items on the other. In most recommender systems based on items rating which is given by users, however, this rating matrix is typically very sparse in real world applications as users usually not fill their satisfaction for all the used items or watched movies. Matrix Factorization has been showed to be able to make very good predictions even on very sparse matrices. The matrix factorization approach reduces the dimensions of the rating matrix r by factorizing it into a product of two latent factor matrices, p for the users and q for items.

$$\begin{bmatrix} r11 & \cdots & r1i \\ \vdots & \ddots & \vdots \\ ru1 & \cdots & rui \end{bmatrix} = \begin{bmatrix} P1 \\ \vdots \\ Pu \end{bmatrix} [q1 \quad \ldots \quad qi];$$

$$\{u * i, u * f, f * i\} \quad (1)$$

f is the number of features extracted, u the number of users and I number of items (in our case, movies).

Each row pu is a vector of features for a user u and each row qi is a vector of features for an item i. The product of these vectors creates an estimate of the original rating.

$$r_{ui} = p_u q_i^T \quad (2)$$

There are multiple ways of factorizing a matrix into multiple components, used in many areas of machine learning and statistics, but most methods do not work when there are missing values in the matrix. If it could be done, not only would the observed values be estimated but all the missing values would be predicted. One approach is to impute the missing values, but doing so could distort the observed data due to the sparseness of the original matrix. Another one is to factorize by only using the observed ratings and try to minimize the squared error.

$$\min \sum_{u,i} (r_{ui} - p_u q_i^T)^2 \quad (3)$$

However, this can be result in over fitting the training data. To prevent over fitting a regularization term is introduced to the squared error. Impact of the regularization is controlled by constant β.

$$\min \sum_{u,i} (r_{ui} - p_u q_i^T)^2 + \beta (||P_u||^2) + ||q_i||^2) \quad (4)$$

Where ||.|| denotes the frobenius norm can be approximated using algorithms explained This approach has been shown to be very effective and at the same time scalable on very big datasets. The factorization can be done beforehand and less memory are used when making a prediction compared to neighborhood approaches where the whole rating matrix or a subset of it need to be kept in memory.

Biased Matrix Factorization. Improvement of Matrix Factorization prediction uses a bias for item and user, then calculates interactions, and on the other way, this model modifies the minimized squared error Equation. 4 to include the bias.

Stochastic Gradient Descent (SGD). SGD algorithm solves the optimization Equation. 4. It works by looping through each rating in the training data, to predict the rating and calculates a prediction error.

C. Experimental Workflow

Movie Lens 100Kdatasets included three attributes named by "user ID", "item ID", and "item ratings given by user", without missing value.

We set the "item ratings given by user" as a label, and "user ID" and "item ID" defined as attributes. In the split data phase, we perform 80% of data as the training set and the remaining 20% as the test data. The evaluation performance of our method we consider two comparison partners: Matrix Factorization and Biased Matrix Factorization, both using SGD. Experimental work flow as shown in Figure 1.

The main objective of this system is to support better recommender system. Firstly, the user chooses one of Movie Lens dataset. The system reads the selected Movie Lens rating data in the project. After reading file, the number of users and movies are obtained. Then, the system will predict accuracy depending on the apply model.

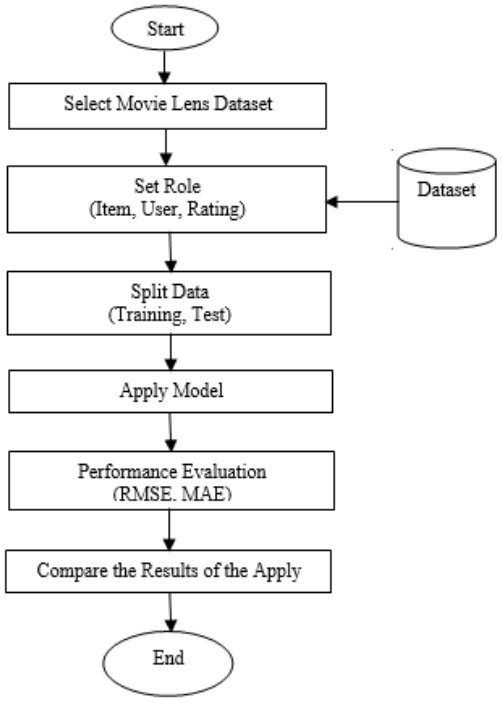

Fig 1. Workflow the Experiment

IV. EXPERIMENTAL RESULTS

In this section, we explain the datasets and experimental results obtained after running the Matrix Factorization and Biased Matrix Factorization approaches combine with SGD for the real-world Movie Lens 100 K dataset.

A. Data Set

In this system, we analyze real-world Movie Lens 100 K dataset and consider user, item and item ratings given by users in dataset.

TABLE I. SAMPLE DATA SET

No.	Data set's name	Number of Users	Number of Movies	Ratings
1	ml-latest-small	706	8,570	100,023
2	ml-100k	943	1,682	100,000
3	ml-20m	138,493	27,278	20,000,263

Movie Lens 100 K dataset were collected by the Group Lens Research Project at the University of Minnesota. This data set consists of: 100,000 ratings (1–5) from 943 users on 1682 movies shown in table 1.

B. Experimental Results

The experimental results are evaluated in Root Mean Square Error (RMSE) and Mean Absolute Error (MAE).

Root Mean Squared Error (RMSE). When evaluating rating predictions, a common metric is the Root Mean Squared Error (RMSE). The Root Mean Squared Error was the primary method used to test the accuracy of the prediction algorithms. RMSE is a statistical metric that represent the standard deviation between a set of estimated values to the actual values. In recommender systems it has been used to measure how far from the true values a set of predictions. RMSE is an objective metric widely used for performance evaluation of recommendation system models, which is defined as

$$\text{RMSE} = \sqrt{\frac{\sum_{t=1}^{n} (y_t^n - y_t)2}{n}} \quad (5)$$

The RMSE has the same measuring unit of the variable y.

Mean Absolute Error (MAE). MAE is the average vertical distance between each point and the identity line. The formula is given by

$$\text{MAE} = \sqrt{\frac{\sum_{t=1}^{n} |y_t^n - y_t|}{n}} \quad (6)$$

where t is estimated value at point, being the observed value in t and being the sample size.

TABLE II. EXPERIMENTAL COMPARISON RESULTS OF MATRIX FACTORIZATION AND BIASED MATRIX FACTORIZATION

Dataset Name	Method	RMSE	MAE
Movie Lens 100 K Rating	Biased Matrix Factorization	0.857	0.622
	Matrix Factorization	**0.895**	**0.724**

Table 2 shows that rating prediction result of Movie Lens 100 K datasets, which outperforms higher result in Biased Matrix Factorization compare with regular Matrix Factorization technique. Compute with a regular Matrix Factorization technique, Biased Matrix Factorization produced the reduction of the RMSE by 19.69% and MAE by 14.08% for Movie Lens 100 K dataset. Our experimental best result materialized RMSE by 0.857 and MAE by 0.622 on Movie Lens 100 K ratings datasets. According to the experimental results, the Biased Matrix Factorization provide more accurate recommendation.

Parameter settings of minimum rating, range, and number of factors depended on collected information of experimental datasets, respectively. Then, some other parameters such as user and item regularizations −0015, iteration number −30, and learning rates −0.01 were applied similarly in each technique. Biased Matrix Factorization technique should adjust bias parameter which toned in 1.0E-4.

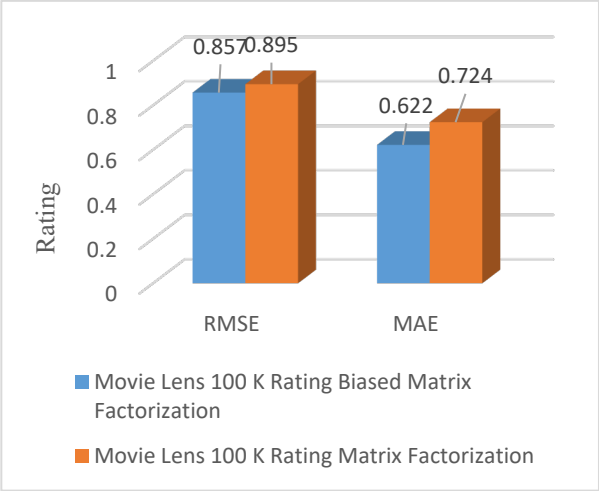

Fig 2. Results Comparison of Biased Matrix Faction and Matrix Factorization

V. CONCLUSION

Recommender systems have become increasingly popular, and utilized in variety of areas to enhance the understanding about customer behavior, therefore support the business processes effectively. In recent years, many kinds of recommender systems were developed, from them collaborative filtering model-based approach used most popular and successfully employed in applications, specially solve the critical part of predicting ratings.

This system used matrix factorization with the Movie Lens 100 K datasets to implement a recommender system since it is the current state of the art for implementing collaborative recommender systems. Matrix factorization techniques can be applied to a number of different systems, not only recommender systems. Matrix Factorization is a viable strategy for both making rating predictions and finding similar movies. Contribution of this system is showed to compare the two kinds of efficient techniques as Matrix Factorization and Biased Matrix Factorization in real-world Movie Lens 100 K datasets for predicting item ratings of users. Biased Matrix Factorization using SGD algorithm more the better performance corresponds to the RMSE and MAE than regular Matrix Factorization. Comparing the results of dataset, Biased Factorization using SGD materialize less prediction error.

ACKNOWLEDGMENT

I would like to express my special thanks to all my teachers who gave me their time and guidance, and all my friends who helped in the task of developing this paper. I am also graceful to all respectable people who directly or

indirectly helped towards the success. Finally, I would like specially to thank my parents for their continuous support and encouragement throughout my whole.

REFERENCES

[1] F. Ricci, L. Rokach, B. Shapira, "Recommender systems: introduction and challenges", In:Recommender Systems Handbook, pp. 1–34. Springer, Boston, MA, 2015.
[2] S. Gong, H. Ye, H. Tan, "Combining memory-based and model-based collaborative filtering in recommender system", Pacific-Asia Conference on Circuits and Communications, 2009.
[3] X. Su, T. M. Khoshgoftaar, "A survey of collaborative filtering techniques", 2009.
[4] R. Katarya and O. P. Verma, "An effective collaborative movie recommender system with cuckoo search," *Egypt. Inform. J.*, vol. 18, no. 2, pp. 105–112, Jul. 2017.
[5] Y. Koren, R. Bell, C. Volinsky, "Matrix factorization techniques for recommender systems", Computer 8, 30–37, 2009.
[6] H. Ma, H. Yang, M. R. Lyu, I. King, "Sorec: social recommendation using probabilistic matrix factorization", In Proceedings of the 17th ACM Conference on Information and Knowledge Management, pp. 931–940, ACM, 2008.
[7] M. Jamali, M. Ester, "A matrix factorization technique with trust propagation for recommendation in social networks", In Proceedings of the fourth ACM Conference on Recommender Systems, pp. 135–142, 2010.
[8] J. Herlocker, J. Konstan, L. Terveen, J. C. s Lui, and T. Riedl, "Evaluating collaborative filtering recommender systems," *ACM Trans. Inf. Syst.*, vol. 22, pp. 5–53, Jan. 2004.
[9] F. Gedikli, D. Jannach, "Recommending based on rating frequencies", In Proceedings of the Fourth ACM Conference on Recommender Systems, pp. 233–236, 2010.
[10] G. Takács, I. Pilászy, B. Németh, and D. Tikk, "Scalable Collaborative Filtering Approaches for Large Recommender Systems," *J. Mach. Learn. Res.*, vol. 10, pp. 623–656, Jun. 2009.
[11] C. J. Willmott, K. Matsuura, "Advantages of the mean absolute error (MAE) over the root mean square error (RMSE) in assessing average model performance" Climate Res. **30**(1),79–82, 2005.
[12] F. Maxwell Harper, J. A. Konstan, "The movielens datasets: history and context", ACM Trans.Interact. Intell. Syst. (TiiS) **5**(4), 19 (December 2015).
[13] Z. Yunhong, W. Dennis, S. Robert, and P. Rong "Large-scale parallel collaborative filtering for the netix prize", In Algorithmic Aspects in Information and Management, pages 337, 2008.
[14] R. Salakhutdinov and A. Mnih, "Probabilistic Matrix Factorization," Pro Advances in Neural Information Processing Systems 20 (NIPS 07), ACM Press, 2008, pp. 1257-1264.
[15] Y. Koren, "Collaborative Filtering with Temporal Dynamics,"Proc. 15th ACM SIGKDD Int'l Conf. Knowledge Discovery and Data Mining (KDD 09), ACM Press, 2009, pp. 447-455.
[16] L. Pasquale, G. D. Marco, and S. Giovanni, "Contentbased recommender systems: State of the art and trends", In Recommender systems handbook, pages 73, 2011.
[17] S. Xiaoyuan and K. M. Taghi, "A survey of collaborative filtering techniques", Advances in arti_cial intelligence, 2009:4, 2009.
[18] K. Yehuda and B. Robert, "Advances in collaborative filtering", In Recommender systems handbook, pages 145, 2011.
[19] S. Badrul, K. George, K. Joseph, and R, John, "Item-based collaborative filtering recommendation algorithms", In Proceedings of the 10th international conference on World Wide Web, pages 285, 2001.
[20] G. Takács et al., "Major Components of the Gravity Recommendation System," *SIGKDD Explorations*, vol. 9, 2007, pp.80-84.

Article ID – JRA6002420

Disaster Forecasting System Using Artificial Neural Network

Thet Su Win
Information Technology Supporting & Maintenance
University of Information Technology
Yangon, Myanmar
thetsuwin@uit.edu.mm

Khaing Htet Win
Faculty of Computer Systems and Technlogies
University of Computer Studies, Yangon
Yangon, Myanmar
khainghtetwin86@gmail.com

Soe Moe Aye
Information Technology Supporting & Maintenance
University of Information Technology
Yangon, Myanmar
soemoeaye@uit.edu.mm

***Abstract*— Natural disasters like floods, drought, Tsunamis, create numerous hazards including risk to human life, disturbance of transport and communication networks, damage to buildings and infrastructure, and the loss of agricultural crops. In addition, Myanmar is a cyclone-stricken country. There are many kinds of natural disasters, including tsunamis and volcanoes earthquakes, floods and landslides. These risks have a significant impact on the poor and the most vulnerable, along with high economic and social costs. In this paper, we develop a disaster forecasting system which can handle 3cases of disaster. This system propose a new technique of weather classification and forecasting using Liebenberg Marquardt Back Propagation Artificial Neural Network. The result of using ANN's approach to disaster prediction based on selected weather conditions is related to the situation in which the network is exposed. This system is effectively useful for weather forecasting and disaster forecasting in our country.**

***Keywords*— Disaster Forecasting System, artificial neural network (ANN), Earthquake, Floods, Landslide**

I. INTRODUCTION

An accident or a sudden natural catastrophe that cause great damage or loss of life can be defined as a disaster. Natural disaster that is a major environment issue creating economic and damage has become a great danger to human lives. Disaster prevention is not a practical task, and it is very useful for policy makers to inform and inform the public and to prevent and minimize energy loss [1]. The underlying mechanism of natural disasters is predicted by developing computational models and hence the historical data on natural disasters are analyzed to determine and recognize the patterns in the natural phenomena.

The artificial neural network is used to analyze complex climate data across a variety of climate applications; provides a powerful disaster risk assessment tool to design and understand. Predictive neural network applications are a problem of classification. It defines a subset of a task based on risk measurement.

To overcome this problem, ANN is applied to this system. Weather database are used to identify in forecasting cases. A critical requirement in disaster forecasting system is the availability of a problem domain expert to build verified database. In this work, ANN is used to train the verified database.

The following is this article: part II lists related works. Part III describes the types of disaster which is mostly caused in Myanmar. Part IV is depicted the framework of ANNs-based disaster forecasting system. Part V describes experimental results and conclusion is given in part VI.

II. RELATED WORKS

Many researchers have been work for weather forecasting system and forecasting system has been an area of active research. In this paper, we will emphasis on disaster forecasting system in Myanmar country. Many methods, rule- oriented or data driven have been proposed to tackle the forecasting problems. It is at times no easy to forecast many disasters.

Over the past decade, there have been several disaster management studies using the sensor network. Some of these are described in [10], [11] and [12]. Many researchers have proposed measures to combat the effects of floods in [2], [3], [5].There are also various models of operational disaster alarming system in [8].

The IMGW measurement network [9] is used for flood management and contains regular rainfall and hydrometric (water gauge) stations. Under normal conditions, information from the signal network sends the information to the IMGW estimator office once or three times daily. Researchers determine the frequency of information updates based on measurements and findings. For example, in the event of a flood, that means the water level goes above the warning level or increases in heavy rainfall and water levels.

Vista [8] uses remote sensing sensor ranging from metrological satellites (METEOSAT, NOAA) to optical satellite (LANDSAT-TM, WiFS) and hyper special air bone sensor (AVIS, DAIS) to SAR-sensor (ERS, ENVISAT-ASAR, SPOT, IKONOS). Depending on the application field Sensors are equipped with the most suitable sensors for extracting surface parameters used as input in the computation model. It uses space technology to send information to the rainfall / hydrodynamic model. However, these models do not have a comprehensive view

of flood estimates for environmental parameters. In addition, a personal study model was used for predicting floods in computer models.

III. Types of Disaster

Disaster is a sudden occurrence, which greatly impedes the functioning of a community or society, using the community and its natural resources beyond the capacity of society, Material and economic or environmental loss. The three main types of natural disasters are earthquakes; Floods and landslides affect people's health immediately. The secondary impacts is floods, landslides, fires, tsunamis.

A. Earthquake Disaster

In addition to geological damage, volcanic activity; Landslides; Other events, such as mining and nuclear tests, have also led to earthquakes. An initial breakpoint of an earthquake is called the focus or hypocenter. The epicene is at the ground level in the hypocenter.

B. Flood Disaster

Flooding can be regarded as over-watering (or over-watering), especially on land that is not drained. Water sources that cause many disasters can have many origins. These include severe and prolonged rainfall, melting snow, and blocking the river bottom from landslides or the collapse of dams or river closures Storm surge waves and tidal waves. Flooding problems are also exacerbated by the presence of man-made barriers such as road networks and canals that prevent natural flow.

C. Landslides Disaster

Slopes disrupt the natural stability of the slopes. They may be subject to heavy rainfall or drought, earthquakes or volcanic eruptions can be followed. When the water quickly collects in the soil, the shells develop and it is a stone. It causes soil and water-saturated damage.

IV. Training Artificial Neural Network

Processing of artificial neural network is done in three phase: training, validating, and testing. Firstly network is trained using input dataset. In this process the weights are adjusted such that the mean squared error obtained between the experimental and obtained result can be minimized. More the input data set used for training accurate will be the result, as it will have more data available for training.

In Back propagation algorithm the error is back propagated and respectively the weights are adjusted so as to reduce the error. The iteration continues until target value with minimum error is reached [4]. At the beginning of the training process, the connections between the neurons are set to random weight values. During the training process, the input and output data from the training data subset are fed into the network. The difference between training output and actual output values is then calculated [4].

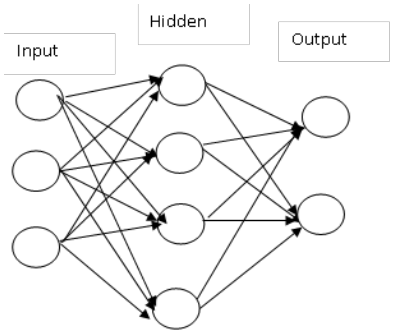

Fig. 1. Feed Forward ANN

V. Disaster Forecasting System

The classification and prediction of weather using back propagation neural network is basically a forecasting system which aims to gather data that is weather parameters, like temperature, pressure, humidity, wind direction. These predictors are taken as input neuron to BPNN. Weather forecast is made by collecting the data regarding the past and current status of the atmosphere and using this data to train neural network.

The system classifies and displays the future weather also it displays the weather information if one of the parameter is varied that is what will be the weather if value of the predictors are changed keeping one predictor value as constant.

A. Feature Selection

Properly forecasting natural disasters is often based on variety of inconsistent data (features) for examples, meteorologists are trained to identify potential threats to handle relevant data from all types of data. Such information is called “features” in the use of neural network.

B. Weather Data Collection

The data related to the predictors is provided to the network input layer. The data can be gathered using weather software also wireless weather sensors can be used like anemometer sensor, thermo hygro sensor etc.

C. Preprocessing

The noise in the data is removed in this step so as to get better Prediction result.

D. Weather Prediction using BPNN Training

The network is feed forward neural network. This network is to be trained using Levenberg Marquardt BPNN.

E. Classification

In neural network classification can be done easily. However it is mainly done using IF-THEN and Decision Table. After classification it should display, whether the future day selected will be sunny, rainy, partly cloudy etc.

F. Data Flow Diagram

The data is recorded using sensors and this data is given as input to the network. The data is preprocessed to remove noise and it is trained and validated. Further the output can

be classified (means weather the weather will be sunny, rainy, cloudy etc.

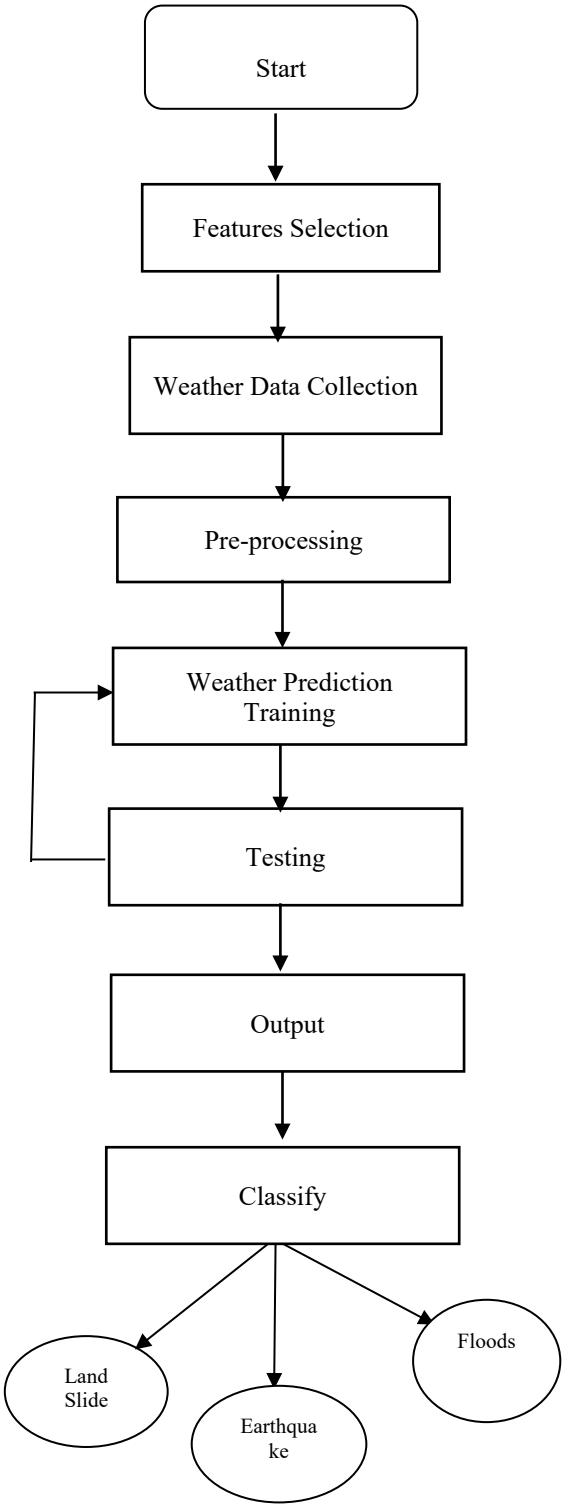

Fig. 2. Flow of Disaster Forecasting

VI. DISASTER FORECASTING SYSTEM

This paper emphasizes on the three disaster forecasting (earthquake, flood and landslide) that can occur the most percentages of Myanmar country. Mat lab 7.9 uses the Neural network toolbox to assess the proposed networks performance. Earthquake is the initial disaster to predict.

A two layer feed forward network was created with 6 inputs and 20 sigmoid latent neurons and 20 sigmoid latent neurons and linear output neurons. As a result, the network was able to predict 92 percent of Earthquake.

Flood is the second disaster to be forecasted. A two-layer feed-forward network was created with 22 inputs and 20 sigmoid hidden neurons and 20 sigmoid hidden neurons and linear output neurons. The network was able to predict 95% of occurrences of trials.

Landslide is third disaster to be forecasted. A two-layer feed-forward network was created with 16 inputs and 20 sigmoid hidden neurons and 20 sigmoid hidden neurons and linear output neurons. The network was able to predict 99 percent of cases from the trial.

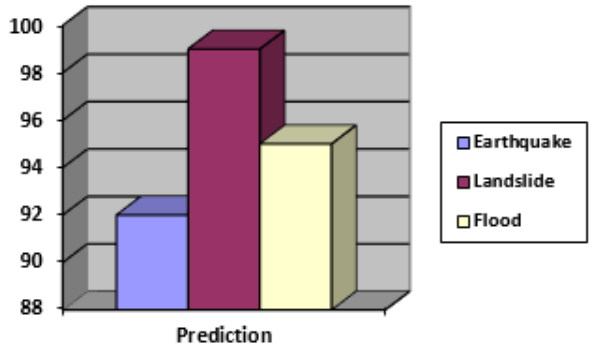

Fig. 3. Evaluation of Disaster Forecasting System

VII. CONCLUSION

The disaster forecasting system is proposed for Myanmar country which can handle 3 disasters.

ANNs act for a potent tool to assist meteorologist. This proposed system has the ability to process large amount of data. In addition, it reduces likelihood of overlooking relevant information and makes the reduction of forecasting time.

However, modern predictions are widely used, they must be considered as a tool to make smooth the last decision of the meteorologist responsible for evaluating the ANN's results. Summarizing and detailing of information and knowledge is constantly evolving and effective, efficient and effective. It can be very helpful for accurate and rapid disaster prediction systems.

ACKNOWLEDGMENT *(Heading 5)*

I would like to thank many of the people who were instrumental in completing this document. Last but not least, I thank my officer (Head of department), my best friend and my sisters from department for encouraging me to write this paper.

REFERENCES

[1] S. Haykin “neural networks A comprehensive foundation”.

[2] S. A. Monadjemi , P. Moallem and S. Moein, “A novel fuzzy-neural based medical diagnosis system”, International Journal of Medical Sciences and Biological , pp. 146-150, No.III, 2009 Volume-4.
[3] G. Canaris, S. D. Flach, B. S. Gerber , R. S. Wigton, P. S. Heckerling and T. G. Tape, “Predictors of urinary Tract infection based on artificial neural networks and genetic algorithms”, International Journal of Medical Informatics; pp. 289-296,Volume.76, No.IV, 2007.
[4] Gill J. et al, “Training back propagation neural networks with geneticAlgorithmfor weather forecasting” IEEE 8th international symposium onIntelligentsystems and informatics Serbia, 2010
[5] P. Moallem & S.A. Monadjemi, “Automatic Diagnosis of Particular Diseases Using a Fuzzy-Neural Approach”, International review on computers and software, pp. 406-411,Volume.3, No-IV, 2008.
[6] R. Lin, “An intelligent model for liver disease diagnosis", pp. 53-62 - Volume.47, No.I, 2009.
[7] J. A. Baker, G. D. Tourassi, P. A. Habas, J. Y. Lo, M. A. Mazurowski and J. M. Zurada, “Training Neural Network Classifiers for Medical Decision Making: The Effects of Imbalanced Datasets on Classification Performance”.
[8] P. Yan, H. Zhao ,G. Zhang and X. Zhang, “A Computer Aided Diagnosis System in Mammography Using Artificial Neural Networks”, International Conference on Bio Medical Engineering and Informatics,2008, pp. 823-826,Volume.2.
[9] K. N. Shruthi and J. B. Siddharth Jonathan , “A Two Tier Neural Inter-Network Based Approach to Medical Diagnosis Using K-Nearest Neighbour Classification for Diagnosis Pruning”.
[10] D. P. Ra, “Remote sensing & GIS for sustainable development: An overview”, On Resource and Enviromental Monitoring: Regional, Local and global, 1998.
[11] B. Zhu and M. King, “Gaming strategies,” in Path Planning to the West, volume. 2, Eds. Xian, M. King and S. Tang: Jiaoda Press, pp. 158-176, 1998.
[12] D. R. Fernandez, M. Johnsson, A. S. Paya , J. M. GariciaChemizo and D. Gil, “Application of Artificial Neural Networks in the Diagnosis of Urological Dysfunctions”, Expert Systems with Applications, pp. 5754-5760, Volume.36, No-III, 2009.
[13] O. Erogul , E. Aydur , Z. Telatar, and S. Altunay, “A New Approach to urinary system dynamics problems: Evaluation and classification of flow meter Signal causing artificial neural networks”, pp. 4891-4895, Volume.36, No-3, 2009.

Article ID – JRA6005320

Emoji-Based Pre-processing for Sentiment Polarity Classification

Su Mon Ko
University of Computer Studies (Meiktila)
Myanmar
sumonko@ucsmtla.edu.mm

Myint Myint Toe
University of Computer Studies (Meiktila)
Myanmar
myintmyinttoe@ucsmtla.edu.mm

Thein Than Thwin
University of Computer Studies (Meiktila)
Myanmar
theinthanthwin@ucsmtla.edu.mm

***Abstract*— As a consequent of the massive social media reviews, specifying the sentiment on user opinions becomes a challenging task. Besides, such social media reviews are unstructured in term of noise, emoticons and slang words. Thus, pre-processing step that eliminate the noise in texts becomes an essential process to promote the accuracy of the sentiment analysis system. In this work, the usage of emoji character is focused and the impact of emoji character on sentiment polarity classification is analyzed. The proposed machine learning based-pre-processing tasks are performed on two options including 'considering' and 'ignoring' emojis in the text. To ensure the achievement of our goal, the accuracy is evaluated with the two classification models including N-gram feature model and Naïve Bayes classifier. As a result, emoji-based approach is an important method in sentiment classification for improving the overall accuracy result. The result of conducted experiment shows that the accuracy of the classifier when applying emoji character recognition process increases 3% more than ignoring emoji characters.**

Keywords*— *Data science, Machine Learning, Sentiment Analysis, Social Media classification

I. INTRODUCTION

Social Media plays a vital part in today's life. Millions of users are using social media applications such as Twitter, Facebook, Instagram, WeChat, and WhatsApp. The social media maintains sophisticated data that is generated by variety of users including text, pictures, audio and videos data. From such heterogeneous data, extracting user opinion or sentiment is a challenging task. Sentiment classification is the process of classifying, defining and analyzing opinions in a given piece of text. The polarity classes considered are positive, negative and neutral.

Social sentiment analysis systems which can retrieve the user' opinion from a social media content are proposed with specific purposes. As the user generated contents in social media are unstructured in terms of noise, emoticons and slang words, machine learning approaches are used to perform the pre-processing process in sentiment analysis systems to achieve the accuracy. However, most researchers [1 - 3] emphasized on the consequence of different pre-processing methods for evaluating the sentiment classifiers' accuracy, the sentiment classification algorithms and feature extraction.

Emojis are uncontrollable emerging characters in recent years, especially in online communication. Team. Emoji report [7] has shown that 92% of online consumers are using emojis in 2015. They enabled social media users to express their emotions more easily than the text. The meaning of a text message can change by a single emoji character. A good instance is that the name of a song will achieve more polarity score by using with emoji. Even using the Emoji along with the song name and content can totally revert the meaning. For example, it can bring positive emotion towards the song when the content included a smiling face Emoji character "☺". On the other hand, putting the angry face Emoji "😩" beyond the song name will revert to negative feeling for that song. Therefore, our work focus and analyze on the usage and impact of emoji sign in the contents of text pre-processing.

Our work evaluated the effect of text preprocessing on sentiment classification, dividing into baseline cleaning with emoji characters recognition and without emoji characters. According to the results of earlier researches, various types of preprocessing techniques are used in baseline cleaning including removing hashtags, tagging, numbers and stop-words, replacing negation and repeated characters and expanding acronyms. In this work, N-gram feature model and Naïve Bayes classifier are used to classify the polarity of the content in sentiment classification process.

The rest of our paper is structured as follows. The earlier researches are discussed in section II. The theoretical background which can support for understanding the work is stated in section III. In section IV, the experimental results of the proposed work is illustrated. Discussion and further extensions are presented in section V and finally, the papers is concluded in section VI.

II. RELATED WORK

Some sentiment polarity classifiers are proposed in [1, 6] to classify the sentiment polarity by applying various text pre-processing methods such as stemming, removing URLs, removing stop-words, Hashtags, replacing negative mentions and expanding acronyms in noise reducing process. They proposed their data pre-processing approach to reduce the noise in the text. They tried to show that their approach can improve the efficiency of the classifier by

evaluating on the classification speed. However, some researchers focused on feature extraction rather than text preprocessing of sentiment analysis; the authors of [1] introduced the effectiveness of text preprocessing on sentiment classification. In their work, six types of pre-processing methods are used on two features model and five datasets to test the importance of text preprocessing in sentiment classification task. They showed that expanding acronyms and replacing negation are significantly affected on the accuracy improvement of the classifiers but slightly changes in removing URL, numbers and stop-words. They tried on various text pre-processing methods on various classifier and reveal that Random forest and Naïve Bayes classifiers get the greatest effect.

Giulio Angiani et al. [2] highlighted the importance of preprocessing phase and how it effects on the performance of the system. Based on Balahur' preprocessing ideas [3], their work focused the effectiveness and performance of preprocessing phase in terms of accuracy by analyzing each method separately. According to the results, stemming increased the performance, stop word enhanced the system and using dictionary did not enhanced the performance of the system. Singh et al. [4] analyzed the twitter data pre-processing approach for sentiment classifier. That approach is based on the slang words. The pros and cons of slang words are checked by binding the existing words and slang words. In computing the random fields and bindings, they used N-gram method to evaluate the significance of slang words. They can present that their method can support both optimized data size and good accuracy for sentiment classifier.

The role of text pre-processing approaches for sentiment analysis on movies reviews dataset are highlighted in [5]. They showed improved accuracy for sentiment classifiers due to the right choice of features and presentation with an appropriate pre-processing in their empirical evaluation. Krouska et al. [6] made a comparison study of sentiment machine learning methods for polarity classification on Twitter data and the role of text pre-processing in sentiment analysis, and the report on experiment results demonstrating that with the feature selection and representation can affect the classification performance positively. They found that the preprocessing operations affect the quality of the classification.

From the above reviews, there is a lack of proper analysis of the effect of emoji characters in text pre-processing on sentiment classification task. Thus, the appearance of Emoji characters in text pre-processing and how they effect on the sentiment analysis process are analyzed in this work. This paper focus on analyzing the effects of text pre-processing on sentiment classification using N-gram feature model and Naïve Bayes classifiers on music review datasets in two types of classification task.

III. THEORETICAL BACKGROUND

A. Pre-processing Analysis

To analyze the effect of pre-processing method on sentiment analysis especially in terms of emoji characters, pre-processing analysis is done by dividing into baseline cleaning with emoji recognition and without emoji character recognition. Different types of processing methods are used in baseline cleaning process. The complete analysis of pre-processing set up is stated as follows:

Baseline Cleaning Process

In social media, content generated by the users is very informal. Thus, such kind of informal text are firstly to be cleaned to determine the polarity of sentiment classification. The baseline pre-processing methods used in this paper are as follows:

Converting Lowercase - To avoid case sensitive issue, all texts in the content are converted into lower case.

Removing URLs, Hashtags, Punctuations, Numbers and stop-words - According to the nature of social media, users create their own words and spell shortcuts, slang, emoji and urls. Most URLs are used to give and study the extra detail information about the facts that the topic stated. They do not carry any sentiment information of the content. Hashtags are especially used to describe the topic of the content in twitter. Punctuations and numbers are also do not carry any information about sentiment polarity. Stop-words are commonly used words which have very little meaning. Therefore, URLs, Hashtags, Punctuations, Numbers and Stop-words are removed from the content to resize the content.

Replacing Contractions - Contractions used in the content plays an important role in determining the sentiment of the content. The process of negation is transforming “hasn’t” and “haven’t” into “has not” and “have not” respectively [1].

Stemming - The users are grammatically structured the contents by using different forms of a word, such as organize, organizes and organizing. There is no need to consider grammatical rules in determining the sentiment polarity. Stemming reduces inflectional forms of a word to a common base form. Example, “the boy’s cars are different colors” as “the boy car be differ color”.

Emoji and Emoticon Recognition Process

There are many unique attributes in twitter messages, which distinguishes twitter data analysis from other research areas. The length of a tweet is the first significant attribute. Twitter accept only maximum 140 characters in a tweet and the average length is 14 words. Due to the nature of this attribute, people use emoji characters and emoticons when expressing special meanings. Emoticons are pictorially represented by using punctuation and letters or pictures to express the user’s opinion.

Emoji were firstly used by mobile operators in Japan. 176 Emojis was first proposed as a message feature. Hundreds of Emoji characters were combined with Unicode characters which introduce Emoji the opportunity to be used worldwide in 2010. Total 1,126 Emoji characters were provided when reaching to Unicode 9.0. Gathering data for SA models differs based on the tools used to collect the data. The researchers may receive various form of the Emoji characters in the collected data depending on the tool used. For example, Twitter API for different language provides these characters in different annotations. The

appropriate Unicode annotation should be used in the software when searching a specific Emoji character. In this paper, our objective was to study the impact of Emoji characters on sentiment classification models. We analyzed the usage of emoji characters and evaluated the impact of ignoring or accepting those characters while developing a model.

A lexicon is prepared to support emoji notations including python, which contain 18 different representations for 843 different Emoji characters. A score among values {-1, 0, 1} is assigned for each emoji character. The text is also given scores, negative, natural, or positive. The average score was obtained by integrating all of the score for each text and emoji. The appearance of Emoji signs on Twitter are monitored by the specific website "Emojitracker.com" [9]. That website also reports the analysis results for containing Emoji signs and all tweets. The incidence of each Emoji signs is counted as number of incidences and the sorting process is performed on the number of incidences. In this way, "Emojitracker.com" website maintains the rank for each Emoji sign and the scores for sentiment on each Emoji sign (between 0 and 1). That information is collected into the lexicon of our proposed system. Thus, our lexicon totally maintains such information for 18 different Emoji sign or notation. Then, the created lexicon is used to detect the Emoji sign from the tweeted data which are globally collected. Table 1 shows the various representation or encoding of a single emoji sign "Face with Tears of Joy" [10] as an example.

B. N-gram feature Model

The simplest feature for Twitter sentiment analysis is n-gram feature. The progressive performance of sentiment analysis system is experimented using a unigram model especially based on twitter data [11, 12]. In this work, word unigram feature (referred to N-grams model) is used in feature extraction process of the sentiment analysis.

C. Twitter Sentiment Classifier

Most researches applied machine learning approaches in sentiment analysis process. According to the result of [1], Naïve Bayes supervised classifier is more sensitive than other classifiers. This paper uses it in the literature to classify the content polarity especially considering and ignoring emoji characters at text pre-processing step.

D. Data Collection

The experiment is performed using music review data on twitter. Twitter allows users to collect data via twitter API. In this task, Twitter API is connected and downloading data by using Python and Tweepy library. A tweet contains 140 characters maximum and use special characters like @ and # are used to indicate the user name and topic of the content. The music review are collected base on only tweets and filtered by using hashtag. Retweets and other factors are rejected in this task. The user generated data for a popular song named "How You Like That" reviews are collected in this work by using #howyoulikethat target word. There are 10947 review tweets for this song. Therefore, the dataset used in this experiment contains 10947 data records containing 66% neutral, 28% positive and 6% negative tweets. Table 2 shows the number of tweets in the created datasets and its sentiment labels.

TABLE 1. SAMPLE EMOJI LEXICON ENTRY

Representation	Value
Emoji Name	FACE WITH TEARS OF JOY
Unicode UTF-8	😂
Character UTF-8 Count	1
HTML Entity (Decimal)	😂
HTML Entity (Hexadecimal)	😂
Code Point (Hexadecimal)	1f602
Unicode Notation	U+1F602
Code Point (Decimal)	128514
UTF-8 Hexadecimal (C Syntax)	0xF0 0x9F 0x98 0x82
Hexadecimal UTF-8	F0 9F 98 82
Octal UTF-8	360 237 230 202
Hexadecimal UTF-16 (C)	0xD83D 0xDE02
Hexadecimal UTF-16	d83dde02
Decimal UTF-16	55357 56834
Hexadecimal UTF-32 (C)	0x0001F602
UTF-32 Hexadecimal	01F602
UTF-32 Decimal	128514
Python	u"\U0001F602"
PHP	"\xf0\x9f\x98\x82"
C/C++/Java	"\uD83D\uDE02"
R-Encoding	<ed><a0><bd><ed><b8><82>
Emojitracker.com rank	1
Sentiment Score	0.805100583

TABLE 2. TOTAL NUMBER OF TWEETS AND ITS TWEET SENTIMENT IN DATASET

	Tweets	#positive	#negative	#neutral
Music review dataset	10947	7206	3051	690

IV. EXPERIMENTAL RESULTS

The dataset is partitioned into training set that is used to train the proposed model and testing set that is used to test the accuracy of the proposed machine learning approach based on 70:30 proportion. Several baseline preprocessing techniques are firstly applied on Twitter music review dataset by dividing with emoji characters and without emoji characters. For each approach, tweets are classified using Naïve Bayes classifier. Afterwards, a comparative analysis of the classification accuracy is performed to estimate the roles of emoji characters in preprocessing on Twitter sentiment classification problems. The accuracy of the classification process on the proposed work is

calculated by using precision, recall, F1-measure and accuracy methods. Table 3 illustrated the total number of words in the dataset before and after the proposed preprocessing methods are applied. According to the table, the preprocessing step reduced the unnecessary words that are useless in the sentiment classification process. This can reduce noise data in the dataset.

TABLE 3. TOTAL NUMBER OF WORDS BEFORE AND AFTER PREPROCESSING

Total Tweets	Word count before Cleaning	Word count after Baseline cleaning without emoji characters	Word count after Baseline cleaning with emoji characters
10947	145924	100971	109345

The ratio of positively or negatively classified tweets which have an actual classification of positive or negative is referred to as precision, whereas recall is the proportion of the actual positive or negative tweets which are also classified as such. The F1 measure is the harmonic mean of precision and recall. Accuracy is the proportion of correctly classified tweets [8].

Table 4 reports the values of precision, recall, and F1 measure for positive, negative and neutral documents without emoji recognition process in pre-processing. Result with accuracy at level of 58% seems to be quite nice result for such basic algorithm like Naive Bayes. This performance may not hold for the final testing set. In order to see how the Naïve Bayes performs in more general cases, 8-fold cross-validation is used, which is a technique that is useful to evaluate a classification algorithm for a given corpora, splitting and evaluating the training set several times. The average accuracy of the sentiment analysis process produced 43% after applying 8-fold cross validation.

TABLE 4. THE ACCURACY RESULT OF THE SENTIMENT CLASSIFICATION PROCESS USING ONLY BASELINE CLEANING

	Negative	Neutral	Positive
F1 measure	0.3895	0.4507	0.7137
Precision	0.4541	0.4843	0.6501
Recall	0.341	0.4215	0.7782
Accuracy	0.5752		
Average Accuracy	43 %		

Table 5 states the values of precision, recall, and F1 measure for positive, negative and neutral documents with emoji recognition process in pre-processing. There were slightly change in the values of precision, recall, f1-measure and accuracy of the classification process. However, the average accuracy of the sentiment analysis process reported 46% accuracy after applying 8-fold cross validation.

Table 5. The accuracy result of the sentiment classification process using baseline cleaning integrated with emoji character recognition process

	Negative	Neutral	Positive
F1 measure	0.245	0.4794	0.7034
Precision	0.4778	0.4919	0.6316
Recall	0.1648	0.4676	0.7936
Accuracy	0.5795		
Average Accuracy	46 %		

V. DISCUSSION AND FURTHER EXTENSION

The experiment result show that the usage of emoji characters effects the performance of the classifier on real time twitter dataset. According to the nature of twitter data, the user uses different types of unstructured text like emoji, acronyms and slang words. Most of the users are directly used emoji characters to express real opinion about the specific topic while others are not. Some users use emoji characters to express opposite feelings of their opinions. For example, the tweet "Blackpink is great ☺" means that the user have positive opinion on Blackpink K-pop group. However, the tweet "Blackpink is great 😩" means opposite opinion. For the sentiment analysis process, the weight of emoji character is more important than the text. Emoji enhancement process is also needed to perform in the pre-processing step. The review tweets upon the specific topic have many forms of aspect. The data is collected based on the music review tweets. Some tweets are given opinion for the song while others are different aspects like visual of singers, sound effect, music types and so on. The sentiment analysis process is performed by calculating the polarity score of sentiments used in the tweets. Therefore, it does not need to consider what the user have positive or negative opinions on what aspects of the music. This may lead to miss information result to the music reviews analyzer.

In the future, sentiment classification will be performed on aspect-based analysis for decision making processes and a comparison analysis will also be performed on the effect of emoji characters of sentiment analysis using other feature models and classifiers on different datasets.

VI. CONCLUSION

This paper studies the usage of emoji characters in user-generated data on twitter and the effect of this on sentiment polarity classification. The experiment is conducted using Naïve Bayes classifier to verify the effectiveness of using emoji characters on real time twitter dataset. According to the experimental results, the usage of emoji characters slightly effects on the sentiment polarity classification process. This work observed that considering emoji in sentiment classification help to improve the overall accuracy result. The performance accuracy of the classifier is increased 3% when applying emoji character recognition process in pre-processing step.

REFERENCES

[1] Z. Jianqiang and G. Xiaolin, "Comparison Research on Text Pre-processing Methods on Twitter Sentiment Analysis," IEEE Access, vol. 5, pp. 2870–2879, 2017, doi: 10.1109/ACCESS.2017.2672677.

[2] G. Angiani et al., "A Comparison between Preprocessing Techniques for Sentiment Analysis in Twitter," 2016.

[3] A. Balahur, "Sentiment Analysis in Social Media Texts," p. 9.

[4] T. Singh and M. Kumari, "Role of Text Pre-processing in Twitter Sentiment Analysis," Procedia Comput. Sci., vol. 89, pp. 549–554, Jan. 2016.

[5] E. Haddi, X. Liu, and Y. Shi, "The Role of Text Pre-processing in Sentiment Analysis," Procedia Comput. Sci., vol. 17, pp. 26–32, Jan. 2013.

[6] A. Krouska, C. Troussas, and M. Virvou, "The effect of preprocessing techniques on Twitter sentiment analysis," in 2016 7th International Conference on Information, Intelligence, Systems Applications (IISA), Jul. 2016, pp. 1–5.

[7] E. R. Team. Emoji report.

[8] Department of Software Engineering, Bahcesehir University, Besiktas, Istanbul, Turkey., S. Ayvaz, and M. O. Shiha, "The Effects of Emoji in Sentiment Analysis," *Int. J. Comput. Electr. Eng.*, vol. 9, no. 1, pp. 360–369, 2017.

[9] Emojitracker: Realtime emoji use on twitter. *Emojitracker.* Retrieved Jan. 30, 2017, from http://emojitracker.com.

[10] Liberatore, S. (2017). New study finds face with tears of joy is world's most popular emoji. *Daily Mail,* Retrieved Jan. 30, 2017, from http://www.dailymail.co.uk/sciencetech/article-4089052/Crying-waychart-Face-tears-joy-revealed-world-s-popular emoji.html.

[11] A. Go, R. Bhayani, and L. Huang, ``Twitter sentiment classi_cation using distant supervision," Stanford, Stanford, CA, USA, Project Rep. CS224N, 2009.

[12] A. Pak and P. Paroubek, ``Twitter as a corpus for sentiment analysis and opinion mining," in *Proc. LREC*, vol. 10. 2010, pp. 1320_1326.

Article ID – JRA6002920

Extraction and Characterization of Arrowroot Starch and its Application in Starch Packaging Films

Thida Tin
Mandalay Technological University, Myanmar
thidatin.mumdy@gmail.com

Thida Win
Technological University (Sagaing), Myanmar

***Abstract*— The arrowroot was selected for extraction and characterization of starch and the preparation of films were studied. Firstly, arrowroot starch was extracted from arrowroot powder. Moreover, the physicochemical properties such as pH, moisture, ash content, water absorption capacity, bulk density, viscosity and swelling power of arrowroot starch were also investigated. In addition, Semi-crystalline nature of arrowroot (Adalut) starch was shown by X-ray diffraction analysis. Furthermore, the starch films were performed by using only starch and starch with different kind of chitosan and poly vinyl alcohol. Finally, the mechanical properties of the different types of films were also determined. Among the prepared films, the starch- chitosan film showed the satisfactory mechanical properties. Therefore, the prepared starch films were used for packing of fresh fruit and extending of their shelf life.**

Keywords— ***arrowroot, starch, films, mechanical properties***

I. Introduction

Arrowroot is a starch rice; it's widely cultivated hilly regions. Arrowroot is relatively safe for human consumption and chiefly valuable as an easily digested. Arrowroot starch is one of the purest forms natural carbohydrate and has a maximum viscosity, although this is adversely affected by the salinity of the processing water. Arrowroot is edible raw, roasted, stewed and fried. The rhizomes are sometimes eaten boiled. The rhizome are used for the production of a very fine, easily digested starch, which appears on world markets as a dry white power known as arrowroot starch. It works due to present of bio-active compound such as alkaloids, carbohydrate, cardiac, glycoside, amino acids, phenolic compounds, terpenoids, saponins and flavones. Arrowroot is a rich source of vitamins [1].

Starch consist of two type of molecules the linear amylose and the branched amylopectin. Depending on the plants, starch generally contains 20 to 25% amylose and 75 to 80% amylopectin by weight. Starch is the common carbohydrate in the human diet and is contained staple foods. The major source of starch intake worldwide are the cereals (rice, wheat and maize) and the root vegetable (potatoes and arrowroot).Many starch foods are grown, some only in specific climate [3].

Food packaging is an important part of food products, both to protect food quality and safety of food products to enhance their added value. Food packaging materials with sufficient thermal stability, antibacterial and antioxidant properties are necessary for food safety and extending the shelf life of packaged food [4].

The main purpose of this research work, arrowroot was chosen to extract starch and to characterize the different types of prepared arrowroot starch film.

A. Botanical Description

Family name	: Marantaceae
Scientific name	: *Maranta arundinacea* L.
English name	: Arrowroot
Myanmar Name	: Ardalut
Part used	: Rhizome

Fig 1. Plants and rhizomes of arrowroot (*Maranta arundinacea* L.)

II. Materials and Methods

A. Sampling

Arrowroot were collected from Thingaton village, Pyin Oo Lwin Township, Mandalay Region. The arrowroots were grinded with blender and sieved with 150 mesh sieve

and the powder sample was stored in plastic bag for studying.

B. Determination of pH and Physicochemical Properties of Arrowroot

The pH of arrowroot powder was measured by using pH meter. The physicochemical properties of arrowroot powder sample such as moisture, ash, fat and crude fiber were determined by using Moisture Analyser, Muffle furnace and Soxhlet extraction methods [2].

C. Extraction of Starch from Arrowroot Powder

100.0 g of arrowroot powder sample and 500mL of 0.05 M sodium hydroxide solution were introduced into a steel container. It was stirred for one hour at a rate of 600 rpm at room temperature. It was allowed to stand for 30 minutes and filtered by using double layer cotton cloth. The residue was washed distilled water until the filtrate was neutral. Then the residue was dried in air and the dried sample was grinded by using the pestle and motor to obtain the starch powder. The weight of extracted arrowroot starch was determined.

D. Iodine Test

About 0.1 g of arrowroot starch was dissolved in 5 mL of distilled water and it was heated in boiling water bath for 30 minutes. When one drops of iodine solution was added into the starch solution, the colour of the solution changes deep blue colour.

E. Determination Bulk Density of Arrowroot Starch

The clean and dry specific gravity bottle (25mL) was weighed. The bottle was filled with the starch powder sample and weighed. Bulk density of the powder sample was calculated as:

$$\text{Bulk density (\%)} = \frac{b-a}{v}$$

Where, a = wt of specific gravity bottle
b = wt of specific gravity bottle and powder sample
v = volume of specific gravity bottle

F. Determination of Water Absorption Capacity of Arrowroot Starch

Arrowroot starch powder (1.0g) was placed in a pre-weighed centrifuge tube and add 10 mL of distilled water. The tube was shaken with shaker for about 2 hours and allowed to stand for 30 minutes. The tube was centrifuged for ten minutes. The supernatant was decanted. The centrifuge tube was weighed. The gain in weight was used to calculate the water absorption capacity.

$$\text{Water absorption capacity} = \frac{c-(a+b)}{b}$$

Where, a = wt of centrifuge tube
b = wt of starch powder
c = wt of centrifuge tube containing sample powder with water uptake

G. Determination of Intrinsic Viscosity

1.0 g of arrowroot starch powder sample and a few ml of distilled water were added to make a paste. The pastes were added into 100 mL boiling water and then boil for 10 minutes to obtain 1% starch solution. Using an Oswald's viscometer, viscosity of starch solution was determined.

$$\eta_1 = \frac{d_1 \times t_1}{d_2 \times t_2} \times \eta_2$$

Where, η = viscosity (centipoises)
η_1 = viscosity of 1% starch solution
η_2 = viscosity of water
d_1 = density of starch
d_2 = density of water (1.00)
t_1 = flow time of starch solution
t_2 = flow time of water

H. Determination of Starch Solubility and Swelling Power

1.0 g of arrowroot starch was weighed and put into the beaker. 100 mL of distilled water was added into the beaker. The suspension was stirred at 1100 rpm and heated at 50°C for 1 hour. Then the suspension was cooled for 30 minutes. After 30 minutes, it was poured into pre -weighed centrifuge tubes and centrifuge for 10 minutes. The supernatant was carefully removed using a pipette. The suspension was added again to the centrifuge tube and the procedure was repeated till the suspension was over. Weight of sediment was determined. Solubility was measured by pouring supernatant into evaporating dishes and evaporated at 110°C and weight of dry solids was determined.

$$\text{Starch solubility (\%)} = \frac{\text{weight of suspension (dry)}}{\text{weight of starch powder (g)}} \times 100$$

$$\text{Swelling power (wt/wt)} = \frac{\text{weight of swollen sediment}}{\text{weight of starch powder (g)}}$$

Swelling power and solubility of the arrowroot starch powder were determined at 50°C, 60°C, 70°C, 80°C and 90°C by using the similar above procedure.

I. X-Ray Powder Diffraction Studies on Arrowroot Starch

The structure of arrowroot starch was investigated by using Rigaku X-ray powder diffractometer (Rigaku, Tokyo, Japan) at Universities' Research Center, Yangon. The powder of arrowroot starch was scanned by using Cu Kαradiation (λ =1.54056 °A) at 40 kV and 40 m.

J. Preparation of only arrowrootstarch Film (1:1)

About 2.0 g of starch powder and 40 mL of distilled water were mixed in a 150 mL beaker and the mixture was stirred with magnetic stirrer at a rate of 500 rpm at 60°C for 50 minutes. 10 mL of paste solution was poured into each petridish and dried in air for three days.

K. Preparation of arrowrootstarch- chitosan Film (1:1)

About 1.0 g of starch powder and 1.0 g of chitosan were weight and put in a 150 mL beaker. Then, 40 mL of distilled water was added into a beaker. It was stirred with magnetic stirrer at a rate of 500 rpm at 60°C for 50 minutes. 10 mL of paste solution was poured into each petridish and dried in air for three days.

L. Preparation of arrowrootstarch- polyvinyl alcohol Film (1:1)

About 1.0 g of starch powder and 1.0 g of chitosan were weight and put in a 150 mL beaker. Then, 40 mL of distilled water was added into a beaker. It was stirred with magnetic stirrer at a rate of 500 rpm at 60°C for 50 minutes. 10 mL of paste solution was poured into each petridish and dried in air for three days.

M. Determination of Mechanical Properties of Prepared Blend Films

Mechanical properties such as thickness, tensile strength, elongation at break and tear strength were determined at Development Center for Rubber Technology, Yangon (8)

III. RESULTS AND DISCUSSION

TABLE I. PHYSICOCHEMICAL PROPERTIES OF ARROWROOT POWDER SAMPLE

No.	Arrowroot powder sample	
1.	pH	6.20 ± 0.10
2.	Ash	14.88 ± 0.02
3.	Moisture	9.50 ± 0.10
4.	Fat	1.10 ± 0.02

From these data, all arrowroot powder sample were found to be slightly acidic. The ash content of the sample was found to be 14.86 –14.90 %. The moisture content of the sample was found to be 9.4 – 9.5 %. The fat content of the sample was found to be 1.08 –1.12%.

A. Extraction of Starch from Arrowroot

The starch was extracted from arrowroot and the yield percent of arrowroot starch was found to be 52.63%.

B. Confirmation of Arrowroot Starch by Iodine Test

The extracted arrowroot starch sample was confirmed by iodine test.

Fig. 2 Iodine test for arrowroot starch sample

The extracted starch sample gave the deep blue color showing the positive test of iodine.

TABLE II. PHYSICOCHEMICAL PROPERTIES OF ARROWROOT STARCH

No.	Arrowroot starch powder sample	
1.	pH	7.40 ± 0.10
2.	Ash	18.30 ± 0.02
3.	Moisture	15.50 ± 0.10
4.	Bulk density (gcm^{-3})	0.57±0.02
5.	Water Absorption Capacity of Starch(g/mL)	1.80±0.04
6.	Intrinsic Viscosity of Starch(cP)	3.92±0.02

According to this table, arrowroot starch was found to be slightly alkaline. The ash content of the sample was found to be 18.28 –18.32 %. The moisture content of the sample was found to be 15.4 –15.6 %.

The bulk density of arrowroot starch samples was found to be in the range of 0.55 to 0.59gcm-3. The water absorption capacity of arrowroot starch samples was observed within the range of 1.76 to 1.84 respectively. Intrinsic viscosity of starch sample was found to be within the range of 3.90 to 3.94 respectively.

TABLE III. SOLUBILITY AND SWELLING POWER OF STARCH

No		Temperature				
		50ºC	60ºC	70ºC	80ºC	90ºC
1	Solubility in water (%)	5.3	5.5	10.2	10.5	12.5
2	Swelling power(g/g)	3.2	5.6	6.7	9.2	13.4

The solubility of arrowroot starch samples was found within the range of 5.3 to 12.5 at various changing temperature. According to the table, the solubility of starch sample was the most soluble at the temperature 90°C. The swelling power of arrowroot starch powder was increase with the increasing temperature.

C. X-Ray Powder Diffraction Studies on Arrowroot Starch

Semi-crystalline nature of arrowroot starch was observed in X-ray powder diffractogram (Figure 2) because of the presence of both sharp and diffuse diffraction peaks.

Arrowroot starch showed strong diffraction peaks at 17.4°, 23.2° and 28.3° of 2□. Parallel double amylopectin molecules result in the formation of crystalline regions, while amylose molecules result in the formation of amorphous regions in the starch structure.

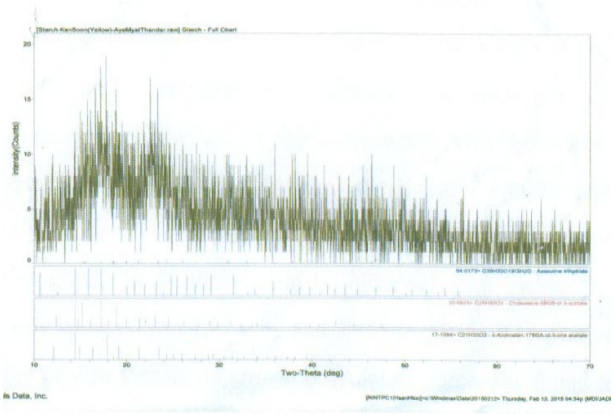

Fig 3. X-ray Diffractogram of Water Insoluble Arrowroot Starch

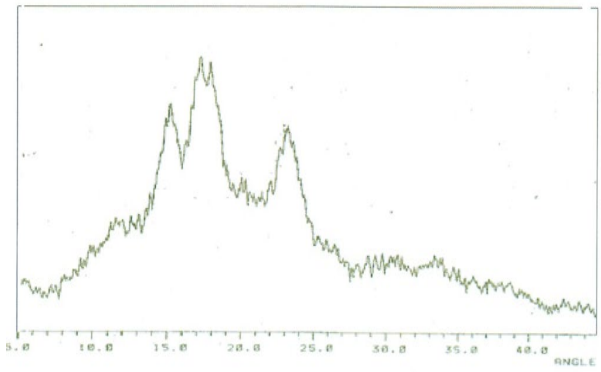

Fig 4. X-ray Diffractogram of Reference Starch

D. Preparation of Starch Blend Films

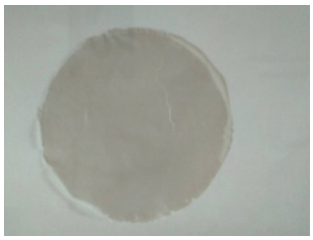

Fig 5. The prepared only arrowroot starch Films

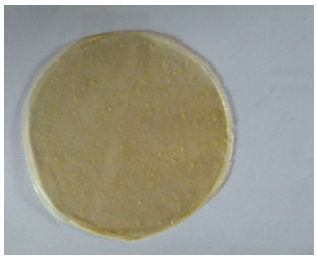

Fig. 6 The prepared arrowroot starch – chitosan Films

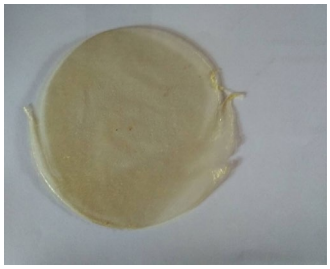

Fig. 7 The prepared arrowroot starch – PVA Films

E. Determination of the Mechanical Properties of Prepared Blend Films

The mechanical properties such as thickness, tensile strength, elongation at break and tear strength of the prepared films were determined and the results are presented in Table (IV).

TABLE IV. MECHANICAL PROPERTIES OF PREPARED BLEND FILMS

No	Mechanical Properties	starch	Starch-Chitosan	Starch-PVA
1	Thickness (mm)	0.10	0.12	0.12
2	Tensile strength (MPa)	20.00	25.20	2.40
3	Elongation at break (%)	6.90	72.00	82.00
4	Tear strength (KN/m)	43.50	186.70	20.00

According to these data, the thickness of only starch film was found to be thinnest and lowest elongation at break. The thickness of starch- chitosan and starch- PVA films were equal. Among the prepared films, the starch-chitosan film shows the medium tensile strength, highest tear strength and medium elongation at break. The starch-PVA film was highest elongation at break.

IV. CONCLUSION

Rhizomes of arrowroot (Marantaarund inacea L.) (adalut) were grinded for the study. The physical properties such as pH, moisture content, ash content and fat content of arrowroot powder samples were determined. pH of arrowroot powder samples was found to be slightly acidic. The moisture and ash content of the sample was found to be 9.40 – 9.50 % and 14.86 – 14.90 %. The fat content of the sample was found to be 1.08 –1.12%. The starch samples were extracted from arrowroot powder samples by using 0.05M sodium hydroxide solution for one hours at 600 rpm stirring. The characteristic properties of starch such as bulk density, water absorption capacity, and intrinsic viscosity, solubility and swelling power were determined. The bulk densities were found to be within the ranges of 0.55 to 0.59. And then the values of water

absorption capacity were found to be within the range of 1.76 to 1.84. Intrinsic viscosities were found to be within the ranges of 3.90 to 3.94 respectively. The higher the temperature, the more solubility of arrowroot starch was obtained. Increasing the temperature can also increase the swelling power of the starch. The arrowroot starch showed characteristic crystalline peaks at 17.4°, 23.2° and 28.3° of 2θ.

The different types of films (only arrowroot starch, arrowroot starch – chitosan and arrowroot starch - PVA) were prepared. The mechanical properties of prepared films (thickness, tensile strength, elongation at break and tear strength) were determined. Thickness of only starch was observed as 0.10 mm, tensile strength was found to be 20.00 MPa, elongation at break was observed as 6.9% and tear strength was 43.50 kN/m. Thickness of only starch-chitosan and starch- PVA films were observed as 0.11 mm and 0.11 mm, tensile strength were found to be 25.20 MPa and 2.40MPa, elongation at break was observed as 72.00% and 82.00%, tear strength were measured as 186.70 kN/m and 20.00 kN/m.

From the comparison of the mechanical properties of prepared films, the thickness of only arrowroot starch film was found to be thinnest. Moreover, the arrowroot starch-chitosan film gave the good tensile strength, good elongation at break and highest tear strength.

Among the prepared films, the starch- chitosan film showed the satisfactory mechanical properties. According to the above results, the prepared arrowroot starch- chitosan film can be used safely in food packaging from the point of view of mechanical properties.

ACKNOWLEDGEMENTS

The author would like to thank Journal of Research & Applications (JRA), UCSMTLA, 2020 for allowing to present this paper. I am extremely grateful to Professor and Head Dr Yi Yi Myint, Department of Chemistry, University of Mandalay and Professor and Head Dr Myat Myat Mon, Department of Engineering Chemistry, Mandalay Technological University for their kind permission, valuable helps, suggestions and good guidance in this research work.

REFERENCES

[1] P. Annie, "Arrowroot Helps Boost Immunity and Soothe Digestion", 2018.
[2] AOAC, "Official Methods of Analysis of Association of Official Analytical Chemists, 2000.
[3] ET. Champagne, "Rice starch composition and characteristics", Cereal Foods World 41:833–38, 1996.
[4] S. A. S. Craig, CG. Maningat, P. A. Serb, R. C. Hoseney, "Starch paste clarity. Cerral Chemistry ", 66, 173-182, 1989.
[5] FAOSTAT., Database of Food and Agricultural Organization, Rome, Italy. 2012.
[6] M. G. Gregory, I. William, Syed and C. Bor-Sen, "Starch Plastic Packaging and Agriculture Application". California, USA: USDA-ARS, Western Regional Research Center, pp: 421- 446, 2010.
[7] H-J. Chung, Q. Liu, Impact of Molecular Structure of amylopectin and amylose on amylose chain association during cooling, Carbohydrates, Polymers 77, 807-815, 2009.
[8] G.F. Mehyar, J. H. Han., "Physical and Mechanical Properties of High amylose Rice and Pea Starch Films as Affected by Relative Humidity and Plasticizer" Journal of Food Science. Vol.69 (9), pp. 449- 453, 2004.
[9] J. B. Pu-you, H. Cai- ying, Z. Lihongand and Young- hong, "Properties of Poly (vinyl alcohol) Plasticized by Glycerin" Journal of Forest Product and Industries. Vol. 3, pp: 151- 153, 2014.
[10] GE. Vandeputte, JA. Delcour, From sucrose to starch granule to physical behaviour: a focus on rice starch. Carbohydrate Polymer 58:245–66, 2004.

Article ID - JRA6000420

Spatial Distribution of Goldsmith Shops in Myitkyina

Aye Aye Moe
Department of Geography
University of Myitkyina
Myitkyina, Myanmar

Thida Aye
Department of Geography
Taunggoke Degree College
Taunggoke, Myanmar

Win Win Nyunt
Department of Geography
Mandalay University
Mandalay, Myanmar

***Abstract*— Myitkyina, the capital of Kachin State, falls in the Humid Subtropical Zone of northern part of Myanmar. It is constituted of 28 wards. It has an area of 40.47 square miles, spreading on the west bank of the Ayeyarwady. The average elevation of the whole study area is about 476' above sea level. With the development of technology, various economic activities have increased and subsequently population has also grown rapidly from 43, 630 persons in 1973 to 190,870 persons in 2019. In accordance with the increase of population and development of economy, trading affairs in all aspects including purchasing and selling of gold and golden ornaments have also improved and consequently goldsmith works have developed more than ever. In this research, spatial distribution of goldsmith works has been examined and analyzed by means of the Nearest Neighbour method, the Concentric Circle method, Graph and Regression analysis. The results show that (1) the spatial distribution of gold shops combined with goldsmith works is "cluster pattern", (2) 92.42 % of gold shops combined with goldsmith works is found in Myoma and Minyat Wards, are located in the Central Business District of Myitkyina Town and are of the core wards, (3) most of gold shops combined with goldsmith works are found concentrated in the southeastern part of Myitkyina Town, the wards of which have large population densities, good accessibility and good commercial centres, and (4) the linear regression equation of y=0.139x+0.487 indicates that the goldsmith work growth appears to have been increasing over the years in relation with the population and urban growth of Myitkyina.**

Keywords— goldsmith, ornament, shop, cluster, accessibility

I. INTRODUCTION

Goldsmith works of a region are directly related to social-economic factors which determine the distribution pattern of population. The increase of population helps the goldsmith works improve in technology and creates the wider market for sales of gold and golden ornaments. In 1973 there were 43,630 persons with 22, 038 males and 21, 592 females. According to 2019 data, the total population of Myitkyina was 190, 870 persons with 94,051 males and 96,819 females.

The main aim of this research is to study the nature of spatial distribution of goldsmith shops in Myitkyina. Objective of this study are (1) to identify of the actual distribution of the goldsmith shops, (2) to study the process of gold accessories, and (3) to describe goldsmith shops near market.

Primary data are collected by field observation, by interviewing whereas the secondary data are obtained from the respective governmental departments. Data on goldsmith shops and their spatial distribution are collected by field survey. The collected data are processed into the appropriate form or tables. Then, the processed data are analyzed by statistical method or graphical method, nearest neighbor method, and concentric circle method. Finally, the results are conducted into a generalization.

II. THE STUDY AREA

Myitkyina is located in Kachin State of northern part of Myanmar. It is the capital of Kachin State. It is situated between the North Latitudes 25° 20' 9" and 25° 27' 25"and between the East Longitudes of 97° 23' 49" and 97° 25' 34". (Figure 1)

Myitkyina is constituted of 28 wards. It has an area of 40.47 square miles (25,900acres), spreading on the west bank of the Ayeyarwady. It has nearly triangle shape. (Figure 2)

The Ayeyarwady bounds the town in the east and south. The huge curvature of the river limits the southern expansion of the town areas.

Myitkyina is situated in the west bank of the Ayeyarwady River. The average elevation of the whole study area is about 476' above sea level. The study area is flat land topography and predominates in almost all urban area. The lowest area of this study area is situated along the Ayeyarwady River.

Major drainage of Myitkyina is the Ayeyarwady River which flow from the eastern and southern part. The Ayeyarwady River originates from the confluence of the Mai Hka and Mali Hka, at about 28 miles 4 furlongs north of Myitkyina.

According to the temperature records for 30 years from 1990 to 2019, the average annual maximum, mean and minimum temperatures of the study area were 89.46° F, 76.8° F and 64.24° F, respectively. January was the coldest month with the average maximum temperature of 80.27°F and the average minimum temperature of

48.72°F. The average mean temperature was found to be 64.39° F. April was the hottest month of the year with the average maximum temperature of 95.34°F and the average minimum temperature of 65.2°F and the average mean temperature of 80.7° F.

The annual range of temperature was therefore, 30.14°F. On studying the 30- year temperature records from 1990 to 2019 of Myitkyina, its highest maximum temperature was found in 2014 with 104° F. The highest mean temperature was found in 1997 with 93.06°F and the least minimum temperature was found in 1990 with 44.6°F.

During 30- year period from 1990 to 2019, the average annual rainfall of Myitkyina was 94.36 inches. Among these 30 years, the highest monthly rainfall occurred in the July with 22.27 inches and the least monthly rainfall in the month of December with 0.36 inch.

According to Koppen's classification, the 30- year data from 1990 to 2019 show that Myitkyina has a Cwa type of climate or Humid Subtropical.

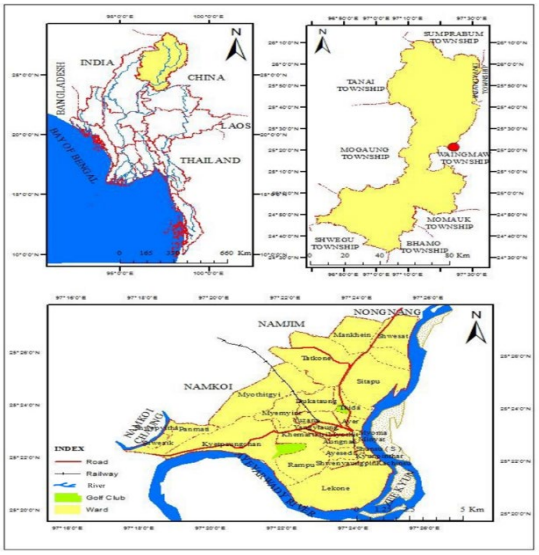

Fig. 1. Location map of Myitkyina

Fig. 2. Wards of Myitkyina

Placer gold has been reported found in many localities of Myitkyina District, mostly in river and stream valleys. Namma-Kangon area in the southern part of the district is another potential mining area for gold.

According to 2019 data, total population of Myitkyina is 190,870 persons and the largest population is found in Rampu Ward with 18,846 people and the smallest population is found in Shweait Ward with 1,209 people. Tatkone is the largest ward with 4.42 square miles of area whereas Minyat Ward is the smallest ward with 0.07 square miles.

III. Spatial Distribution of Goldsmth Shops

In Myanmar-sar-lon-baung Thatpon-kyan , "Pantein" is defined as "badein" where ornament sets are made with jewellery or gold and silver. The "badein" appeared, relying on gold. People all over the world like and admire gold. It is due to having distinct characteristics and ever-

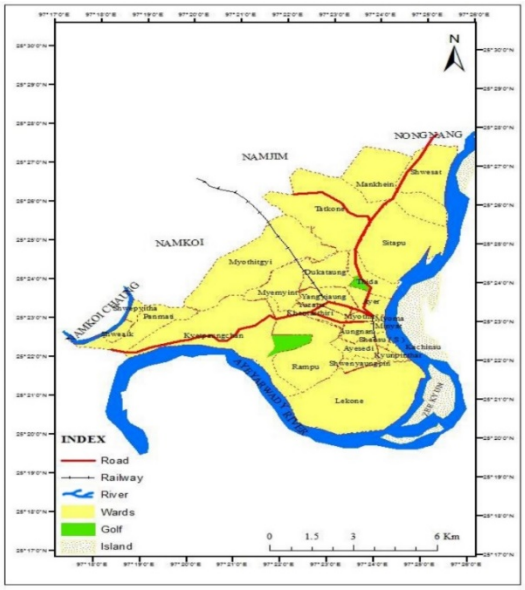

bright and yellow colour which never changes in colour although it is made mixed with other metal. It never loses its specific weight though it is melt a lot of times. Therefore, everybody admires gold and wears gold as ornaments and thus the goldsmith work has also expanded more than ever.

Goldsmith means a person who forges things out of gold, especially jewellery and a person who makes gold articles (Oxford Dictionary of English, 1948).

In 2019, Myitkyina has a total of 66 goldsmith works combined golden ornaments (Table 1). Located wards, established year, number of labourers, and places from which raw material of gold being used is purchased. According to the field observation, it is known that all of the goldsmiths mostly create and produce necklaces, ear-rings and rings.

A. Analysis on the spatial distribution by graph and linear gression

Based on field survey data, the growth of the goldsmith shops in Myitkyina are analyzed by graph (Figure 3). According to the found that, it is found that the goldsmith works of the town had grown regularly before 2007 but rapidly since that year, particularly very significantly and rapidly during the 2007-2019 years. According to the Linear Regression, the goldsmith shops of Myitkina is known to have been increasing according to the equation of $y = 0.139x + 0.487$. This goldsmith work growth appears to be related with the population and urban growth of Myitkyina. The graph indicates that goldsmith works in Myitkyina accounted for 23 works in 2006 and had increased by 38 works between 2007 and 2018. After 2017, it appears to increase regularly.

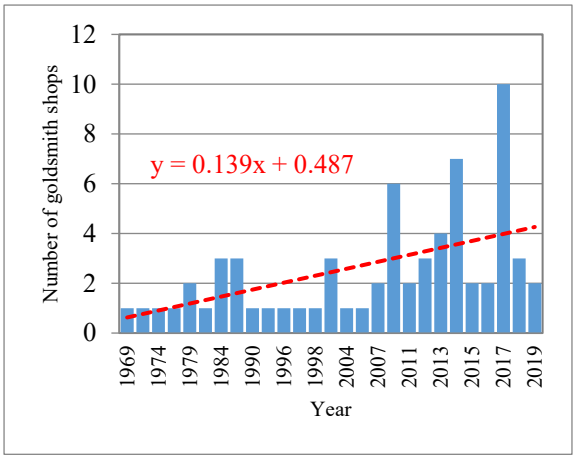

Fig. 3. The growth of goldsmith shops in Myitkyina (1969-2019)

TABLE I. SPATIAL DISTRIBUTION OF GOLDSMITH SHOPS IN MYITKYINA (2019)

No.	Name of Goldsmith & Shops	Established Year	Wards
1	Daw Mya Yin	2014	Bazaar No.1,Minyat
2	Thitsarmon	2004	Bazaar No.1,Minyat
3	Thamardi	1984	Bazaar No.1,Minyat
4	Winwarhtun	1979	Bazaar No.1,Minyat
5	Sanyadanar	2009	Bazaar No.1,Minyat
6	Naymarlar	1984	Bazaar No.1,Minyat
7	Shweyadanar	1994	Bazaar No.1,Minyat
8	Htunyadanar	1969	Bazaar No.1,Minyat
9	San	2014	Bazaar No.1,Minyat
10	Shweyiwin	1996	Bazaar No.1,Minyat
11	Myittar	1989	Bazaar No.1,Minyat
12	Daw Mya Yin	1971	Bazaar No.1,Minyat
13	Daw Li Li Myint	1982	Bazaar No.1,Minyat
14	Myayadanar	1979	Bazaar No.1,Minyat
15	Shwekabar	2006	Bazaar No.1,Minyat
16	Yanaungmyin	2013	Bazaar No.1,Minyat
17	Khinemyewai	2014	Bazaar No.1,Minyat
18	Kyiyadanar	1984	Minyat
19	Tikepyar	1974	Minyat
20	Theingi	2012	Minyat
21	Golden Star	2016	Minyat
22	Seinyadanr	2015	Minyat
23	Panthazin	2013	Minyat
24	Zabuyitshwesin	2007	Bazaar No. 2, Myoma
25	Seinsoso	2012	Bazaar No. 2, Myoma
26	Hteiktan	2017	Bazaar No. 2, Myoma
27	Linyadanar	1989	Bazaar No. 2, Myoma
28	Thandaraung	2009	Bazaar No. 2, Myoma
29	Aungtharaphu	2017	Bazaar No. 2, Myoma
30	Thahtaylaung	2012	Bazaar No. 2, Myoma
31	Yadanarmaung	2015	Bazaar No. 2, Myoma
32	Shwebeikman	2009	Bazaar No. 2, Myoma
33	ShwesinOo	2017	Bazaar No. 2, Myoma
34	Shwesinhtun	2014	Bazaar No. 2, Myoma
35	Nawarat	1997	Bazaar No. 2, Myoma
36	Winshwesin	2014	Bazaar No. 2, Myoma
37	Shwesanli	2004	Bazaar No. 2, Myoma
38	Khusutpan	1999	Bazaar No. 2, Myoma
39	Kanpwint	2014	Bazaar No. 2, Myoma
40	Tawwin	1999	Bazaar No. 2, Myoma
41	Shweyiwin	2013	Bazaar No. 2, Myoma
42	Meik	2013	Bazaar No. 2, Myoma
43	Khinemyintsi	2009	Bazaar No. 2, Myoma
44	Moe & Nyein	2017	Bazaar No. 2, Myoma
45	Shwengonmin	2017	Bazaar No. 2, Myoma
46	Zabuyit	1998	Bazaar No. 2, Myoma
47	Shwemyodaw	1990	Bazaar No. 2, Myoma
48	Yadanarphyo	1977	Bazaar No. 2, Myoma
49	Naymarlar	2017	Bazaar No. 2, Myoma
50	Hteiktan	2019	Bazaar No. 2, Myoma
51	Daw Mya Yin	2017	Bazaar No. 2, Myoma
52	Shwemyanmar	2018	Bazaar No. 2, Myoma
53	Cheinhman	2018	Myoma
54	Shweyunein	2017	Myoma
55	Phurant	2011	Myoma
56	Kyawmyanmar	2011	Myoma
57	OVI	2017	Myoma
58	Moe & Nyein	2019	Myoma
59	Shwezabu	2007	Myoma
60	Yahteik	2009	Aungnan
61	Shwesin	2009	Aungnan
62	Hteiktan	2016	Aungnan
63	Yuzana	2017	Yuzana
64	Thamardi	1989	Khaymarthiri
65	Daw Mya Yin	1999	Shansu North
66	Shweminthamee	2018	Tatkone

B. Analysis on the spatial distribution by Nearest Neighbour Method

In this part, spatial distribution of goldsmith works and shops in Myitkyina Town is analyzed by using *Nearest Neighbour Analysis Method* of Clark and Ivans (1954) after examined by using Google Satellite Images.

This analysis distinguishes objectively between clustered and dispersed spatial distributions and that also distinguishes between degree and intensity of clustering or random or dispersal.

This method quantitatively defiles a scale related to three absolute benchmarks. The scale measures the degree of departure of an observed spatial distribution from a theoretical random distribution. The maximum departure at one end of the scale is absolute clustering and at the one end of the scale is absolute dispersal. The nearest neighbor scale can be calculated as follows: where

$$R = \frac{\bar{r}A}{\bar{r}E}$$

$$\bar{r}A = \frac{\Sigma r}{N}$$

or the mean of the series of distances to nearest neighbors, r being the distance from each point to its nearest neighbor (A meaning "actual") and

$$\bar{r}E = \frac{1}{2\sqrt{P}}$$

or the expected mean distance to a nearest neighbor in an infinitely large random distribution of density P (E meaning expected): P being defined as

$$P = \frac{\text{Number of points (N)}}{\text{total area}}$$

The individual R scores can therefore take on any value between *Zero*, signifying absolute clustering, to 2.1491, signifying maximum dispersion, with unity indicating the presence of a random observed distribution. This means that there is *Zero* (clustering) at the one end and 2.1491 (dispersion) at another end while the central numbers (unity or random) are in the middle.

Following the above-mentioned formulae, distribution pattern of goldsmith works in Myitkyina Town is

calculated. Before calculation, the three formulae are transformed into one as shown below:

$$R = \frac{\Sigma r \times 2\sqrt{P}}{N} \quad \textbf{or} \quad R = \frac{\Sigma r}{N} \times 2\sqrt{P}$$

$$R = \frac{\Sigma\, distance \times 2\sqrt{\Sigma\, of\ points/\Sigma\, Area}}{\text{Number of points (N)}} \quad \textbf{or} \quad R = 2\,\bar{d}\,\sqrt{\frac{N}{A}}$$

According to this formula, at first distribution of goldsmith works combined with shops in Myitkyina town is needed to know. In order to know the exact locations of them are observed and recorded in field survey by using GPS. Then, based on the locations are plotted on the 2019 Google earth image of Myitkyina Town. Afterwards, nearest neighbours of each goldsmith work combined with shop are identified and respective distances are measured on the image by using measuring tool. The out-coming results are described in Table (2).

According to the table, it is found that Σ distance is 27, 924 feet (5.2886 miles), number of points is 66, Σ area of the town is 40.47 square miles. Substituting these figures in the formula, the score for the nearest neighbor of the goldsmith works combined with shops is calculated as follow:

$$R = \frac{\Sigma\, distance \times 2\sqrt{\Sigma\, of\ points/\Sigma\, Area}}{\text{Number of points (N)}}$$

$$R = \frac{5.2886 \times 2\sqrt{66/40.47}}{66}$$

$$R = \frac{5.2886 \times 2 \times 1.2770}{66}$$

$$R = 0.204$$

According to the calculated result, as the score *R* value (0.204) is close to *Zero,* the distribution pattern of goldsmith works combined with shops in the town can be assumed to be "clustering".

TABLE II. NEAREST NEIGHBOURS OF GOLDSMITH SHOPS IN MYITKYINA (2019)

No.	Name of Goldsmith & Shops	Location (North Latitute and East Longitude)		Nearest distance (feet)	Nearest Goldsmith Shop No.
1	Daw Mya Yin	25° 22' 58"	97°˙24 ' 5"	0	7
2	Thitsarmon	25° 22' 56"	97°24' 5"	0	4
3	Thamardi	25° 22' 57"	97°24' 5"	0	7
4	Winwarhtun	25°22 ' 56"	97°24' 5"	0	2
5	Sanyadanar	25° 22' 56"	97° 24' 4"	0	8
6	Naymarlar	25° 22' 58"	97°24 ' 5"	0	7
7	Shweyadanar	25° 22' 57"	97° 24' 5"	0	3
8	Htunyadanar	25° 22' 56"	97° 24' 4"	0	5
9	San	25° 22' 56"	97° 24' 7"	183	11
10	Shweyiwin	25° 22' 57"	97° 24' 1"	270	28
11	Myittar	25° 22' 56"	97° 24' 5"	0	4
12	Daw Mya Yin	25° 22' 58"	97° 24' 4"	0	13
13	Daw Li Li Myint	25° 22' 58"	97° 24' 4"	0	12
14	Myayadanar	25° 22' 56"	97° 24' 5"	0	15
15	Shwekabar	25° 22' 56"	97° 24' 5"	0	14
16	Yanaungmyin	25° 22' 56"	97° 24' 5"	0	15
17	Khinemyewai	25° 22' 54"	97° 24' 5"	183	30
18	Kyiyadanar	25° 22' 54"	97° 23' 60"	0	23
19	Tikepyar	25° 22' 55"	97° 24' 0"	0	21
20	Theingi	25° 22' 57"	97° 23' 57"	88	54
21	Golden Star	25° 22' 55"	97° 23' 60"	0	19
22	Seinyadanr	25° 22. 55"	97° 24' 8"	323	40
23	Panthakhin	25° 22' 54"	97° 24' 6"	0	18
24	Zabuyitshwesin	25° 23' 4"	97° 24' 6"	110	50
25	Seinsoso	25° 23' 3"	97° 24' 6"	0	31
26	Hteiktan	25° 23' 4"	97° 24' 5"	91	33
27	Linyadanar	25° 23' 3"	97° 24' 4 E	0	35
28	Thandaraung	25° 22' 59"	97° 23' 59"	270	10
29	Aungtharaphu	25° 23' 1"	97° 24' 4"	216	34
30	Thahtaylaung	25° 22' 54"	97° 24' 3"	366	40
31	Yadanarmaung	25° 23' 3"	97° 24' 6"	0	24
32	Shwebeikman	25° 23' 2"	97° 24' 6"	92	31

33	ShwesinOo	25° 23' 4"	97° 24' 4"	91	26
34	Shwesinhtun	25° 23' 1"	97° 24' 6"	210	41
35	Nawarat	25° 23' 3"	97° 24' 4"	0	27
36	Winshwesin	25° 23' 0"	97° 24' 49"	618	58
37	Shwesanli	25° 23' 3"	97° 24' 5"	0	38
38	Khusutpan	25° 23' 3"	97° 24' 5"	0	37
39	Kanpwint	25° 23' 3"	97° 24' 4"	0	27
40	Tawwin	25° 22' 57"	97° 24' 5"	101	48
41	Shweyiwin	25° 22' 59"	97° 24' 5"	0	42
42	Meik	25° 22' 59"	97° 24' 5"	0	41
43	Khinemyintsi	25° 23' 3"	97° 24' 4"	91	46
44	Moe & Nyein	25° 22' 58"	97° 24' 4"	109	44
45	Shwengonmin	25° 23' 4"	97° 24' 4"	90	46
46	Zabuyit	25° 23' 4"	97° 24' 5"	0	50
47	Shwemyodaw	25° 23' 3"	97° 24' 4"	0	39
48	Yadanarphyo	25° 22' 59"	97° 24' 4"	85	49
49	Naymarlar	25° 22' 58"	97° 24' 5"	85	48
50	Hteiktan	25° 23' 4"	97° 24' 5"	0	46
51	Daw Mya Yin	25° 23' 3"	97° 24' 4"	0	47
52	Shwemyanmar	25° 23' 2"	97° 24' 6"	1613	50
53	Cheinhman	25° 23' 2"	97° 24' 59"	277	55
54	Shweyunein	25° 22' 57"	97° 23' 56"	85	20
55	Phurant	25° 23' 3"	97° 24' 1"	88	57
56	Kyawmyanmar	25° 23' 1"	97° 23' 59"	0	58
57	OVI	25° 23' 3"	97° 24' 2"	88	57
58	Moe & Nyein	25° 23' 1"	97° 23' 56"	0	56
59	Shwezabu	25° 23' 3"	97° 24' 1"	90	57
60	Yahteik	25° 22' 56"	97° 23' 57"	89	20
61	Shwesin	25° 22' 55"	97° 23' 56"	139	60
62	Hteiktan	25° 22' 49"	97° 23' 43"	1163	64
63	Yuzana	25° 23' 17"	97° 23' 23"	3451	64
64	Thamardi	25° 22' 43"	97° 23' 32"	3119	65
65	Daw Mya Yin	25° 22' 45"	97° 24' 6"	3119	64
66	Shweminthame e	25° 25' 4"	97° 23' 35"	10931	63
		Total Distance (in feet)		27924	

C. Analysis by Concentric Circle Method

In this analysis, centre of Myitkyina Town is marked at the intersection point of 25˚23'17" North Latitude and 97˚23'23" East Longitude, according to the map shape of the town. Centering that point, concentric circles are drawn in 1 kilometre (0.8 mile) interval. According to the map with concentric circles, 1 goldsmith with gold shop is found within 1 kilometre from the centre of the town, 2 goldsmith works attached with shops within the distance between 1 kilometre and 2 kilometres, and the remaining 63 goldsmith works attached with shops within the distance between 2 kilometres and 3 kilometres from the centre of the town (Figure 4).

According to the directions, majority (92.42 %) of goldsmith works attached with shops are closely distributed in the southeastern part of the town, particularly 87.77% in the east-southeastern portion and 4.55% in the south-southeastern portion, and 1.52% in the north-northeastern part. Especially most of goldsmith works combined with shops are located within the core wards of Myoma and Minyat, especially in 43.94% in Myoma Bazaar No.2, 25.76% in Minyat Bazaar No. 1, 10.61% in Myoma Ward, 9.09% in Minyat ward, and 3.03% in Aungnan ward. Myoma and Minyat wards are the Central Business District of Myitkyina Town. This is why majority of goldsmith works combined with gold shops are found within these wards.

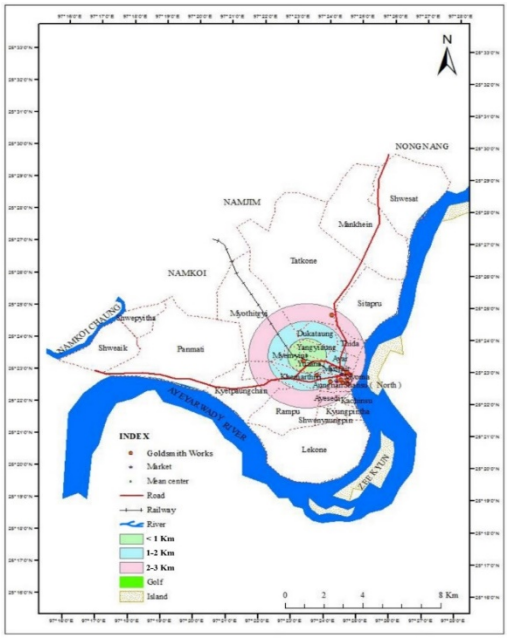

Fig. 1. Distribution of goldsmith works combined with gold shops in Myitkyina

IV. RESULTS AND FINDINGS

This research provides the following results and findings.

(1) There are a total of 66 gold shops combined with goldsmith works in Myitkyina Town which has a total population of 190,870 persons in 2019.

(2) The *Nearest Neighbour Analysis* shows that the score of 0.204 indicates the spatial distribution of gold shops combined with goldsmith works is "cluster pattern".

(3) The concentric circle method reveals that 1 gold shop combined with goldsmith work within 1 kilometre from the centre of the town, 2 within the distance between 1 kilometre and 2 kilometres, and the remaining 63 within the distance between 2 kilometres and 3 kilometres from the centre of the town.

(4) According to the directions, (92.42 %) of gold shops combined with goldsmith works is found in Myoma and Minyat Wards, especially in 54.53% in Myoma Ward, 34.84% in Minyat ward. And then 3.03% is found in Aungnan ward, 1.51% each in Yuzana, Khaymarthiri, Shansu North, and Tatkone Wards. Why majority of goldsmith works combined with gold shops are found within Myoma and Minyat wards is that they are located in the Central Business District of Myitkyina Town and are of the core wards.

(5) Moreover, most of gold shops combined with goldsmith works are found concentrated in the southeastern part of Myitkyina Town, the wards of which have large population densities, good accessibility and good commercial centres.

(6) Finally, the linear regression equation of $y = 0.139x + 0.487$ indicates that the goldsmith work growth appears to have been increasing over the years in relation with the population and urban growth of Myitkyina.

V. CONCLUSIONS

According to the results, it is known that the goldsmith works in Myitkyina has been increasing with a rapid increase rate of 4.2 works per year during the 2007-2017 years but with a regular increase rate of 2.5 after 2017. If compared to the population of the town (190,870 persons in 2019), it is found that there is a goldsmith work in every 2861 persons in Myitkyina Town. If compared to the number of wards, it is found that there are 2.36 goldsmith works per ward. However, actually, out of 28 wards, there are 10 wards which have goldsmith works and the remaining 18 wards have no goldsmith work. Most of the works are found mostly in Minyat Bazaar No.1 and Myoma Bazaar No. 2 wards which lie in the CBD area of the town, and a few in the six wards adjacent to Myoma and Minyat. This indicates that goldsmith works are found in the wards which are busy with customers and have good transportation and tranquility. If population of the town increases at the present increase rate of 3.99 %, the goldsmith works will grow at least 2 works per year. Unless it is so, the present goldsmith works combined with shops will become grown and developed in near future. However, as most of the customers usually buy small things of golden ear-rings, rings and necklaces, the works should have created the ornaments with new modern styles and designs. If it is so, the works will certainly be developed more than ever.

ACKNOWLEDGMENT

We are greatly indebted to Dr Ja Kham, Professor and Head of Department of Geography and Dr Seng Aung, Professor, Department of Geography, Myitkyina University for their exhortation and helpful comments on this research. Special thanks to faculty of University for giving permission and cooperation to prepare this research.

REFERENCES

[1] P. J. Clark and F. C. Evans, "Distance to Nearest Neighbor as a Measure of Spatial Relationships in Populations," *Ecology*, vol. 35, no. 4, pp. 445–453, 1954, doi: 10.2307/1931034.

[2] K. R. Cox, "Analogy and Human Geography," *Unfashionable Geographies*, Feb. 23, 2020.

[3] P. A. Rogerson, *Statistical Methods for Geography: A Student's Guide*, Fifth Edition. LA: SAGE Publications Ltd, 2019.

[4] G. C. Cameron and E. M. Hoover, "An Introduction to Regional Economics.," *The Economic Journal*, vol. 82, no. 328, p. 1447, Dec. 1972, doi: 10.2307/2231342.

[5] D. Wheeler, G. Shaw, and S. Barr, *Statistical Techniques in Geographical Analysis*. London: Routledge, 2004.

[6] Z. Htet, "A Geographical Study on Transportation Network of Myitkyina District," PhD Dissertation, Department of Geography, University of Mandalay, 2011.

Article ID – JRA6001220

Finding Minimal Weight by Using Prim's Algorithm in Flipped Classroom

Khin Hla Thi
Mathematics Department
Meiktila University
khinhlathi19@gmail.com

Abstract – In this paper, firstly basic terminology is illustrated. Then Prim's Algorithm is presented and considered with example. Finally, finding minimal weight between the fourteen cities in the network and muddy city problem are studied.

Keywords- graph, subgraph, simple path, weighted graph, spanning tree, minimal spanning tree.

I. INTRODUCTION

In general, a graph will have several spanning trees, since it must contain all the vertices, it must be connected, and it must have a unique simple path between each pair of vertices. Thus, a needed spanning tree is the sum of whose minimal weights. Such a tree is called minimal spanning tree [1]. There are many ways of finding a minimal spanning tree in a connected weighted graph. The minimal weight provides many effective in the real world likes:

To find the shortest path that visits each point at least once (solve the travelling sale person problem).

To solve Telephone, electrical, hydraulic, TV cable, computer, road, water supply, network problems.

For example, at the business with several offices, we want to lease phone lines to connect them up with each other and connect all the business offices with a minimum total cost. It should be a spanning tree, since if a network isn't a tree we can always remove some edges and save money. There are many minimal spanning tree algorithms such as Prim's algorithm, Kruskal's algorithm and Boruvka's algorithm. Among them Prim's algorithm is presented in this paper.

II. BASIC TERMINOLOGY

A graph G is defined to be a pair (V(G), E(G)), where V(G) is a non-empty finite set of elements called vertices (or points or notes) and E(G) is a finite family of unordered pair of elements of V(G) called edges (or lines) [2]. Two vertices x, y of G are adjacent, if they are joined by an edge of G. An edge is incident to its endpoints. A simple graph in which each pair of distinct vertices is joined by an edge is called a complete graph [1]. A spanning subgraph of G is a subgraph H with V(H) = V(G). A walk in G is a finite non-null sequence W = v0e1v1e2v2,⋯, ekvk, whose terms are alternately vertices and edges, such that, for 1 ≤ i ≤ k, the ends of ei are vi-1 and vi . The integer k is the length of W. If the vertices in W are all distinct, then W is called a path. A k-path is a path of length k. The n-cycle for n ≥ 3, denoted by Cn, is the graph with n vertices, v1, v2, ⋯, vn and edge set E = {v1v2, v2v3, ⋯, vn-1vn, vnv1}. Cn has n vertices and n edges. A cycle is odd (even) cycle if its length is odd (even). A k-cycle is a cycle of length k. An acyclic graph is one that contains no cycles. A tree is a connected acyclic graph. A spanning tree of G is a spanning subgraph of G that is a tree.

III. PRIM'S ALGORITHM

We will apply Prim's Algorithm to the graph of Figure 1 with vertex ordering a, b, c, d, e, f to obtain a minimal spanning tree.

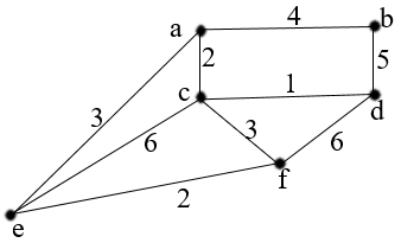

Fig.1. A Graph G

At line 1, we select the vertex a. At this point, T consists of the vertex a and no edges. Since T does not have five edges, we proceed to line 3. We select the edge (a, c) incident on a that has minimum weight and add it to T. Again, T does not have five edges, so we move to line 3.

Among the edges {(a, b), (a, e), (c, d), (c, e), (c, f)} not in T that are incident on a vertex in T and do not complete a cycle if added to T, we select (c, d), which has minimum weight, and add it to T. At this point T consists of the edges (a, c) and (c, d). Since T does not have five edges, we proceed to line 3.

Among the edges{(a, b), (a, e), (c, e), (c, f),(d, b), (d, f)} not in T that are incident on a vertex in T and do not complete a cycle if added to T, both (a, e) and (c, f) have minimum weight 3. In this case we select (a, e), since a

precedes c in the vertex ordering given. At this point T consists of the edges (a, c), (c, d) and (a, e). Since T does not have five edges, we proceed to line 3.

Among the edges {(a, b), (c, f), (d, b), (d, f), (e, f)} not in T that are incident on a vertex in T and do not complete a cycle if added to T, we select (e, f), which has minimum weight, and add it to T. At this point T consists of the edges (a, c), (c, d), (a, e) and (e, f). Since T does not have five edges, we proceed to line 3. [2]

Among the edges {(a, b), (d, b)} not in T that are incident on a vertex in T and do not complete a cycle if added to T, we select (a, b), which has minimum weight, and add it to T. At this point T consists of the edges (a, c), (c, d), (a, e), (e, f) and (a, b). Since T has five edges, the algorithm terminates. The minimal spanning T is shown in Figure 2.

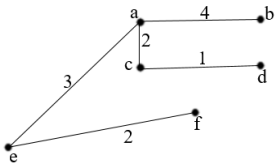

Fig.2. The minimal spanning tree of G

Its minimal spanning tree is (a, c), (c, d), (a, e), (e, f), (a, b). Its lowest total cost is 2 + 1 + 3 + 2 + 4 = 12.

IV. FINDING MINIMAL WEIGHT BETWEEN GIVEN FOURTEEN CITIES

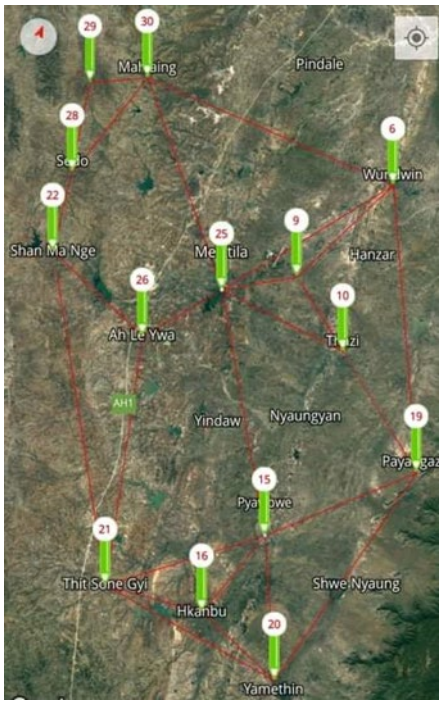

Fig.3. The given fourteen cities in the Network

Now we will construct the graph model the above given fourteen cities in the network to find the minimal weight between them as the following:

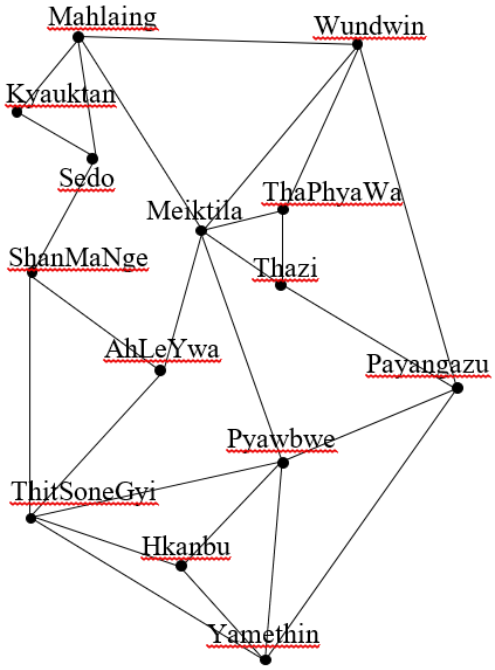

Fig.4 Graph model of the road system

The weighted graph G of Figure 4 shows fourteen cities and the costs of building roads between certain pairs of cities. We want to build the lowest-cost road system that will connect the fourteen cities. The solution can be represented by a subgraph.

TABLE 1 THE DISTANCES (MILES) BETWEEN GIVEN FOURTEEN CITIES IN THE NETWORK

(Mahlaing-Wundwin)	24.01 miles
(Mahlaing-Meiktila)	19.99 miles
(Mahlaing-Sedo)	10.7 miles
(Mahlaing-Kyauktan)	5 miles
(Kyauktan-Sedo)	8 miles
(Sedo-ShanMaNge)	9.55 miles
(ShanMaNge-AhLeYwa)	9.26 miles
(ShanMaNge-ThitSoneGyi)	27.69 miles
(Meiktila-AhLaYwa)	8.75 miles
(AhLeYwa-ThitSoneGyi)	21.57 miles
(Meiktila-Wundwin)	17.65 miles
(Meiktila-ThaPhayWa)	9.14 miles
(Meiktila-Thazi)	11.41 miles
(Meiktila-Pyawbwe)	23.29 miles
(ThaPhayWa-Wundwin)	9.54 miles
(ThaPhayWa-Thazi)	8.79 miles
(Thazi-Payangazu)	13.89 miles
(Payangazu-Wundwin)	24.22 miles

(Payangazu-Pyawbwe)	14.82 miles
(Payangazu-Yamethin)	47.6 miles
(Pyawbwe-Hkanbu)	9.24 miles
(Pyawbwe-ThitSoneGyi)	16.23 miles
(ThitSone-Hkanbu)	11.53 miles
(ThitSoneGyi-Yamethin)	65.05 miles
(Hkanbu-Yamethin)	7.84 miles
(Pyawbwe-Yamethin)	11.44 miles

We will apply Prim's Algorithm to the graph of Figure 4 with vertex ordering given fourteen cities to obtain a minimal spanning tree or minimal weight.
Ml = Mahlaing, Kt = Kyauktan, Sd = Sedo,
Smn= ShanMaNge, Aly = AhLaYwa,
Tsg = ThitSoneGyi, Wdn = Wundwin, Mtla = Meiktila,
Tpwa = ThaPhayWa, Tzi = Thazi, Pyzu = Payangazu,
Pbw = Pyawbwe, Hkbu = Hkanbu, Ymt = Yamethin.

At line 1, we select the vertex Ml. At this point, T consists of the vertex Ml and no edges. Since T does not have thirteen edges, we proceed to line 3. We select the edge (Ml, Kt) incident on Ml that has minimum weight and add it to T. Again, T does not have thirteen edges, so we move to line 3.

Among the edges {(Ml, Wdn), (Ml, Sd), (Ml, Mtla), (Kt, Sd)} not in T that are incident on a vertex in T and do not complete a cycle if added to T, we select the edge (Kt, Sd) which has minimum weight and add it to T. At this point T consists of the edges (Ml, Kt) and (Kt, Sd). Since T does not have thirteen edges, we proceed to line 3.

Among the edges {(Ml, Wdn), (Ml, Sd), (Ml, Mtla), (Sd, Smn)} not in T that are incident on a vertex in T and do not complete a cycle if added to T, we select (Sd, Smn) and add it to T. At this point T consists of the edges (Ml, Kt), (Kt, Sd) and (Sd, Smn). Since T does not have thirteen edges, we proceed to line 3.

Among the edges {(Ml, Wdn), (Ml, Sd), (Ml, Mtla), (Smn, Aly), (Smn, Tsg)} not in T that are incident on a vertex in T and do not complete a cycle if added to T, we select (Smn, Aly), and add it to T. At this point T consists of the edges (Ml, Kt), (Kt, Sd), (Sd, Smn) and (Smn, Aly). Since T does not have thirteen edges, we proceed to line 3.

Among the edges{(Ml, Wdn), (Ml, Sd), (Ml, Mtla), (Aly, Mtla), (Aly, Tsg)} not in T that are incident on a vertex in T and do not complete a cycle if added to T, we select (Aly, Mtla), which has minimum weight, and add it to T. At this point T consists of the edges (Ml, Kt), (Kt, Sd), (Sd, Smn), (Smn, Aly) and (Aly, Mtla). Since T does not have thirteen edges, we proceed to line 3.

Among the edges{(Ml, Wdn), (Ml, Sd), (Ml, Mtla), (Aly, Tsg), (Mtla, Wdn), (Mtla, Tpwa), (Mtla, Pbw), (Mtla, Tzi)} not in T that are incident on a vertex in T and do not complete a cycle if added to T, we select (Mtla, Tpwa), which has minimum weight, and add it to T. At this point T consists of the edges (Ml, Kt), (Kt, Sd), (Sd, Smn), (Smn, Aly), (Aly, Mtla) and (Mtla, Tpwa). Since T does not have thirteen edges, we proceed to line 3.

Among the edges {(Ml, Wdn), (Ml, Sd), (Ml, Mtla), (Aly, Tsg), (Smn, Tsg), (Mtla, Wdn), (Wdn, Tpwa), (Mtla, Pbw), (Mtla, Tzi)} not in T that are incident on a vertex in T and do not complete a cycle if added to T, we select (Wdn, Tpwa), which has minimum weight, and add it to T. At this point T consists of the edges (Ml, Kt), (Kt, Sd), (Sd, Smn), (Smn, Aly), (Aly, Mtla), (Mtla, Tpwa) and (Tpwa, Wdn). Since T does not have thirteen edges, we proceed to line 3.

Among the edges{(Ml, Wdn), (Ml, Sd), (Ml, Mtla), (Aly, Tsg), (Smn, Tsg), (Mtla, Wdn), (Mtla, Pbw), (Mtla, Tzi) and (Tpwa, Tzi)} not in T that are incident on a vertex in T and do not complete a cycle if added to T, we select (Tpwa, Tzi), which has minimum weight, and add it to T. At this point T consists of the edges (Ml, Kt), (Kt, Sd), (Sd, Smn), (Smn, Aly), (Aly, Mtla), (Mtla, Tpwa), (Tpwa, Wdn) and (Tpwa, Tzi). Since T does not have thirteen edges, we proceed to line 3.

Among the edges{(Ml, Wdn), (Ml, Sd), (Ml, Mtla), (Aly, Tsg), (Smn, Tsg), (Mtla, Wdn), (Mtla, Pbw), (Mtla, Tzi), (Wdn, Pyzu), (Tzi, Pyzu)} not in T that are incident on a vertex in T and do not complete a cycle if added to T, we select (Tzi, Pyzu), which has minimum weight, and add it to T. At this point T consists of the edges (Ml, Kt), (Kt, Sd), (Sd, Smn), (Smn, Aly), (Aly, Mtla), (Mtla, Tpwa), (Tpwa, Wdn), (Tpwa, Tzi) and (Tzi, Pyzu). Since T does not have thirteen edges, we proceed to line 3.

Among the edges{(Ml, Wdn), (Ml, Sd), (Ml, Mtla), (Aly, Tsg), (Smn, Tsg), (Mtla, Wdn), (Mtla, Pbw), (Mtla, Tzi)} (Wdn, Pyzu), (Pyzu, Ymt), (Ymt, Pbw)} not in T that are incident on a vertex in T and do not complete a cycle if added to T, we select (Pyzu, Pbw), which has minimum weight, and add it to T. At this point T consists of the edges (Ml, Kt), (Kt, Sd), (Sd, Smn), (Smn, Aly), (Aly, Mtla), (Mtla, Tpwa), (Tpwa, Wdn), (Tpwa, Tzi) and (Tzi, Pyzu) and (Pyzu, Pbw). Since T does not have thirteen edges, we proceed to line 3.

Among the edges{(Ml, Wdn), (Ml, Sd), (Ml, Mtla), (Aly, Tsg), (Smn, Tsg), (Mtla, Wdn), (Mtla, Pbw), (Mtla, Tzi), (Wdn, Pyzu), (Pyzu, Ymt), (Pbw, Ymt), (Pbw, Tsg), (Pbw, Hkbu)} not in T that are incident on a vertex in T and do not complete a cycle if added it to T, we select (Pbw, Hkbu), which has minimum weight, and add it to T. At this point T consists of the edges (Ml, Kt), (Kt, Sd), (Sd, Smn), (Smn, Aly), (Alya, Mtla), (Mtla, Tpwa), (Tpwa, Wdn), (Tpwa, Tzi), (Tzi, Pyzu), (Pyzu, Pbw) and (Pbw, Hkbu). Since T does not have thirteen edges, we proceed to line 3.

Among the edges{(Ml, Wdn), (Ml, Sd), (Ml, Mtla), (Aly, Tsg), (Smn, Tsg), (Mtla, Wdn), (Mtla, Pbw), (Mtla, Tzi), (Wdn, Pyzu), (Pyzu, Ymt), (Pbw, Tsg), (Hkbu, Tsgi), (Hkbu, Ymt)} not in T that are incident on a vertex in T and do not complete a cycle if added to T, we select (Hkbu, Tsg), which has minimum weight, and add it to T. At this point T consists of the edges (Ml, Kt), (Kt, Sd), (Sd, Smn), (Smn, Aly), (Aly, Mtla), (Mtla, Tpwa), (Tpwa, Wdn), (Tpwa, Tzi), (Tzi, Pyzu), (Pyzu, Pbw), (Pbw, Hkbu)

and (Hkbu, Tsg). Since T does not have thirteen edges, we proceed to line 3.

Among the edges{(Ml, Wdn), (Ml, Sd), (Ml, Mtla), (Aly, Tsg), (Smn, Tsg), (Mtla, Wdn), (Mtla, Pbw), (Mtla, Tzi), (Wdn, Pyzu), (Pyzu, Ymt), (Ymt, Pbw), (Pbw, Tsg), (Hkbu, Ymt)} not in T that are incident on a vertex in T and do not complete a cycle if added to T, we select (Hkbu, Ymt), which has minimum weight, and add it to T. At this point T consists of the edges (Ml, Kt), (Kt, Sd), (Sd, Smn), (Smn, Aly), (Aly, Mtla), (Mtla, Tpwa), (Tpwa, Wdn), (Tpwa, Tzi), (Tzi, Pyzu), (Pyzu, Pbw), (Pbw, Hkbu), (Hkbu, Tsg) and (Hkbu, Ymt). Since T has thirteen edges, the algorithm terminates. The minimal spanning tree T is shown in Figure 5.

Its minimal weight is

5 + 8 + 9.55 + 9.26 + 8.75 + 9.14 + 9.54 + 8.79 + 13.89 + 14.82 + 9.24 + 11.53 + 7.84 = 125.35 miles.

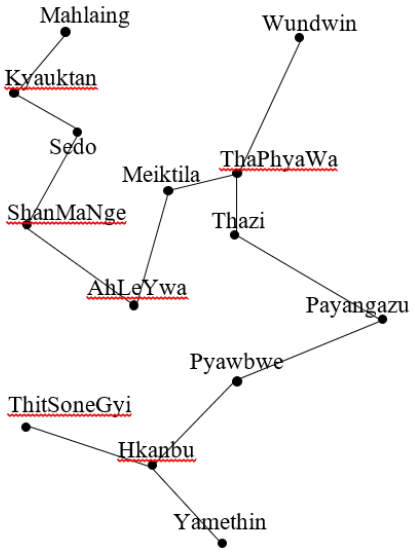

Fig.5. The minimal distance between given fourteen cities

V. Practical Problem in the Real World

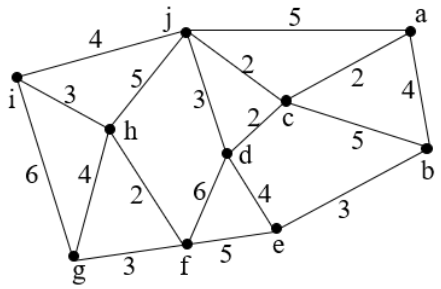

Fig.6. The layout of the city

Once upon a time there was a city that has no roads. Getting around the city was particularly difficult after rainstorms because the ground became very muddy cars got stuck in the mud and people got their boots dirty. The mayor of city decided that some of the streets must be paved, but didn't want to spend more money than necessary because the city also wanted to build a swimming pool. The mayor therefore specified two conditions:

(i) Enough streets must be paved so that it is possible for everyone to travel from their house to anyone else house only along paved roads, and

(ii)The paving should cost as little as possible. Figure 6 is the layout of the city. The number of paving stones between each house represents the cost of paving that road. We can find the best route that connects all the houses, but uses as few counters (paving stones) as possible.

We will apply Prim's Algorithm to the graph of Figure 6 with vertex ordering given ten houses to obtain a minimal spanning tree or minimal weight of Figure 7.

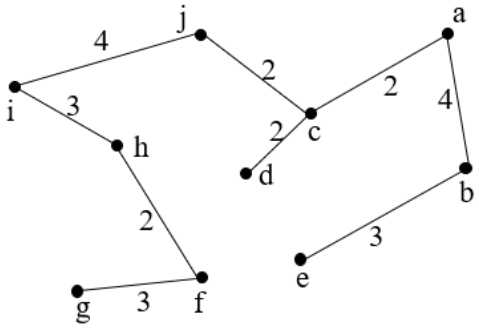

Fig.7. The lowest-costs of paving stones between ten houses

Its minimal spanning tree is

(a, c), (c, d), (c, j), (j, i), (a, b) ,(b, e), (i, h), (h, f) , (f, g).

Its lowest total cost is

2 + 2 + 2 + 4 + 4 + 3 + 3 + 2 + 3 = 25 .

VI. Conclusion

This paper presents finding the minimal weight between the fourteen cities in the network and the lowest-costs of paving stones between certain pairs of houses by using Prim's algorithm (a greedy algorithm). A greedy algorithm is an algorithm that optimizes the choice at each iteration we supply add an available edge with minimum weight [3].

ACKNOWLEDGEMENTS

I would like to express my grateful thanks to Head and Professor, Dr Aung Kyaw Min and Professor, Dr Khin Myat Myat Aung, Department of Mathematics, Meiktila University for their hearty attention, advice and encouragement. I also thank all my colleagues of our department for their warm friendship and kind advices.

REFERENCES

[1] A. Bondy and U. S. R. Murty, "GRAPH THEORY WITH APPLICATIONS," p. 270.

[2] R. J. Wilson, *Introduction to graph theory*, 4. ed., [Nachdr.]. Harlow: Prentice Hall, 20.

[3] K. H. Rosen, *Discrete mathematics and its applications (2nd ed.)*. USA: McGraw-Hill, Inc., 1991.

Article ID – JRA6004020

Servo Motor Control System by Using Microcontroller

Mar Mar Cho
University of Magway, Myanmar
marmarcho406@gmail.com

Aung Naing Oo
University of Magway, Myanmar

***Abstract*- Light detection unit formed by light dependent resistor and LM339 produces output voltage according to the presence or absent of automobile. This voltage is sent to PIC16F877A microcontroller. Two conditions namely no car condition and car stop condition are present in this system. These conditions are shown by both different coloured light emitting diodes and liquid crystal display simultaneously. The gate on and off is made by PIC16F84A microcontroller. Normally gate is closed and if motor switch is pressed, gate is opened. The required programs are written in Pic BASIC Pro language in MicroCode Studio software. The programs are compiled and downloaded into PIC16F84A micro-controller and PIC16F877A micro- controller respectively via PICKIT 2 programmer.**

Keywords- PIC16F84A micro-controller, PIC16F877A microcontroller, Servo Motor, Pic BASIC Pro language.

I. INTRODUCTION

The most common form of photo- conductive cell is the cadmium sulphide cell, named after the material used as a photoconductor. This is often referred to as a light dependent resistor. The cadmium sulphide is deposited as a thread pattern on an insulator, and since the length of this pattern affects the sensitivity, the shape is usually a zigzag line. The cell is then encapsulated in a transparent resin or encased in glass to protect the cadmium sulphide from contamination by the atmosphere. The cell is very rugged and can withstand a considerable range of temperatures, either in storage or during operation. The OPR 12 type of light dependent resistor has the following characteristics: peak spectral response is 610 nm, cell resistance at 50 lux is 2400 Ω, cell resistance at 1000 lux is 130 Ω, dark resistance is 10 MΩ, maximum voltage (DC or peak AC) is 110 V, maximum dissipation at 25°C is 200 mW, typical resistance rise time is 75 ms and typical resistance fall time is 350 ms.

The servo motor is most commonly used for high technology devices in the industrial application like automation technology. It is self contained electrical devices that rotate parts of a machine with high efficiency and great precision. The output shaft of this motor can be moved to a particular angle. Servo motors are mainly used in home electronics, toys, cars, airplanes, etc. This article discusses about what is a servo motor, servo motor working, servo motor types and its applications. Continuous rotation servo motor is quite related to the common positional rotation servo motor, but it can go in any direction indefinitely. The control signal, rather than set the static position of the servo, is understood as the speed and direction of rotation. The range of potential commands sources the servo to rotate clockwise or anticlockwise as preferred, at changing speed, depending on the command signal. This type of motor is used in a radar dish if you are riding one on a robot or you can use one as a drive motor on a mobile robot [3].

A microcontroller is a single chip computer. Micro suggests that the device is small, and controller suggests that the device can be used in control applications.

A microcontroller differs from a microprocessor in many ways. The main difference is that a microprocessor requires several other components for its operation, such as program memory and data memory, I/O devices and external clock circuit. A microcontroller on the other hand has all the support chips incorporated inside the same chip. All microcontrollers operate on a set of instructions (or the user program) stored in their memory. A microcontroller fetches the instructions from its program memory one by one, decodes these instructions, and then carries out the required operations [1].

In this work, light sensing unit determines whether there is an automobile or not. Depending on the situation, the analog output voltage is produced. This voltage is sent to microcontroller control unit which makes the processing. The output signals are sent to display unit and indicator unit simultaneously. The operation of servo motor is controlled by servo motor control unit. Fig (1) shows the block diagram of the constructed system.

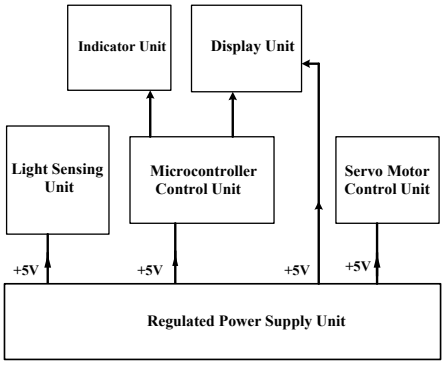

Fig 1. The block diagram of the constructed system

II. DESCRIPTION OF DEVICES

A. PIC16F877A Microcontroller

In the constructed system, PIC16F877A is used as the main control device which is manufactured by the Microchip Technology Inc. It is a 40-pin device with 8K bytes of flash program memory. The PIC16F877A has five I/O ports, PORTA, PORTB, PORTC, PORTD and PORTE. Some pins for these I/O ports are multiplexed with an alternate function for the peripheral features on the device. In general, when a peripheral is enabled, that pin may not be used as a general purpose I/O pin.

Some important features of PIC16F877A are it requires only 35 single word instructions for RISC CPU, operating speed of DC-20MHz clock input, 8K x 14 words of flash program memory, wide operating voltage range: 2V to 5.5V, 1000,000 erase/write cycles and 8 channels of analog-to-digital converter [5]. Fig (2) and Fig (3) shows the pin diagram and photograph of PIC16F877A microcontroller.

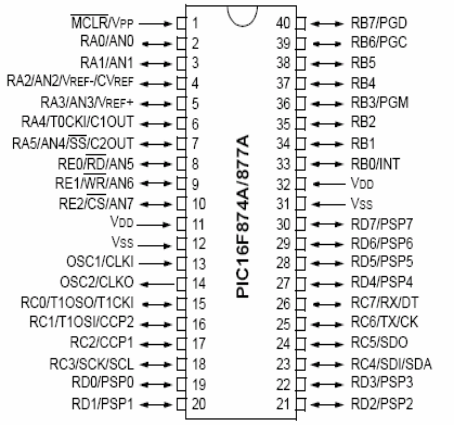

Fig 2. The pin diagram of PIC16F877A microcontroller

Fig 3. The photograph of PIC16F877A microcontroller

B. PIC16F84A Microcontroller

A microcontroller is an inexpensive single-chip computer. Single-chip computer means that the entire computer system lies within the confines of the integrated circuit chip. The microcontroller has features similar to those of standard personal computer. Primarily, the microcontroller is capable of storing and running a program. The microcontroller contains a CPU (central processing unit), RAM (random-access memory), ROM (read-only memory), I/O (input/output) lines, serial and parallel ports, timers and sometimes other built-in peripherals such as A/D (analog-to-digital) and D/A (digital-to-analog) converters [1].

The PIC16F84A microcontroller is an 18-pin device and it offers 1024 x 14 flash program memory, 68 bytes of data RAM, 64 bytes of non-volatile EEPROM (electrically erasable programmable read only memory), data memory, 13 I/O pins, a timer, a watchdog, and internal and external interrupt sources. The timer is 8-bits wide but can be programmed to generate internal interrupts for timing purposes. PIC16F84A can be operated from a crystal or a resonator for accurate timing. A resistor-capacitor can also be used as a timing device for application where accurate timing is not required [6]. Fig (4) and Fig.(5) show the photograph and pin configuration of PIC16F84A microcontroller.

Fig 4. The photograph of PIC16F84A Microcontroller

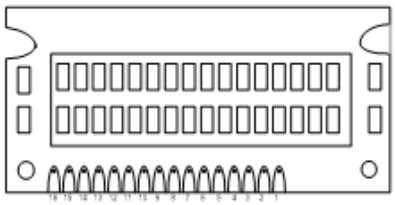

Fig 5. Pin configuration of PIC16F84A microcontroller

C. Liquid Crystal Display (LCD)

Alphanumeric dot matrix liquid crystal displays are used for displaying visual information, symbols, alphanumeric and icons in an impressive fashion. These modules have built-in controllers, drivers, character generator RAM/ROM, and associated circuitry for easy implementation of the logic for refreshing, multiplexing and updating the display. It has a LMB162A controller IC. The LMB162A module incorporates the control circuits, data RAM, and character generator RAM required for display. This module provides both 8 bit and 4 bit parallel interfaces and allows the controlling microprocessor to read and write data directly [2]. Fig (6) and Fig (7) shows the photograph and pin layout of the LCD (LMB162A).

Fig 6 The photograph of LCD (LMB162A)

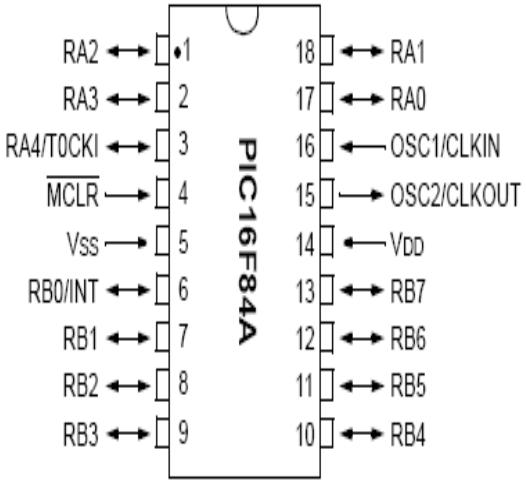

Fig 7. Pin layout of the LCD (LMB162A)

D. *Servo Motor*

The servo motor is most commonly used for high technology devices in the industrial application like automation technology. It is a self-contained electrical device that rotates parts of a machine with high efficiency and great precision. The output shaft of this motor can be moved to a particular angle. Servo motors are mainly used in home electronics, toys, cars, airplanes, etc. This article discusses about what is a servo motor, servo motor working, servo motor types and its applications. Continuous rotation servo motor is quite related to the common positional rotation servo motor, but it can go in any direction indefinitely. The control signal, rather than set the static position of the servo, is understood as the speed and direction of rotation. The range of potential commands sources the servo to rotate clockwise or anticlockwise as preferred, at changing speed, depending on the command signal. This type of motor is used in a radar dish if you are riding one on a robot or you can use one as a drive motor on a mobile robot [3]. Fig (8) shows the photograph of servo motor.

Fig 8. The photograph of servo motor

III. DESIGN AND CONSTRUCTION OF THE SYSTEM

There are six main parts in the work of "Servo Motor Control System by Using Microcontroller". They are regulated power supply unit, light sensing unit, microcontroller control unit, indicator unit, display unit and servo motor control unit.

A. *Regulated Power Supply Unit*

The PIC16F84A microcontroller and PIC16F877A microcontroller function properly at DC +5V. The required DC voltage is taken from voltage regulator (LM7805). The pin 1(input pin) of LM7805 is connected to positive terminal of DC +6V, 4A battery. The pin 2(ground pin) of LM7805 and negative terminal of battery are connected to ground. The output voltage of DC +5V is taken from pin 3(output) of LM7805.

B. *Light Sensing Unit*

This unit senses whether there is an automobile in front of the gate. This unit is formed by light dependent resistor and LM339 (Quad comparator). The pin 3(VCC) is connected to DC +5V and pin 12(VSS) is grounded. The reference voltage is set by 1 kΩ resistor and 10 kΩ variable resistor. This voltage is sent to pin 4(inverting) of LM339. The input voltage is set by LDR and 10 kΩ resistor. This voltage is sent to pin 5(noninverting) of LM339. The output voltage (at Pin 2) is pulled up by 1 kΩ resistor. This output voltage is sent to pin 2(AN0) of PIC16F877A microcontroller.

C. *Microcontroller Control Unit*

This unit controls the whole operation of the system. PIC16F877A microcontroller is used in this unit. The pin 11(VDD) and pin 32(VDD) are connected to DC +5 V and pin 12(VSS) and pin 31(VSS) are grounded. A 4 MHz crystal oscillator is fixed at pin 13(OSC1) and pin 14(OSC2). Two 22 pF capacitors are connected to the crystal oscillator and ground. The pin 1($\overline{\text{MCLR}}$) is connected to DC +5 V through 10 kΩ resistor. When RESET SWITCH is pressed, the pin 1($\overline{\text{MCLR}}$) is grounded and the microcontroller is reset condition. The pin 2(AN0) is connected to the pin 2 of LM339. The pin 33(RB0), pin 34(RB1), pin 35(RB2), pin 36(RB3), pin 37(RB4) and pin 38 (RB5) are connected to pin 11(DB4), pin12 (DB5), pin 13 (DB6) and pin 14 (DB7), pin 6(E) and pin 4(RS) of liquid crystal display (LMB162A) respectively. The pin 15(RC0), pin 16(RC1) and pin 17(RC2) of PIC16F877A are connected to anodes of YELLOW LED, GREEN LED and RED LED through 100Ω resistor respectively.

D. *Indicator Unit*

This unit shows the presence or absence of automobile in front of the gate and to switch on the servo motor. If there is no automobile, YELLOW LED is off, GREEN LED is on and RED LED is off. When there is an automobile, YELLOW LED is on, GREEN LED is off and RED LED is on. The light emitting diodes are energized by PIC16F877A micro-controller. Each anode pin of YELLOW LED, GREEN LED and RED LED is connected to pin 15(RC0), pin 16(RC1) and pin 17(RC2) of PIC16F877A microcontroller through 100Ω resistor respectively. The cathode pins of three light emitting diodes are grounded.

E. Display Unit

The operating condition of the constructed system is shown by display unit. A 16 characters x 2 lines liquid crystal display (LMB162A) is used in this unit. The pin 2(VDD) is connected to DC +5 V. The pin 1(VSS), pin 5(R/$\overline{W}$) and pin 16 (K) are grounded. The pin 15 (A) is connected to DC +5 V through 100 Ω resistor. The pin 3(VEE) is connected to middle pin of 10 kΩ variable resistor. The pin 11(DB4), pin 12(DB5), pin 13(DB6), pin 14(DB7), pin 6(E) and pin 4(RS) are connected to pin 33(RB0), pin 34(RB1), pin 35(RB2), pin 36(RB3), pin 37(RB4) and pin 38(RB5) of PIC16F877A microcontroller respectively.

F. Servo Motor Control Unit

The unit opens and closes the gate. PIC16F84A microcontroller and servo motor form this unit. MOTOR SWITCH is fixed at Pin 4($\overline{MCLR}$) of PIC16F84A microcontroller. The pin 6(RB0) of PIC16F84A is connected to YELLOW pin of servo motor. RED pin is connected to DC +5V and BROWN pin is grounded.

IV. RESULT AND DISCUSSION

There are two microcontrollers in this work. They are PIC16F877A microcontroller for system control operation and PIC16F84A microcontroller for servo motor control operation. The required programs are written in Pic BASIC Pro language. They are compiled and downloaded into microcontrollers. For PIC16F84A microcontroller, pin 2(RA0) is defined as input pin. The pin 33(RB0), pin 34(RB1), pin 35(RB2), pin 36(RB3), pin 37(RB4), pin 38(RB5), pin 15(RC0), pin 16(RC1) and pin 17(RC2) are configured as output pins. The RESET SWITCH is fixed at pin 1($\overline{MCLR}$) of PIC16F877A microcontroller.

The light dependent resistor senses whether there is an automobile on it or not. If there is no automobile, the output of LM339 produces logic HIGH states. If there is an automobile, the output of LM339 produces logic LOW state. The output logic states are sent to PIC16F877A microcontroller as analog voltage. If voltage is 0 V to 2.5 V, it is defined as car stop condition. YELLOW LED is turned on. GREEN LED is turned off. RED LED is turned on. The first line of liquid crystal display is “CAR STOP”. The second line of liquid crystal display is “GATE ON”. These two lines are displayed.

If voltage is 2.6 V to 5 V, it is defined as no car condition. YELLOW LED is turned off. GREEN LED is turned on. RED LED is turned off. The first of liquid crystal display is “NO CAR”. The second line of liquid crystal display is “GATE OFF”. These two lines are displayed. YELLOW LED is designed to signal the operation of servo motor. If it is turned on that signs to switch on servo motor and if it is turned off that signs to switch off servo motor.

For PIC16F84A microcontroller, pin 6(RB0) sends control signal to servo motor. This pin is defined as output pin. The MOTOR SWITCH is fixed at pin 4 ($\overline{MCLR}$) of PIC16F84A microcontroller. When this switch is pressed, servo motor is turned on. The servo motor is designed as gate control of the system. The photograph and complete circuit diagram of “Servo Motor Control System by Using Microcontroller” as shown in Fig (9) and Fig (10). Fig (11) and Fig (12) show the flowchart of the servo motor operation and coding for the servo motor.

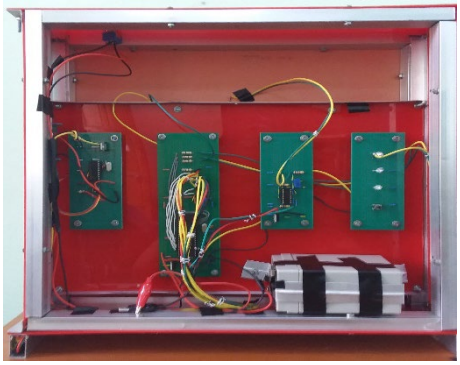

Fig 9. Photograph of “Servo Motor Control System by Using Microcontroller”

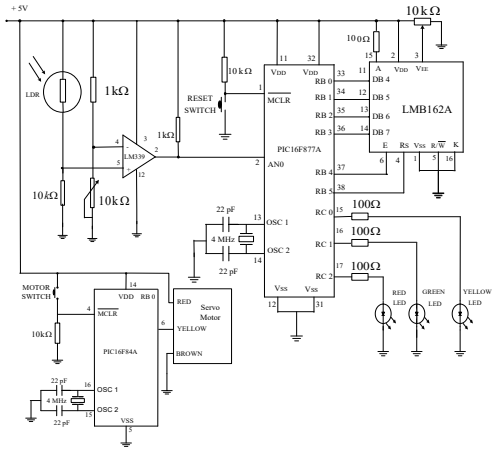

Fig 10. Complete circuit diagram of “Servo Motor Control System by Using Microcontroller”

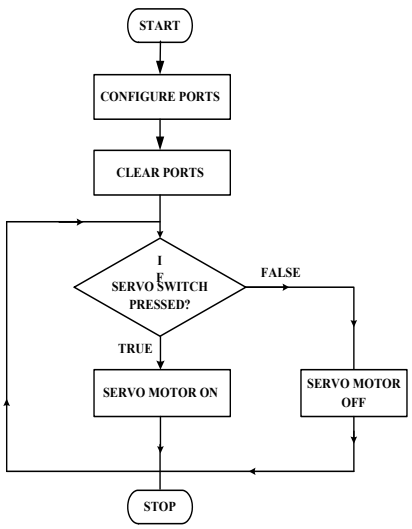

Fig 11. The flowchart of the servo motor operation

```
DEFINE OSC 4
B3        VARB   BYTE
      TRISA = $00
      TRISB = $00
      PORTB = $00
      B3 = 100
SWEEP:
     PULSOUT 0, B3
     PAUSE 18
     B3 = B3 + 1
     IF B3 > 200 THEN SWEEPBACK
    GOTO SWEEP
SWEEPBACK:
     B3 = B3 – 1
     PULSOUT 0, B3
     PAUSE 18
     IF B3 < 100 THEN SWEEP
    GOTO SWEEPBACK
    END
```

Fig 12. Coding for the servo motor

V. CONCLUSION

Toll gate can be found in high way traffic. The operation of the constructed system is designed on toll gate operation. In this work light dependent sensor and servo motor are used as required electronic devices. The other electronic devices of sensing automobile and gate control are also suggested to be carried out as further works.

ACKNOWLEDGEMENTS

We would like to express our gratitude to Dr Khin Maung Oo, Rector, Dr Win Soe, Pro-Rector and Dr Than Than Oo, Pro-Rector of University of Magway for their suggestion and permission to perform this project work. We would also like to express our great thanks to Dr Sandar Maung, Professor (Head of Department), Dr Nwe Nwe Yee, Professor and all the teachers and staff from the Department of Physics, University of Magway for their help and discussion throughout this research work.

REFERENCES

[1] D. G. Ibrahim, “Pic Basic Projects” Elsevier, Oxford UK (2006).
[2] "How to use Liquid Crystal Display (LCD)", PIC Microcontroller Course Electronics Training Center, 2004.
[3] http://www.circuitdigest.com, “Servo Motor”, 2015.
[4] J. Iovine, “PIC MICROCONTROLLER PROJECT BOOK”, McGraw-Hill, New York, 2000.
[5] Microchip Technology Inc, “Microchip PIC16F877A Data Sheet, 40 pin Enhanced FLASH/ EEPROM 8-bit Microcontroller”, 2001.
[6] Microchip Technology Inc, “Microchip PIC16F84A Data Sheet, 18 pin Enhanced FLASH/ EEPROM 8-bit Microcontroller”, 2001.
[7] T. L. Floyd, ninth edition, “Digital Fundamentals”, New Jersey, 2006.

Article ID – JRA6009020

Automatic Water Filling System Using Communication Between Microcontrollers

Nilar Winn
Natural Science
University of Computer Studies
Meiktila, Myanmar
drnilarwinn@ucsmtla.edu.mm

Khin Khin Sein
Natural Science
University of Computer Studies
Meiktila, Myanmar
drkhinkhinsein@ucsmtla.edu.mm

Myint Myint Aye
Engineering Physics
Technological University
Meiktila, Myanmar
myintmyintaye@tumeiktila.edu.mm

***Abstract*—An automatic water filling system was designed and constructed to be used as a home appliance. It was constructed using microcontrollers, liquid crystal display (LCD), pressure sensors, operational amplifiers, and a few active as well as passive components. It can be used as stand-alone control device or communicate with other tank controls. The automatic water filling system composes of two control units, master and slave controls which contain PIC16F877A microcontrollers as main control devices. In this system two water pumps are used for two water tanks. Pressure sensors MPX4115A and MPXA4115A sense the ambient atmospheric pressure and pressure of water level respectively. We have achieved to sense water level to an accuracy of ± 1 cm using these sensors. Self-developed programs were developed in Pic Basic Pro programming language for both of the master and slave control units. The master unit implements to sense the ambient atmospheric pressure and total pressure, i.e atmospheric pressure plus water pressure, of one tank. From these pressure values, the water pressure and therefore, water level in the tank is computed. Two control units were communicated with Universal Synchronous and Asynchronous Receiver Transmitter (USART) modules of the PIC 16F877A microcontrollers via the MAX485 transceiver ICs. Two relay operated pumps for two water tanks are controlled by the master unit and the system displays the information of water levels of tanks and pumps on GDM20464C LCD.**

***Keywords*—microcontrollers, pressure sensor, water level sensing**

I. Introduction

There are many different kinds of water filling systems in local market, some operates with mechanical switch, which will accordingly operate with the weight of water, but some are probe switches which use the filling water itself as conductor switch. In anyway, it is to fill the water with safe operation, and the water in the overhead tank must be always in high level. It is important to fill every tank in one's house to be in maximum tank level. Most of the local and foreign designed operate for a single tank filling systems, but not for multi tanks control. Moreover, the display is only available with LED indicators [1, 2]. The constructed system has two unit; master and slave unit. The master unit is used as main control device. The main jobs of the master unit are investigating the status of the level of tank1, controlling the pump1 and pump2 according to the received data from slave unit, displaying messages from tanks and pumps on the LCD display. The slave will receive the command from the master, investigate the status of the water level sensors of tank2 and send this status to the master unit. The master unit will perform the decision making. This research work investigates the communication between microcontroller based systems or communication between master and slave systems [3]. The system demonstrates how to control the water levels of two tanks. Both hardware and software are developed for the automatic water filling system. The communication between master and slave controller was investigated. The software design is simply created with Pic Basic Pro programming language [10]. In this program, it is initiated with oscillator setting and LCD pin assignments [5]. Then transmit and receive of serial communication pin configuration, pump control and pressure sensor pin definitions were made. The sensor pin is always checked for water level condition and this condition was displayed on the LCD screen. According to the water level, an operation condition for the pump was generated if the level is less than 50 cm, the pump will operate and fill the water. If the level is greater than 99 cm, the pump will be stopped. And it will remain stop until low level is detected again. The two systems, master and slave were communicated using MAX485 transceiver IC.

II. System Design

A. The Block Diagram of System

The master and slave control unit consist of a power supply unit, PIC16F877A microcontroller, pressure sensor, summing operational amplifier and interface circuit. 20 characters 4 lines LCD display is also used in the master unit. The PIC microcontroller based water filling system was constructed by using two PIC16F877A microcontrollers which are used as main controlling devices. One microcontroller is used for master unit and another is used for slave. MPX4115A/MPXA4115A series pressure sensor will sense pressure of water in tank.

The conditioning circuit for pressure sensor is developed by non-inverting summing amplifier. Water levels of tank1 and tank2 and on/off condition of their associated pumps are displayed on LCD display. MAX485 transceiver communicates between two microcontrollers. The block diagram of the constructed system is shown in Fig.1.

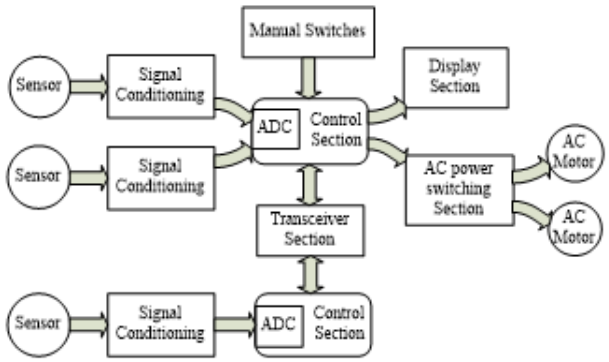

Fig 1. Block diagram of the constructed system

B. The Analog to Digital Converter (ADC)of PIC16F877A

There are eight analog inputs (RA0, RA1, RA2, RA3, RA5, RE0, RE1, and RE2) in the analog-to-digital (A/D) converter module of the PIC16F877A microcontroller. In this project, RA0 analog input is used to sample the conditioned voltage from pressure sensor. The A/D converter generates a digital result for an analog voltage level via successive approximation. The A/D conversion of the analog input signal results a corresponding 10-bit digital number. The A/D module has four registers. These registers are A/D Result High Register (ADRESH), A/D Result Low Register (ADRESL), A/D Control Register0 (ADCON0), and A/D Control Register1 (ADCON1). In the software program for the functions of the PIC, the ADCON0 register is set 0 × 40 for selecting the A/D conversion clock as FOSC/8(FOSC = frequency of oscillator). The ADCON1 register is configured to 0 × 82 to store the A/D result in right justification and specify all of RA pins as analog inputs.

C. MPX4115A/MPXA4115A Series Pressure Sensor

The MPX4115A/MPXA4115A series piezo resistive transducer is a state-of-the-art, monolithic, signal conditioned, silicon pressure sensor. This sensor combines advanced micromachining techniques, thin film metallization, and bipolar semiconductor processing to provide an accurate, high level analog output signal that is proportional to applied pressure. Fig.2 and Fig.3 show pressure sensors MPX4115A and MPX4115AS which were used in our work.

The pressure sensor can be used to measure 15 kPa to 115 kPa (2.2 to 16.7 psi). The respective voltages are 0.2 to 4.8 volts. These sensors have 1.5% maximum errors over 0° to 85°C. It is ideally suited for microprocessor or microcontroller based systems. Temperature compensation is from -40°C to +125°C. The pressure sensor can be used in aviation altimeters, industrial controls, engine control, and weather stations and weather reporting devices [4].

According to the measurements and observations, the output voltage of atmospheric pressure in local region pointed out by the sensor is about 4 V. the maximum applicable sensor output voltage for water level sending is 0.8 V. So the analog signal processing has to be made for the pressure sensor output.

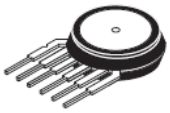

Fig 2. Pressure sensor MPX4115A

Fig 3. Pressure sensor MPX4115AS

D. MAX485Transceiver

The MAX485 IC is a low-power transceiver for RS485 communication. Each part contains one driver and one receiver. The driver slew rates of the MAX485 is not limited, allowing it to transmit up 2.5Mbps. The transceiver draws between 120µA and 500µA of supply current when unloaded or fully loaded with disable drivers. All parts operate from a single 5V supply. Drivers are short-circuit current limited and are protected against excessive power dissipation by thermal shutdown circuitry that places the driver outputs into a high-impedance state. The receiver input has a fail-safe feature that guarantees a logic-high output if the input is open circuit. Pin diagram of MAX485 is shown in Fig.4.

It has a low quiescent current of 300µA. Common-mode input voltage is -7V to +12V. It has three-state outputs. Propagation delay of this IC is 30ns and skew is 5ns. It can be operated by using a single 5V supply. Maximum number of transceivers that can be used on the Bus is 32. Data rate is 2.5Mbps [6].

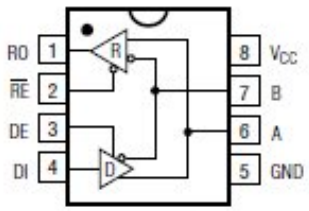

Fig 4. Pin diagram of MAX485 transceiver IC

E. Signal Conditioning for Pressure Sensort

The input voltage Vin is the sum of sensor output voltage and output voltage of voltage divider circuit. The input voltage of noninverting summing amplifier circuit is obtained as follows.

$$V_{in} = \frac{V_s R_{eq} + V_{th} R_1}{R_1 + R_{eq}} = [V_s + (-4)] \times \frac{1}{2} = \frac{(V_s - 4)}{2}$$

A noninverting amplifier is implemented by operational amplifier A1 with resistors R4 and R5. The gain is obtained as follows.

$$A_{V1} = \frac{R_5}{R_4} + 1 = \frac{3.9}{2.7} + 1 = 2.44$$

The output voltage V_{O1} is thus

$$V_{o1} = V_{in} \times A_{V1} = \frac{(V_s - 4)}{2} \times 2.44 = 1.22V_s - 4.88$$

The output voltage V_{o1} is then fed into another noninverting amplifier A_1. The second noninverting amplifier circuit consists of the feedback resister R_8 and R_7 is connected to the inverting input of operational amplifier A_2. The gain is obtained as follows.

$$A_{V2} = \frac{R_8}{R_7} + 1 = \frac{100}{24} + 1 = 5.166$$

Hence the output voltage V_{o2} is obtained as

$$V_{o2} = V_{o1} \times A_{V2} = (1.22\,\text{Vs} - 4.88) \times 5.166$$

$$V_{o2} = 6.3025\,\text{Vs} - 25.21$$

The signal conditioning circuit is as shown in Fig. 5. The two op-amps as designed in the summing amplifier and each gain was about 2.44 and 5.166, therefore total gain for two amplifiers is about 12.6 [7,8,9]. The results obtained are tabulated and is as shown in Table 1. The characteristic graphs are shown in Fig.6.

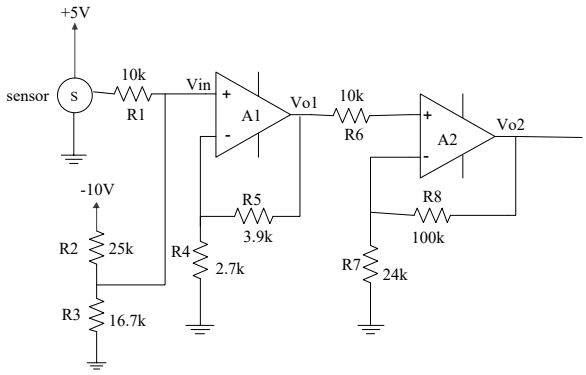

Fig 5. The diagram of the signal conditioning circuit

F. Hardware Development of the System

In this system master control unit senses the ambient atmospheric pressure and total pressure of atmospheric pressure and water level of the tanks. The master control performs these two pressures sensing by using the MPX4115A and MPX4115AS pressure sensors.

The output signal of pressure sensor is fed to the signal conditioning system. The output voltage for each water level was measured. Level height of 104 cm was used for this system. The +5 V is connected to Vs pin of the pressure sensor. The output voltage of this pressure sensor will change according to the pressure. The sensor produces +4 V. This voltage is fed into the potential divider circuit and from this circuit -4 V is taken out and then fed into the input of noninverting amplifier. Thus whenever the pressure changes the voltage difference is fed into the noninverting input. Hence output VO1 is obtained at the first amplifier output. This is again fed into another noninverting amplifier. Finally, output VO2 is obtained at the second amplifier output. After signal conditioning is made the signal is input to RA0 pin which is analog input of the PIC16F877A microcontroller. The upper nibble of PortD is used to transfer the data to LCD display and then RD2 and RD3 are connected to the register select (RS) and enable(E) pins of LCD. 4-bit interface is used to operate the LCD display. The voltage Vin, VO1 and VO2 are measured by digital multi-meters. Finally, automatic water filling system using pressure sensors is implemented and the circuit diagram of the master and slave unit are as shown in Fig.7 and Fig 8.

TABLE I. THE INPUT AND OUTPUT VOLTAGE OF THE SIGNAL CONDITIONING CIRCUIT

Sr. No	V_{in}	V_{out}	Sr.No	V_{in}	V_{out}	Sr.No	V_{in}	V_{out}
1	2.5	-9.7	22	3.6	-3.1	43	4.65	3.84
2	2.55	-9.3	23	3.65	-2.8	44	4.7	4.16
3	2.6	-9.0	24	3.7	-2.4	45	4.75	4.46
4	2.65	-8.7	25	3.75	-2.1	46	4.8	4.77
5	2.7	-8.4	26	3.8	-1.8	47	4.85	5.09
6	2.75	-8.1	27	3.85	-1.5	48	4.9	5.39
7	2.8	-7.8	28	3.9	-1.2	49	4.95	5.72
8	2.85	-7.4	29	3.95	-0.8	50	5.0	6.0
9	2.9	-7.1	30	4.0	-0.5	51	5.05	6.32
10	2.95	-6.8	31	4.05	-0.3	52	5.1	6.63
11	3.0	-6.5	32	4.1	0.4	53	5.15	6.97
12	3.05	-6.2	33	4.15	0.7	54	5.2	7.31
13	3.1	-5.9	34	4.2	1.0	55	5.25	7.6
14	3.15	-5.5	35	4.25	1.4	56	5.3	7.91
15	3.2	-5.3	36	4.3	1.6	57	5.35	8.24
16	3.25	-4.9	37	4.35	2.0	58	5.4	8.55
17	3.3	-4.6	38	4.4	2.3	59	5.45	8.85
18	3.35	-4.3	39	4.45	2.6	60	5.5	9.14
19	3.4	-4.0	40	4.5	2.9	61	5.55	9.5
20	3.45	-3.7	41	4.55	3.2			
21	3.5	-3.4	42	4.6	3.52			

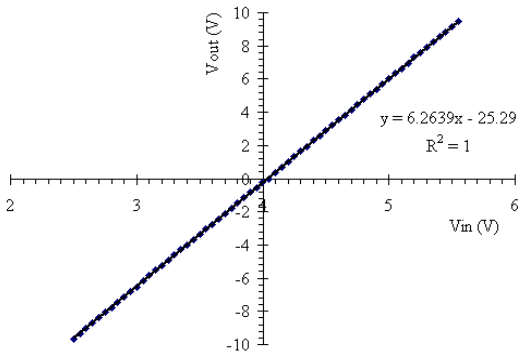

Fig 6. Characteristics of signal conditioning circuit

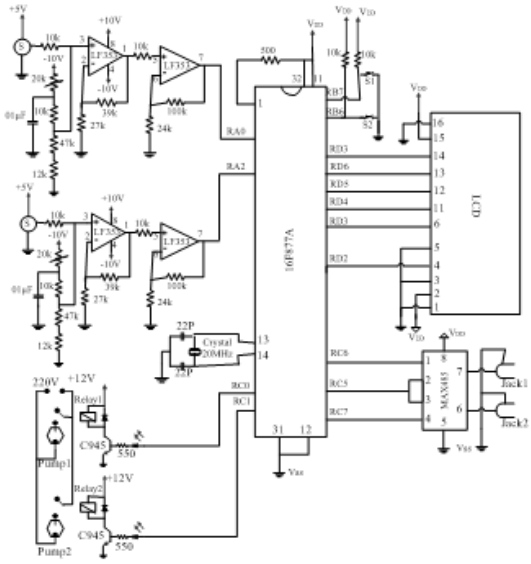

Fig 7. Circuit diagram of the master control unit

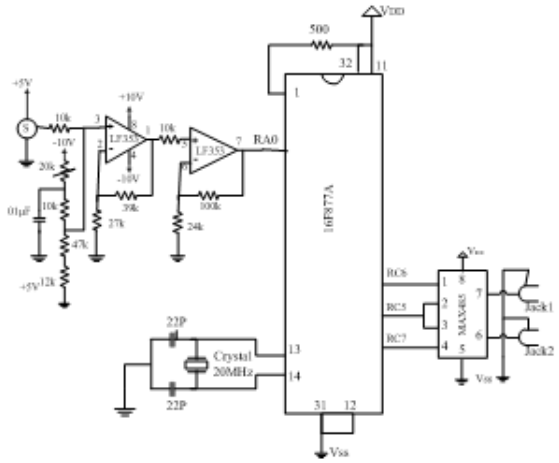

Fig 8. Circuit diagram of the slave control unit

G. Software Development of the System

In the master unit programs for ADC module, receiving data from slave, calculating the pressure of water level, decision making for pumps, LCD displaying were developed. The firmware embedded in slave involves analog to digital conversion program for analog pressure signal and data sending program from USART module to master control.

The master program firstly makes variable declaration, port configuration and initialization for ADC module and LCD display function. Analog channel 0 and 1 are used to sample data from RA0 and RA2 pins. After making the required configurations, program reads the data from slave via USART module. Serial data sending from USART module is made with 2400 baud rate (bit per second). Then the ambient atmospheric pressure and value of atmospheric pressure and water pressure are read from channel 0 and 1 of master controller. Then water level pressure of tank2 is calculated by the difference of pressure value from the slave and atmospheric pressure. The values of water level are averaged by the 5 terms moving average method [8].

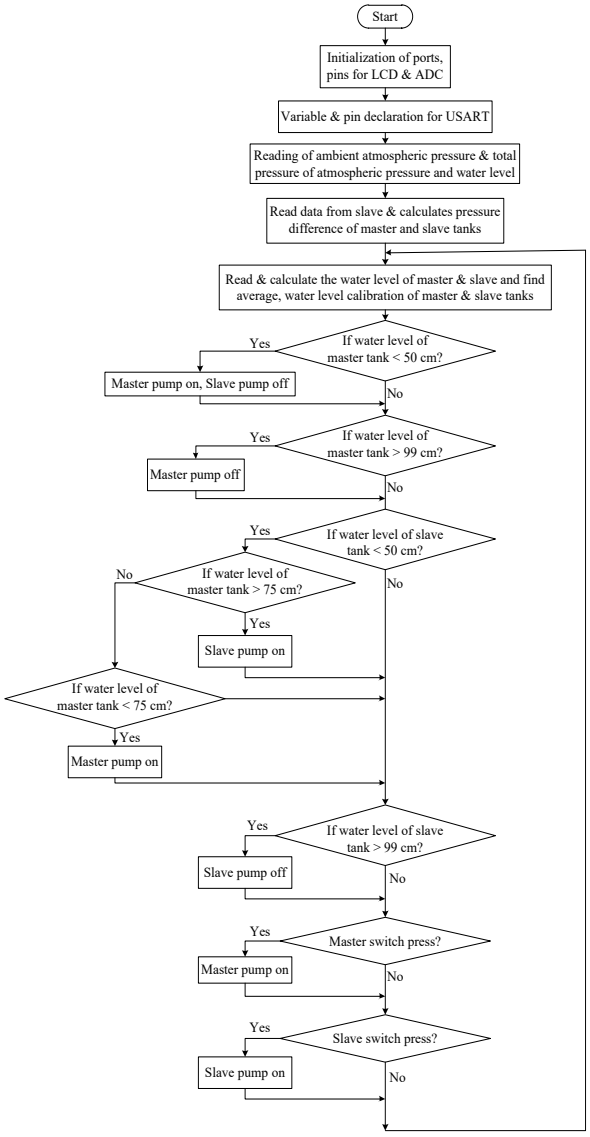

Fig 9. The flow diagram of the master control unit

Data acquisition is established by using the averaging method and reliable data can be obtained. The water level sensed by the master controller is sensed and averaged in the above way. The calibrations for water levels sensed by master and slave are performed then water levels in 'cm' unit are displayed on first line of the LCD display. And the program checks water levels of tank1 and tank2, and makes the respective command to relay operated pump1 and pump2. The flow diagram of the master program depicts in the Fig.9.

According to the flow diagram in Fig.10 the slave control program initializes variables and ports and configures the analog to digital module and USART serial port. Analog output voltage from pressure sensor is read by analog channel 0 and the resultant 10 bit digital data is divided into two byte. This low byte and high byte data are sent to master unit from USART module via MAX485 transceiver IC.

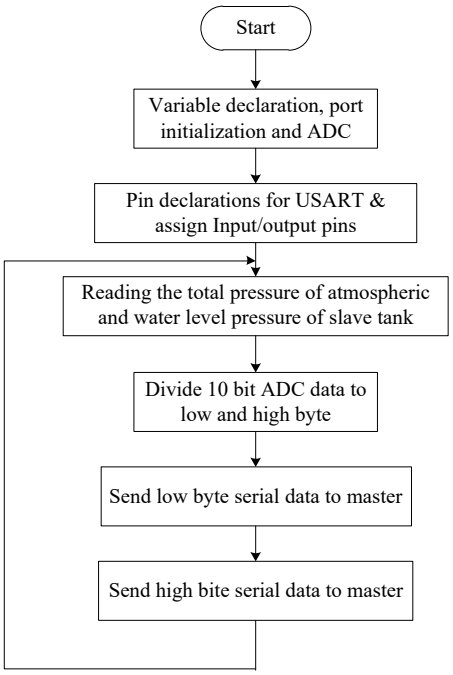

Fig 10. The flow diagram of the slave control unit

III. RESULT AND DISCUSSION

A. *Measurement of the Respective Voltages for Various Water Levels*

When the water level is set at 1 cm, voltage at the pressure sensor output of master unit is measured by using digital multi-meter. After doing this process water level is set at 10 cm, 50 cm and 100 cm. Voltages for those levels are measured in similar manner. Finally output voltages are measured at the second non-inverting amplifier. The results are given in Table 2. An ambient atmospheric pressure is measured at the same time. The output voltages for the circuit of ambient atmospheric pressure sensor are also measured in similar manner. Voltages values are as shown in Table 3. Experiment is repeated for the slave unit. Voltage measurements are given in Table 4. From Table 2 and Table 4, it is found that the voltage values do not differ. We have conducted experimental works to investigate performance of MPX4115AS sensor for water level sensing application and the characteristics is shown in Fig.11.

Analog signal preprocessing is made on sensor output voltage with the signal conditioning circuit. At the first stage of summing amplifier, the variation of output voltage 0.01 V is obtained for 2 cm water level difference. The output characteristic of the first stage of summing amplifier is shown in Fig.12. At the second stage of summing amplifier, the variation of output voltage 0.05 V is obtained for 2 cm water level difference. The output characteristic of the second stage of summing amplifier is shown in Fig.13.

The measurable range of pressure sensor is from 15kPa to 115kPa, and the relative output voltage ranges from 0.2 V to 4.8 V. It is an applicable range of sensitivity to use in this system. According to the measurements and observations, the output voltage of atmospheric pressure in local region pointed out by the sensor is about 4 V. According to manufacturer's datasheet, maximum output voltage difference of pressure sensor is 4.6 V. The maximum applicable sensor output voltage for water level sending is found to be about 0.8 V.

Actually when we measure the pressure of water level in tank, the resultant pressure value is atmospheric pressure plus pressure of water level in the tank. Atmospheric pressure depends on the ambient weather condition and altitude. So we developed the system with two pressure sensing units and one is to measure the ambient atmospheric pressure and another for combination of water pressure and atmospheric pressure. The system calculates the pressure difference of them and actual water level pressure can be obtained.

The conditioned voltage is fed to the analog to digital converter (ADC) of PIC16F877A microcontroller. Since the resolution of the built in analog to digital converter of PIC16F877A is 5 V/1023 = 0.005 V, the significant result is detected for each 1 cm of water level and the better sensitivity can be obtained by using MPX4115AS sensor. The characteristic of the signal conditioning is shown in Fig.14. Maximum water level that can be measured is expected to be about 200 cm (~6.5 ft) with resolution of 1 cm, by this system.

The photograph of testing the constructed system is shown in Fig. 15. The photograph of water level display is shown in Fig. 16. The photograph of master control system is shown in Fig. 17. The photograph of slave control system is shown in Fig. 18.

TABLE II. MEASURE MENT OF OUTPUT VOLTAGES OF MASTER UNIT FOR VAUIOUS WATER LEVELS

Water Level (cm)	**Voltage (V)**		
	Sensor output	***First non-inverting amplifier output***	***Second non-inverting amplifier output***
1	4.8	0.31	1.65
10	4.12	0.35	1.88
50	4.29	0.57	3.00
100	4.51	0.83	4.36

TABLE III. MEASURE MENT OF OUTPUT VOLTAGES OF MASTER UNIT FOR AMBIENT ATMOSPHERIC PRESSURE

Voltage (V)		
Sensor output	***First non-inverting amplifier output***	***Second non-inverting amplifier output***
4.08	0.28	1.52

TABLE IV. MEASURE MENT OF OUTPUT VOLTAGES OF SLAVE UNIT FOR VAUIOUS WATER LEVELS

Water Level (cm)	**Voltage (V)**		
	Sensor output	***First non-inverting amplifier output***	***Second non-inverting amplifier output***
1	4.09	0.32	1.62
10	4.13	0.36	1.90
50	4.30	0.58	2.97
100	4.52	0.84	4.36

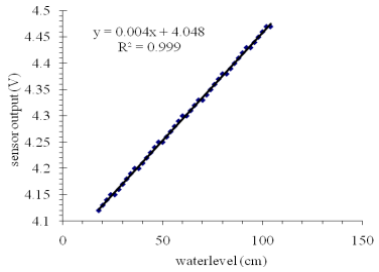

Fig 11. Sensor output versus water level graph of master unit

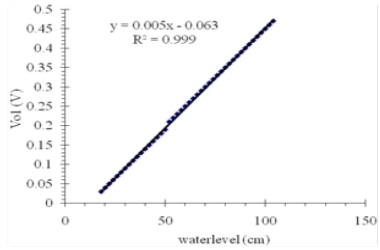

Fig 12. V_{O1} versus water level graph of first non-inverting amplifier

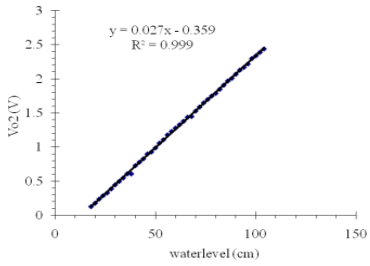

Fig 13. V_{O2} versus water level graph of second non-inverting amplifier

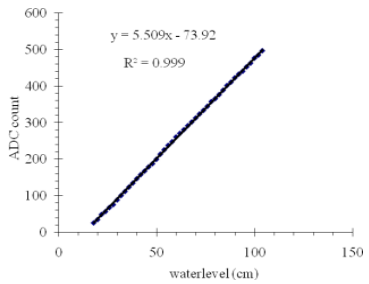

Fig 14. Analog to digital converter count versus water level graph

Fig 15. The photograph of testing the constructed system

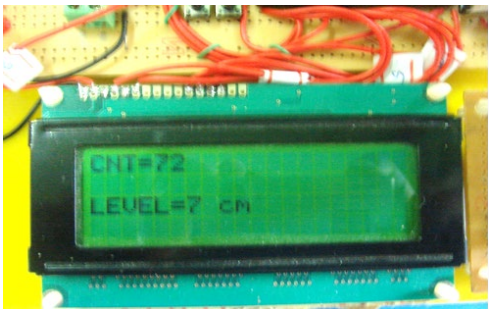

Fig 16. The photograph of automatic water level display

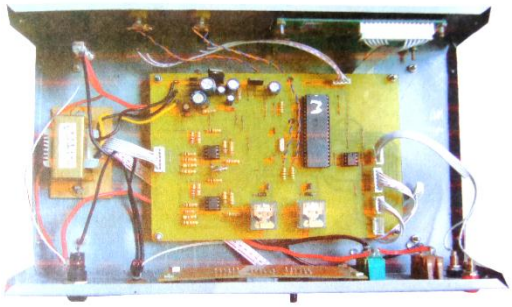

Fig 17. The photograph of master control system

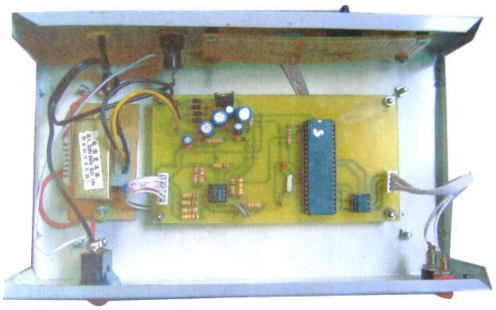

Fig 18. The photograph of slave control system

IV. CONCLUSION

MPX4115A and MPX4115AS pressure sensors provides an accurate and high level analog output signal that is proportional to applied pressure. By the help of software and special features of PIC16F877A microcontroller accuracy and system reliability can be enhanced. Furthermore the system can be upgraded not

only for liquid level sensing but also level control application. For some factories and plants liquid level control is essential needed and some control algorithm such as Fuzzy and Neural control system has to be used. The basic construction of hardware has been developed in this work and the software only has to be modified for such cases. Since the programs developed in constructed system is in Basic Pro software, high level and reliable C programming can be used for more complicated algorithm.

ACKNOWLEDGMENT

We would like to express our gratitude to Dr. Mie Mie Khin, the Rector, University of Computer Studies (Meiktila) for her permission and encouragement to perform this research. We would like to thank to Dr. Min Soe Tun, Associate Professor, Department of Physics, Mandalay University of Distant Education, for his valuable supervision and guidance.

REFERENCES

[1] A. March, "Tank Water Level Indicator", Everyday Practical Electronics Magazine, Wimbrone Publishing Ltd., United Kingdom, 2009.
[2] Orbit Communications Pty Ltd., "Dual Pump control/monitor", Australia, 2010.
[3] Microchip Technology Inc., "PIC 16F877A Data Sheet, 8-Bit CMOS FLASH Microcontrollers," United State of America, 2007.
[4] Freescale Semiconductor Inc., "Integrated Silicon Pressure Sensor, MPX4115A/MPXA4115A Series," United State of America, 2009.
[5] J. Ilett, "How to Use Intelligent L.C.D," Wimbrone Publishing Ltd., New York, 1997.
[6] Maxin Integrated Products, "MAX485 Transceivers Data Sheet," United State of America, 2007.
[7] D. L. Terrell, "OP AMPS Design, Application, and Troubleshooting," Second Edition, Terrell technologies Inc., United State of America, 1996.
[8] R. F. Coughlin and F. F. Driscoll, "Operational Amplifiers and Linear Integrated Circuits," Prentice Hall Inc., United State of America, 1997.
[9] National Semiconductor Corporation, "LF353 Wide Bandwidth Dual JFET Input Operational Amplifiers Data Sheet," United State of America, 2003.
[10] H. Hutching, "Interfacing with C", Second Edition, Newnes, United State of America, 2001.

Article ID – JRA6009720

Simulation of Diffraction with Circular Aperture

Aye Aye Soe
Department of Natural Science
University of Computer Studies (Meiktila)
Mandalay, Myanmar
ayeayesoe11620@gmail.com

Zar Zar Win
Department of Physics
Technological University (Kyaukse)
Mandalay, Myanmar
zarzarwin76@gmail.com

Naw Ku Ma
Department of Natural Science
University of Computer Studies (Taunggyi)
Taunggyi, Myanmar
nawkuma76@gmail.com

***Abstract*—Diffraction occurred when the wave is encountered an obstacles or objects [1]. It is also the slight bending of light after passing around the edges of an object. There are basically two types of diffraction namely: Fresnel diffraction and Fraunhofer diffraction. The Fresnel diffraction is occurred when the wave is passed through an aperture and diffracted field is emerged in near field. And the Fraunhofer diffraction is the far-field diffraction when the wave passed through an aperture or slit [2]. The circular aperture of diffraction is the crucial in optical devices. The results from the circular aperture's pattern are the set of co-centric circular bright and the highest peak in the center is described with the dark bands. In this paper, all of the simulation for analyzing diffraction pattern of Fresnel diffraction and Fraunhofer diffraction with circular aperture are implemented by using Matlab programming language. The main contribution of this paper is to analyze the optical intensity distribution with two different diffractions of circular aperture pattern.**

***Keywords*-** diffraction, aperture, Fresnel, fraunhofer

I. INTRODUCTION

The diffraction concept is observed by Francesco Grimaldi since 1665 in order to notice when the light waves spread out in passing through a slit. The diffraction is occurred when the light is passed through an obstacle, the light can spread due to the edges of these obstacles. The diffraction phenomenon can be described by using Huygens' Principle. The diffrcted field can be calculated by using analytical models such as Kirchhoff-Fresnel diffraction equation, Fraunhofer diffraction and Fresnel diffraction. The Fraunhofer diffraction is the approximation of Kirchhoff equation and applied the far field whereas the Fresnel diffraction is applied the near filed. The regions of the electromagnetic filed around the object is referred to as near filed and far filed. The Kirchhoff equation is derived from the wave equation, second-order diffraction linear partial differential equation. The slit in is the spreading of downstream of the wave and moreover when the slit is getting wider, the pattern of diffraction is also getting narrows. In the fraunhofer diffraction, it breaks up the slit into the half of the wavelength ($\lambda/_2$) and consider how to combine these divided slits. The circular aperture is thinking of projecting of the slit into a circle by spinning. The series of decreased intensity rings around it can give the diffraction pattern [3].

The types of diffraction and its further extension types are illustrated in the following figure 1. The next section is described the methods used to implement the diffraction pattern with circular aperture and the simulation of fresnel diffraction and fraunhofer diffraction is experimented by using Matlab programming in Section III. The Section IV is shown the conclusion of the whole system of this paper.

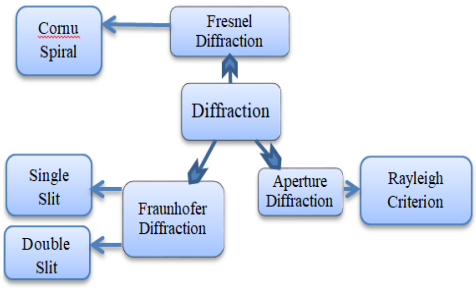

Fig. 1. Branches Diagram of Diffraction Pattern

The observation of diffraction from source of light is passed through the aperture is shown in figure 2.

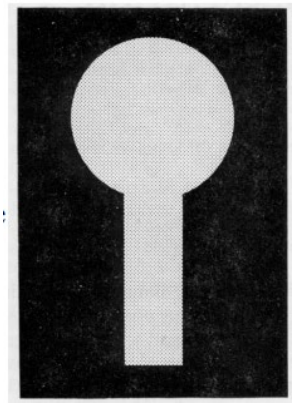

Fig. 2. Sample of Diffraction at Aperture [4]

II. METHODOLOGY

In this paper, the diffraction pattern with circular aperture is analyzed by using Fresnel and Fraunhofer diffraction methods. The previous research work studied the Fresnel or Fraunhofer diffraction with different apertures such as rectangular, circular and so on. They didn't study only one type of aperture in two types of diffraction: Fresnel and Fraunhofer.

A. Fresnel Diffraction

The Fresnel diffraction was made as a contribution for transversing the nature of light and diffraction theory by Augustin Jean Fresnel [5]. It is the near field diffraction type with curved wavefront. In the Fresnel diffraction, the aperture is divided into regions is called the Fresnel zones.

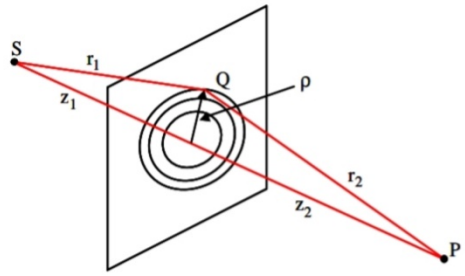

Fig. 3. Sample of illuminating aperture from Sphere Wave

The Fresnel zones are called when the Fresnel diffraction is divided the aperture into regions. In above figure, the source of point S is illuminating the aperture distance z1 to away and then the distance to aperture's right is the observation point P. The field in the plane (x1, y1) can be calculated [6] by using equation 1:

$$r=r_0+\frac{x_1^2+y_1^2}{2r_0}-\frac{x_1x_2+y_1y_2}{r_0} \quad (1)$$

The equation 2 is the expansion using binomial theorem.

$$U_2(P) = -\frac{i}{\lambda r_0}exp(ikr_0)\iint_s (U_1(x_1,y_1)exp\left[-\frac{ik}{r_0}(x_1x_2+y_1y_2)\right] \exp\left[\frac{ik}{2r_0}\left(x_1^2+y_1^2\right)\right])dx_1dy_1 \quad (2)$$

B. Circular Aperture Fresnel Diffraction

The circular aperture by Fresnel, it simplifies the law of Fresnel diffraction, which is near the aperture with the Fresnel number F. The circular spot at the center, Airy disc is the representation of best spot of light.

The Fresnel diffraction for circular aperture in illuminating by a plane wave can be calculated by using the equation 3:

$$U_2(R_2,r_0)=-\frac{ik}{r_0}\exp\ (ikr_0)\int_0^a J_0\left[\frac{kR_1R_2}{r_0}\right]\exp\left[\frac{ikR_1^2}{2r_0}\right]R_1dR_1 \quad (3)$$

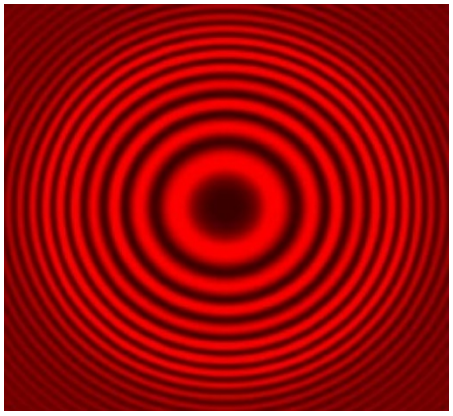

Fig. 4. Sample of Fresnel Diffraction with Circular

C. Fraunhofer Diffraction

The Josef von Fraunhofer developed related to the diffraction for the gratings and increasing understanding [5]. The planar wavefronts are used in this Fraunhofer diffraction.

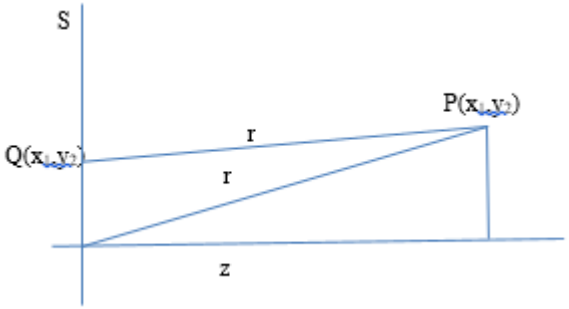

Fig. 5. Sample of Fraunhofer diffraction [6]

The observation point is far from aperture but the diffraction pattern doesn't change only the changes in size when the distance is increased. This type of phenomenon is called the Fraunhofer diffraction. This is occurred with small Fresnel number F≪1. The fraunhofer diffraction pattern can achieve at very larger distance from the aperture. The Fraunhofer diffraction is applied the Huygens' Fresnel diffraction in splitting the incoming wave into the several outgoing waves after passing through an aperture or slit. The source of diffraction pattern in far-field can observe in the focal plane of lens. The filed vector in Huygens' Principle is

$$U(P)=-\frac{i}{\lambda}\iint_s \frac{e^{ikr}}{r}U(Q)dS \quad (4)$$

Where, U(Q) is strength of the illumination of Q, $\frac{e^{ikr}}{r}$ is a sphere wave emanating from Q.

When the aperture from a point with distance(s) illuminated by spherical wave is shown following equations 5 and 6.

$$U(Q)=A\frac{e^{iks}}{s}, \quad (5)$$

$$U(P)=-A\frac{i}{\lambda}\iint_s \frac{e^{ik(r+s)}}{rs}dS \quad (6)$$

The formula for Huygens' diffraction is described in the above equation. The value of r in the field vector doesn't change as much as the value of Q [6]. It is necessary to consider the changes in exponent due to the multiplicative factor. Therefore, the value of r is considered as constant at the value of r0 described in below equation 7.

$$U_2(P)=-\frac{i}{\lambda r_0}\iint_s e^{ikr}U_1(Q)dS \quad (7)$$

$$r^2=(x_2-x_1)^2+(y_2-y_1)^2+z^2 \quad (8)$$

$$=r_0^2+(x_1^2+y_1^2)+2(x_1x_2+y_1y_2)$$

$$r=r_0-\frac{(x_1x_2+y_1y_2)}{r_0}$$

The approximation of Fraunhofer diffraction equation is

$$U_2(P)=-\frac{i}{\lambda r_0}\exp(ikr_0)\iint_s U_1((x_1,y_1)\exp\left[\frac{-ik}{r_0}(x_1x_2+y_1y_2)\right]dx_1dy_1 \quad (9)$$

D. Circular Aperture Fraunhofer Diffraction

This section is described the circular aperture with radius a of Fraunhofer diffraction. The structure of circular aperture like a ring and it has maximum central brightest.

The polar coordinates [6]: of x_1 and y_1 can be expressed by using following equations:

$$x_1 = R_1 cos\emptyset, \qquad x_2 = R_2 cos\varphi,$$

$$y_1 = R_1 sin\emptyset, \qquad y_2 = R_2 sin\varphi,$$

The equation for diffraction by Fraundhofer with circular aperture is:

$$U_2(P)=-\frac{i}{\lambda r_0}\exp(ikr_0)\int_0^{2\pi}\int_0^{a}\exp\left[\frac{ikR_1R_2\cos(\phi-\varphi)}{r_0}\right]R_1dR_1d\phi \quad (10)$$

E. Procedure for Simulation

The simulation can be performed by using Matlab programming in order to know how light is diffracted by going through the slit. The image by diffraction pattern with circular aperture for Fresnel and Fraunhofer is simulated in this paper. The Matlab programming can analyze the optical intensity distribution by Fresnel and Fraunhofer by generating for any wavelength. The circular aperture is plotted with Fourier transform using fft and shift fft function in Matlab.

III. SIMULATION RESULTS

The diffraction pattern of Fresnel and Fraunhofer with circular aperture is simulated by using Matlab programming language. The following figures are shown the Fraunhofer and 59Fresnel diffraction and then the modulus of these two diffraction patterns with aperture of circular shape. The diffraction pattern of circular aperture produced as an "Airy pattern or Airy Disc". The Airy disc is produced the light as a diffuse circular disc. Finally, their results are also described by the mesh grid figures.

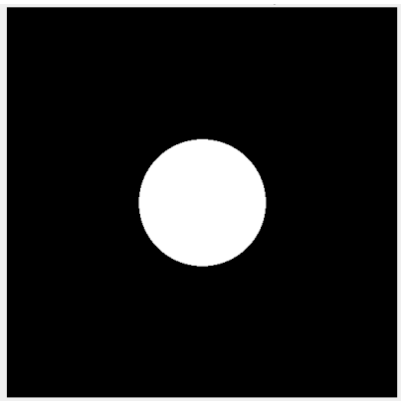

Fig. 6. Simulation of Fresnel Diffraction

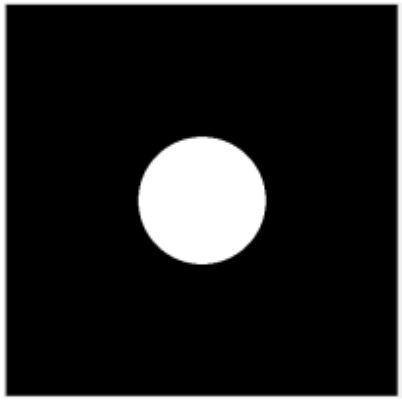

Fig. 7. Simulation of Fraunhofer Diffraction

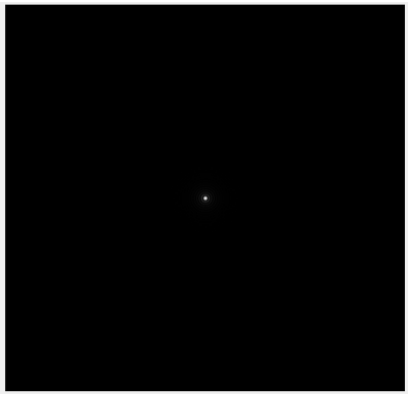

Fig. 8. Simulation of Fraunhofer Diffraction

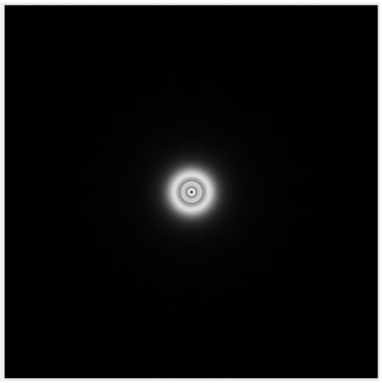

Fig. 9. Simulation of Fresnel Diffraction

In optics, the point image is produced from a point object according to the geometric optics. The result at the screen can be found when the aperture treated as whole bunch of point object. The results of simulation for two diffraction types in above figure are not different but after finding their modulus of these two results, they are significantly different as shown in figure 8 and 9.

The mesh plot is a three-dimensional surface and described with solid edge and face colors.

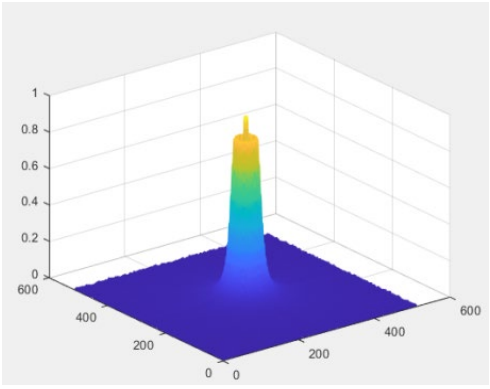

Fig. 10. Simulation of Fresnel Diffraction with Mesh Grid

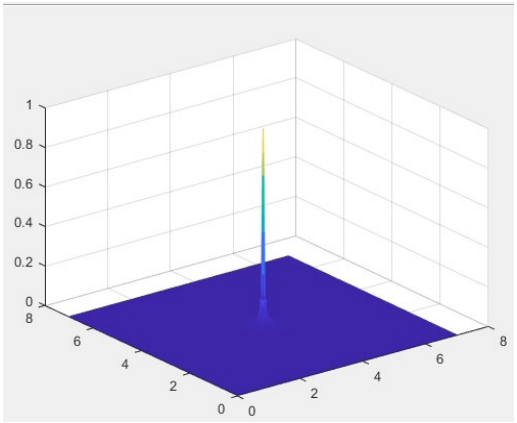

Fig. 11. Simulation of Fresnel Diffraction with Mesh Grid

IV. Conclusion

The diffraction pattern depends on the distance between aperture and the observation point. The near-field diffraction pattern (Fresnel) is the observed points are closely from the aperture with an intermediate distance whereas the far-field diffraction (Fraunhofer) has a long distance from the aperture to the observation point. The wave fronts in Fraunhofer are planar wave whereas the Fresnel is cylindrical wave. The observation distance in two diffraction patterns: infinite observation in Fraunhofer and finite distance observation in Fresnel. For the further extension from this paper, Fraunhofer diffraction with line source and single slit and so on. The Fresnel diffraction can contribute by considering the number of Fresnel zones. Moreover, the aperture types such as rectangular, sphere can also extend.

References

[1] http://www.wikipedia.org, Diffraction.
[2] http://www.sites.ualberta.ca, Diffraction on circular apertures Text Book, Page 1253-1256.
[3] M. Creech-Eakman, Radiation and Optics, “Diffraction”.
[4] LASER 51, “Diffraction.pdf”, April 03.
[5] W. C. James, “13 Fresnel Diffraction”, Optics 505.
[6] D. A. Boas, C. Pitris, N. Ramanujam, Sheppard CJR (2011), “Diffraction Optics”, Handbook of Biomedical Optics, Page. 11-31.

Article ID – JRA6002320

Analysis on Socio-Economic Development of Pyawbwe Township

Win Win Nyunt
Department of Geography and Environmental Studies
University of Mandalay
Mandalay, Myanmar
winwinnyunt@mu.edu.mm

Aye Aye Moe
Department of Geography
University of Myitkyina
Myitkyina, Myanmar

Htar Ei Chaw
Department of Geography
University of Meiktila
Meiktila, Myanmar

***Abstract*- This research paper is "A Geographic Analysis on Socio-Economic Development in Pyawbwe Township". Development is a multi – dimensional phenomenon such as level of economic growth, level of education, level of health services, level of social development and level of transportation and communication. This study is to investigate the social economic changes in Pyawbwe Township, and to make an assessment of the growing prosperity and welfare of Pyawbwe Township. Levels of Socio-Economic Development are examined (13) indicators with help of each village in Pyawbwe Township by using the formula of composite index of development. For investigation study, spatial analysis of socio-economic development clearly indicates that only 53.72 percent of the study area under high level development and remaining 68.35 percent is under low level and moderate level development. It is essential to avoid the spatial disparity in the development special attention government and non-government agencies for future.**

***Keywords*: multi – dimensional phenomenon, socio-economic development, government, non-government.**

I. INTRODUCTION

The pattern of socio-economic development of Pyawbwe Township are examined the basis for future socio-economic improvements and planning. It studies the aspects of society and economy of a region. Therefore, it needs to study socio economic changes for habitat of the region.

II. STUDY AREA

Pyawbwe Township is situated in the Mandalay region of the central Myanmar. It lies between 20o 21' 59.11" to 20o 23' 19.2" north latitudes and 95o 35' 4.813" to 96o 22' 40.75" east longitudes. It is surrounded by Meiktila Township to the north, Thazi Township to the north–east, Yemathin Township to the south, and Natmauk Township to the west. The study area has an area of 1653.567 km2 (408603.7 acre). It has plain in the central part, mountain range in

the eastern part, and gentle slope in the western part of study area. Climatically, it falls Bsh climate according to the Koppen's classification. Soil of the study area is mainly derived alluvial, red brown savanna soil, and primitive crushed stone soil. Alluvial and Irrawaddy formation is covering in this study. Economy in this study area has agriculture base. Irrigation has played an important role in transforming agricultural landscape and life of rural people in the study area. The study area has fairly rail and road network. Transportation plays an important role in the economic development and rural-urban interaction (Figure 1).

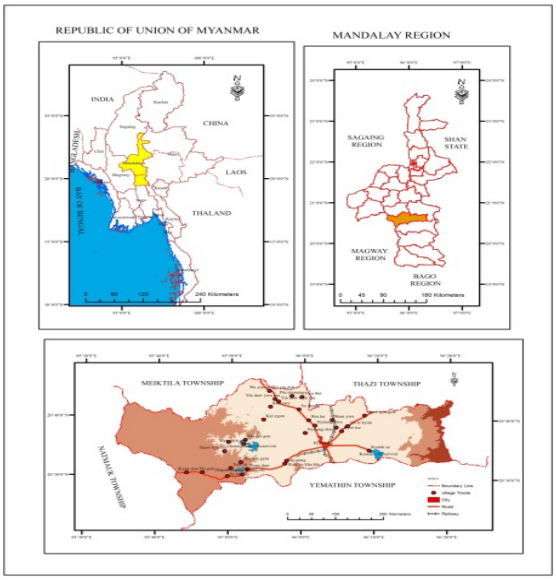

Fig 1. Location of Pyawbwe Township

III. OBJECTIVES

The objectives in this study area are; to investigate the social economic changes in Pyawbwe Township, and to make an assessment of the growing prosperity and welfare of Pyawbwe Township.

IV. METHODOLOGY

Developmental activities of rural areas cannot be evaluated fully by any single indicator because it is a multi-dimensional process [1]. Moreover, when analyzed, a number of indicators do not provide an integrated and easily comprehensive picture of reality. Hence, there is a need of combining the effect of different indicators for

assessing the level of development. Rural development of a region depends on agricultural growth, economic and social infrastructural facilities, provisions for public health, education, communication and transportation facilities etc [2]. In this analysis, the composite index of development has been obtained for different groups by using data pertaining to the year 2019 on the developmental indicators, particularly cultivation, secondary and tertiary activities, irrigation, agro-economic sector, population density as social indicator, high schools and middle schools in education sector, clean water as sanitation, dispensaries, rural health centres, and sub-rural health centres in health sector, electricity, and transportation roads in infrastructural facilities. A total of 13 developmental indicators are included in this analysis that has used mainly ratio index, transformed from the indicators. The level of socio-economic development is identified and delineated for village tracts with the help of certain indices. It is measured by using the formula of composite index of development. The following variables are considered for determining the levels of socio-economic development.

1. Percentage of land under cultivation.
2. Percentage of land under irrigation.
3. Percentage of population engaged in secondary and tertiary activities
4. Population density
5. Percentage of urban population.
6. Percentage of village tracts having school.
7. Percentage of village tracts having primary health care center.
8. Percentage of village tracts having supply of water
9. Percentage of village tracts having toilet system.
10. Percentage of village tracts having transportation system.
11. Percentage of village tracts having electricity.
12. Percentage of village tracts having tele-communication facilities.
13. Percentage of literacy

The method adopted to determine level of development involves two stages, first determination of level of development of Pyawbwe Township. In terms of discrete variables and then integration of the values of obtained to give a composite index of development [3] taking all the variables in to account. The co-efficient of a single variable is expressed as:

$$CDI = Pi / PI \ X100$$

where, CDI = the co-efficient of development for variable i,
Pi =Percentage of variable i, in the areal unit.
PI =Mean percentage of variable i, in the study region.

By summing the development indices taking account all variable, we get the composite index of development by the following equation.

$$CID = (CDI\ 1+CDI\ 2+CDI\ 3\ldots\ldots CDIn) / N$$

Where, CID= Composite index of development and N=Number of variables.

V. FINDING AND DISCUSSION

The pattern of socio-economic development of Pyawbwe Township are examined the basis for future socio-economic improvements and planning. It studies the aspects of society and economy of a region. Therefore, it needs to study socio economic changes for habitats of the region. Levels of socio-economic development are calculated for all village tracts on the above formula. The patterns of socio-economic development in Pyawbwe Township are described as the three categories by using the composite development indices in the table (1) and figure (2).

TABLE 1. THE COMPOSITE INDEX OF DEVELOPMENT IN PYAWBWE TOWNSHIP (2019)

Sr	Town & Village Tracts	CDI	CID	Classification
1	Pyawbwe	18964.83	1458	High
2	Shan Su Gon	1184.78	91.13	Low
3	San Daw	3777.04	290.54	High
4	Seywa	2256.39	173.56	Moderate
5	Thibin	2306.97	177.46	Moderate
6	Mipayagon	288.43	22.19	Low
7	Kyaungywa	2295.27	176.55	Moderate
8	Taung Le	2683.93	206.46	High
9	Kende	2053.16	157.93	Moderate
10	Myinde	3795.26	291.94	High
11	Hlaing Pan	418.36	32.18	Low
12	Taung Nyaunggo	1375.41	105.8	Moderate
13	Gegyi	427.68	32.89	Low
14	Pebin she	3878.37	298.33	High
15	Thapanchaung	768.49	59.11	Low
16	Bawdigon	749.04	57.82	Low
17	Natsonehmaw	271.03	20.84	Low
18	Telaybin	2408.83	185.29	Moderate
19	Let thegyo	2458.89	189.14	Moderate
20	Magyi gon	417.82	32.14	Low
21	Shan Su	5082.91	390.99	High
22	Htadawgyi	851.25	65.48	Low
23	Naunggon North	4070.60	313.12	High
24	Me Dee	2317.88	178.29	Moderate
25	Kyiywa	2463.33	189.48	Moderate
26	Seikgyo	1007.27	77.48	Low
27	Yindaw Myoma	4083.37	314.1	High
28	Ywarhtin	276.80	206	High
29	Yanaung	5577.46	429.03	High
30	Yagyi	615.23	47.32	Low
31	Htayanga	1355.67	104.28	Moderate
32	Tawdwinhla	800.42	61.57	Low
33	Hlwebaukkon	624.84	48.06	Low
34	Pyinzin	572.18	44.01	Low
35	Hpwe thin	926.74	71.28	Low
36	Pin myaing	410.95	31.61	Low
37	Yindaw ywama	675.94	51.99	Low

38	Pyawgon	542.70	41.76	Low
39	Dahatgon	836.01	64.30	Low
40	Wayindok	792.48	60.96	Low
41	Wayon	328.39	25.26	Low
42	Akaritgon	3440.41	264.65	High
43	Sadaung	542.55	41.73	Low
44	Tamagon	2526.85	194.37	Moderate
45	Chaungmagyi	2718.00	209.07	High
46	Kyeni	5652.20	434.78	High
47	Thapayoe	1207.20	92.86	Low
48	Wetlet	1059.42	81.49	Low
49	Nyaung Shwe	3672.17	282.47	High
50	Thaphaypin	942.62	72.50	Low
51	Hpettaw	687.78	52.90	Low
52	Batta	2933.67	225.66	High
53	Minlann	5301.22	407.78	High
54	Kyoegon	437.56	33.65	Low
55	Thanakhadaw	612.80	47.13	Low
56	Kyettee	2555.54	196.58	Moderate
57	Kyudawwa	2721.76	209.36	High
58	Kantha	1066.95	82.07	Low
59	Ohnbin	840.20	64.63	Low
60	Moenangon	901.26	69.32	Low
61	Gwezee	427.98	32.92	Low
62	Zagyan taung	881.42	67.80	Low
63	Phayagyi	527.29	40.56	Low
64	Sugyingon	987.91	75.99	Low
65	Ossanwe	990.42	76.81	Low
66	Theingon	528.85	40.68	Low
67	Myenigon	951.51	73.19	Low
68	Twinywa	1014.68	78.05	Low
69	Gwebinyoe	527.50	40.57	Low
70	Hpaung daw	613.69	47.20	Low
71	Kountha	1152.61	88.66	Low
72	Moegaung	2434.37	187.25	Moderate
73	Shwenyaungpu	3951.87	303.98	High
74	Kyaukse	1177.33	90.56	Low
75	Kangyi	3131.86	240.91	High
76	Sabegon	754.69	58.05	Low

A. High socio-economic development

High socio-economic development is found in Pyawbwe, Shan Su, Kyeni, Nyaung Shwe, Minlann, Sandaw, Taungle, Myinde, Pebinshe, Nyaunggon north, Yindaw Myoma, Ywarhtin, Yanaung, Akaritgon, Chaungmagyi, Kyudawwa, Shwenyaungpu, Kangyi and Twinywa village tracts. It covers nearly 53.72 percent of total geographical area. Pyawbwe is located in the southern part of Pyawbwe Township with an administrative status as townships headquarter. Other village tracts and Pyawbwe are connected good communication and transportation such as roads and rail routes, infrastructural facilities and electric light. Expect Pyawbwe, it is sufficient the irrigation facilities in other regions which made for agricultural development and iron industry in other regions.

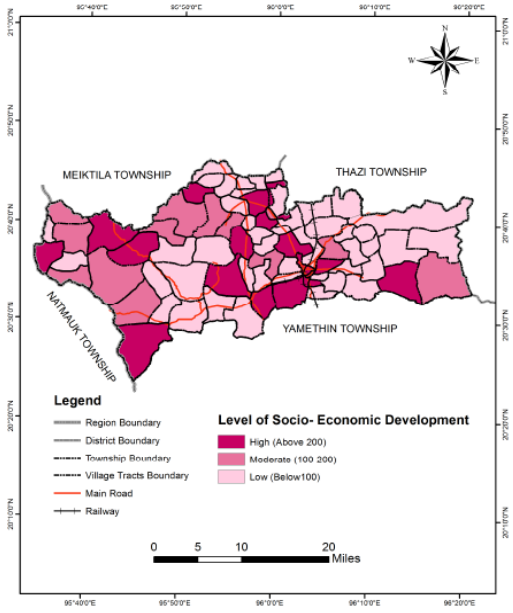

Fig.2. The Level of socio–economic development of Pyawbwe Township

B. Moderate socio-economic development

Moderate socio-economic development is found in Seywa, Thibin, Kyaungywa, Kande, Nyaunggon Taung, Telaybin, Lethegyo, Medee, Kyiywa, Htayanga, Tamagon, Kyettee and Moegaung village tracts. It covers nearly 21.33 percent of total geographical area. These regions have good amount of cultivated land for agricultural facilities and livestock. It has moderate electric light, transportation and communication in these regions.

C. Low socio-economic development

Low socio-economic development is found in Shansugon, Mipayagon, Hlaingpan, Gegyi, Thapanchaung, Bawdigon, Natsonemaw, Magyigon, Htadawgyi, seikgyo, Yagyi, Tawdwinhla, Hlwebaukgon, Pyinzin, Hpwethin, Pinmyaing, Yindaw Ywama, Pyawgon, Dahatgon, Wayindok,, Wayon, Sadaung, Thapayoe, Wetlet, Thaphaypin, Hpettaw, Batta, Kyoegon, Thanakhadaw, Kantha, Ohnbin, Moenangon, Gwezee, Zagyantaung, Phayagyi, Sugyingon, Ossanwe, Theingon, Myenigon, Twinywa, Gwebinyoe, Haungdaw, Kountha, Kyaukse and Sabegon village tracts. It covers nearly 47.02 percent of total geographical area. This is because those village tracts do not electric light, health center and poor transportation. Those regions are available for cultivation, but it is retarded the irrigation facilities.

Spatial analysis of socio-economic development clearly indicates that only 53.72 percent of the study area under high level development and remaining 68.35 percent is under low level and moderate level development. The development of a region depends upon the economic activities, future plans, region's authorities and local people [4]. It seems that there is vast contrast in the socio-

economic development. It is essential to avoid the spatial disparity in the development special attention of government and non-government agencies. As the economy of Pyawbwe Township has basic priority the connected with the farming and the use of land for farming in development process should be given to agricultural sector through modern measures. Social development will automatically take place with the economic development.

VI. CONCLUSION

The socio - economic development level in village tracts has increased in Pyawbwe Township in 2019, their more use of fertilizers and pesticides, and paying more attention to paddy cultivation is more than ever. At present the villages are using more of have found electricity, road transportation and health care centres. It now has more developments in all aspects like other regions of Myanmar.

A. Suggestion and Future Prospect

According to the research, some suggestions are concerned:

- to maintain soil conservation for cultivation due to the cultivated multi-cropping pattern
- to upgrade the irrigation facilities
- to control crops price and support suitable agricultural loans for farmers
- to give the agricultural knowledge and use the modern technique for farming
- to encourage the export to foreign market for the iron industry
- to upgrade the breeding of livestock for household
- to promote the road quality and upgrade at least to the level of tarred roads and bridge on the roads for the transportation activity

The most the transportation, the economic activities of the Pyawbwe Township will certainly be development. Therefore, the future of Pyawbwe township can be expected to be more prosperous than today.

ACKNOWLEDGEMENT

Thanks to faculty of University Technical for giving permission and cooperation to prepare this research. Special thanks to supervisor for comments and guidance to improve this article.

REFERENCES

[1] International Journal of Humanities and Social Sciences (2010): *Disparity in Socio-Economic Development and its Implications on Communal Conflicts*.

[2] H. Andrew, "*Canada's Global Cities: Socio-economic Conditions in Montreqal, Toronto and Vancouver"*, 2006.

[3] V. K. Bhatia and S. C. Ral, "*Evaluation of Socio-Economic Development in Small Areas",* Project Report, Planmng Commission, Government of India, New Delhi, 2004.

[4] D. Abhiman, "*Socio - Economic Development in India"*, A Regional Analysis Reserve Bank of India, 1999.

Article ID - JRA6000920

A Sequential Algorithm for Poisson Equation on a Thin Plate

Thant Thant Soe
Faculty of Computing
University of Computer Studies(Monywa)
Monywa, Myanmar
thantthantsoethelma@gmail.com

***Abstract*— This paper presents a sequential algorithm for solving Dirichlet problem associated with Poisson equation on a thin plate. At first, Poisson equation for Dirichlet problem is introduced. Secondly, Fourier coefficients of solution for the Dirichlet problem is evaluated. Besides, recursive relations by using domain discretization are also derived. Then, sequential implementation and two variants of the integration scheme are described as algorithm. Finally, numerical example for exact solution and maximum errors is performed using Matlab programming.**

Keywords*— *sequential algorithm, Poisson equation, thin plate, Dirichlet, recursive relations, Matlab programming

I. INTRODUCTION

A variety of problems in computational science and engineering requires the solution of Poisson equation. Poisson equation is a partial differential equation named after the French mathematician and physicist Siméon – Denis Poisson. There are many numerical approaches to solve Poisson equation. Fast, accurate and reliable numerical solver play a significant role in the development of applications for scientific problems. Here, we solve Poisson equation on a thin plate using Green's function method. Thin plate is a flat slice neglecting thickness and here we will use thin plate as a disk. To determine completely the solution of the Poisson equation, it is necessary to specify a boundary condition on the solution. The common boundary condition is Dirichlet condition, in which the values of the solution are specified on the boundary.

We consider Poisson equation for the Dirichlet problem on a disk Ω as

$$\Delta u = f \text{ in } \Omega, \tag{1}$$

$$u = g \text{ on } \partial\Omega \tag{2}$$

where $\Omega = B(0,R) = \{x \in R^2 : |x| < R\}$, $R > 0$.

II. SOLUTION OF DIRICHLET PROBLEM ON A DISK

Let v satisfy

$$\Delta v = f \text{ in } \Omega, \tag{3}$$

and w be the solution of the homogeneous problem

$$\Delta w = 0 \text{ in } \Omega$$
$$w = g - v \text{ on } \partial\Omega. \tag{4}$$

Then, the solution of (1) and (2) is given by

$$u = v + w.$$

A general solution of (3) is

$$v(x) = \int_{\Omega} f(\xi)G(x;\xi)d\xi, \quad x \in \Omega, \tag{5}$$

where $G(x;\xi) = \frac{1}{2\pi}\ln|x-\xi|$ is the Green's function for the Laplacian [1].

The value v (.) is expanded in terms of Fourier series with Fourier coefficients of v (.). To construct an efficient algorithm, in the evaluation of Fourier coefficients of Fourier series, a theorem will be needed and it is represented as follow [2].

A. Theorem

If $u(r,\theta)$ is the solution of (1) and (2) for $x = re^{i\theta}$ and $f(re^{i\theta}) = \sum_{n=-\infty}^{\infty} f_n(r)e^{in\theta}$, then the nth Fourier coefficient $u_n(r)$ of $u(r,.)$ can be written as

$$u_n(r) = v_n(r) + \left(\frac{r}{R}\right)^{|n|}\left(g_n - v_n(R)\right), \quad 0 < r < R, \tag{6}$$

where g_n are the Fourier coefficients of g on $\partial\Omega$, and

$$v_n(r) = \int_0^r p_n(r;\sigma)d\sigma + \int_r^R q_n(r;\sigma)d\sigma, \tag{7}$$

$$p_n(r;\sigma) = \begin{cases} \sigma \ln r f_0(\sigma) & , n = 0, \\ \frac{-\sigma}{2|n|}\left(\frac{\sigma}{r}\right)^{|n|} f_n(\sigma), & n \neq 0, \end{cases} \tag{8}$$

$$q_n(r;\sigma) = \begin{cases} \sigma \ln \sigma f_0(\sigma) & , n = 0, \\ \frac{-\sigma}{2|n|}\left(\frac{r}{\sigma}\right)^{|n|} f_n(\sigma), & n \neq 0. \end{cases} \tag{9}$$

Proof

The solution w of (4) by using the Poisson integral formula is [1]

$$w(r,\theta)=\frac{1}{2\pi}\int_0^{2\pi}\phi(\tau)\,K(\frac{r}{R},\theta-\tau)\,d\tau,\ 0<r<R,$$

where the Poisson kernel is [1]

$$K(\rho,\tau)=\frac{1-\rho^2}{1+\rho^2-2\rho\cos\tau},\ 0\le\rho<1, \tag{10}$$

and the boundary condition

$$\phi(\tau)=g(\tau)-v(R,\tau) \tag{11}$$

For $z=\rho e^{i\tau}$, (10) becomes

$$\begin{aligned}K(\rho,\tau)&=\frac{1-\rho^2}{(1-\rho\cos\tau)^2+(\rho\sin\tau)^2}\\&=\frac{1-|z|^2}{|1-z|^2}\\&=\frac{Re(1-z\bar{z}+z-\bar{z})}{|1-z|^2}\\&=Re\left(\frac{1+z}{1-z}\right)\end{aligned} \tag{12}$$

Since $|z|<1$, we can write (12) as

$$K(\rho,\tau)=Re(1+2(z+z^2+\ldots))=\sum_{n=-\infty}^{\infty}\rho^{|n|}e^{in\tau} \tag{13}$$

From (13), we get $K_n(\rho)=\rho^{|n|}$.

If we let $w(r,\theta)=\sum_{n=-\infty}^{\infty}w_n(r)e^{in\theta}$, we have

$$\begin{aligned}w_n(r)&=\frac{1}{2\pi}\int_0^{2\pi}\left[\frac{1}{2\pi}\int_0^{2\pi}\phi(\tau)K(\frac{r}{R},\theta-\tau)\,d\tau\right]e^{-in\theta}\,d\theta\\&=\frac{1}{2\pi}\int_0^{2\pi}\phi(\tau)\left[\frac{1}{2\pi}\int_0^{2\pi}K(\frac{r}{R},\theta-\tau)e^{-in\theta}\,d\theta\right]d\tau\\&=\frac{1}{2\pi}\int_0^{2\pi}\phi(\tau)\left[\frac{1}{2\pi}\int_0^{2\pi}K(\frac{r}{R},\theta-\tau)e^{-in(\theta-\tau)}\,d\theta\right]e^{-in\tau}d\tau\\&=\frac{1}{2\pi}\int_0^{2\pi}\phi(\tau)K_n(\frac{r}{R})e^{-in\tau}\,d\tau\\&=K_n(\frac{r}{R})\,\phi_n,\end{aligned}$$

where $K_n(\frac{r}{R})=\frac{1}{2\pi}\int_0^{2\pi}K(\frac{r}{R},\theta-\tau)e^{-in(\theta-\tau)}\,d\theta$

and $\phi_n=\frac{1}{2\pi}\int_0^{2\pi}\phi(\tau)e^{-in\tau}d\tau.$

The Fourier coefficients $w_n(r)$ are

$$w_n(r)=\left(\frac{r}{R}\right)^{|n|}\phi_n. \tag{14}$$

When we use (11), (14) becomes

$$w_n(r)=\left(\frac{r}{R}\right)^{|n|}\left(g_n-v_n(R)\right),\ 0<r<R.$$

The notations of domain Ω will be introduced as

$${}_0\Omega_r \quad =B(0;r),$$

$${}_{r-\varepsilon}\Omega_{r+\varepsilon}=B(0;r+\varepsilon)\setminus B(0;r-\varepsilon),$$

$${}_r\Omega_1 \quad =B(0;1)\setminus B(0;r).$$

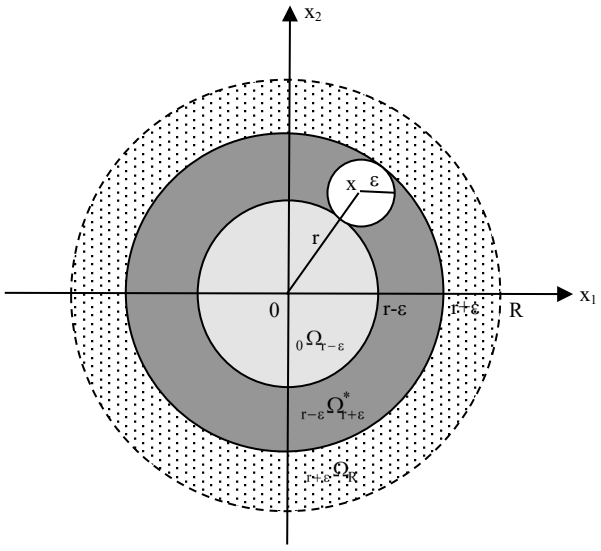

Fig. 1. Domain discretization

Using these notations for $x=re^{i\theta}$, (5) can be written as

$$\begin{aligned}v(x)&=\frac{1}{2\pi}\lim_{\varepsilon\to0}\int_{\Omega\setminus B(x;\varepsilon)}f(\xi)\ln|x-\xi|\,d\xi\\&=\frac{1}{2\pi}\lim_{\varepsilon\to0}\Bigg[\int_{{}_0\Omega_{r-\varepsilon}}f(\xi)\ln|x-\xi|\,d\xi+\\&\int_{r-\varepsilon\Omega^*_{r+\varepsilon}}f(\xi)\ln|x-\xi|\,d\xi+\int_{r+\varepsilon\Omega_R}f(\xi)\ln|x-\xi|\,d\xi\Bigg],\end{aligned}$$

where ${}_{r-\varepsilon}\Omega^*_{r+\varepsilon}={}_{r-\varepsilon}\Omega_{r+\varepsilon}\setminus B(x;\varepsilon).$

The Fourier decomposition is given by

$$\begin{aligned}v_n(r)&=\frac{1}{4\pi^2}\int_{{}_0\Omega_r}f(\xi)\int_0^{2\pi}\ln|x-\xi|\,e^{-in\theta}d\theta d\xi\\&+\frac{1}{2\pi}\int_0^{2\pi}\left(\frac{1}{2\pi}\lim_{\varepsilon\to0}I_\varepsilon\right)e^{-in\theta}d\theta\\&+\frac{1}{4\pi^2}\int_{{}_r\Omega_R}f(\xi)\int_0^{2\pi}\ln|x-\xi|\,e^{-in\theta}d\theta d\xi,\end{aligned}$$

where $I_\varepsilon=\int_{r-\varepsilon\Omega^*_{r+\varepsilon}}f(\xi)\ln|x-\xi|\,d\xi.$

Since

$$|I_\varepsilon| \le \sup_{\xi\in_{r-\varepsilon}\Omega^*_{r+\varepsilon}} |f(\xi)| \sup_{\xi\in_{r-\varepsilon}\Omega^*_{r+\varepsilon}} |\ln|x-\xi|\,|\,\pi\left((r+\varepsilon)^2-(r-\varepsilon)^2\right)$$
$$\le \sup_{\xi\in_{r-\varepsilon}\Omega^*_{r+\varepsilon}} |f(\xi)|\,4\pi r\varepsilon\left|\ln|\varepsilon|\right|,$$

we obtain $\lim_{\varepsilon\to 0}|I_\varepsilon| = 0$. If $\xi = \sigma e^{i\beta}$ and $\alpha = \theta - \beta$, then

$$v_n(r) = \frac{1}{2\pi}\Big[\int_0^r\int_0^{2\pi}\sigma\, f(\sigma,\beta)e^{-in\beta}\left(\frac{1}{2\pi}\int_{-\beta}^{2\pi-\beta}\ln|x-\xi|\,e^{-in\alpha}d\alpha\right)d\beta d\sigma\Big]$$
$$+\frac{1}{2\pi}\Big[\int_r^R\int_0^{2\pi}\sigma\, f(\sigma,\beta)e^{-in\beta}\left(\frac{1}{2\pi}\int_{-\beta}^{2\pi-\beta}\ln|x-\xi|\,e^{-in\alpha}d\alpha\right)d\beta d\sigma\Big]. \quad (15)$$

Letting $\tilde{G}(r;\sigma,\alpha) = \ln|x-\xi| = \ln\left|r^2+\sigma^2-2r\sigma\cos\alpha\right|^{1/2}$, (15) becomes

$$v_n(r) = \frac{1}{2\pi}\left[\int_0^r\int_0^{2\pi}\sigma f(\sigma,\beta)e^{-in\beta}\tilde{G}_n(r;\sigma)d\beta d\sigma\right]$$
$$+\frac{1}{2\pi}\left[\int_r^R\int_0^{2\pi}\sigma\, f(\sigma,\beta)e^{-in\beta}\tilde{G}_n(r;\sigma)d\beta d\sigma\right]$$
$$= \int_0^r f_n(\sigma)\tilde{G}_n(r;\sigma)\sigma\, d\sigma$$
$$+\int_r^R f_n(\sigma)\tilde{G}_n(r;\sigma)\sigma\, d\sigma,\ 0\le r<R, \quad (16)$$

where f_n and $\tilde{G}_n$ are the nth Fourier coefficients of f and $\tilde{G}$, respectively [1], [3].

We define $\zeta = \frac{\sigma}{r}e^{-i\alpha}$ for $r > \sigma$ and $\eta = \frac{r}{\sigma}e^{i\alpha}$ for $r < \sigma$.

$$\tilde{G}(r;\sigma,\alpha) = \ln\left|(r-\sigma\cos\alpha)^2+\sigma^2\sin^2\alpha\right|^{\frac{1}{2}}$$
$$= \ln\left|r-\sigma(\cos\alpha - i\sin\alpha)\right|$$
$$= \ln\left(r\left|1-\frac{\sigma}{r}e^{-i\alpha}\right|\right)$$
$$= \ln r + \ln|1-\zeta|.$$

Similarly, $\tilde{G}(r;\sigma,\alpha) = \ln\left|(\sigma-r\cos\alpha)^2+r^2\sin^2\alpha\right|^{\frac{1}{2}}$

$$= \ln\left|\sigma-r(\cos\alpha+i\sin\alpha)\right|$$
$$= \ln\left(\sigma\left|1-\frac{r}{\sigma}e^{i\alpha}\right|\right)$$
$$= \ln\sigma + \ln|1-\eta|.$$

Furthermore, for $r > \sigma$, we have $|\zeta| < 1$ and

$$\ln|1-\zeta| = \frac{1}{2}\left[\ln(1-\zeta)+\ln(1-\bar{\zeta})\right]$$
$$= \frac{1}{2}\left(-\sum_{n=1}^{\infty}\frac{\zeta^n}{n}-\sum_{n=1}^{\infty}\frac{\bar{\zeta}^n}{n}\right)$$
$$= -\sum_{n=1}^{\infty}\frac{1}{2n}\left(\frac{\sigma}{r}\right)^n\left(e^{-in\alpha}+e^{in\alpha}\right)$$
$$= -\sum_{0\ne n=-\infty}^{\infty}\frac{1}{2|n|}\left(\frac{\sigma}{r}\right)^{|n|}e^{in\alpha}.$$

Similarly, for $r < \sigma$, we have $|\eta| < 1$ and

$$\ln|1-\eta| = -\sum_{0\ne n=-\infty}^{\infty}\frac{1}{2|n|}\left(\frac{r}{\sigma}\right)^{|n|}e^{in\alpha}.$$

Therefore,

$$\tilde{G}(r;\sigma,\alpha) = \begin{cases}\ln r - \sum_{0\ne n=-\infty}^{\infty}\frac{1}{2|n|}\left(\frac{\sigma}{r}\right)^{|n|}e^{in\alpha}, & r>\sigma,\\ \ln\sigma - \sum_{0\ne n=-\infty}^{\infty}\frac{1}{2|n|}\left(\frac{r}{\sigma}\right)^{|n|}e^{in\alpha}, & r<\sigma.\end{cases} \quad (17)$$

Using (17), (16) can be written as

$$v_n(r) = \int_0^r p_n(r;\sigma)d\sigma + \int_r^R q_n(r;\sigma)d\sigma,$$

where $p_n(r;\sigma) = \begin{cases}\sigma\ln r\, f_0(\sigma), & n=0,\\ \frac{-\sigma}{2|n|}\left(\frac{\sigma}{r}\right)^{|n|}f_n(\sigma), & n\ne 0,\end{cases}$

and $q_n(r;\sigma) = \begin{cases}\sigma\ln\sigma\, f_0(\sigma), & n=0,\\ \frac{-\sigma}{2|n|}\left(\frac{r}{\sigma}\right)^{|n|}f_n(\sigma), & n\ne 0.\end{cases}$

Hence, the Fourier coefficients $u_n(r)$ of $u(r,.)$ are [3]

$$u_n(r) = v_n(r) + w_n(r)$$
$$= v_n(r) + \left(\frac{r}{R}\right)^{|n|}(g_n - v_n(R)),\ 0<r<R.$$

The above theorem follows from (7) and (9) that $v_n(0) = 0$ for $n \ne 0$, [2].

II. Fourier Coefficients for the Discretized Problem

The strength of the previous theorem is evident when considering the disk $\overline{B(0;R)}$ discretized by $M\times N$ lattice points with M distinct points in the radial direction and N equidistant points in the angular direction. Let $0 = r_0 < r_1 < r_2 < \ldots < r_M = R$ be the radii defined on the discretization [2], [3].

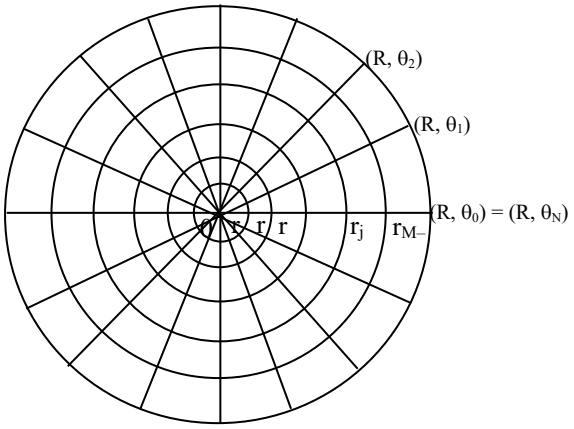

Fig. 2. Discretization of domain in radial and angular directions

Use of the previous theorem in constructing an efficient algorithm requires the following theorem.

A. Theorem

Let $0 = r_0 < r_1 < r_2 < \ldots < r_M = R$, and

$$C_n^{m,j} = \int_{r_m}^{r_j} \frac{\sigma}{2n}\left(\frac{r_j}{\sigma}\right)^n f_n(\sigma)d\sigma, \quad n < 0, \tag{18}$$

$$D_n^{m,j} = -\int_{r_m}^{r_j} \frac{\sigma}{2n}\left(\frac{r_m}{\sigma}\right)^n f_n(\sigma)d\sigma, \quad n > 0. \tag{19}$$

We define, for $n < 0$,

$$\begin{aligned} &v_n^-(r_0) = 0, \\ &v_n^-(r_j) = \left(\frac{r_j}{r_{j-1}}\right)^n v_n^-(r_{j-1}) + C_n^{j-1,j}, \quad j = 1,2,3,\ldots,M, \end{aligned} \tag{20}$$

and, for $n > 0$,

$$\begin{aligned} &v_n^+(r_M) = 0, \\ &v_n^+(r_j) = \left(\frac{r_j}{r_{j+1}}\right)^n v_n^+(r_{j+1}) + D_n^{j,j+1}, \\ &\qquad j = M-1, M-2, \ldots, 0. \end{aligned} \tag{21}$$

Then, for $j = 0,1,\ldots,M$ we have

$$v_n(r_j) = \begin{cases} v_n^-(r_j) + \overline{v_{-n}^+(r_j)}, & n < 0, \\ v_n^+(r_j) + \overline{v_{-n}^-(r_j)}, & n > 0. \end{cases} \tag{22}$$

Proof

If $n < 0$, (20) implies

$$\begin{aligned} v_n^-(r_j) &= \left(\frac{r_j}{r_{j-1}}\right)^n \left[\left(\frac{r_{j-1}}{r_{j-2}}\right)^n v_n^-(r_{j-2}) + C_n^{j-2,j-1}\right] + C_n^{j-1,j} \\ &= \left(\frac{r_j}{r_{j-2}}\right)^n v_n^-(r_{j-2}) + \left(\frac{r_j}{r_{j-1}}\right)^n C_n^{j-2,j-1} + C_n^{j-1,j} \\ &= \left(\frac{r_j}{r_{j-2}}\right)^n \left[\left(\frac{r_{j-2}}{r_{j-3}}\right)^n v_n^-(r_{j-3}) + C_n^{j-3,j-2}\right] + \left(\frac{r_j}{r_{j-1}}\right)^n C_n^{j-2,j-1} + C_n^{j-1,j} \\ &\vdots \\ &= \left(\frac{r_j}{r_0}\right)^n v_n^-(r_0) + \left(\frac{r_j}{r_1}\right)^n C_n^{0,1} + \left(\frac{r_j}{r_2}\right)^n C_n^{1,2} + \cdots \\ &\qquad + \left(\frac{r_j}{r_{j-1}}\right)^n C_n^{j-2,j-1} + C_n^{j-1,j} \\ &= \left(\frac{r_j}{r_1}\right)^n \int_{r_0}^{r_1} \frac{\sigma}{2n}\left(\frac{r_1}{\sigma}\right)^n f_n(\sigma)d\sigma + \left(\frac{r_j}{r_2}\right)^n \int_{r_1}^{r_2} \frac{\sigma}{2n}\left(\frac{r_2}{\sigma}\right)^n f_n(\sigma)d\sigma + \cdots \\ &\quad + \left(\frac{r_j}{r_{j-1}}\right)^n \int_{r_{j-2}}^{r_{j-1}} \frac{\sigma}{2n}\left(\frac{r_{j-1}}{\sigma}\right)^n f_n(\sigma)d\sigma + \int_{r_{j-1}}^{r_j} \frac{\sigma}{2n}\left(\frac{r_j}{\sigma}\right)^n f_n(\sigma)d\sigma \\ &= \int_0^{r_j} \frac{\sigma}{2n}\left(\frac{r_j}{\sigma}\right)^n f_n(\sigma)d\sigma. \end{aligned} \tag{23}$$

If $n > 0$, (21) implies

$$\begin{aligned} v_n^+(r_j) &= \left(\frac{r_j}{r_{j+1}}\right)^n \left[\left(\frac{r_{j+1}}{r_{j+2}}\right)^n v_n^+(r_{j+2}) + D_n^{j+1,j+2}\right] + D_n^{j,j+1} \\ &= \left(\frac{r_j}{r_{j+2}}\right)^n v_n^+(r_{j+2}) + \left(\frac{r_j}{r_{j+1}}\right)^n D_n^{j+1,j+2} + D_n^{j,j+1} \\ &= \left(\frac{r_j}{r_{j+2}}\right)^n \left[\left(\frac{r_{j+2}}{r_{j+3}}\right)^n v_n^+(r_{j+3}) + D_n^{j+2,j+3}\right] + \left(\frac{r_j}{r_{j+1}}\right)^n D_n^{j+1,j+2} + D_n^{j,j+1} \\ &\vdots \\ &= \left(\frac{r_j}{r_M}\right)^n v_n^+(r_M) + \left(\frac{r_j}{r_{M-1}}\right)^n D_n^{M-1,M} \\ &\quad + \left(\frac{r_j}{r_{M-2}}\right)^n D_n^{M-2,M-1} + \cdots + \left(\frac{r_j}{r_{j+1}}\right)^n D_n^{j+1,j+2} + D_n^{j,j+1} \\ &= \left(\frac{r_j}{r_{M-1}}\right)^n \int_{r_{M-1}}^{r_M} \frac{\sigma}{2n}\left(\frac{r_{M-1}}{\sigma}\right)^n f_n(\sigma)d\sigma \\ &\quad - \left(\frac{r_j}{r_{M-2}}\right)^n \int_{r_{M-2}}^{r_{M-1}} \frac{\sigma}{2n}\left(\frac{r_{M-2}}{\sigma}\right)^n f_n(\sigma)d\sigma - \cdots \\ &\quad - \left(\frac{r_j}{r_{j+1}}\right)^n \int_{r_{j+1}}^{r_{j+2}} \frac{\sigma}{2n}\left(\frac{r_{j+1}}{\sigma}\right)^n f_n(\sigma)d\sigma - \int_{r_j}^{r_{j+1}} \frac{\sigma}{2n}\left(\frac{r_j}{\sigma}\right)^n f_n(\sigma)d\sigma \\ &= -\int_{r_j}^{R} \frac{\sigma}{2n}\left(\frac{r_j}{\sigma}\right)^n f_n(\sigma)d\sigma. \end{aligned} \tag{24}$$

From (7), we have

$$v_n(r) = \begin{cases} \int_0^r \frac{\sigma}{2n}\left(\frac{r}{\sigma}\right)^n f_n(\sigma)d\sigma + \\ \quad \int_r^R \frac{\sigma}{2n}\left(\frac{\sigma}{r}\right)^n f_n(\sigma)d\sigma, & n < 0, \\ \int_0^r \frac{-\sigma}{2n}\left(\frac{\sigma}{r}\right)^n f_n(\sigma)d\sigma + \\ \quad \int_r^R \frac{-\sigma}{2n}\left(\frac{r}{\sigma}\right)^n f_n(\sigma)d\sigma, & n > 0. \end{cases} \tag{25}$$

Substituting (23) into (25) for $n < 0$, we get

$$\begin{aligned} v_n(r_j) &= v_n^-(r_j) + \int_{r_j}^{R} \frac{\sigma}{2n}\left(\frac{\sigma}{r_j}\right)^n f_n(\sigma)d\sigma \\ &= v_n^-(r_j) - \int_{r_j}^{R} \frac{\sigma}{-2n}\left(\frac{r_j}{\sigma}\right)^{-n} \overline{f_{-n}(\sigma)}\, d\sigma (\text{where } f_n = \overline{f_{-n}}) \\ &= v_n^-(r_j) + \overline{v_{-n}^+(r_j)} \end{aligned}$$

Substituting (24) into (25) for $n > 0$, we get

$$\begin{aligned} v_n(r_j) &= \int_0^{r_j} \frac{-\sigma}{2n}\left(\frac{\sigma}{r_j}\right)^n f_n(\sigma)d\sigma + v_n^+(r_j) \\ &= \int_0^{r_j} \frac{\sigma}{-2n}\left(\frac{r_j}{\sigma}\right)^{-n} \overline{f_{-n}(\sigma)}\, d\sigma + v_n^+(r_j) \\ &= \overline{v_{-n}^-(r_j)} + v_n^+(r_j). \end{aligned}$$

B. Corollary

Let $0 = r_0 < r_1 < r_2 < \ldots < r_M = R$, and

$$C_0^{m,j} = \int_{r_m}^{r_j} \sigma f_0(\sigma)d\sigma \text{ and } D_0^{m,j} = \int_{r_m}^{r_j} \sigma \ln \sigma f_0(\sigma)d\sigma, \qquad (26)$$

then for $\ell = 1, 2, \ldots, M$, we have

$$v_n(r_\ell) = \begin{cases} \ln r_\ell \sum_{j=1}^{\ell} C_0^{j-1,j} + \sum_{j=\ell}^{M-1} D_0^{j,j+1} & \text{, for } n = 0, \\ \sum_{j=1}^{\ell}\left(\frac{r_\ell}{r_j}\right)^n C_n^{j-1,j} + \sum_{j=\ell}^{M-1}\left(\frac{r_j}{r_\ell}\right)^n \overline{D_{-n}^{j,j+1}}, & \text{for } n < 0, \\ \sum_{j=\ell}^{M-1}\left(\frac{r_\ell}{r_j}\right)^n D_n^{j,j+1} + \sum_{j=1}^{\ell}\left(\frac{r_j}{r_\ell}\right)^n \overline{C_{-n}^{j-1,j}}, & \text{for } n > 0. \end{cases} \qquad (27)$$

Proof

When $n = 0$, by using (26) we get

$$\begin{aligned} \sum_{j=1}^{\ell} C_0^{j-1,j} &= \int_{r_0}^{r_1} \sigma f_0(\sigma)d\sigma + \int_{r_1}^{r_2} \sigma\, f_0(\sigma)d\sigma + \cdots + \int_{r_{\ell-1}}^{r_\ell} \sigma f_0(\sigma)d\sigma \\ &= \int_0^{r_\ell} \sigma f_0(\sigma)d\sigma \end{aligned}$$

and

$$\begin{aligned} \sum_{j=\ell}^{M-1} D_0^{j,j+1} &= \int_{r_\ell}^{r_{\ell+1}} \sigma \ln \sigma\, f_0(\sigma)d\sigma + \int_{r_{\ell+1}}^{r_{\ell+2}} \sigma \ln \sigma f_0(\sigma)d\sigma + \cdots \\ &\quad + \int_{r_{M-1}}^{r_M} \sigma \ln \sigma f_0(\sigma)d\sigma \\ &= \int_{r_\ell}^{R} \sigma \ln \sigma f_0(\sigma)d\sigma \end{aligned}$$

By (7),

$$\begin{aligned} v_0(r_\ell) &= \int_0^{r_\ell} \sigma\, \ln r_\ell\, f_0(\sigma)d\sigma + \int_{r_\ell}^{R} \sigma \ln \sigma\, f_0(\sigma)d\sigma \\ &= \ln r_\ell \sum_{j=1}^{\ell} C_0^{j-1,j} + \sum_{j=\ell}^{M-1} D_0^{j,j+1}. \end{aligned}$$

When $n < 0$, by using (18) and (23) we get

$$\begin{aligned} \sum_{j=1}^{\ell}\left(\frac{r_\ell}{r_j}\right)^n C_n^{j-1,j} &= \left(\frac{r_\ell}{r_1}\right)^n \int_{r_0}^{r_1} \frac{\sigma}{2n}\left(\frac{r_1}{\sigma}\right)^n f_n(\sigma)d\sigma + \\ &\quad \left(\frac{r_\ell}{r_2}\right)^n \int_{r_1}^{r_2} \frac{\sigma}{2n}\left(\frac{r_2}{\sigma}\right)^n f_n(\sigma)d\sigma + \cdots \\ &\quad + \left(\frac{r_\ell}{r_\ell}\right)^n \int_{r_{\ell-1}}^{r_\ell} \frac{\sigma}{2n}\left(\frac{r_\ell}{\sigma}\right)^n f_n(\sigma)d\sigma \\ &= \int_0^{r_\ell} \frac{\sigma}{2n}\left(\frac{r_\ell}{\sigma}\right)^n f_n(\sigma)d\sigma \\ &= v_n^-(r_\ell). \end{aligned}$$

If we use (19) and (24), we get

$$\begin{aligned} \sum_{j=\ell}^{M-1}\left(\frac{r_j}{r_\ell}\right)^n \overline{D_{-n}^{j,j+1}} &= -\left(\frac{r_\ell}{r_\ell}\right)^n \int_{r_\ell}^{r_{\ell+1}} \frac{\sigma}{-2n}\left(\frac{r_\ell}{\sigma}\right)^{-n} \overline{f_{-n}(\sigma)}\, d\sigma \\ &\quad -\left(\frac{r_{\ell+1}}{r_\ell}\right)^n \int_{r_{\ell+1}}^{r_{\ell+2}} \frac{\sigma}{-2n}\left(\frac{r_{\ell+1}}{\sigma}\right)^{-n} \overline{f_{-n}(\sigma)}\, d\sigma - \cdots \\ &\quad -\left(\frac{r_{M-1}}{r_\ell}\right)^n \int_{r_{M-1}}^{r_M} \frac{\sigma}{-2n}\left(\frac{r_{M-1}}{\sigma}\right)^{-n} \overline{f_{-n}(\sigma)}\, d\sigma \\ &= -\int_{r_\ell}^{R} \frac{\sigma}{-2n}\left(\frac{r_\ell}{\sigma}\right)^{-n} \overline{f_{-n}(\sigma)}\, d\sigma \\ &= \overline{v_{-n}^+(r_\ell)}. \end{aligned}$$

According to the first term of (22), we have

$$\begin{aligned} v_n(r_\ell) &= v_n^-(r_\ell) + \overline{v_{-n}^+(r_\ell)} \\ &= \sum_{j=1}^{\ell}\left(\frac{r_\ell}{r_j}\right)^n C_n^{j-1,j} + \sum_{j=\ell}^{M-1}\left(\frac{r_j}{r_\ell}\right)^n \overline{D_{-n}^{j,j+1}}, \text{ for } n < 0. \end{aligned}$$

When $n > 0$, by using (19) and (24), we get

$$\begin{aligned} \sum_{j=\ell}^{M-1}\left(\frac{r_j}{r_\ell}\right)^n D_n^{j,j+1} &= -\left(\frac{r_\ell}{r_\ell}\right)^n \int_{r_\ell}^{r_{\ell+1}} \frac{\sigma}{2n}\left(\frac{r_\ell}{\sigma}\right)^n f_n(\sigma)d\sigma \\ &\quad -\left(\frac{r_\ell}{r_{\ell+1}}\right)^n \int_{r_{\ell+1}}^{r_{\ell+2}} \frac{\sigma}{2n}\left(\frac{r_{\ell+1}}{\sigma}\right)^n f_n(\sigma)d\sigma \\ &\quad -\cdots -\left(\frac{r_\ell}{r_{M-1}}\right)^n \int_{r_{M-1}}^{r_M} \frac{\sigma}{2n}\left(\frac{r_{M-1}}{\sigma}\right)^n f_n(\sigma)d\sigma \\ &= -\int_{r_\ell}^{R} \frac{\sigma}{2n}\left(\frac{r_\ell}{\sigma}\right)^n f_n(\sigma)d\sigma \\ &= v_n^+(r_\ell). \end{aligned}$$

If we use (18) and (23), we get

$$\sum_{j=1}^{\ell}\left(\frac{r_j}{r_\ell}\right)^n \overline{C_{-n}^{j-1,j}} = \left(\frac{r_1}{r_\ell}\right)^n \int_{r_0}^{r_1} \frac{\sigma}{-2n}\left(\frac{r_1}{\sigma}\right)^{-n} \overline{f_{-n}(\sigma)}d\sigma + \left(\frac{r_2}{r_\ell}\right)^n \int_{r_1}^{r_2} \frac{\sigma}{-2n}\left(\frac{r_2}{\sigma}\right)^{-n} \overline{f_{-n}(\sigma)}d\sigma + \cdots + \left(\frac{r_\ell}{r_\ell}\right)^n \int_{r_{\ell-1}}^{r_\ell} \frac{\sigma}{-2n}\left(\frac{r_\ell}{\sigma}\right)^{-n} \overline{f_{-n}(\sigma)}d\sigma$$

$$= \int_0^{r_\ell} \frac{\sigma}{-2n}\left(\frac{r_\ell}{\sigma}\right)^{-n} \overline{f_{-n}(\sigma)}\,d\sigma = \overline{v_{-n}^-(r_\ell)}.$$

According to the last term of (22), we have

$$v_n(r_\ell) = v_n^+(r_\ell) + \overline{v_{-n}^-(r_\ell)} = \sum_{j=\ell}^{M-1}\left(\frac{r_\ell}{r_j}\right)^n D_n^{j,j+1} + \sum_{j=1}^{\ell}\left(\frac{r_j}{r_\ell}\right)^n \overline{C_{-n}^{j-1,j}},\ \text{for } n > 0, [1].$$

III. A Sequential Algorithm for Dirichlet Problem on a Thin Plate (Disk)

In this section, we describe an algorithm which requires the radial one- dimensional integrals $C_n^{j,j+1}$ and $D_n^{j,j+1}$ to be calculated between two successive points on a given radial direction, and it is as follow [1].

Given M, N, $0 = r_0 < r_1 < r_2 < \ldots < r_M = R$, $\theta_k = \frac{2\pi}{N}k$, the grid values $f(r_j e^{i\theta_k})$ and the boundary conditions $g(Re^{\frac{2\pi}{N}ki})$, $0 \le j \le M$, and $1 \le k \le N$, the algorithm gives the values $u(r_j e^{\frac{2\pi}{N}ki})$ of the solution for (1) and (2).

Step 1. Compute the Fourier coefficients $f_n(r_j)$, $n \in [-\frac{N}{2}, \frac{N}{2}]$, for M sets of data at $0 \le j \le M$, and the Fourier coefficients g_n on $\partial\Omega$.

Step 2. For $0 \le j \le M-1$, compute the radial one-dimensional integrals $C_n^{j,j+1}$, $n \in [-\frac{N}{2}, 0]$ as defined in (18) and (26); and compute $D_n^{j,j+1}$, $n \in [0, \frac{N}{2}]$ as defined in (19) and (26).

Step 3. Compute coefficients $v_n^-(r_j)$ for each of the negative modes $n \in [-\frac{N}{2}, 0]$ as defined in (20) and (27):

(a) Set $v_n^-(r_0) = 0$.

(b) For j = 1, …, M, $v_n^-(r_j) = \left(\frac{r_j}{r_{j-1}}\right)^n v_n^-(r_{j-1}) + C_n^{j-1,j}$.

Step 4. Compute coefficients $v_n^+(r_j)$ for each of the positive modes $n \in [0, \frac{N}{2}]$ as defined in (21) and (27):

(a) Set $v_n^+(r_M) = 0$.

(b) For $j = M-1, \ldots, 0$, $v_n^+(r_j) = \left(\frac{r_j}{r_{j+1}}\right)^n v_n^+(r_{j+1}) + D_n^{j,j+1}$.

Step 5. Combine coefficients v_n^+ and v_n^- as defined in (22) and (27). For j=1,2,…, M,

$$v_0(r_j) = \ln r_j\, v_0^-(r_j) + v_0^+(r_j).$$

$$v_n(r_j) = \overline{v_{-n}(r_j)} = v_n^-(r_j) + \overline{v_{-n}^+(r_j)},\quad n \in [-\frac{N}{2}, -1].$$

Step 6. Apply the boundary conditions as defined in (6). For j=1,2,…, M,

$$u_n(r_j) = v_n(r_j) + \left(\frac{r_j}{R}\right)^{|n|}(g_n - v_n(R)),\ n \in [-\frac{N}{2}, \frac{N}{2}].$$

Step 7. Compute $u(r_j e^{i\theta_k}) = \sum_{n=-\frac{N}{2}}^{\frac{N}{2}} u_n(r_j)e^{i\theta_k}$, $1 \le k \le N$, for each radius r_j, $1 \le j \le M$.

IV. Numerical Example

In this section, example is presented for Dirichlet problem associated with Poisson equation using Matlab programming [4].

We will consider Poisson equation with Dirichlet boundary value on a disk $\Omega = \{(r,\theta) | r < 1, 0 \le \theta \le 2\pi\}$ as

$$\Delta u = \frac{1}{r} - \frac{3}{r}\cos 2\theta \quad \text{in } \Omega \qquad (28)$$

and $$u(1,\theta) = \cos 2\theta + 1.1. \qquad (29)$$

The exact solution is $u(r,\theta) = r(1+\cos 2\theta) + 0.1$ and Fourier coefficients $f_n(r)$ of $f(r,\theta) = \frac{1}{r} - \frac{3}{r}\cos 2\theta$ are

$$f_n(r) = \begin{cases} \frac{1}{r} & \text{for } n = 0, \\ -\frac{3}{2r} & \text{for } n = \pm 2, \\ 0 & \text{otherwise.} \end{cases}$$

The Fourier coefficients g_n of $g(\theta) = \cos 2\theta + 1.1$ are

$$g_n = \begin{cases} 1.1 & \text{for } n = 0, \\ 0.5 & \text{for } n = \pm 2, \\ 0 & \text{otherwise.} \end{cases}$$

We take M=32, $\delta r = \frac{1}{32}$, $r_j = j\delta r$, $j = 1,2,...,M$ and N=32, $\delta\theta = \frac{2\pi}{N} = \frac{2\pi}{32} = \frac{\pi}{16}$, $\theta_k = \frac{2\pi}{N}k$, $k = 1,2,...,N$.

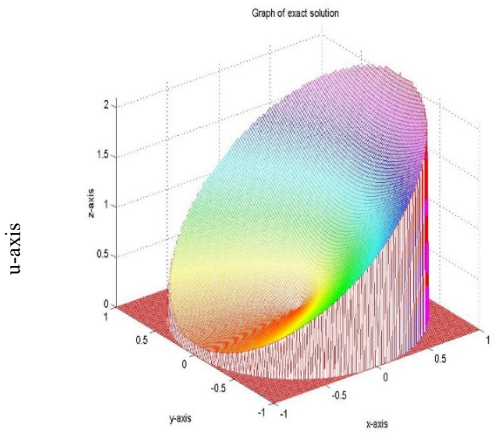

Fig. 3. Graph of exact solution of Dirichlet problem

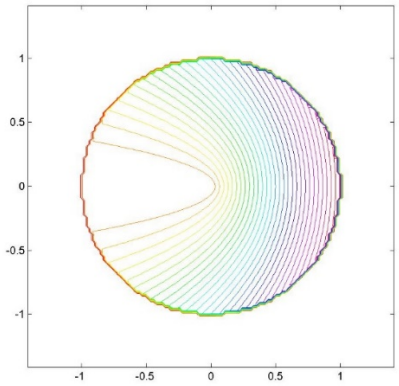

Fig. 4. Contour of exact solution of Dirichlet problem

By using step by step of sequential algorithm, numerical solution of (28) with Dirichlet conduction (29) will be obtained. Here, for $1 \le j \le M$ and $1 \le k \le N$, various use of number of grid points (power of two) M and N will give many numerical solutions.

Then, denoting by u the exact solution and by U the computed solution, the maximum error is

$$\max_{j,k} \left| U(r_j, \theta_k) - u(r_j, \theta_k) \right|,$$

over the $N(M-1)$ points (that is, $1 \le j \le M-1$, $1 \le k \le N$) in the domain.

Now, to know the accuracy of the method, maximum errors of Dirichlet problem (28)-(29) are calculated using Matlab programming as shown in following table.

TABLE I. MAXIMUM ERRORS OF SOLUTION OF POISSON EQUATION (28) WITH DIRICHLET CONDUCTION (29)

(M , N)	maximum error
(32 , 32)	3.20 E-03
(64 , 64)	4.42 E-04
(128 , 128)	2.89 E-05
(256 , 256)	7.28 E-06

By viewing the maximum errors, one can say that using more number of grid points M and N gives smaller than the maximum error. And since obtained maximum errors are very small, we can conclude that the method is accurate.

V. CONCLUSIONS

In fact, in the algorithm using Green's function method, the solution of Poisson equation is expressed in terms of Fourier series by deriving radius-dependent Fourier coefficients. These Fourier coefficients can be obtained by recursive relations which only utilize one-dimensional integrals in the radial directions of the domain. In future, we can survey three-dimensional elliptic equation (for example ellipsoid) using the numerical method (Green's function method) based on Fourier series.

There are many everyday purposes for Poisson equation. Applications of Poisson equation are surveying, navigation, metrology, astrometry, binocular vision, modern rocketry and gun direction of weapons. Poisson equation is also applied in fluid dynamics for computing pressure field when velocity field is known. For example, in a numerical iterative algorithm one computes velocity field from Navier-Stokes equations, then it can be computed pressure by Poisson equation.

ACKNOWLEDGMENT

I am grateful to the journal committee and the editorial board for permitting the submission of this paper.

I would like to deepest thanks to my father for his kind-help and encouragement.

REFERENCES

[1] T. M. U, *Partial differential equations of mathematical physics*. New York: American Elsevier Pub. Co, 1973.
[2] L. Borges and P. Daripa, "A Fast Parallel Algorithm for the Poisson Equation on a Disk," *J. Comput. Phys.*, vol. 169, no. 1, pp. 151–192, May 2001.
[3] R. Bracewell, "The Fourier Transform and Its Applications," 1965.
[4] J. Cooper, *Introduction to Partial Differential Equations with MATLAB*. Birkhäuser Basel, 1998.

Article ID – JRA6002020

Correlation Analysis among Water Quality Parameters of Water Sources in Kayin State, Myanmar

Shwe Sin Oo
Department of Physics
Panglong University
Myanmar
77floralshwesin@gmail.com

Nyein Thida
Department of Physics
University of Yangon
Myanmar
nyein151270@gmail.com

Mu Mu Win
Department of Physics
Dagon University
Myanmar
mumuwin2002@gmail.com

***Abstract*- This paper aims to determine the water quality of both surface water and ground water sources in two Districts of Kayin State, lower Myanmar to help the decision maker while implementing a scientifically pretty water quality management plan to improve smoothly. Three water samples from various water sources were collected and made a laboratory analysis for physico-chemical parameters like pH, electrical conductivity (EC), turbidity, hardness, total dissolved solids (TDS) and alkalinity, metal such as cadmium, lead, copper, zinc, potassium, sodium and calcium using World Health Organization (WHO) and the Bureau of Indian Standards (BIS). Correlation coefficients (r) were analyzed Pearson correlation method to develop mathematical relationship between different physical and chemical parameters and water quality indices (WQIs) were determined using measured results obtained from two laboratories, Yangon. WQI was found to be 138.782 for sample-1 and 109.188 for sample-2 but 27.014 for sample-3. Based on the experimental results and water quality indices (WQIs), two sampling stations in study area were found to be unfit for drinking purpose in accordance with the rating of water quality. However, water from sampling station-3 was good for drinking and domestic uses.**

Keywords: Correlation coefficients, Water *Quality Indices (WQIs), physico -chemical parameters, metals concentration, water quality.*

I. INTRODUCTION

Water is essential for the survival of living beings and is an excellent indicator of environmental change. [6] In its purest form, water is odorless, colorless and tasteless. The various sources of water pose the greatest risk to human health due to contamination of solid and human waste, effluents from chemical industries and dissolved gases.

Drinking water is achieved from a variety of original water sources like different kinds of wells, rivers, streams, lakes, various sorts of reservoirs, ponds etc. Water pollutants mainly consist of heavy metals, micro- organisms, fertilizers and thousands of toxic organic compounds. The objective of this investigation is to discuss the suitability of water for the daily use of local people based on the physico-chemical data and metals' concentration with reference to drinking water standards, correlation coefficients and computed WQI values. Correlation coefficients between water parameters were determined statistically conducting Pearson correlation analysis in order to point the sources of contaminated substances and the nature of ground. The goal of water quality index (WQI) is valuable and effective to interpret the whole water quality status into a single indicator that is very useful to meet the concerned issues. Evaluation of WQI is one of the effective and efficient ways to address water quality. This investigation imagined and studied (i) to experimental measurement of some of the physico-chemical parameters and molarities of dissolved metals in sample water and compare with drinking water quality guidelines provided by WHO and the Bureau of Indian Standards (BIS),(ii) to evaluate the interrelationship of the water quality parameters using correlation coefficients (r) and (iii) to calculate WQIs for a preferable interpretation of water quality data to support a water quality management plan for the residences in this study area.

II. EXPERIMENT

The workflow of the entire study was shown in figure (1).

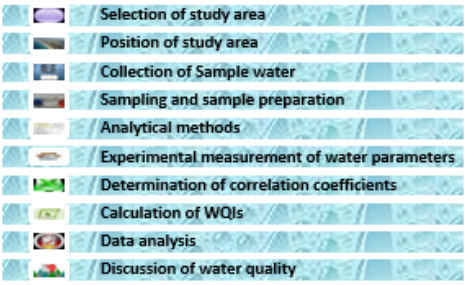

Fig 1. Procedures of water study.

A. Position of Study Area

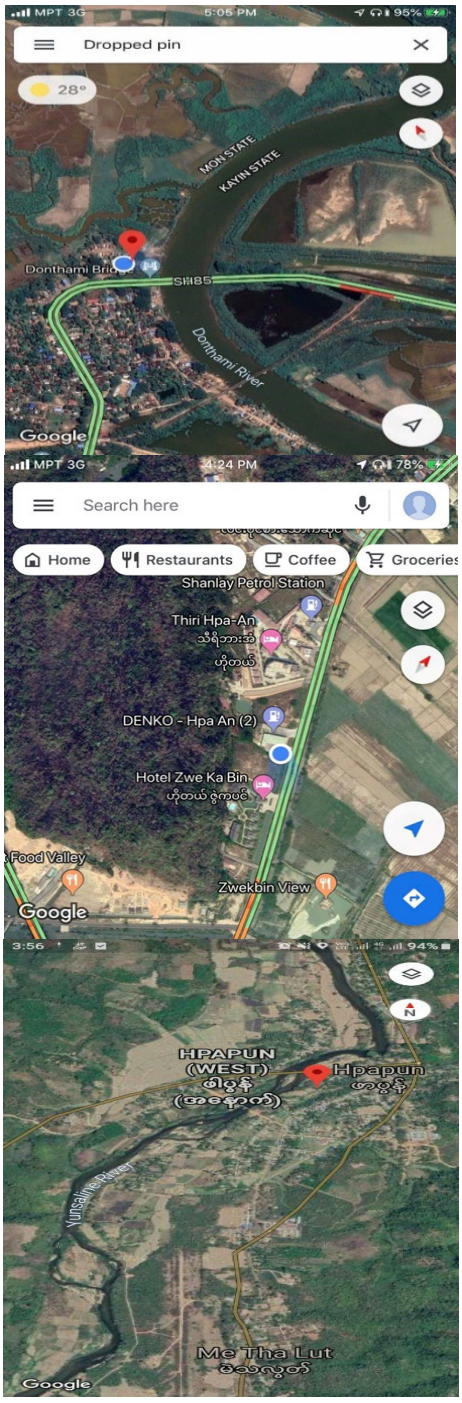

Fig 2. Map of study area.[4]

Donthami river at Hpa-an district and Yunsaline river at Hpapun district, Kayin State were chosen and then ground water sample was fetched from Denko Petrol Station (2) in Hpa-an Township, Hpa-an district. All study areas are situated in Kayin State, Lower Myanmar. Sample 1 (HS-1) was collected from Donthami river near Donthami bridge with GPS coordinates of 16˚ 58' 51" N 97˚ 26' 31"E, sample-2 (HS-2) was fetched from Denko Petrol Station (2) of 16˚ 52' 12" N 97˚ 39' 36"E and sample 3 (HS-3) was taken from Yunsaline river located across 18˚ 03' 38" N 97˚ 26' 17"E. [4] The study area has temperate weather as it is located in the low latitude zone. The sampling locations of study area have been presented in table-1 and displayed in figure-2.

TABLE I. DESCRIPTIONS OF SAMPLING STATIONS.

Sampling stations	Descriptions
HS-1	Water from Donthami river near Donthami bridge which flow in Thanlwin river. Most of the local people along river bank depend on this river water for various purposes. It is one kind of surface water . There are some villages, orchards and very little plantations.
HS-2	Water from drilled well which is 300 feet depth at Denko Hpa-an (2) petrol station in Hpa-an township. It is obtained from aquifer and so it's ground water. There are many trees and plantations around its surrounding. It is still used as drinking water and domestic uses.
HS-3	Water from Yunsaline river near Hpapun township. It's also surface water. There are many paddy fields, trees and rubber plantations. All the residences along river bank rely on this river for different purpose.

B. Experiment apparatus

B.1 Sampling and Sample Preparation

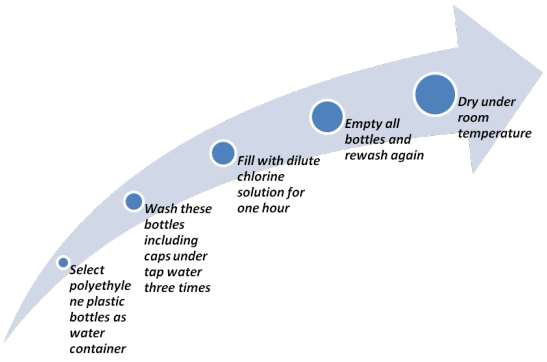

Fig 3. Sample preparation steps.

Water samples were collected from three sites in this study area and then brought into two laboratories for the measurement of various parameters to evaluate correlation coefficients (r) between water quality parameters and to compute WQI values of both surface and ground water in order to know the status of water quality. Water samples were collected from each site to assess it for a winter season of December, 2019. All water samples were collected in the evening hour from 5:00 to 6:00 pm using dry and sterile plastic bottle using the standard procedures. The water of all rivers and drilled well are used for drinking, domestic usage and agriculture.

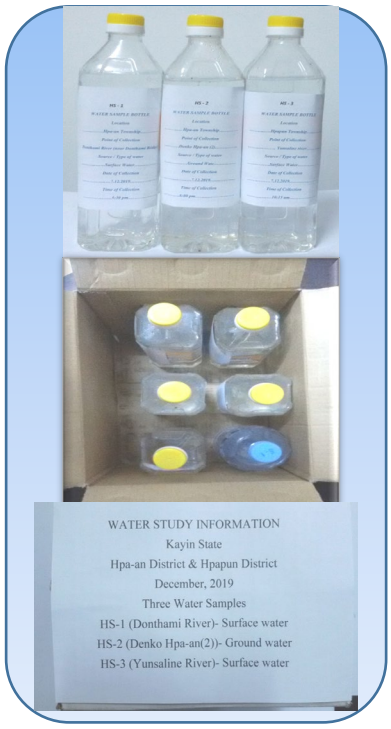

Fig 4. Sampling procedures.

Before collecting water sample, polyethylene plastic water bottles with caps were washed under the tap water and filled with 2 ml diluted chlorine water for one hour. And then, these bottles were slightly shaken and removed caps and made empty bottles. Water bottles and caps were rinsed under the flowing tap water until no foamed was seen. After that, three bottles including caps were rinsed with pure water. Finally, water sample bottles were dried at room temperature for a day. Before sampling, empty bottles were labeled with permanent marker not to rub off the written information. These dried bottles were packed with papers not to enter any effect including sunlight and brought to the area that is getting sample.

In getting sample water, water bubbles were not to be allowed during collecting water. After collecting water, bottles were screwed with caps immediately and tightly. Clean, dry and dark conditions must be needed throughout the transportation to the laboratory. Therefore, collected water sample bottles were put in a paper box, closed, and then labeled with sample information i.e. sample collection data as shown in figure (4). Finally, three sample water bottles were put to University Research Centre, University of Yangon and ALARM Ecological Laboratory situated at Kamayut Township. The total time for sampling and transportation was during 24 hours to obtain correct and definite values for water parameters.

B.2 Analytical Techniques

Turbidity and hardness were analyzed by spectro direct method using Lovibond Spectro Direct. Turbidity parameter was tested by Spectro Direct method No 385. The measurement of pH and electrical conductivity (EC) were done by HANNA HI 98129, 98130 water proof pH tester and EC tester. Testing the TDS was made using TDS meter by electrode method. For the analysis of metals, water samples were added with 2 ml HNO3 per one bottle to avoid the precipitation of metals at the bottom of sample bottles. Cadmium, lead, copper, zinc, potassium, sodium and calcium concentrations were determined by atomic absorption spectrometry method (AAS). Concentrations of (7) metals dissolved in sample water were measured using high-performance PinAAcle™ 900H S/N PHCS16091301 atomic absorption spectrometer instrument in the laboratory of URC at University of Yangon.

All the water quality parameters were analyzed according to standard methods for the examination of water and waste water in two laboratories, Yangon. Analyzed water parameters were distinguished into two parts namely heavy metals and physico-chemical parameters presented in figure (5).

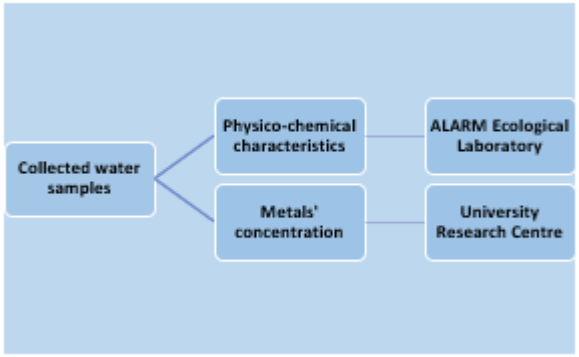

Fig 5. Procedures for sample analysis.

B.3 Statistical Analysis

Pearson correlation coefficients (r) for three water samples were determined to find the relationship between water quality parameters for the water's characteristics.[7] In computing WQI values, Weighted Arithmetic Index Method which was originally proposed by Horton (1965) and developed by Brown et al (1972) was used in this research paper. Standards of drinking water quality recommended by WHO which are universally accepted as the permissible values for the water-quality parameters are very important factors for all living things because the quality of water relates to the human health directly.

III. RESULT AND DISCUSSION

A. Physico-chemical parameters

Fresh water –bodies all over the world are threatened by water pollution day by day. Degradation or reduction of water quality due to water pollution can impact human health safety. Drinking and using for households the contaminated water can cause water-borne disease. Assessment of water quality in study area using some physico-chemical parameters to seek the status of water sources was reported. pH is very significant indicator to determine the status of water sources because water from three sampling stations have been used by local people in these areas as drinking water and domestic uses. pH value of

pure water is 7.0 but it may be accepted the range from 6.5 – 8.5 by WHO. The measured results of pH values range from 7.1 to 7.9 and were well below the acceptable limits set by WHO (2011), BIS and Myanmar Emission Guidelines (2015).[1][2][3] There was little industrial work but no factories and mineral production near the surrounding of sampling sites-3. Therefore, electrical conductivity was apparently low in sample-3 but the rest of the samples had more than that of sample-3. Turbidity for three samples was less than 5 and it was valid within the standard of WHO. The acceptable limit for hardness was 200 mg/L provide by WHO. The obtained results for hardness were less than WHO standards. Standard for TDS was 600 mg/L given by WHO and the achieved results for all samples were much less than the standard value. The permissible limit for alkalinity was 120 mg/L set by the Bureau of Indian Standards (BIS) but the experimental values of alkalinity for all samples were greater than that of permissible standard. According to the measured results of six kinds of physico-chemical parameters, we said that water stations were good for various purposes because no direct discharge of domestic and industrial waste water has been noticed. Table-3 gave the measured values of various selected physico-chemical characteristics in collected water samples during December 2019.

TABLE II. MEASURED VALUES OF PHYSICO-CHEMICAL CHARACTERISTICS OF THREE WATER SAMPLES AND STANDARD PERMISSIBLE VALUES ACCORDING TO WHO AND BIS.

Sr No	S_i	pH	Electrical Conductivity	Turbidity	Hardness	Total Dissolved Solids	Alkalinity
1	WHO	6.5-8.5	2500	5	200	600	-
2	BIS	6.5-8.6	-	-	-	500	120
3	HS-1 (river)	7.9	300	<5	80	188	167
4	HS-2 (ground)	7.5	400	<5	160	215	380
5	HS-3 (river)	7.1	43	<5	100	195	230

All values are measured in mg/L except pH, turbidity and electrical conductivity.

B. Metal concentration

Variety of metals can enter the rivers and diffuse into the ground water due to the various sources such as either natural process or human activities. River water can be polluted according to the discharge of domestic and industrial waste carelessly day by day. This event can make that river water be contaminated or concentration of metals' levels in river water can be increased. Most of the metals impact on human health but some are essential for nutrition for living things.

Among (7) kinds of metal concentration, content of lead (Pb) is greater than the permissible value set by WHO and BIS. In addition, the amounts of cadmium (Cd) for sample-1 and sample -2 were nearly closed to WHO standard. This fact can be caused by releasing untreated waste water from households and traditional industries indirectly. The concentrations of potassium for HS-1 and HS-2 were not detected. The rest of metals dissolved in sample water were within the allowed limits of WHO. The progression of various metals' concentration both in the river water and in the ground water and standards of drinking water guidelines provided by WHO and the Bureau of Indian Standards (BIS) have been prescribed in table-3.[1][2][3]

TABLE III. METALS' CONTENTS DISSOLVED IN BOTH RIVER WATER AND GROUND WATER.

Sr No	S_i	Cadmium	Lead	Copper	Zinc	Potassium	Sodium	Calcium
1	WHO	0.03	0.01	2	5	100	130	100
2	BIS	0.01	0.05	0.05	5	-	150	200
3	HS-1 (river)	0.014	0.914	0.044	0.168	ND	1.203	44.97
4	HS-2 (ground)	0.011	1.278	0.037	0.166	ND	4.167	52.05
5	HS-3 (river)	0.0027	1.05	1.581	0.197	0.9	4.81	55.02

All the metals' levels were measured in mg/L.

IV. DATA ANALYSIS

A. Correlation coefficient (r)

TABLE IV. CORRELATION COEFFICIENTS MATRIX OF PHYSICAL AND CHEMICAL PARAMETERS.

Parameters	pH	Electrical Conductivity	Hardness	Total Dissolved Solids	Alkalinity	Cadmium	Lead	Copper	Zinc	Potassium	Sodium	Calcium
pH	1											
Electrical Conductivity	0.69	1										
Hardness	-0.24	0.53	1									
Total Dissolved Solids	-0.25	0.52	0.99	1								
Alkalinity	-0.29	0.49	0.99	0.99	1							
Cadmium	-0.54	-0.71	-0.31	-0.31	-0.28	1						
Lead	-0.37	0.41	0.99	0.99	0.99	-0.22	1					
Copper	-0.86	-0.96	-0.28	-0.27	-0.23	0.70	-0.15	1				
Zinc	-0.82	-0.96	-0.33	-0.32	-0.28	0.53	-0.19	0.98	1			
Potassium	-0.87	-0.96	-0.28	-0.27	-0.23	0.69	-0.14	0.99	0.98	1		
Sodium	-0.94	-0.41	0.56	0.57	0.60	0.35	0.67	0.64	0.58	0.64	1	
Calcium	-0.97	-0.51	0.46	0.47	0.50	0.42	0.57	0.73	0.67	0.73	0.99	1

In this study paper, to determine how much of the amount will be related directly or reversely between measured water quality parameters, correlation coefficient (r) were evaluated. Table-4 indicated clearly that the correlation coefficient between (i) hardness and total dissolved solids (TDS), (ii) hardness and alkalinity (iii) hardness and lead (iv) total dissolved solids and alkalinity (v) total dissolved solids and lead (vi) alkalinity and lead (vii) copper and potassium (viii) sodium and calcium was +0.99, strong positive relationship and therefore it was said to be perfect correlation.

Besides, highly correlation coefficient between zinc and copper (ii) zinc and potassium was +0.98. (i) pH and electrical conductivity (ii) electrical conductivity and hardness (iii) electrical conductivity and total dissolved solids (iv) hardness and sodium (v) total dissolved solids and sodium (vi) alkalinity and sodium (vii) alkalinity and calcium (viii) cadmium and copper (ix) cadmium and zinc (x) cadmium and potassium (xi) lead and sodium (xii) lead and calcium (xiii) copper and sodium (xiv) copper and

calcium (xv) zinc and sodium (xvi) zinc and calcium (xvii) potassium and sodium (xviii) potassium and calcium were positive correlated moderately.

Positive correlation means one parameter will increase while another parameter will also increase for one pair. Based on the results of table-4, (i) electrical conductivity and alkalinity (ii) electrical conductivity and lead (iii) hardness and calcium (iv) total dissolved solids and calcium (v) cadmium and sodium (vi) cadmium and calcium had weak positive correlation. From the results of evaluated correlation coefficients, it was distinctly found that (i) pH and copper (ii) pH and zinc (iii) pH and potassium (iv) pH and sodium (v) pH and calcium (vi) electrical conductivity and copper (vii) electrical conductivity and zinc (viii) electrical conductivity and potassium were strongly uncorrelated. Electrical conductivity illustrated negative correlation with cadmium (r= -0.71).

By studying correlation table, (i) pH and cadmium (ii) pH and lead (iii) electrical conductivity and sodium (iv) electrical conductivity and calcium (v) hardness and cadmium (vi) hardness and zinc (vii) total dissolved solids and cadmium (viii) total dissolved solids and zinc presented low negative correlation with each pair. It meant that no significant correlation between each pair. In addition, pH had very low correlation with (i) hardness (ii) total dissolved solids (iii) alkalinity. Hardness was very low correlated with (i) copper (ii) potassium. Total dissolved solids poorly correlated with (i) copper (ii) potassium. It was observed that alkalinity showed very low negative correlation with (i) cadmium (ii) copper (iii) zinc and (iv) potassium. Cadmium had very poor correlation with lead (r = - 0.22). It is said to be likely unimportant. According to table-4, lead very negatively low correlated with (i) copper (ii) zinc and (iii) potassium. Low negative correlation coefficients and weak positive correlation coefficients meant that they had no expressive correlation (or) no linear relationship between each parameter of a pair. The evaluated correlation coefficients of water quality parameters were displayed in table-4.

B. Technology of water quality indices (WQIs)

Calculation of water quality index was carried out in this work by Weighted Arithmetic Index Method which was originally proposed by Horton (1965) and developed by Brown et al (1972) to find the quality of surface water for drinking purpose. Using the following equation, the weighted arithmetic water quality index (WQI) is calculated. [5]

$$WQI = \frac{\sum_{i=1}^{n} W_i q_i}{\sum_{i=1}^{n} W_i} \qquad (1.1)$$

In the first step, the value of quality rating or sub index (qi) is calculated according to Brown et al (1972) as follow:

$$q_i = 100 \left[\frac{measured\ values\ of\ i^{th}\ parameter - ideal\ value\ of\ i^{th}\ parameter}{standard\ value - ideal\ value}\right] \qquad (1.2)$$

In the second step, the calculation of relative weight (Wi) of the parameters was carried out. The unit weight (Wi) which is inversely proportional to the values of the recommended standards is obtained as:

$$W_i = \frac{k}{S_i} \qquad (1.3)$$

$$k = \frac{1}{\sum_{i=1}^{n}\left[\frac{1}{S_i}\right]} \qquad (1.4)$$

Calculated water quality index of water samples is usually distinguished into five categories shown in table-5.

TABLE V. WATER QUALITY INDICES (WQIS) ANDCORRESPONDING WATER QUALITY STATUS.
(C. CHATTERJEE AND RAZIUDDIN2002)

WQI values	Status of Water Quality
0-25	Excellent
26-50	Good
51-75	Poor
76-100	Very Poor
Above 100	Unfit for Drinking Purpose

TABLE VI. COMPUTATIONAL RESULTS OF WATER QUALITY INDICES (WQIS) FOR BOTH SURFACE WATER AND GROUND WATER IN STUDY AREA.

Sr No	Parameters	HS-1 (river) W_i Q_i	HS-2 (ground) W_i Q_i	HS-3 (river) W_i Q_i
1	pH	0.0696	0.0386628	0.0174
2	Electrical Conductivity	0.000048	0.000064	0.00000688
3	Turbidity	-	-	-
4	Hardness	0.002	0.004	0.0025
5	Total Dissolved Solids	0.0006266	0.0007166	0.00065
6	Alkalinity	0.01113336	0.0253336	0.0153336
7	Cadmium	138.46	108.79	26.703
8	Lead	0.226215	0.316305	0.259875
9	Copper	0.000726	0.001188	0.0017391
10	Zinc	0.0066528	0.0065736	0.0078012
11	Potassium	-	-	0.000081
12	Sodium	0.0000703	0.00024396	0.0002812
13	Calcium	0.00445203	0.00515295	0.00544698
	WQIs	138.7815241	109.1882405	27.01411496

WQIs for three sampling water from various locations have been calculated using the presented equation in above and then the suitability of drinking water quality is determined according to the rating of water quality shown in table-5.[6] Studying the results of computed WQIs displayed in table-6, the value of water quality indices for HS-1 and HS-2 were larger than 100 and therefore they were unfit for drinking water according to table-5. HS-1 &2 had high WQI

values because of very high concentration of cadmium (Cd). Sample-1 (HS-1) was collected from Donthami river near Donthami bridge and it is a population-dense area. Moreover, river water in this area was released indirectly with waste water and waste-products from traditional industries and production. It can be caused by the inflow of toilets' wastewater. River water management must be needed for Donthami river due to the results of HS-1. Reliable monitoring and management will be required for keeping a close watch on water quality of water sources in this study to have a healthy environment. Nevertheless, water quality index for sample-3 was 27.014 and thus the rate of water quality was good for drinking and domestic usage.

V. CONCLUSION

This research paper will help for the public health care sectors and all measured data were based on the scientific observations. This study can be applied in the water studies and water management system within the following areas:

- Heavy metals and trace elements contaminants
- Water quality modelling
- Environmental water quality
- Water policy and regulation
- Water technologies

Pearson correlation coefficients were evaluated to know the power of a linear relationship between two water parameters. In evaluating, if r-value is "1", it means that these two parameters have a perfect positive correlation and if r-value is "-1", it means that these two parameters have a perfect negative correlation.[7] The value of WQI for HS-1 was 138.782, for HS-2 was 109.188 and HS-3 was 27.014 computed by weighted arithmetic method as displayed in table-6. Therefore, the obtained results are the clear indication that the water in HS-1 and HS-2 are not suitable for both drinking purpose and domestic uses without treatment but also water in HS-3 is safe for drinking purpose. According to calculated WQIs presented in table-6, high concentration of cadmium makes larger values of WQI in HS-1&2. Although WQIs for HS-1&2 is very high, WQI for HS-3 is low because of the small value of cadmium content dissolved in it. After all, the obtained results from this investigation will be essential requirement for the planner, decision makers, government agencies, and the residents. More technological approaches will be needed to get a better management plan for clean and safe drinking water.

ACKNOWLEDGEMENT

First and foremost, praises and thanks to the Buddha, for his kind throughout my research work to complete the research successfully. I am extremely grateful to my parents for their love, prayers, nurturing and sacrifices for my future. I would like to thank Dr Khin May Aung, Pro-rector, Panglong University. I would like to express my gratitude to Dr Than Than Win (Professor and Head), Department of Physics, Panglong University for her kind permission to give me the opportunity to do research. I also thank to Dr Myo Lwin (Professor and Head) Department of Physics, University of Maubin for his help and critical suggestions.

REFERENCES

[1] 2018 Edition of drinking water standards and Health Advisories (EPA 822-F-18-001)
[2] Guidelines for Drinking water Quality, Fourth Edition, WHO 2011, ISBN 978 924 154 81 51.
[3] https://en.wikipedia.org/wiki/Drinking_water_quality_standards.
[4] https://www.googlemap.com
[5] R. K. Horton, An index number for rating water quality, *Journal of Water Pollution Control Federation*, 37(3), 1965.
[6] www.ajer.org (Volume-5, Issue-10).
[7] https://www.socscistatistics.com/tests/pearson/default.aspx

Article ID – JRA6002520

Comparison of Explicit Numerical Method and Analytical Method in solving Laplace's Equation

Khaing Khaing Thant
Faculty of Computing
University of Computer Studies
Monywa, Myanmar
khaingkhaing2019m@gmail.com

Aye Khaing Soe
Faculty of Computing
University of Computer Studies
Monywa, Myanmar
aye564856@gmail.com

Aye Aye Win
Engineering Mathematics
Technological University
Loikaw, Myanmar
ayeayewin2002@gmail.com

***Abstract*— Finite difference approximations to derivatives and the explicit finite difference methods of Laplace's equation are presented. The explicit finite difference methods for the Laplace's equation is explained with two examples. And then, the centered time and the centered space are applied into Laplace's equation. Moreover, in example A, numerical solutions of Laplace's equation by explicit method at $\Delta x = \Delta y = h = k = \pi/2$, at $\Delta x = \Delta y = h = \pi/3$, at $\Delta x = \Delta y = h = \pi/4$ and, in example B, numerical solutions of Laplace's equation by explicit method at $\Delta x = \Delta y = h = \pi/2$, at $\Delta x = \Delta y = h = \pi/3$ are discussed. In both examples, the truncation errors are calculated. The solution of the Laplace's equation converges to the exact solution of the problem as $\Delta x, \Delta y \to 0$.**

Keywords—Variables, Laplace's Equation, Partial Derivatives, Explicit Schemes, Matlab.

I. INTRODUCTION

Finite difference approximations to derivatives is introduced by [3], [9], [12], [13]. Explicit finite difference Method of the Laplace's Equation is presented by [3], [8], [10], [12], [13] and [14]. The analytical solutions are obtained by [1], [4], [5], [6], [7], [9], [11], [13] and [14]. The following figures are drawn by Matlab, [2]. Steady state problems in two dimensions and three dimensions give rise to elliptic partial differential equations. These equations are due to Laplace and Poisson. In vector notation, Laplace's equation can be written as $\nabla^2 u = 0$. Typically, the Laplace's equation is the very core of the theory of analytic functions of a complex variable. It describes the temperature distribution in an isotropic medium. It summarizes the gravitational or electrostatic potentials at point of empty space. It also characterizes the slow motion of an incompressible viscous fluid. Many more physical situations can be cited where this equation occurs. For a well-posed problem in Laplace's equation, a closed boundary is desirable.

II. FINITE DIFFERENCE APPROXIMATIONS TO DERIVATIVES

The Taylor series expansion of a function $u(x, y)$ of two independent variables x, y is

$$u(x_i \pm h, y_j) = u_{i\pm1}{}^j = u_i{}^j \pm h u_{xi}{}^j + \frac{h^2}{2!} u_{xxi}{}^j + \ldots (1)$$

and

$$u(x_i, y_j \pm k) = u_i{}^{j\pm1} = u_i{}^j \pm k u_{yi}{}^j + \frac{k^2}{2!} u_{yyi}{}^j + \ldots \quad (2)$$

where $u_i{}^j = u(x, y), u_{i\pm1}{}^j = u(x \pm h, y)$ and $u_i{}^{j\pm1} = u(x, y \pm k)$. We choose a set of uniformly spaced rectangles with vertices at $p_i{}^j$ with coordinates (ih, jk) where i, j are positive or negative integers or zeros. We denote $u(ih, jk)$ by $u_i{}^j$. The approximate expressions for u_x at $p_i{}^j$ in terms of $u_i{}^j, u_{i+1}{}^j$ and $u_{i-1}{}^j$ are

$$u_x \approx \frac{1}{h}(u_{i+1}{}^j - u_i{}^j) + O(h) \quad (3)$$

$$u_x \approx \frac{1}{h}(u_i{}^j - u_{i-1}{}^j) + O(h) \quad (4)$$

$$u_x \approx \frac{1}{2h}(u_{i+1}{}^j - u_{i-1}{}^j) + O(h^2) \quad (5)$$

The equation (3), equation (4) and the equation (5) are called the first order forward difference formula, the first order backward difference formula and the first order central difference formula of u_x respectively. The quantity $O(h)$ or $O(h^2)$ is known as the truncation error in this discretization process.

$$u_{xx} \approx \frac{1}{h^2}(u_{i+1}{}^j - 2u_i{}^j + u_{i-1}{}^j) + O(h^2) \quad (6)$$

Similarly, the approximate formulas for u_y and u_{yy} at $p_i{}^j$ are

$$u_y \approx \frac{1}{k}(u_i^{j+1} - u_i^{j}) + O(k) \tag{7}$$

$$u_y \approx \frac{1}{k}(u_i^{j} - u_i^{j-1}) + O(k) \tag{8}$$

$$u_y \approx \frac{1}{2k}(u_i^{j+1} - u_i^{j-1}) + O(k^2) \tag{9}$$

$$u_{yy} \approx \frac{1}{k^2}(u_i^{j+1} - 2u_i^{j} + u_i^{j-1}) + O(k^2) \tag{10}$$

All these difference formulas are extremely useful in finding numerical solution of first or second order partial differential equations, [3], [9], [12], [13].

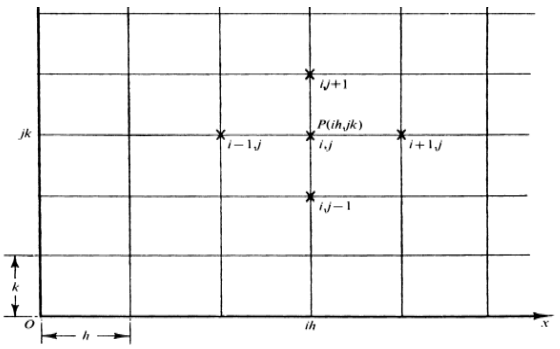

Fig. 1. Mesh on a semi-infinite strip.

III. Explicit Finite Difference Method for Laplace's Equation

Consider the Dirichlet problem for Laplace's equation

$$\frac{\partial^2 u}{\partial x^2} + \frac{\partial^2 u}{\partial y^2} = 0, 0 \le x \le a, 0 \le y \le b \tag{11}$$

Where the value of $u(x, y)$ is prescribed everywhere on the boundary of the rectangular domain.

The rectangular grid system is the most common and convenient system for this problem. We choose the vertices of the rectangular domain as the nodal points and set $h = \Delta x = a/m$ and $k = \Delta y = b/n$ where *m* and *n* are positive integers so that the domain is divided into *m n* sub-rectangles.

The central difference approximations to the Laplace's equation (11) is

$$\frac{u_{i+1}^{j} - 2u_i^{j} + u_{i-1}^{j}}{h^2} + \frac{u_i^{j+1} - 2u_i^{j} + u_i^{j-1}}{k^2} = 0 \tag{12}$$

Where, $1 \le i \le m-1$ and $1 \le j \le n-1$.

The prescribed conditions on the boundary of the rectangular domain determines the values u_0^j, u_m^j, u_i^0 and u_i^n for a square grid system, $h = k = \Delta x = \Delta y$, so that equation (12) becomes

$$u_i^j = \frac{u_{i+1}^{j} + u_{i-1}^{j} + u_i^{j+1} + u_i^{j-1}}{4} \tag{13}$$

Thus the value of *u* at any nodal point (*i, j)* is the average of the value of *u* at four adjacent points. This is well known mean value theorem for harmonic functions that satisfy the Laplace's equation. As *i* and *j* vary, the present numerical scheme reduces to a set of (*m*-1)(*n*-1) linear non-homogeneous algebraic equations (*m*-1)(*n*-1) unknown values of *u* at interior nodal points. It can be shown the solution of equation (13) converges to the exact solution of the problem as $\Delta x, \Delta y \to 0$. The proof of the existence of the solution and its convergence to the exact solution as Δx and Δy tend to zero is essentially based on the Maximum Modulus Principle, [13]. It follows from the finite difference equation (13) that the values of $|u|$ at the interior nodal point do not exceed to its value at any of the four adjoining nodal points. In other words, the value of u_i^j at p_i^j cannot exceed its values at the four adjoining points $p_{i+1}^j, p_{i-1}^j, p_i^{j+1}$ and p_i^{j-1}. The successive application of this argument at all interior nodal points leads to the conclusion that $|u|$ at the interior nodal points cannot be greater than the maximum value on the boundary. This may be recognized as the finite difference analogue of the Maximum Modulus Principle. Thus, the success of the numerical method is directly associated with the existence of the Maximum Modulus Principle, [3], [8], [10], [12], [13] and [14].

A. Example

Consider the Laplace's equation

$$\frac{\partial^2 u}{\partial x^2} + \frac{\partial^2 u}{\partial y^2} = 0, 0 \le x \le \pi, 0 \le y \le \pi \tag{14}$$

$$u(0, y) = u(\pi, y) = 0, 0 \le y \le \pi \tag{15}$$

$$u(x, 0) = x(\pi - x), u(x, \pi) = 0, 0 \le x \le \pi \tag{16}$$

The finite difference approximation to equation (14) is

$$u_i^j = \frac{u_{i+1}^{j} + u_{i-1}^{j} + u_i^{j+1} + u_i^{j-1}}{4} \ . \tag{17}$$

For case (i), Let $\Delta x = \Delta y = h = k = \pi/2$.

Putting i=1, j=1, in equation (17),

$$4u_1^1 - u_2^1 - u_0^1 - u_1^2 - u_1^0 = 0 .$$

On the boundary,

$$u_2^1 = u_1^2 = u_0^1 = 0, u_1^0 = \pi^2/4 .$$

Therefore

$$u_{1,1} = \pi^2/16 = 0.61685.$$

For case (ii), Let $\Delta x = \Delta y = h = k = \pi/3$.

Putting i=1, j=1, 2 and i=2, j=1,2 in equation (17),

$$4u_1^1 - u_2^1 - u_0^1 - u_1^2 - u_1^0 = 0$$
$$4u_1^2 - u_2^2 - u_0^2 - u_1^3 - u_1^1 = 0$$
$$4u_2^1 - u_3^1 - u_1^1 - u_2^2 - u_2^0 = 0$$
$$4u_2^2 - u_3^2 - u_1^2 - u_2^3 - u_2^1 = 0$$

By using boundary conditions,

$u_0^1 = u_0^2 = u_1^3 = u_2^3 = u_3^1 = u_3^2 = 0, , u_1^0 = 2\pi^2/9, u_2^0 = 2\pi^2/9$, obtain the system of equation becomes

$$4u_1^1 - u_2^1 - u_1^2 = 2\pi^2/9,\ 4u_1^2 - u_2^2 - u_1^1 = 0,$$
$$4u_2^1 - u_2^2 - u_1^1 = 2\pi^2/9,\ 4u_2^2 - u_1^2 - u_2^1 = 0.$$

The matrix notation is

$$\begin{bmatrix} 4 & -1 & -1 & 0 \\ -1 & 4 & 0 & -1 \\ -1 & 0 & 4 & -1 \\ 0 & -1 & -1 & 4 \end{bmatrix} \begin{bmatrix} u_1^1 \\ u_1^2 \\ u_2^1 \\ u_2^2 \end{bmatrix} = \begin{bmatrix} 2\pi^2/9 \\ 0 \\ 2\pi^2/9 \\ 0 \end{bmatrix}.$$

The solutions are obtained by Gauss elimination. Thus,

$u_1^1 = u_2^1 = 0.8225, u_1^2 = u_2^2 = 0.2742$.

For case (iii), Let $\Delta x = \Delta y = h = k = \pi/4$.

Putting i=1, j=1, 2, 3, i=2, j=1, 2, 3 and i=3, j=1, 2, 3 in equation (17), nine algebraic equations can be obtained,

$$4u_1^1 - u_2^1 - u_0^1 - u_1^2 - u_1^0 = 0$$
$$4u_1^2 - u_2^2 - u_0^2 - u_1^3 - u_1^1 = 0$$
$$4u_1^3 - u_2^3 - u_0^3 - u_1^4 - u_1^2 = 0$$
$$4u_2^1 - u_3^1 - u_1^1 - u_2^2 - u_2^0 = 0$$
$$4u_2^2 - u_3^2 - u_1^2 - u_2^3 - u_2^1 = 0$$
$$4u_2^3 - u_3^3 - u_1^3 - u_2^4 - u_2^2 = 0$$
$$4u_3^1 - u_2^1 - u_3^2 - u_3^0 - u_4^1 = 0$$
$$4u_3^2 - u_2^2 - u_3^3 - u_3^1 - u_4^2 = 0$$
$$4u_3^3 - u_2^3 - u_3^4 - u_3^2 - u_4^3 = 0$$

By using boundary conditions,

$u_0^1 = u_0^2 = u_0^3 = u_1^4 = u_2^4 = u_3^4 = u_4^3 = u_4^2 = u_4^1 = 0,$

$u_1^0 = 3\pi^2/16, u_2^0 = \pi^2/4, u_3^0 = 3\pi^2/16$, the system of equations can be got,

$$4u_1^1 - u_2^1 - u_1^2 = 3\pi^2/16,\ 4u_1^2 - u_2^2 - u_1^3 - u_1^1 = 0,$$
$$4u_1^3 - u_2^3 - u_1^2 = 0,\ 4u_2^1 - u_3^1 - u_1^1 - u_2^2 = \pi^2/16,$$
$$4u_2^2 - u_3^2 - u_1^2 - u_2^3 - u_2^1 = 0,$$
$$4u_2^3 - u_3^3 - u_1^3 - u_2^2 = 0,\ 4u_3^1 - u_2^1 - u_3^2 = 3\pi^2/16,$$
$$4u_3^2 - u_2^2 - u_3^3 - u_3^1 = 0,\ 4u_3^3 - u_2^3 - u_3^2 = 0$$

The matrix notation is

$$\begin{bmatrix} 4 & -1 & 0 & -1 & 0 & 0 & 0 & 0 & 0 \\ -1 & 4 & -1 & 0 & -1 & 0 & 0 & 0 & 0 \\ 0 & -1 & 4 & 0 & 0 & -1 & 0 & 0 & 0 \\ -1 & 0 & 0 & 4 & -1 & 0 & -1 & 0 & 0 \\ 0 & -1 & 0 & -1 & 4 & -1 & 0 & -1 & 0 \\ 0 & 0 & -1 & 0 & -1 & 4 & 0 & 0 & -1 \\ 0 & 0 & 0 & -1 & 0 & 0 & 4 & -1 & 0 \\ 0 & 0 & 0 & 0 & -1 & 0 & -1 & 4 & -1 \\ 0 & 0 & 0 & 0 & 0 & -1 & 0 & -1 & 4 \end{bmatrix} \begin{bmatrix} u_1^1 \\ u_1^2 \\ u_1^3 \\ u_2^1 \\ u_2^2 \\ u_2^3 \\ u_3^1 \\ u_3^2 \\ u_3^3 \end{bmatrix} = \begin{bmatrix} 3\pi^2/16 \\ 0 \\ 0 \\ \pi^2/16 \\ 0 \\ 0 \\ 3\pi^2/16 \\ 0 \\ 0 \end{bmatrix}$$

The solutions are computed

$u_1^1 = u_3^1 = 0.8537, u_1^2 = u_3^2 = 0.3855, u_1^3 = u_3^3 0.1487$

$u_2^1 = 1.1786, u_2^2 = 0.5397, u_2^3 = 0.2093$ by using Matlab.

To obtain analytical solution, assume a solution of the form

$$u(x, y) = F(x)G(y) \tag{18}$$

where F is a function of x alone and G is a function of y alone. Substituting $u(x, y)$ in equation (14),

$$F'' - \lambda F = 0 \tag{19}$$
$$G'' + \lambda G = 0 \tag{20}$$

where λ is the separation constant. Since the boundary conditions are homogeneous on $x = 0$ and $x = \pi$, choose $\lambda = -\alpha^2$ with $\alpha > 0$ in order to obtain nontrivial solutions of the eigenvalue problem

$$F'' + \alpha^2 F = 0,$$
$$F(0) = F(\pi) = 0.$$

It is easily found that the eigenvalues are

$\alpha = n,\ n = 1, 2, \ldots$. and the corresponding Eigen functions are $\sin nx$. Hence

$$F_n(x) = A_n \sin nx.$$

The solutions of equation (20) is

$G(y) = B\cosh \alpha y + C\sinh \alpha y$, which may also be written in the form

$$G(y) = E\sinh \alpha(y + H),$$

Where $E = (C^2 - B^2)^{\frac{1}{2}},\ H = 1/\alpha \tanh^{-1}(B/C)$.

By using remaining homogeneous boundary condition $u(x, \pi) = F(x)G(\pi) = 0$, it is obtained as

$$G(\pi) = E\sinh \alpha(\pi + H) = 0$$

And hence

$$H = -\pi, E \neq 0$$

For a nontrivial solution $u(x, y)$. Thus,

$$G_n(y) = E_n \sinh n(y - \pi).$$

Because of linearity, the solution is

$$u(x, y) = \sum_{n=1}^{\infty} a_n \sin nx \sinh n(y - \pi), a_n = A_n E_n.$$

Now, applying the nonhomogeneous boundary condition to obtain

$$u(x, 0) = x(\pi - x) = \sum_{n=1}^{\infty} a_n \sin nx \sinh(-n\pi),$$

This is a Fourier sine series and hence

$$a_n = \frac{-2}{\pi \sinh(n\pi)} \int_0^{\pi} x(\pi - x) \sin nx dx.$$

Thus, formal solution is given by

$$u(x, y) = \sum_{n=1}^{\infty} a_n^* \frac{\sinh n(\pi - y) \sin nx}{\sinh n\pi},$$

where $a_n^* = \frac{2}{\pi} \int_0^{\pi} x(\pi - x) \sin nx dx.$

$$a_n^* = \frac{2}{\pi} \left[\left(\pi x - x^2 \right) \left(\frac{-\cos nx}{n} \right) + \left(\frac{(\pi - 2x)}{n^2} \right) \sin nx - \frac{2 \cos nx}{n^3} \right]_0^{\pi},$$

$$a_n^* = \frac{-4\left((-1)^n - 1 \right)}{n^3},$$

$$a_n^* = \begin{cases} 0, n = \text{even} \\ \frac{8}{\pi n^3}, n = \text{odd} \end{cases}$$

So,

$$u(x, y) = \sum_{n=1,3,5,\ldots} \frac{8}{\pi n^3} \frac{\sinh n(\pi - y) \sin(nx)}{\sinh(n\pi)}$$, [1], [4], [5], [6], [7], [9], [11], [13], and [14].

The partial sum for $n = 7$ is considered. The analytical solution of case (i) is $u(\pi/2, \pi/2) = u_1^1 = 0.5066.$

The analytical solution of case (ii) are

$u(\pi/3, \pi/3) = u_1^1 = 0.7635$

$u(\pi/3, 2\pi/3) = u_1^2 = 0.2386 = u(2\pi/3, 2\pi/3) = u_2^2$,

$u(2\pi/3, \pi/3) = u_2^1 = 0.7635$.

The analytical solution of case (iii) are

$u(\pi/4, \pi/4) = u_1^1 = 0.8212$

$u(\pi/4, 2\pi/4) = u_1^2 = 0.3594 = u(3\pi/4, 2\pi/4) = u_3^2$,

$u(\pi/4, 3\pi/4) = u_1^3 = 0.1355 = u(3\pi/4, 3\pi/4) = u_3^3$

$u(2\pi/4, 3\pi/4) = u_2^3 = 0.1915, u(3\pi/4, 2\pi/4) = u_3^2 = 0.8212.$

In this example, the truncation error of case (i) is -0.11025. In case (ii) and case (iii), the truncation errors, analytical solutions and numerical solutions are as shown in the following table I, table II and table III.

TABLE I. THE VALUES OF $u(x, y)$ FROM $x = 0$ TO $x = \pi$ AND $y = 0$ TO $y = \pi$ (RUN BY MATLAB)

	$u(x, y)$			
	u_1^1	u_2^1	u_1^2	u_2^2
F.D.S	0.8225	0.8225	0.2742	0.2742
A.S	0.7635	0.7635	0.2386	0.2386
T.E	-0.059	-0.059	-0.0356	-0.0356

TABLE II. THE VALUES OF $u(x, y)$ FROM $x = 0$ TO $x = \pi$ AND $y = 0$ TO $y = \pi$ (RUN BY MATLAB)

	$u(x, y)$		
	$u_1^1 = u_3^1$	$u_1^2 = u_3^2$	$u_1^3 = u_3^3$
F.D.S	0.8537	0.3855	0.1487
A.S	0.8212	0.3594	0.1355
T.E	-0.0325	-0.0261	-0.0132

TABLE III. THE VALUES OF $u(x, y)$ FROM $x = 0$ TO $x = \pi$ AND $y = 0$ TO $y = \pi$ (RUN BY MATLAB)

	$u(x, y)$		
	u_2^1	u_2^2	u_2^3
F.D.S	1.1786	0.5397	0.2093
A.S	1.1442	0.5066	0.1915
T.E	-0.0344	-0.0331	-0.0178

The A.S represents analytical solutions and F.D.S represents numerical solutions and the T.E represents the truncation errors. The truncation error can be obtained by

differencing between analytical solution and numerical solution.

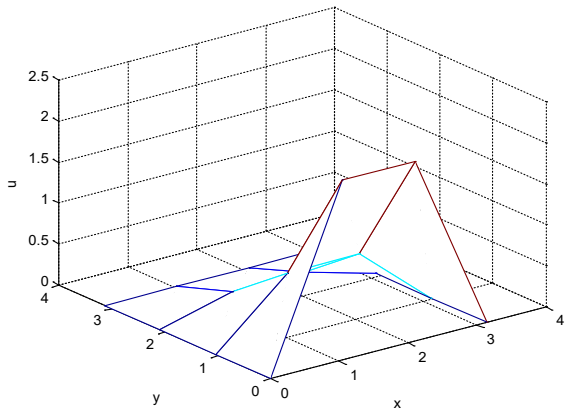

Fig. 2. Graph of the analytical solutions of $u(x,y)$ form $x=0$ to $x=\pi$ and form $y=0$ to $y=\pi$

B. Example

Consider the Laplace's equation

$$\frac{\partial^2 u}{\partial x^2}+\frac{\partial^2 u}{\partial y^2}=0, 0\le x\le\pi, 0\le y\le\pi \qquad (21)$$

$$u(0,y)=u(\pi,y)=0, 0\le y\le\pi \qquad (22)$$

$$u(x,0)=\sin^2 x, u(x,\pi)=0, 0\le x\le\pi \qquad (23)$$

The finite difference approximation to equation (21) is

$$u_i^j=\frac{u_{i+1}^j+u_{i-1}^j+u_i^{j+1}+u_i^{j-1}}{4}\ . \qquad (24)$$

For case (i), Let $\Delta x=\Delta y=h=k=\pi/2$.

Putting i=1, j=1, in equation (24), the equation becomes

$4u_1^1-u_2^1-u_0^1-u_1^2-u_1^0=0$.

On the boundary,

$u_2^1=u_1^2=u_0^1=0, u_1^0=1$. Therefore $u_{1,1}=0.25$.

For case (ii), Let $\Delta x=\Delta y=h=k=\pi/3$.

Putting i=1, j=1, 2 and i=2, j=1, 2 in equation (24),

$$4u_1^1-u_2^1-u_0^1-u_1^2-u_1^0=0$$
$$4u_1^2-u_2^2-u_0^2-u_1^3-u_1^1=0$$
$$4u_2^1-u_3^1-u_1^1-u_2^2-u_2^0=0$$
$$4u_2^2-u_3^2-u_1^2-u_2^3-u_2^1=0$$

By using boundary conditions,

$u_0^1=u_0^2=u_1^3=u_2^3=u_3^1=u_3^2=0,,u_1^0=3/4, u_2^0=3/4$, obtain the system of equation

$$4u_1^1-u_2^1-u_1^2=3/4, \qquad 4u_1^2-u_2^2-u_1^1=0,$$
$$4u_2^1-u_2^2-u_1^1=3/4, \qquad 4u_2^2-u_1^2-u_2^1=0.$$

The matrix notation is

$$\begin{bmatrix}4&-1&-1&0\\-1&4&0&-1\\-1&0&4&-1\\0&-1&-1&4\end{bmatrix}\begin{bmatrix}u_1^1\\u_1^2\\u_2^1\\u_2^2\end{bmatrix}=\begin{bmatrix}3/4\\0\\3/4\\0\end{bmatrix}.$$

The solutions are obtained by Gauss elimination. Thus,

$u_1^1=u_2^1=0.28125, u_1^2=u_2^2=0.09357$.

To obtain analytical solution, assume a solution of the form

$$u(x,y)=F(x)G(y) \qquad (25)$$

where F is a function of x alone and G is a function of y alone. Substituting $u(x,y)$ in equation (14),

$$F''-\lambda F=0 \qquad (26)$$

$$G''+\lambda G=0 \qquad (27)$$

where λ is the separation constant. Since the boundary conditions are homogeneous on $x=0$ and $x=\pi$, choose $\lambda=-\alpha^2$ with $\alpha>0$ in order to obtain nontrivial solutions of the eigenvalue problem

$$F''+\alpha^2 F=0,$$
$$F(0)=F(\pi)=0.$$

It is easily found that the eigenvalues are

$\alpha=n,\ n=1,2,\ldots$ and the corresponding Eigen functions are $\sin nx$. Hence

$$F_n(x)=A_n\sin nx.$$

The solutions of equation (20) is

$G(y)=B\cosh\alpha y+C\sinh\alpha y$, which may also be written in the form

$$G(y)=E\sinh\alpha(y+H),$$

where $E=(C^2-B^2)^{\frac{1}{2}}$, $H=1/\alpha\tanh^{-1}(B/C)$.

By using remaining homogeneous boundary condition $u(x,\pi)=F(x)G(\pi)=0$, it is obtained as

$$G(\pi)=E\sinh\alpha(\pi+H)=0$$

And hence

$$H=-\pi, E\neq 0$$

For a nontrivial solution $u(x,y)$. Thus,

$$G_n(y) = E_n \sinh n(y-\pi).$$

Because of linearity, the solution is

$$u(x,y) = \sum_{n=1}^{\infty} a_n \sin nx \sinh n(y-\pi), a_n = A_n E_n.$$

Now, applying the nonhomogeneous boundary condition to obtain

$$u(x,0) = \sin^2 x = \sum_{n=1}^{\infty} a_n \sin nx \sinh(-n\pi),$$

This is a Fourier sine series and hence

$$a_n = \frac{-2}{\pi \sinh(n\pi)} \int_0^{\pi} \sin^2 x \sin nx dx.$$

Thus, formal solution is given by

$$u(x,y) = \sum_{n=1}^{\infty} a_n^* \frac{\sinh n(\pi-y)\sin nx}{\sinh n\pi},$$

where $a_n^* = \frac{2}{\pi} \int_0^{\pi} \sin^2 x \sin nx dx.$

$$a_n^* = \frac{1}{\pi}\left[\frac{-\cos nx}{n} - \frac{1}{2}\left(\frac{-\cos(n+2)x}{n+2} - \frac{\cos(n-2)x}{n-2}\right)\right]_0^{\pi},$$

$$a_n^* = \frac{1}{\pi}\left[\frac{-1}{n}\left((-1)^n - 1\right) - \frac{1}{2}\frac{2n\left(1-(-1)^n\right)}{n^2-4}\right],$$

$$a_n^* = \begin{cases} 0, & n = \text{even} \\ \dfrac{-8}{\pi n(n^2-4)}, & n = \text{odd}. \end{cases}$$

So,

$$u(x,y) = \sum_{n=1,3,5,\ldots} \frac{-8}{\pi n(n^2-4)} \frac{\sinh n(\pi-y)\sin(nx)}{\sinh(n\pi)}$$

Of this problem is obtained by the method of separation of the variables, [1], [4], [5], [6], [7], [9], [11], [13] and [14].

The partial sum for $n = 7$ is considered.

The analytical solution of case (i) is $u(\pi/2, \pi/2) = u_1^1 = 0.1707$.

The analytical solutions of case (ii) are

$u(\pi/3, \pi/3) = u_1^1 = 0.2546,$

$u(\pi/3, 2\pi/3) = u_1^2 = 0.0795 = u(2\pi/3, 2\pi/3) = u_2^2,$

$u(2\pi/3, \pi/3) = u_2^1 = 0.2546.$

In this example, the truncation error of case (i) is -0.0793. In case (ii), the truncation errors, the analytical solutions and numerical solutions are as shown in the following table IV.

TABLE IV. THE VALUES OF $u(x,y)$ FROM $x = 0$ TO $x = \pi$ AND $y = 0$ TO $y = \pi$ (RUN BY MATLAB)

	$u(x,y)$			
	u_1^1	u_2^1	u_1^2	u_2^2
F.D.S	0.28125	0.28125	0.09375	0.09375
A.S	0.2546	0.2546	0.0795	0.0795
T.E	-0.02665	-0.02665	-0.01425	-0.01425

The analytical values of $u(x,y)$ from $x = y = 0$ to $x = y = \pi$ is as shown in the following figure by using Matlab.

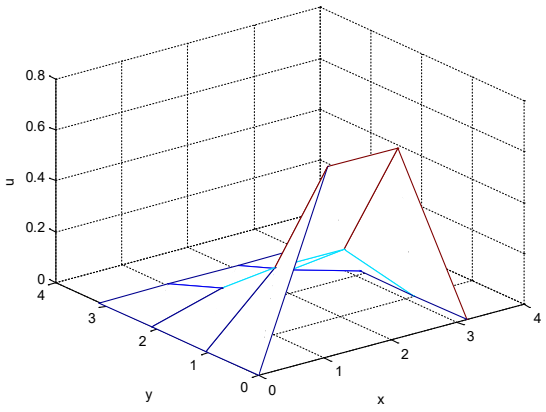

Fig. 3. Graph of analytical solutions of $u(x,y)$ form $x = 0$ to $x = \pi$ and form $y = 0$ to $y = \pi$

IV. CONCLUSIONS

Two examples of Laplace's equation are computed. Example A is computed by explicit method at $h = k = \pi/2$, at $h = k = \pi/3$ and at $h = k = \pi/4$. In example A, the analytical solutions of $u(x,y)$ from $x = 0$ to $x = \pi$ and $y = 0$ to $y = \pi$ are computed by using MATLAB. It is observed that the values of $u(x,y)$ are between 0 and 0.8225. Example B is computed by explicit method at $h = k = \pi/2$ and at $h = k = \pi/3$. In example B, the analytical solutions of $u(x,y)$ from $x = 0$ to $x = \pi$ and $y = 0$ to $y = \pi$, are computed by using MATLAB. It is observed that the values of $u(x,y)$ are between 0 and 0.28125. In example A, the truncation errors of case (iii) is smaller than the truncation errors of case (i) and case (ii). In example B, the truncation errors of case (ii) is smaller than the truncation errors of case (i). It is observed that the more the exact solution is near, the less the value of h.

ACKNOWLEDGMENT

We are grateful to the committee of JRA and the editorial board for permitting the submission of this paper. This research, appreciation is also due to Dr. Moe Moe Hlaing, Professor and Head of department of faculty

of computing, University of Computer Studies (Monywa) who has given us various guidelines and knowledge. We would like to deepest thanks to our family for their kind help and encouragement.

REFERENCES

[1] L.Arthur Schoenstadt, "An Introduction to Fourier Analysis", Monterey, California, 2006.
[2] Aung Myint (M.E.Australia), Matlab & Simulin, ch-1.
[3] N.P. Bali, Manish Goyal, A Textbook of Engineering Mathematics, Laxmi Publications LTD 113, Golden House, Daryagani, New Delhi 110002, 2007 pp.1432-1448.
[4] R.V. Churchill, "Fourier Series and Boundary Value Problems", *New* York, M.C Graw Hill, 1963.
[5] E.C.Zachmanoglou and W.Dale Thoe, An Introduction to Partial Differential Equations with applications, Dover Publications,Inc.,New York, 1986, pp.249-257.
[6] Gordon C. Everstine, Numerical Solution of Partial differential Equations, 2010.
[7] J.W.Thomas, Numerical Partial differential Equations: Finite Difference Methods, New York, Inc., 1995, pp.1-8.
[8] Kandasamy, P., Thilagavathi, K. and Gunavathi, K., Engineering Mathematics, Volume III, S.Chand &Company Ltd., New York, 1996.
[9] K .Sankara Rao, Numerical Methods for Scientists and Engineers, PHI Learning Private Ltd, New Delhi-110001, 2009.
[10] K .Sankara Rao, Introduction to partial differential equations, PHI Learning Private Ltd, New Delhi, 1995, pp.210-216, pp.240-247.
[11] E.Kreyszig, Advanced Engineering Mathematics, New York John Wiley & Sons, Inc., 1999, pp.564-567.
[12] G. D. Smith, "Numerical Solution of Partial differential Equations: Finite Difference Method", Clarendon Press, 1985, pp.1-8, pp.239, pp.240.
[13] U. Tyn Myint, "Partial Differential Equations for Scientists and Engineers", *New York,* PTR Prentice-Hall, Inc., 1987, pp.448-508.
[14] Yehuda Pinchover and Jacob Rubinstein, An Introduction to Partial Differential Equations, New York, 2005, pp.173-187, pp.309-318.

Article ID – JRA6002620

Risks Associated with the Human Resources Management in Computer University

Tue Tue Mar
Faculty of Information Science,
University of computer Studies
(Pakokku), Myanmar
tuetuemar38@gmail.com

Yi Yi Win
Faculty of Computer Science
University of computer Studies
(Meikhtila), Myanmar
yiyipku941@gmail.com

Nuyee Win
Faculty of Computer Science
University of computer Studies
(Magway), Myanmar
nuyeewin@gmail.com

***Abstract*- Education is very import sectors in every life, every country and every government. The Education Policy is right and strong. Actions of school and university are associated with the quality of human resources in the sector. Their lack causes serious problems in selected areas and in the long run, it leads to a reduction or loss of country competitiveness. Education policy and the related national level strategic and legislative documents set the targets and measures to achieve these targets, which imply risks and responsibilities for country. The article presents a methodical advancement which enables to find risk factors to Computer University in the HR field, determines their significance and impact on the quality results of the university.**

***Keywords*- Software Engineering, Risk factor; risk management; human resource management;**

I. INTRODUCTION

World is managed by people. People are managed by people. Manage person is called manager. In university manager is called rector or pro-rector. Rector manages staff, teacher, and students. So, they have many human risks. Risk is the part of work life of individuals and organizations. Risk is uncertainties that may give birth to loss [1]. They are not HR managers.

Rectors solve technical and nontechnical problem for university by using the most effective ways. They have to motivate people, plan and organize their work and ensure that the work is being done properly. Poor management of people is one of the most significant contributors to bad smell in university environment. But they cannot select the staff, teacher and students.

II. CRITICAL FACTORS IN PEOPLE MANAGEMENT

The management people may know that the four critical factors in people management from the following [2]:

(1) Consistency: People in a university should all be treading in comparable way. No one expects all rewards to be identical; people should not feel that their contribution to the organization is undervalued.

(2) Respect: Different people have different skills and should respect these differences. All teachers and staffs of the university should be given an opportunity to make a contribution. In some case, they will find that people simply don't fit into a team and cannot continue, but it is important not to jump to conclusions about this.

(3) Inclusion: People contribute effectively when they feel that others listen to them and take account of their proposals. It is important to develop a working environment where all views, even the most of junior staff or demonstrator are considered.

(4) Honesty: As a principle or rector, should always be honest about what is going well and what is going badly in the life. Should also be honest about their technical knowledge and be willing to defer to staff with more knowledge when necessary.

In introduction, the rector cannot select the teacher, staff and student. But any appoint select the staff to take the work. Information provided by staff about their background and experience. Recommend from people who have worked with the staff [3].

III. RISK IN UNIVERSITY

A. Strategic Risk

- Failure to publish adequate high-quality research outputs
- Failure to recognize and deliver student expectations
- Failure to maintain teaching quality and standards
- Failure to achieve widening participation
- Failure to maintain effective corporate relationships with key external and internal stakeholder
- Failure to maintain financial viability
- Failure to accurately create, securely manage and store data
- Failure to meet international student recruitment targets
- Failure to deliver a healthy and safe environment

B. Optional

- Failure Logistics in university
- Failure Project in university

C. Compliance
- Internal controls
- Ethics

D. People
- Fraud
- Incompetence
- Lack of talent

E. Technology
- Poor use of technology
- Change in technology

To reduce the risk in university, the head of department motivates their staff, teachers and student. To motivate the people, use people capability maturity model and know three types of professional.

IV. MOTIVATING PEOPLE

After selected the people for appoint or project (online teaching), motivate the staff who work for them. Motivation means the organizing the work and the working environment sot that people are stimulated to work effectively as possible. If the people are not motivating, they will not be interested in the work they are doing. They will work slowly, be more likely to make mistakes and will not contribute to the broader of the organization.

Fig 1. Human needs hierarchy

In Figure 1; People working in university organizations are not usually hungry or thirsty and generally do not feel physically threatened by their environment. So, ensuring the satisfaction of social, esteem and self-realization needs is most significant from management point of view.

To satisfy social needs, rector or head of department need to give staff time to meet their co-workers and to provide places for them to meet. Electronic communication may be used to support this working. My experience with electronic communications is that they do not really satisfy social needs. If the group is distributed, should arrange periodic face-to-face, so that people experience direct interaction with other member.

To satisfy esteem needs, need to show people that they are valued by the organization. Public recognition of achievements is a simple yet effective way of doing this. Wonderfully, people must also feel that they are paid at a level that reflects their skills and experience. Maslow's hierarchy of needs includes five levels of needs and argues that individuals will act only to meet their higher needs when their lower needs are met. Abraham Maslow's hierarchy of needs theory is seen as the basis of many later developed theories. Herzberg's two-factor theory transforms Maslow's needs into two areas of need as hygiene factors and motivation factors [4].

Last, to satisfy self-realization needs, need to give people responsibility for their work, assign them demanding tasks and provide a training teaching course and office course where people can develop their skills.

V. THREE TYPES OF PROFESSIONALS

Timely detection risk ability, importance assignment of individual risk factors and the subsequent division into risk groups will allow then to determine the appropriate measures that will help reduce the risk to a predetermined level or eliminate risk causes, and thus overall to reduce the enterprise risk. Our country is in the application of computer technology in the human resource management is the requirement of building a modern society in the new era of the construction of science and technology. Human resource information management is also fully reflected in politics government department people-oriented service concept, and promotes the harmonious development of society.

Heads of department also know the types of professionals. There are three types of professionals

(1) Task-oriented people: are motivated by the work. In IT environment, they are technicians who are motivated by the intellectual challenge. We need task-oriented people because of it is IT university.
(2) Self-oriented people: are motivated by personal success and recognition. This does not mean that these people are selfish and think only of their own concerns. They have good idea we permission to do research.
(3) Interaction-oriented people: are motivated by the presence and actions of coworkers. In software development becomes more user-centered. In computer university teachers is most women. Women are more likely to be interaction-oriented than man [3].

Certainly, we need to try to get task-oriented and self-oriented people because of it are Computer University. The quality of HR management system functioning depends, first of all, not only on the employees' qualification level, but also on the particular specialist's load. It is the performance level. According to the specialists' recommendations, such load should not exceed 2-3 applicants per month. Heads of department, while seeking to make a fairly reasonable decision to hire a new technician for training rely primarily on these characteristics from their previous job. "Hiring good people is hard. Hiring great people is brutally hard. And yet nothing matters more in winning than in getting the right people on the field. All the clever strategies and advanced technologies in the world are nowhere near as effective without great people to put them to work." [5].

VI. PEOPLE CAPABILITY MATURITY MODEL

The Software Engineering Institute (SEI) in the UK is engaged in a long-term program of process improvement. The PCMM is five-level model, as shown Figure 2.

P-CMM is a practical tool for improving the management of people in an organization because it provides a framework for motivating, recognizing, standardizing and improving good practice.

1) Initial: People informal practices management.
2) *Repeatable*: Policies for developing the capability of the staff.
3) Defined: Standardization of the best people management practice cross the organization.

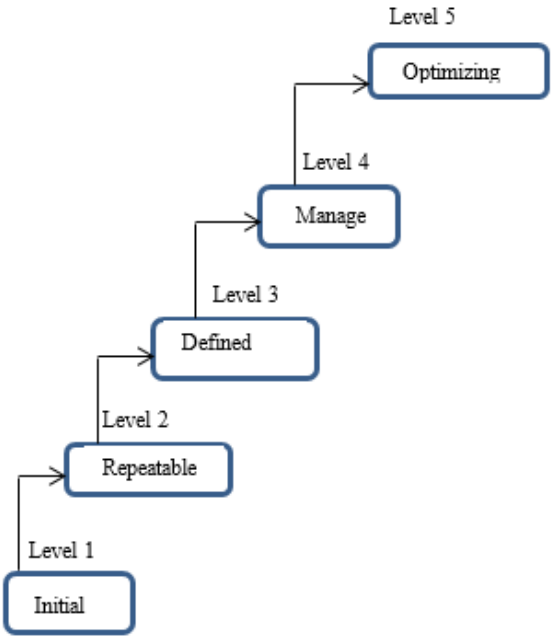

Fig 2. The People Capability Maturity Model

1) *Managed:* Quantitative goals for people management
2) Optimizing: Continuous focus on improving individual competence and work-force motivation.

VII. CONCLUSIONS

HR are important everywhere and everything. University structure's is a game, and as with all games, the team that puts the best people on the field and gets them playing together wins [6]. Correct identification of human resources risk is an integral part of the conscious management within turbulent environments and, most importantly, the key stage in the process of effective risk management. As emerge from the analyses, the ongoing, inevitable changes of the demographic situation associated with the aging population, declining job resources, and increased burden on the population of working age are crucial global human resources risk factors. In order to reduce the risk, employers will need to adopt a new approach to human resources management [7].

ACKNOWLEDGEMENT

The authors would like to thank the support given by the paper and would like to acknowledgement our deep thanks and respect go to Prof. Dr. Mie Mie Khin, Rector, University of Computer Studies (Meiktla) for allowing us an opportunity to write paper in AUJIRP. I would like to thank the support given by the paper and would like to acknowledgement our deep thanks and respect go to Prof. Dr. Tin Tin Thein, Pro-Rector (acting) University of Computer Studies (Pakokku). I would like to thanks to dear friends and teachers at University of Computer Studies (Pakokku) for kind support and empathy on my requisiteness. Also thank for my department heart Dr. Shwe Sin Thein.

REFERENCES

[1] Kasidi, "Risk Mangement", 2010.
[2] V. Frederickson, "Risk Management and The HR Executive", 2010.
[3] C. F. Gray and E. W. Larson, Project management: the managerial process, Sixth edition. New York, NY: McGraw-Hill Education, 2014.
[4] A. H. Maslow, "'Higher' and 'Lower' Needs," J. Psychol., vol. 25, no. 2, pp. 433–436, Apr. 1948.
[5] J. Welch and S. Welch, Winning, 1st ed. New York: HarperBusiness Publishers, 2005.
[6] H. V. Poor, An Introduction to Signal Detection and Estimation, 2nd Edition. New York: Springer, 1994.
[7] D. Anaraki-Ardakani and A. Ganjali, "Human Resource Risk Management," p. 14, 2014.

Article ID – JRA6003120

Finite Difference Method and its Application on One- and Two-Dimensional Domains

Thant Thant Soe
Faculty of Computing
University of Computer Studies(Monywa)
Monywa, Myanmar
thantthantsoethelma@gmail.com

Khin Cho Lin
Faculty of Computing
University of Computer Studies(Monywa)
Monywa, Myanmar
khincholin2@gmail.com

***Abstract*—This paper presents finite difference method for solving second order differential equations and application of this method on one- and two-dimensional domains. At first, finite difference method is introduced for second order ordinary differential equation on one-dimensional domain and it is applied to linear and nonlinear ordinary differential equations using first and second order approximations. Secondly, five–point finite difference method using Taylor's formula and discrete problem for Poisson equation are described. Then, discretization error is expressed for Dirichlet problem. Finally, example is treated for Poisson equation on two-dimensional domain and discretization error is also calculated between finite difference solution and analytical solution.**

Keywords—finite difference method, five-point finite difference, Poisson equation, Taylor's formula, Dirichlet, one- and two-dimensional domains

I. INTRODUCTION

In numerical analysis, finite difference method is discretization used for solving differential equations by approximating them with difference equations that finite differences approximate the derivatives. Even though the method was known by such workers as Gauss and Boltzmann, it was not widely used to solve engineering problems until the 1940s. During 1950-1970, finite difference method was the most important numerical method used to solve practical problems. This method converts linear or nonlinear differential equations into a system of equations that can be solved by matrix algebra techniques.

A finite difference approximation involves the following steps.

(a) Generate a grid, (x_i, y_i), to find an approximate solution.

(b) Substitute the derivatives in a differential equation or a system differential equations with finite difference schemes. The differential equation becomes a linear or non-linear system of algebraic equations.

(c) Solve the system of algebraic equations.

(d) Do the error analysis, both analytically and numerically.

There are three formulas for finite difference approximation and they are forward finite difference, backward finite difference and central finite difference.

II. FINITE DIFFERENCE METHOD FOR SECOND ORDER ORDINARY DIFFERENTIAL EQUATION ON AN INTERVAL

In this section, finite difference method for solving second order ordinary differential equation on an interval and discretization on this domain are proposed. And finite difference method is applied in solving linear and nonlinear boundary value problems. The most general linear second order differential equation is in the form [1]

$$y''(x) + p(x)y'(x) + q(x)y(x) = r(x),\ a \le x \le b, \qquad (1)$$

with boundary conditions $y(a) = A$ and $y(b) = B$.

We divide the interval $[a, b]$ into a chosen number n of subintervals of equal width. That is, $x_i = a + ih\ (i = 0.1, 2, ..., n)$.

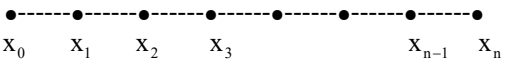

Thus, the step size h (that is, Δx) of each of the n subintervals is given by $h = \frac{b-a}{n}$. Notation y_i is denoted by the value of the function at i-th node of the computational grid. Using first derivative, central finite difference [3]

$$f'(x) = \frac{f(x+h) - f(x-h)}{2h} + O(h^2)$$

and second derivative, central finite difference

$$f''(x) = \frac{f(x+h) - 2f(x) + f(x-h)}{h^2} + O(h^2)$$

in (1), $y_1, y_2, ..., y_{n-1}$ can be calculated.

At any mesh point $x = x_i$, the finite-difference representation of the differential equation (1) can be written-as

$$\frac{y_{i+1}-2y_i+y_{i-1}}{h^2}+p_i\frac{y_{i+1}-y_{i-1}}{2h}+q_iy_i=r_i,\ (i=1,2,...,n-1),$$

$$2(y_{i+1}-2y_i+y_{i-1})+hp_i(y_{i+1}-y_{i-1})+2h^2q_iy_i=2h^2r_i,\quad (i=1,2,...,n-1).$$

And arranging the equation, we obtain the system of linear equations

$$(2+hp_i)y_{i+1}+(2h^2q_i-4)y_i+(2-hp_i)y_{i-1}=2h^2r_i,(i=1,2,...,n-1).$$

The boundary conditions $y_0=A$ and $y_n=B,$ provide of the solution at the two ends of the grid.

We can interpret y as a vector and write the equation formally as an algebraic matrix equation, $A_hY_h=R_h,$ where

$$A_h=\begin{bmatrix} 2h^2q_1-4 & 2+hp_1 & 0 & ... & ... & 0\\ 2-hp_2 & 2h^2q_2-4 & 2+hp_2 & 0 & ... & 0\\ 0 & 2-hp_3 & 2h^2q_3-4 & 2+hp_3 & ... & 0\\ \vdots & \vdots & \ddots & \ddots & \ddots & \vdots\\ 0 & ... & 0 & 2-hp_{n-2} & 2h^2q_{n-2}-4 & 2+hp_{n-2}\\ 0 & ... & ... & 0 & 2-hp_{n-1} & 2h^2q_{n-1}-4 \end{bmatrix}$$

$$R_h=\begin{bmatrix} 2h^2r_1-(2-hp_1)A\\ 2h^2r_2\\ 2h^2r_3\\ \vdots\\ 2h^2r_{n-2}\\ 2h^2r_{n-1}-(2+hp_{n-1})B \end{bmatrix},\quad \text{and}\quad Y_h=\begin{bmatrix} y_1\\ y_2\\ y_3\\ \vdots\\ y_{n-2}\\ y_{n-1} \end{bmatrix}.$$

A. Example

We will approximate the solution of the linear ordinary differential equation

$$y''-(1-\frac{x}{5})y=x,\quad y(1)=2\ \text{ and }\ y(3)=-1 \qquad (2)$$

on the interval $1\le x\le 3.$

Let $x_n=x_0+nh,\ x_0=1,\ h=0.5$ and y_n be the calculated approximation for $y_n=y(x_n).$

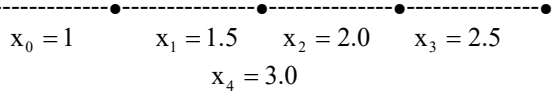

Using the central finite difference approximation [3], (2) gives

$$\frac{y_{i+1}-2y_i+y_{i-1}}{\Delta x^2}-(1-\frac{x_i}{5})y_i=x_i,\quad i=1,2,3,$$

$$y_{i-1}-\left[2+(1-\frac{x_i}{5})\Delta x^2\right]y_i+y_{i+1}=x_i\Delta x^2,\quad i=1,2,3.$$

For i=1,

$$y_0-\left[2+(1-\frac{1.5}{5})(0.5)^2\right]y_1+y_2=(1.5)(0.5)^2.$$

For i=2,

$$y_1-\left[2+(1-\frac{2}{5})(0.5)^2\right]y_2+y_3=(2)(0.5)^2.$$

For i=3,

$$y_2-\left[2+(1-\frac{2.5}{5})(0.5)^2\right]y_3+y_4=(2.5)(0.5)^2.$$

Setting $y_0=2,\ y_4=-1,$ the linear system is

$$\begin{bmatrix} -2.175 & 1 & 0\\ 1 & -2.15 & 1\\ 0 & 1 & -2.125 \end{bmatrix}\begin{bmatrix} y_1\\ y_2\\ y_3 \end{bmatrix}=\begin{bmatrix} -1.625\\ 0.5\\ 1.625 \end{bmatrix}.$$

By solving the linear system, we get $y_1=0.552,\ y_2=-0.4244,\ y_3=-0.9644.$

B. Example

We will approximate the solution of nonlinear ordinary differential equation

$$8y''+yy'=2x^3+32,\ y(1)=17,\ y(4)=45 \qquad (3)$$

on the interval $1\le x\le 4,$ with h = 1.

Since h = 1, the interval [1, 4] is divided into 3 equal subintervals.

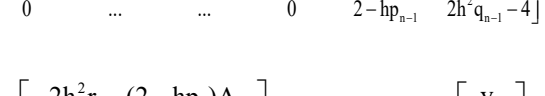

Using the central finite difference approximation [3], (3) gives

$$8\frac{y_{i+1}-2y_i+y_{i-1}}{\Delta x^2}+\frac{y_{i+1}-y_{i-1}}{2\Delta x}y_i=2x_i^3+32,\ i=1,2,$$

$$16(y_{i+1}-2y_i+y_{i-1})+\Delta x(y_{i+1}-y_{i-1})y_i=(2x_i^3+32)2\Delta x^2,\ i=1,2.$$

Rearranging the terms, we have

$$16y_{i+1}-32y_i+16y_{i-1}+y_{i+1}y_i\Delta x-y_{i-1}y_i\Delta x=(2x_i^3+32)2\Delta x^2,\ i=1,2.$$

For i=1, $16y_2-32y_1+16y_0+y_2y_1-y_0y_1=(2.2^3+32)2.$

For i=2, $16y_3-32y_2+16y_1+y_3y_2-y_1y_2=(2.3^3+32)2.$

By given that $y_0=17,\ y_3=45,$ the nonlinear system is

$$16y_2-32y_1+272+y_2y_1-17y_1=96,$$
$$720-32y_2+16y_1+45y_2-y_1y_2=172.$$

The nonlinear system can be expressed as a matrix with a corresponding vector,

$$F(Y)=\begin{bmatrix} f_1(y_1,y_2)\\ f_2(y_1,y_2) \end{bmatrix}=\begin{bmatrix} y_1y_2-49y_1+16y_2+176\\ -y_1y_2+16y_1+13y_2+548 \end{bmatrix}=\begin{bmatrix} 0\\ 0 \end{bmatrix}.$$

To approximate the solution to this nonlinear algebraic system, we will use the Newton's iterative method.
We can do this by taking an initial approximation $Y^0,$

$$Y^{n+1}=Y^n-(J(Y^n))^{-1}F(Y^n),\quad n\ge 0,$$

where $(J(Y^n))^{-1}$ is the inverse of the Jacobian matrix [4],

$$J(Y)=\begin{bmatrix} \frac{\partial f_1}{\partial y_1} & \frac{\partial f_1}{\partial y_2}\\ \frac{\partial f_2}{\partial y_1} & \frac{\partial f_2}{\partial y_2} \end{bmatrix}=\begin{bmatrix} y_2-49 & y_1+16\\ -y_2+16 & -y_1+13 \end{bmatrix}.$$

The first iteration:

If we take $Y^0 = \begin{bmatrix} 0 \\ 0 \end{bmatrix}$, then $F_0 = F(Y^0) = \begin{bmatrix} 176 \\ 548 \end{bmatrix}$.

$$J(Y^0) = J_0 = \begin{bmatrix} -49 & 16 \\ 16 & 13 \end{bmatrix}, \quad J_0^{-1} = \begin{bmatrix} -0.0146 & 0.0179 \\ 0.0179 & 0.0549 \end{bmatrix}.$$

$$Y^1 = Y^0 - J_0^{-1}F^0 = \begin{bmatrix} 0 \\ 0 \end{bmatrix} - \begin{bmatrix} -0.0146 & 0.0179 \\ 0.0179 & 0.0549 \end{bmatrix}\begin{bmatrix} 176 \\ 548 \end{bmatrix} = \begin{bmatrix} -7.2396 \\ -33.2356 \end{bmatrix}.$$

The second iteration:

We have $Y^1 = \begin{bmatrix} -7.2396 \\ -33.2356 \end{bmatrix}$,

then $F^1 = F(Y^1) = \begin{bmatrix} 239.5832 \\ -240.5088 \end{bmatrix}$.

$$J_1 = \begin{bmatrix} -82.2356 & 8.7604 \\ 49.2356 & 20.2396 \end{bmatrix}, \quad J_1^{-1} = \begin{bmatrix} -0.0097 & 0.0042 \\ 0.0235 & 0.0392 \end{bmatrix}.$$

$$Y^2 = \begin{bmatrix} -7.2396 \\ -33.2356 \end{bmatrix} - J_1^{-1}\begin{bmatrix} 239.5832 \\ -240.5088 \end{bmatrix} = \begin{bmatrix} -3.9055 \\ -29.4379 \end{bmatrix}.$$

III. Five-Point Finite Difference Method and Discrete Problem for Poisson Equation

In this section, five-point finite difference method for numerical solution of Poisson equation is proposed on two-dimensional domain. The method is mostly preferred method for irregular and regular domains. If the shape of the boundary is irregular, placing grid points on the boundary is difficult.

We consider a physical problem. An elastic membrane is fixed round a contour whose projection onto the horizontal plane is the boundary Γ of an open, bounded, connected domain Ω of this same plane. Suppose that the membrane is subjected to the action of a given vertical force $\Gamma F(x,y)dxdy$ per surface element of the horizontal plane and Γ being the tension of the membrane. The problem can be posed of the determination of the vertical displacement $U(x,y), (x,y) \in \Omega,$ of points of the membrane when subjected to this force [1],[3].

The function U satisfy the partial differential equation

$$-\left(\frac{\partial^2 U}{\partial x^2} + \frac{\partial^2 U}{\partial y^2}\right) = F(x,y), \quad (x,y) \in \Omega, \tag{4}$$

and (4) is called Poisson equation.

A function $U : \overline{\Omega} \to R$ is the solution of (4) and

$$U(x,y) = g, \quad (x,y) \in \Gamma,$$

where g is the height of the contour of the membrane, and is given. If the data F and g, as well as the boundary Γ, are sufficiently smooth, then the problem has a unique solution, continuous in $\overline{\Omega}$.

Let P be a point of Ω and let h_i be the distance of the point P from the point P_i. And let $P_i, 1 \le i \le 4$, be the four points of the set $\overline{\Omega}$ as shown in Fig. 1.

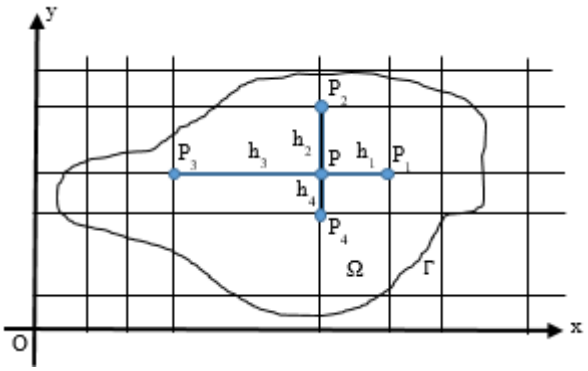

Fig 1. Finite difference discretization for membrane.

Using Taylor's formula [4],

$$U(P_1) = U(P) + h_1\frac{\partial U(P)}{\partial x} + \frac{h_1^2}{2!}\frac{\partial^2 U(P)}{\partial x^2} + \frac{h_1^3}{3!}\frac{\partial^3 U(\rho_1)}{\partial x^3}, \quad \rho_1 \in (P, P_1),$$

$$U(P_3) = U(P) - h_3\frac{\partial U(P)}{\partial x} + \frac{h_3^2}{2!}\frac{\partial^2 U(P)}{\partial x^2} - \frac{h_3^3}{3!}\frac{\partial^3 U(\rho_3)}{\partial x^3}, \quad \rho_3 \in (P, P_3),$$

$$\frac{\partial^2 U(P)}{\partial x^2} = \frac{2}{h_1^2 + h_3^2}\left[U(P_1) - 2U(P) + U(P_3) - (h_1 - h_3)\frac{\partial U(P)}{\partial x} - \left(\frac{h_1^3}{6}\frac{\partial^3 U(\rho_1)}{\partial x^3} - \frac{h_3^3}{6}\frac{\partial^3 U(\rho_3)}{\partial x^3}\right)\right].$$

If $h_1 = h_3$, we obtain

$$\frac{\partial^2 U(P)}{\partial x^2} = \frac{2}{h_1^2 + h_3^2}U(P_1) - \frac{4}{h_1^2 + h_3^2}U(P) + \frac{2}{h_1^2 + h_3^2}U(P_3) - \frac{h_1^3}{3(h_1^2 + h_3^2)}\frac{\partial^3 U(\rho_1)}{\partial x^3} + \frac{h_3^3}{3(h_1^2 + h_3^2)}\frac{\partial^3 U(\rho_3)}{\partial x^3}.$$

Neglecting terms involving third or higher order derivatives of the function U, the above equation becomes

$$\frac{\partial^2 U(P)}{\partial x^2} \approx \frac{2}{h_1^2 + h_3^2}U(P_1) - \frac{4}{h_1^2 + h_3^2}U(P) + \frac{2}{h_1^2 + h_3^2}U(P_3).$$

Similarly if $h_2 = h_4$,

$$\frac{\partial^2 U(P)}{\partial y^2} \approx \frac{2}{h_2^2 + h_4^2}U(P_2) - \frac{4}{h_2^2 + h_4^2}U(P) + \frac{2}{h_2^2 + h_4^2}U(P_4).$$

If $h_1 = h_2 = h_3 = h_4 = h$, the Laplacian operator approximates as

$$\frac{\partial^2 U(P)}{\partial x^2} + \frac{\partial^2 U(P)}{\partial y^2} \approx \frac{U(P_1) + U(P_2) + U(P_3) + U(P_4) - 4U(P)}{h^2}.$$

Denoting the approximate value of U at the representative mesh point $P(ih, jh)$ by $u(P) = u(ih, jh) = u_{i,j}$,

$$\left(\frac{\partial^2 U}{\partial x^2} + \frac{\partial^2 U}{\partial y^2}\right)_p = \left(\frac{\partial^2 U}{\partial x^2} + \frac{\partial^2 U}{\partial y^2}\right)_{i,j} \approx \frac{u_{i+1,j} + u_{i-1,j} + u_{i,j+1} + u_{i,j-1} - 4u_{i,j}}{h^2}.$$

This is called the five-point approximation of the Laplacian operator [5].

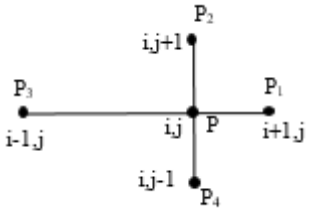

Fig 2. Five-point stencil in two-dimension.

Now, let Ω_h be the set of nodes of the mesh belonging to Ω, and Γ_h be the set of points of the plane which fall on the intersection of the boundary Γ and a horizontal and (or) vertical line of the mesh and $\overline{\Omega}_h$ be the set of all mesh points in $\overline{\Omega} = \Omega \cup \Gamma$. Then, the discrete problem over the discrete set $\Omega_h \cup \Gamma_h$ can be defined by

$$-\left(\frac{\partial^2 U_h(P)}{\partial x^2} + \frac{\partial^2 U_h(P)}{\partial y^2}\right) = F(P), \quad P \in \Omega_h,$$

$$U_h(P) = g(P), \quad P \in \Gamma_h.$$

The finite difference formula for solving Poisson equation takes the form

$$-\frac{u_{i+1,j} + u_{i-1,j} + u_{i,j+1} + u_{i,j-1} - 4u_{i,j}}{h^2} = F_{i,j}. \tag{5}$$

The linear system associated with this problem is the form

$$A_h' u_h = b_h,$$

where u_h is a column vector whose components are arranged in the particular order under consideration and b_h is known vector.

IV. Discretization Error for Poisson Equation on Rectangular Domain

Discretization error is difference between exact solution and numerical solution of model equation. It arises because of exact solution to the considered equation being solved is not obtained easily but is numerically approximated [1]. Several consistency requirements have to be fulfilled by the discretization scheme in order to ensure that the solution of the discretised equations closely approximates the solution of the original equation.

For the Dirichlet Problem

$$-\left(\frac{\partial^2 U}{\partial x^2} + \frac{\partial^2 U}{\partial y^2}\right) = F(x,y), \quad (x,y) \in \Omega = (0,a) \times (0,b), \tag{6}$$

$$U(x,y) = g, \qquad (x,y) \in \Gamma,$$

where g is known on the boundary Γ. We define $x_i = ih,\ i = 0(1)M$ and $y_j = jh,\ j = 0(1)N$, where $Mh = a$ and $Nh = b$.

The five-point difference approximation to (6) at the point (ih, jh) is

$$-\frac{u_{i+1,j} + u_{i-1,j} + u_{i,j+1} + u_{i,j-1} - 4u_{i,j}}{h^2} = F_{i,j}.$$

If we denote $Lu_{i,j} = \dfrac{u_{i+1,j} + u_{i-1,j} + u_{i,j+1} + u_{i,j-1} - 4u_{i,j}}{h^2}$,

$Lu_{i,j} = -F_{i,j}, \quad (ih, jh) \in \Omega_h$ and $u_{i,j} = g_{i,j}, \quad (ih, jh) \in \Gamma_h$.

If $e_{i,j}$ is defined by the discretization error at the point (ih, jh), then

$$e_{i,j} = U_{i,j} - u_{i,j}, \quad (ih, jh) \in \Omega_h.$$

V. Example for Two-Dimensional Domain

In this section, example is presented for Dirichlet problem associated with Poisson equation using finite difference method. We consider the function U which satisfies the equation

$$-\left(\frac{\partial^2 U}{\partial x^2} + \frac{\partial^2 U}{\partial y^2}\right) = 2, \tag{7}$$

at every point inside the square bounded by the straight lines $x = \pm 1, y = \pm 1$ and is zero on the boundary.

To get exact solution of Poisson equation, two common methods are variation iteration method and Adomian decomposition method. But variation iteration method provides the solution of problem without calculating Adomian's polynomials and also this method has a higher order of convergence to the solutions. Here, by using variation iteration method [4], exact solution of (7) is

$$U(x,y) = 1 - y^2 - \frac{32}{\pi^3}\sum_{n=0}^{\infty} \frac{(-1)^n}{(2n+1)^3} \operatorname{sech}\frac{(2n+1)\pi}{2} \cosh\frac{(2n+1)\pi x}{2} \cos\frac{(2n+1)\pi y}{2}. \tag{8}$$

The domain is made discretization into small squares using a square mesh of side $\frac{1}{4}$. From (5), the simplest finite difference approximation to (7) is the five-point equation

$$-\frac{1}{h^2}(u_{i+1,j} + u_{i-1,j} + u_{i,j+1} + u_{i,j-1} - 4u_{i,j}) = 2.$$

Since $h = \frac{1}{4}$, the difference equation is

$$-16(u_{i+1,j} + u_{i-1,j} + u_{i,j+1} + u_{i,j-1} - 4u_{i,j}) = 2,$$

$$8(u_{i+1,j} + u_{i-1,j} + u_{i,j+1} + u_{i,j-1} - 4u_{i,j}) = -1.$$

By using symmetry [2], there are only ten unknowns as shown in Fig. 3 and they are

$\tilde{u}_1$ at $P_1(0,0)$, $\tilde{u}_2$ at $P_2(\frac{1}{4},0)$, $\tilde{u}_3$ at $P_3(\frac{2}{4},0)$, $\tilde{u}_4$ at $P_4(\frac{3}{4},0)$,

$\tilde{u}_5$ at $P_5(\frac{1}{4},\frac{1}{4})$, $\tilde{u}_6$ at $P_6(\frac{2}{4},\frac{1}{4})$, $\tilde{u}_7$ at $P_7(\frac{3}{4},\frac{1}{4})$,
$\tilde{u}_8$ at $P_8(\frac{2}{4},\frac{2}{4})$, $\tilde{u}_9$ at $P_9(\frac{3}{4},\frac{2}{4})$, and $\tilde{u}_{10}$ at $P_{10}(\frac{3}{4},\frac{3}{4})$.

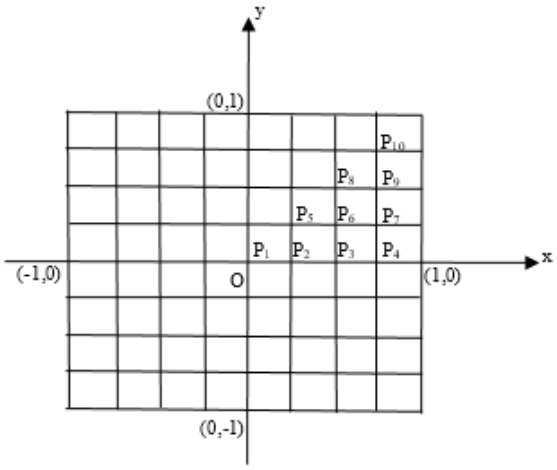

Fig 3. Finite difference discretization for square domain.

Thus,

$$P_1: 8(4\tilde{u}_2 - 4\tilde{u}_1) = -1,$$
$$P_2: 8(\tilde{u}_1 + \tilde{u}_3 + 2\tilde{u}_5 - 4\tilde{u}_2) = -1,$$
$$P_3: 8(\tilde{u}_2 + \tilde{u}_4 + 2\tilde{u}_6 - 4\tilde{u}_3) = -1,$$
$$P_4: 8(\tilde{u}_3 + 2\tilde{u}_7 - 4\tilde{u}_4) = -1,$$
$$P_5: 8(2\tilde{u}_2 + 2\tilde{u}_6 - 4\tilde{u}_5) = -1,$$
$$P_6: 8(\tilde{u}_3 + \tilde{u}_5 + \tilde{u}_7 + \tilde{u}_8 - 4\tilde{u}_6) = -1,$$
$$P_7: 8(\tilde{u}_4 + \tilde{u}_6 + \tilde{u}_9 - 4\tilde{u}_7) = -1,$$
$$P_8: 8(2\tilde{u}_6 + 2\tilde{u}_9 - 4\tilde{u}_8) = -1,$$
$$P_9: 8(\tilde{u}_7 + \tilde{u}_8 + \tilde{u}_{10} - 4\tilde{u}_9) = -1,$$
$$P_{10}: 8(2\tilde{u}_9 - 4\tilde{u}_{10}) = -1.$$

In matrix form,

$$\begin{bmatrix} -32 & 32 & 0 & 0 & 0 & 0 & 0 & 0 & 0 & 0 \\ 8 & -32 & 8 & 0 & 16 & 0 & 0 & 0 & 0 & 0 \\ 0 & 8 & -32 & 8 & 0 & 16 & 0 & 0 & 0 & 0 \\ 0 & 0 & 8 & -32 & 0 & 0 & 16 & 0 & 0 & 0 \\ 0 & 16 & 0 & 0 & -32 & 16 & 0 & 0 & 0 & 0 \\ 0 & 0 & 8 & 0 & 8 & -32 & 8 & 8 & 0 & 0 \\ 0 & 0 & 0 & 8 & 0 & 8 & -32 & 0 & 8 & 0 \\ 0 & 0 & 0 & 0 & 0 & 16 & 0 & -32 & 16 & 0 \\ 0 & 0 & 0 & 0 & 0 & 0 & 8 & 8 & -32 & 8 \\ 0 & 0 & 0 & 0 & 0 & 0 & 0 & 0 & 16 & -32 \end{bmatrix} \begin{bmatrix} \tilde{u}_1 \\ \tilde{u}_2 \\ \tilde{u}_3 \\ \tilde{u}_4 \\ \tilde{u}_5 \\ \tilde{u}_6 \\ \tilde{u}_7 \\ \tilde{u}_8 \\ \tilde{u}_9 \\ \tilde{u}_{10} \end{bmatrix} = \begin{bmatrix} -1 \\ -1 \\ -1 \\ -1 \\ -1 \\ -1 \\ -1 \\ -1 \\ -1 \\ -1 \end{bmatrix}.$$

Solving this matrix form with the use of Matlab, we get finite difference solutions as shown in Table 1. In this table, analytical solutions are computed from (8) for required (x, y) coordinates. And discretization errors are calculated by using $e_{i,j} = U_{i,j} - u_{i,j}$ described in section IV.

TABLE I. TABLE FOR FINITE DIFFERENCE SOLUTION AND ANALYTICAL SOLUTION

i	finite difference solution ($\tilde{u}_i$)	analytical solution(U_i)	Discretization error ($\tilde{e}_i$)
1	0.58245	0.58938	6.93×10^{-3}
2	0.55120	0.55777	6.57×10^{-3}
3	0.45316	0.45867	5.51×10^{-3}
4	0.27620	0.27947	3.27×10^{-3}
5	0.52171	0.52829	6.58×10^{-3}
6	0.43012	0.43560	5.48×10^{-3}
7	0.26332	0.26666	3.34×10^{-3}
8	0.35729	0.36228	4.99×10^{-3}
9	0.22196	0.22548	3.52×10^{-3}
10	0.14223	0.14564	3.41×10^{-3}

By viewing the discretization errors, obtained maximum errors are very small. And approximate solutions are related to number of grids given region is divided. If the grids are more used, the approximation will be better.

VI. CONCLUSIONS

In this paper, we have discussed and applied finite difference method for numerical solutions of second order differential equations on one- and two- dimensional domains subject to boundary conditions. By using the central finite difference approximations, numerical results show good performance and efficiency of proposed method. For Poisson equation, (5) is also the central finite difference with five-point stencil. In solving second order differential equations, finite difference method is used as direct conversion of the differential equation by replacing derivative operators with approximate finite difference. This converts entire problem into a system of linear equations that may be readily solved by means of matrix inversion and we get the required function values.

A common usage is for things like solving differential equations numerically, and approximating derivatives for root finding and numerical optimization schemes. The mentioned areas of use span application in many domains, whether it is engineering, science, business, etc.

ACKNOWLEDGMENT

We are grateful to the journal committee and the editorial board for permitting the submission of this paper.

REFERENCES

[1] D. M. Causon, and C. G. Mingham, "Introductory Finite Difference Methods for PDEs", Bookboon. Com., 2010.
[2] P. K. Pandey and S. S. A. Jaboob, "A finite difference method for a numerical solution of elliptic boundary value problems", Applied Mathematics and Nonlinear Sciences, June 2018.
[3] G. G. Smith, "Numerical Solution of Partial Differential Equations", Clarendan Press, Oxford, 1985.
[4] J. C. Strikwerda, "Finite Difference Schemes and Partial Differential Equations", Wadsworth & Books / Cole California, 1989.
[5] Ubaidullah and Muhammad Saleem Chandio, "Finite Difference Method with Dirichlet Problems of 2D Laplace's Equation in Elliptic Domain", Pakistan Journal of Engineering Technology and Science(PJETS), V0lume 6, No 2, December 2016.

Article ID – JRA6004520

Analysis on Transportation Network of Shwebo Township

Thida Aye
Department of Geography
Taunggoke Degree College, Taunggoke, Myanmar
thidaaye140769@gamil.com

Aye Aye Moe
Department of Geography
University of Myitkyina, Myitkyina, Myanmar

Seinn Seinn Min
Department of Geography
Taunggoke Degree College, Taunggoke, Myanmar

***Abstract*- Development gap between rich and poor and also between urban and rural areas is a major problem of globalization age today. The term 'development' is defined by very different ways, very different criteria and even very different parameters. However, there is no universally accepted definition of that term up to present. Instead of this, advanced technology is generally accepted as an essential element of development and one of the most possible ways to portray development is the creation of better transportation and communication systems within a particular area or region. Based on this concept, geographic traces on initial development pattern in Shwebo Township are made focusing on the transportation network. In this analysis, β index method is used. According to the result, it is found that the study area has improved network connectivity from β index= 1.1(complete simple connection, 1948-1965), β index=1.2(interconnection, 1980-1997), β index= 1.3 interconnection,2011) to β index = 1.4 (advanced interconnection, 2020).**

Keywords- development, transportation, network, connectiity, interconnection

I. INTRODUCTION

In general, development and improvement in transportation is an important factor for the future development of any region. Shwebo Township is situated at the central position within Shwebo District and hence its influential role in local transportation and trade must be known. The available modes of transportation and transportation network are important for the right time transshipment of goods and movement of people. For the future development planning of any region, transportation network is one of the basic infrastructures and it plays a significant role.

The main aim of this research work is to know the development of transportation network in Shwebo Township. The objectives are (1) to know the physical conditions are the best outline in term of its more important transportation**,** (2) to study the importance of transportation, (3) to examine transportation network, (4) to know flow and connection of transportation network, (5) to point out its vital role in national economic development, and (6) to form an essential part of the infrastructure of the country's economy.

The motor-car roads, the railways and the waterways are studied carefully and presented. The materials concerned with this research paper are location map and transportation map. The data and information about transportation modes and flows of commodities and people are also basic materials for this research paper.

The require data and information were obtained from the various department of Shwebo District. These obtained data are processed, computerized and required graphical presentation are made. The basic statistical technique used in this paper is: **β index = e/v (e = edges, v = vertices).**

II. STUDY AREA

Shwebo Township lies in the Central Dry Zone of Myanmar Naing Ngan, between north latitudes of 220 29 ' and 220 41', and east longitudes of 950 24' and 950 50'. The township is bounded on the north by Khin-U Township, on the east by Singu Township, on the south by Wetlet Township and on the west by Depeyin Township. It extends 30 miles from east to west and 14 miles from north to south, with a total area of 412.19 square miles or 263,803 acres. Shwebo Township comprises Shwebo and Kyaukmyaung Towns and 72 village tracts. The boundary of Shwebo Township is of two kinds, the land boundary and the river boundary. River boundaries are found on the eastern and western sides of the township with the Ayeyarwady and Mu rivers respectively, while the administrative ones are on the northern and southern border of the township. Shwebo Township has a rectangular shape elongating from east to west. (Figure 1)

Generally, the topography of the township can be mainly divided into two regions: (a) the western lowland and (b) the eastern region of low hills with narrow riverine plains. The western lowland is located on the east bank of Mu River and it is almost flatland area. This region is known as Mu Valley, the area drained by north-south running. The eastern region is on the east of Mandalay-Myitkyina railroad and consists of eastern low hills of Minwun range with parts of Ayeyarwady. The chief rivers of Shwebo Township are Ayeyawady and Mu rivers. Only these two rivers are perennial. Mu River is very important for agriculture and and it can be said as

the artery of the township. The Ayeyawady passes through for about

27 miles along the eastern boundary of the township. Mu River is the most important river for rice cultivation of Shwebo Township. The river is navigable by local craft in the rainy season before the construction of Kabo Dam. The river is a perennial stream which has a shallow depth of water during the dry period. (Figure2)

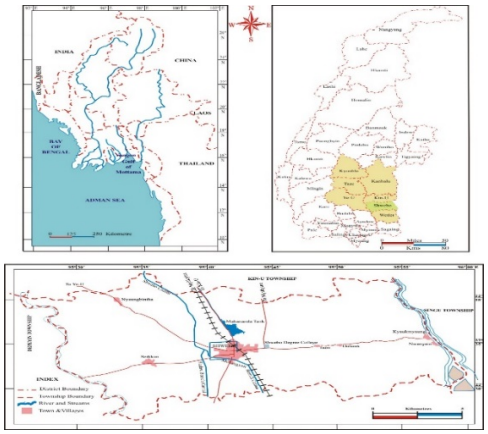

Fig.1. Location map of Shwebo Township

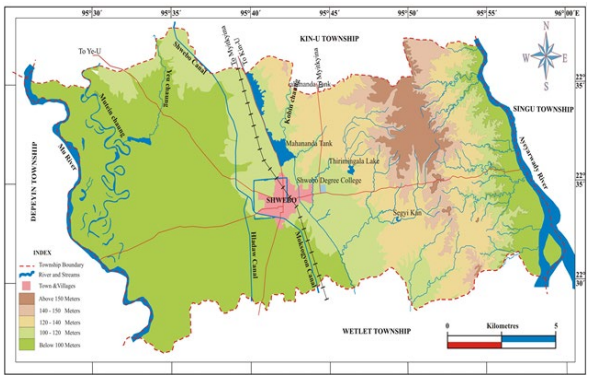

Fig.2. Topography and drainage of Shwebo Township

The climatic condition has a great impact on the socio-economic aspects of a region. In the study area, the temperature is high in summer for every year. Since it lies in Dry Zone of Central Myanmar, the average annual temperature of 30-years period from 1990 to 2019 is 79.68˚F. During this period, the average maximum temperature is 92.07˚F, while the average minimum temperature is 67.19˚F. The average annual total rainfalls amount to 39.51 inches. According to Koppen's classification, this area belongs to the Tropical Savanna (Aw) type of climate.

III. MODES OF TRANSPORTAION

The transportation modes of Shwebo Township are of two types and they are water transportation and land transportation. During the regions of the Burmese (Myanmar) Kings the inland waterways is a transportation route connected with the economic activities within the region. After the annexation of the British of upper Myanmar (Burma) in 1885, railway lines and motorcar roads were built. Before 1894, the transportation connected with the economic activities within the region by railroads (trains) was more important than the transportation by car roads (cars). But since 1944, motorcar roads were being used more as a means of transportation than the water routes. The mode of the transportation of Shwebo Township is described as waterway transport, rail transport, and road transport excluding air transport.

A. Waterway transportation

The Ayeyarwady River, the life artery of Myanmar, plays an important role in the transportation and communication of Myanmar as well as in Shwebo Township.

Kyaukmyaung river port lies 17 miles east of Shwebo and it is an important port of Shwebo Township. The up-stream and down-stream water crafts plying between Mandalay-Bhamo and Mandalay - Thabeikkyin stop at Kyaukmyaung. Steamers plied back and forth between them with monthly trips of 21 trips. They transported 30422 passengers and 6168 tonnage of freight from and to Shwebo Township in 2010-11. In 2019, steamers plied back and forth between them with monthly trips of 17 trips. After the construction of Ayeyarwady Bridge, the passenger and freight are dropped to 27 passengers and 10 tons of freight respectively. But the small villages along the river channel are connected with Kyaukmyaung port which serves as the central base of transportation and commerce.

B. Rail transportation

One of the chief means of transportation of Shwebo Township is railway. The major railway lines of the township are Mandalay –Myitkyina Railroad and Shwebo - Ye-U Railroad. Today the Department of Rail Transport has servicing the up and down trips between Mandalay – Myitkyina, Mandalay – Nabar, Shwebo – Kyunhla, and Shwebo – Monyin. They all totaled 5 up and down trains and transported about 10000 passengers per day in 2019.

C. Road transportation

In Myanmar car roads are the most important and that most used means of transportation lines for passengers and the flow of commodities. Motor roads radiate from Shwebo to different regions of Myanmar. They are the most important mean of transportation of the township. In Shwebo Township, there are:

(1) Shwebo-Myitkyina Road,
(2) Shwebo-Mandalay Road,
(3) Shwebo-Kyaukmyaung Road,
(4) Shwebo-Nyaungbintha-Ye-u Road,
(5) Shwebo-Seikkhun-Tebin Road,
(6) Shwebo-Chibar-Plaing Road
(7) Shwebo-Monywa Road,
(8) Shwebo-Tagaung Road,
(9) Shwebo-Khin U-Ye U – Tantze Road,
(10) Shwebo-Zegone-Kanbalu-Kyunhla Road,
(11) Shwebo-Mogok Road,
(12) Shwebo-Yangon Road,
(13) Shwebo-Naypyidaw Road,
(14) Shwebo-Wetlet Road,
(15) Shwebo-Sagaing Road, etc.

There are 24 motorcar associations plying the daily total of 106 various cars (passenger express and Dyna) to the various part of Myanmar (table 1). They have different carrying capacities.

In addition to the mentioned modes of transportation, canal bank tracks and cart-tracks are important means of transportation for local transportation of agricultural products and local communication. They are widely spread within the township; especially canal is in the western and southwestern part of the township.

TABLE 1. DAILY SERVICING MOTORCARS BY MOTORCAR ASSOCIATIONS AND THEIR TRIP DIRECTION IN SHWEBO TOWNSHIP (2020)

From	To	motorcar Associations	Daily Trips	Direction
Shwebo	Mandalay	Yangyiaungman	12	South
		Aungnaingman	10	
		Nanmyint	2	
		Yanaungman	8	
		Aungtheinkhaman	3	
		Nanmyint	2	
Seikkhun	Mandalay	Aungnaingman	1	Southwest, South
Nyaungbintha	Mandalay	Aungnaingman	1	West, South
Yegyiwa	Mandalay	Aungnaingman	1	S Southwest, South
		Yanaungman	1	
Kyaukmyaung	Mandalay	Aungnaingman	1	East, South
Kyunhla	Mandalay	Aungnaingman	1	North, South
Mandalay	Zeegone	Yangyiaungman	3	South, North
Kabore-Zeegone	Mandalay	Shwekyiesin	5	Northwest, South
Shwebo	Yangon	Aungnaingman	2	South
		Famous	1	
		Aungyadana	2	
		New Seinhtayhlaing	1	
		Winthitsar	3	
		Waiphyoaung	1	
Kyunhla-Kantbalu	Yangon	Aungnaingman	1	North, South
		Winthitsar	1	
		Aungyadana	1	
Shwebo	Naypyidaw	Kyetagon	1	Southwest
Shwebo	Kyunhla	Yanaungman	1	North
Shwebo	Monywa	Kanyarmin	12	South
		Yangyiaungman	2	
Shwebo	Monywa-Pakkoku	Kanyarmin	1	South, Southwest
Sagaing	Shwebo	Shweman	1	South, North
		Sataungman	1	
		Manshwetaung	1	
Shwebo	Zin	Yadanatheinkha	2	North
		Yadanathiha	1	
Shwebo	Zin-Katha	Yadanathiha	1	North
Shwebo	Tagaung	Yadanathiha	3	North
Shwebo	Ye - U	Mandalaroo	3	Northwest
Shwebo	Khin – U - Ye-U	Ayaungmyeoo	1	N-Northwest
		Kyethonepwint	1	
Tantze	Singu - Mogok	Yanaungpadamyar	1	Southwest, East
Ye – U	Shwebo - Mogok	Padamyarmye	1	Southwest, East
Shwebo	Mogok	Yanaungpadamyar	4	East
		Padamyarmye	4	
		24	106	

D. The value of traffic and their flow direction

Shwebo Township is situated on the Mu Valley of the Central Dry Zone of Myanmar Naing Ngan. It has good agricultural bases and sufficient amount of agricultural water resource. Thus the region is surplus in agricultural products like rice and pulses. These facts support for the transport of surplus goods to other required regions of Myanmar. Moreover, its central location within Mu Valley plays a major role in the development of transportation and communication of Shwebo Township. Shwebo Township and its hinterlands have high consumption power and thus the purchasing for needed goods also comprises in the development of transportation and in the increase of traffic flow.

The main agricultural surpluses of the region are rice, wheat, and pulses. The local need commodities are various kinds of household goods, construction materials, chemicals such as pesticides and fertilizer, salted fish, dry fish, and fish source. These surplus and needs caused to the high traffic flow to the east and south direction.

As shown in Table (2) the direction of trips and the flow of traffic are highest to the south with the daily trips of 12 and daily traffic flow of 79. In this amount should be added the freight cargo of Road Transport Department. It shows the "interaction" among the surplus regions and required regions.

The second high in direction of flow and trips is to the north with the daily trips of 7 and daily traffic flow of 15. The remaining directions have low trips and decrease flow because of local connection and communication.

TABLE 2. DAILY TRAFFIC FLOW DIRECTION FROM AND TO SHWEBO

Direction	No. of Trips	No. of Traffic
South	12	79
North	7	15
East	5	11
West	1	1
Southeast	1	1
Southwest	4	4
Northwest	3	10
S-Southwest	1	2

IV. ANALYSIS ON TRANSPORTATION NETWORK

Transportation Network or Communication Network is an inter-connected system of fixed lines of movement between Activity Nodes. The main means of carrying traffic are roads, footpaths, railways, and inland waterways. Sea-travel routes and Air Corridors also form part of transport networks but are neither fixed in position nor visible. Each section if fixed line forms a link in a national network connecting junction points at which travelers change mode of travel or terminate a journey.

The transportation routes of Shwebo Township are motorcar roads, railroads and waterways which connect one region to another. The connectivity of transportation network can be measured by means of Graph Theory. In studying it, the tarred roads and every weather route within the township are analyzed. The Indices obtained after calculation can be used as β index. β index is the ratio between the number of the transportation lines "e" and the main stopping or resting region "v".

A network with a β index of less than one means partially connected. If the β index is zero, there is no network system, but less than one there are some routes along which goods or commodities can flow. A network

with a β index of equal to unity can be described as a complete simple network connection (Figure 3).

As shown in Figure (4) β index of the transportation network of Shwebo Township during 1948 and 1965 was 1.1. It means that the network connectivity of Shwebo Township was in the stage of complete simple connection since that time.

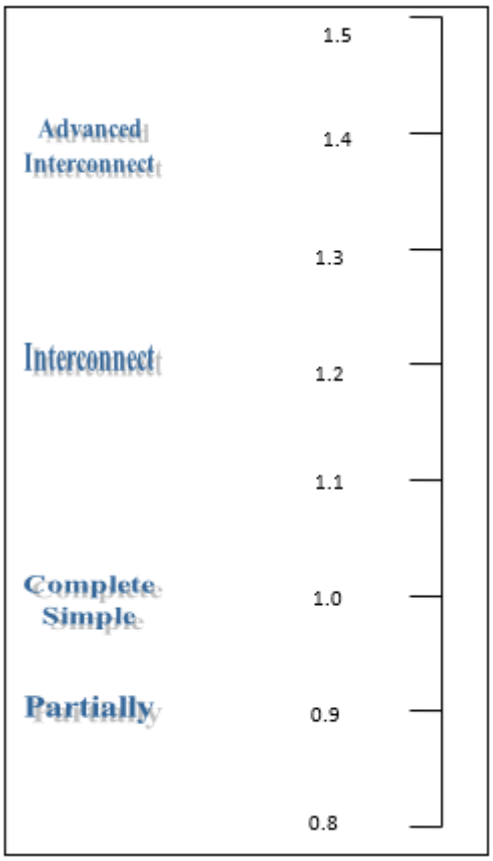

Fig. 3. Connectivity of transportation network (β index value)

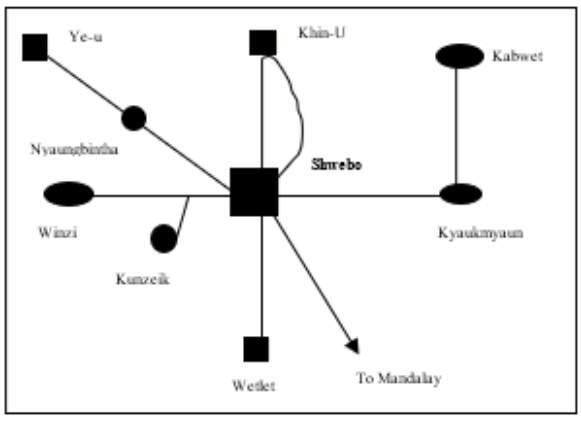

Fig. 4. Development of the connectivity of transportation network β index value of Shwebo Township (1948-1965)

$$\beta = e/v$$
$$= 11/10$$
$$= 1.1\#$$

As shown in Figure (5) β index of the transportation network of Shwebo Township during 1980 and 1997 was 1.2. It means that the network connectivity of Shwebo Township was in the stage of interconnection at that time.

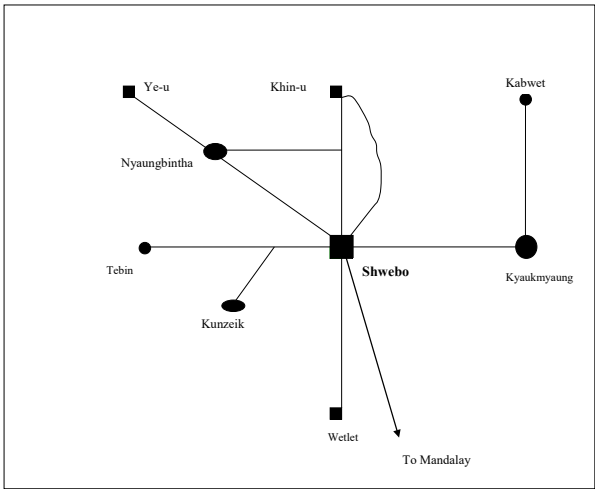

Fig.5. Development of the connectivity of transportation network β index value of Shwebo Township (1980-1997)

$$\beta = e/v$$
$$= 13/11$$
$$= 1.2\#$$

As shown in Figure (6) β index of the transportation network of the township in the year of 2011 was 1.3. It means that the network connectivity of Shwebo Township has been improving and developed to complete interconnection at that time.

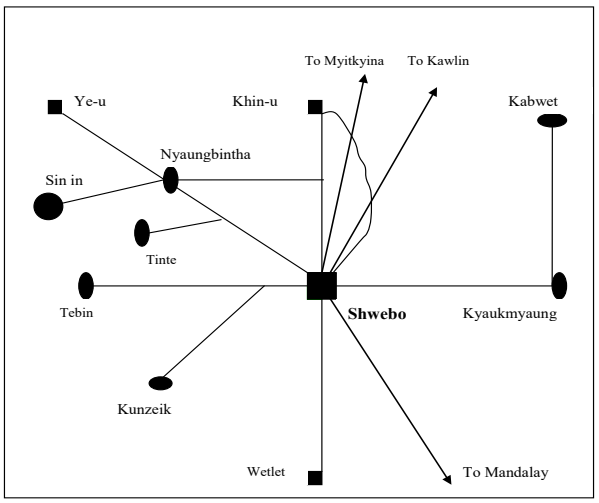

Fig. 6. Development of the connectivity of transportation network β index value of Shwebo Township (2011)

$$\beta = e/v$$
$$= 18/14$$
$$= 1.3\#$$

As shown in Figure (7) β index of the transportation network of the township in the year of 2020 was 1.4. It means that the network connectivity of Shwebo Township is in advanced network connection at the present time.

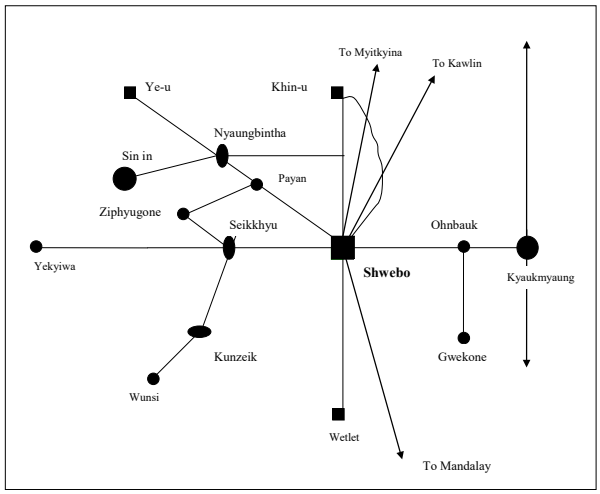

Fig. 7 Development of the Connectivity of Transportation Network β Index Value of Shwebo Township (2020)

$$\beta = e/v$$
$$= 22/16$$
$$= 1.4\#$$

V. FINDING AND RESULTS

This research provides the following results and findings.

(1) In waterway transportation, steamers plied back and forth between Mandalay - Bhamo and Mandalay - Thabeikkyin stop at Kyaukmyaung with monthly trips of 21 trips in 2010-11. In 2019, steamers plied back and forth between them with monthly trips of 17 trips. They have decreased with monthly trips of four trips. After the construction of Ayeyarwady Bridge, the passenger and freight are dropped to 27 passengers and 10 tons respectively.

(2) The major railway lines of the township are Mandalay –Myitkyina Railroad and Shwebo - Ye-U Railroad. Today the Department of Rail Transport has servicing the up and down trips between Mandalay – Myitkyina, Mandalay – Nabar, Shwebo – Kyunhla, and Shwebo – Monyin.

(3) In road transportation, there are 24 motor car associations plying the daily total of 106 various cars (passenger express and Dyna) to the various part of Myanmar.

(4) The direction of trips and the flow of traffic are highest to the south with the daily trips of 12 and daily traffic flow of 79. It shows the "interaction" among the surplus regions and required regions.

(5) The study area has improved network connectivity from β index = 1.1(complete simple connection, 1948-1965), β index = 1.2 (interconnection, 1980-1997), β index = 1.3 (improving and developed to complete interconnection, 2011) to β index = 1.4 (advanced interconnection, 2020).

VI. CONCLUSION

The transportation modes of Shwebo Township are waterway transport, rail transport, and road transport. The Ayeyarwady River plays an important role in the transportation and communication of Shwebo Township. Kyaukmyaung port is the chief port of Shwebo Township. The up-stream and down-stream water crafts plying between Mandalay-Bhamo and Mandalay - Thabeikkyin stop at Kyaukmyaung.

One of the chief means of transportation of Shwebo Township is railway. The major railway lines of the township are Mandalay- Myitkyina Railroad and Shwebo - Ye-U Railroad.

Motorcar roads radiate from Shwebo to different regions of Myanmar. In Shwebo Township, the all-weather motorcar roads are Shwebo - Myitkyina Road, Shwebo - Mandalay Road, Shwebo - Kyaukmyaung Road, Shwebo - Nyaungbintha -Ye-u Road, Shwebo - Seikkhun - Tebin Road, and Shwebo - Chibar - Plaing Road, etc.

The transportation network of Shwebo Township is improving in connectivity, and the traffic flows are also increasing, especially toward the south and the north. With the economic development of the region, there is ever increasing use of motor cycles, private owned light trucks, and agricultural used machinery are on the roads within the township. Thus, the quality of roads, such as width, should be upgraded to avoid unnecessary accidents and death of lives.

ACKNOWLEDGEMENT

We are grateful to various departments for their permission to copy facts, tables, maps and illustrations. We are also thanking our former teachers who thought us geography and leading us to become a studious learner of higher learning.

REFERENCES

[1] Annual Reports: The Long Distance United (combined) Motorcar Associations Maintenance and Supervision Committee, Shwebo District.

[2] Annual Reports: Sub-division of Inland Waterway, Kyaukmyaung, Shwebo District.

[3] J. P. Rodrigue, "The Geography of Transport System", Department of Economic and Geography, Hofstra University, 2006.

[4] E. J. Taffee & H. L. Gauthier, "Geography of Transportation", 2nd ed, Prentice-Hall Ins, New Jersey, 1996.

[5] http://webspace.ship.edu/pgmarr/TransMeth/Lec%25202ConneConnect.pdf&sa=U&ved=2ahUKEwi46ID9i4HsAhUDVHOKHHsAhUDVHOKHVpvCROQF&usg=AOvVaw3Muio3MpQkx-aQbMA70huF. PP.22-26.

[6] A. M. Abbas1, R. B. Hashidu2, Department of Geography, Faculty of Humanities Management and Social Sciences, Federal University of Kashere, Gombe State, Nigeria. Transportation Network Analysis, Connectivity and Accessibility Indices in North East, Nigeria. PP.62.

Article ID – JRA6005720

Convexity of Sets and Set-Valued Mappings

Wai Wai Moe
Department of Mathematics
University of Magway
Magway, Myanmar
moewaiwai111@gmail.com

***Abstract*- In this paper, firstly, some definitions and properties concerning convexity of sets are presented. And then some properties of convex cone are also described. And some various types of convexity for set-value mappings are established. Moreover, the set-valued mapping on a given interval is quasiconvex is calculated with four cases. Finally, the set-valued mapping is closure convexlike on the given interval and it is not convexlike on it is described with the example.**

Keywords: Convex sets, convex cones, set-valued mappings

I. Introduction

We first introduce the definitions of convex, nearly convex and closure convex. Then we study some properties of convexity in a real Hausdorff topological vector space. And then the cone generated by a nonempty set is also defined. Moreover, we described the generated cone is a closed convex cone. We also discus the tangent cone is closed. Next we express (i) S-convex, (ii) nearly S-convex and (iii) closure S-convex. Then the converse implications of these are not generally true is illustrated with examples. Moreover, we state that convexity of set-valued mapping, quasiconvexity of set-valued mapping, convexlike set-valued mapping and closure convexlike set-valued mapping. Then we illustrate that the set-valued mapping on a given interval is quasiconvex with four cases. And then the set-value mapping is convexlike on a given set if and only if it is convex on it is also proved.

II. Preliminaries on Convex Sets

Let C be a subset of a real Hausdorff topological vector space Y. Let $\overline{C}$ (resp. int C) denote the closure (resp. the interior) of C.

A. Convex, Nearly Convex, and Closure Convex

A subset C of Y is said to be:

(i) convex if, for any $y_1, y_2 \in C$ and $\alpha \in (0,1)$, $\alpha y_1 + (1-\alpha)y_2 \in C$;

(ii) nearly convex if there exists $\alpha \in (0,1)$ such that, for any $y_1, y_2 \in C$, $\alpha y_1 + (1-\alpha)y_2 \in C$;

(iii) closure convex if its closure $\overline{C}$ is convex.

In particular, if $\alpha = \frac{1}{2}$ in (ii), we say that C is midpoint convex. It is clear that if C is convex, then it is also nearly convex, but not conversely.

Simple examples of convex sets are the empty set, the singleton set $\{x_0\}$, the complete spaces R^n.

Lemma

Let A be a convex subset of a topological vector space Y. If x is interior to A and y in the closure of A, the open line segment joining x and y is interior to A.

Proof

Let λ, $0 < \lambda < 1$, be fixed; we have to show that $\lambda x + (1-\lambda)y \in \text{int } A$. By a translation if necessary we can arrange that $\lambda x + (1-\lambda)y = 0$. Now $y = \alpha x$ where $\alpha < 0$. Since $\omega \to \alpha\omega$ is a homeomorphism of Y and $x \in \text{int } A, y \in \overline{A}$, there exists a $z \in \text{int } A$ such that $\alpha z \in A$. Let $\mu = \alpha/(\alpha - 1)$; then $0 < \mu < 1$ and $\mu z + (1-\mu)\alpha z = 0$. Hence

$$U = \{\mu\omega + (1-\mu)\alpha z \mid \omega \in \text{int } A\}$$

is a neighborhood of 0 since $\omega \to \mu\omega + (1-\mu)\alpha z$ is a homeomorphism of Y mapping $z \in \text{int } A$ onto 0. But $\omega \in \text{int } A$ and $\alpha z \in A$ imply $U \subset A$, since A is convex; hence $0 \in \text{int } A$.

Lemma

Let $C \subset Y$ be a convex subset. Then its closure $\overline{C}$ is convex. If, moreover, $\text{int } C \neq \varnothing$, then $\text{int } C$ is convex and $\overline{C} = \overline{\text{int } C}$; $\text{int } C = \text{int } \overline{C}$.

Proof

Assume that C is convex. Take any $x, y \in \overline{C}$ and $\alpha > 0, \beta > 0$ such that $\alpha + \beta = 1$. Let W be a neighborhood of $\alpha x + \beta y$. Define $g: Y \times Y \to Y$ by $g(u, v) = \alpha u + \beta v$. Then g is continuous from $Y \times Y$ into Y. Therefore g is continuous at (x,y) and $g(x, y) = \alpha x + \beta y$. Since W is a neighborhood of $\alpha x + \beta y$, $g^{-1}(W)$ is a neighborhood of (x,y) in $Y \times Y$. Therefore there exist a neighborhood U of x and a neighborhood V of y such that $U \times V \subset g^{-1}(W)$. Since $x, y \in \overline{C}$, we get $U \cap C \neq \varnothing$ and $V \cap C \neq \varnothing$. Therefore there exist $a \in U \cap C$ and $b \in V \cap C$. So $a \in U$, $a \in C$ and $b \in V$, $b \in C$. Then $(a,b) \in U \times V$. Hence $(a,b) \in g^{-1}(W)$ and $g(a,b) \in W$. Therefore

$\alpha a+\beta b\in W$. Since C is convex, $\alpha a+\beta b\in C$. Thus $W\bigcap C\neq\varnothing$. Hence $\alpha x+\beta y\in\overline{C}$ and $\overline{C}$ is convex.

Take any $x,y\in \operatorname{int} C$ and $\lambda\in(0,1)$. Hence $x\in \operatorname{int} C$ and $y\in\overline{C}$. Thus $\lambda x+(1-\lambda)y\in \operatorname{int} C$ by Lemma. Therefore $\operatorname{int} C$ is convex.

Since $\operatorname{int} C\subset C$, $\overline{\operatorname{int} C}\subset\overline{C}$ holds trivially. Since $\operatorname{int} C$ is nonempty, there exists $x\in \operatorname{int} C$ and let $y\in\overline{C}$. Because of $\operatorname{int} C\subset C\subset\overline{C}$, we get $x\in\overline{C}$. By the convexity of $\overline{C}$, we have

$$\lambda x+(1-\lambda)y\in\overline{C}.$$

Since $x\in \operatorname{int} C$ and $y\in\overline{C}$, $\lambda x+(1-\lambda)y\in \operatorname{int} C$ by Lemma. Therefore $\overline{C}\subset \operatorname{int} C\subset\overline{\operatorname{int} C}$. Thus $\overline{C}=\overline{\operatorname{int} C}$.

To prove $\operatorname{int} C=\operatorname{int}\overline{C}$, it suffices to show that $0\in \operatorname{int}\overline{C}$ implies $0\in \operatorname{int} C$ if C is convex with nonempty interior. There exists a circled neighborhood V of 0 such that $V\subset\overline{C}$. Since $\overline{C}=\overline{\operatorname{int} C}$, $0\in\overline{\operatorname{int} C}$; hence $\operatorname{int} C$ and V intersect. Let $y\in \operatorname{int} C\bigcap V$. Since $V\subset\overline{C}$ and V is circle, we have $-y\in\overline{C}$. It follows now from Lemma, that $0\in \operatorname{int} C$ since $0=\frac{1}{2}y+\frac{1}{2}(-y)$.

III. Some Various Types of Convex Cones

A. Cone, Pointed Cone

A subset S of Y is called a cone if, for any $y\in S$ and $\lambda\geq 0$, $\lambda y\in S$. A cone S is pointed if $S\bigcap(-S)=\{0\}$.

Hence S is a convex cone if and only if $\lambda S\subset S$ for all $\lambda\geq 0$ and $S+S=S$. Let B be a nonempty subset of Y. The cone

$$\text{cone (B)} = \{\lambda b\,|\,\lambda\geq 0, b\in B\}$$

is called the cone generated by B. By $\overline{\text{cone}}(B)$ we denote the closure of cone (B).

Lemma

Let $B\subset Y$ be a convex subset and $y_0\in B$. Then $\overline{\text{cone}}(B-y_0)$ is a closed convex cone.

Proof

We begin by stating the following consequence of convexity:

$\forall\, y\in \text{cone}(B-y_0)$, $\exists h>0, \forall\, t\in[0,h], y_0+ty\in B$, since we can write that for any $t\in[0,h]$,

$$y_0+ty=\left(1-\frac{t}{h}\right)y_0+\frac{t}{h}(y_0+hy)$$

is a convex combination of elements of B.

For any $y_1,y_2\in \text{cone}(B-y_0)$ and $\alpha\in[0,1]$ there exists $h>0$ such that $y_0+\alpha h\, y_1\in B$ and $y_0+(1-\alpha)h\, y_2\in B$. Hence

$$\alpha y_1+(1-\alpha)y_2\in\frac{B-y_0}{h}\subset \text{cone}(B-y_0).$$

Thus cone $(B-y_0)$ is convex, and so $\overline{\text{cone}}(B-y_0)$ is also convex by Lemma.

B. Sequential Tangent Cone

Let B be a subset of Y. For a given point $y_0\in\overline{B}$, the sequential tangent cone $T(B,y_0)$ for the set B at the point y_0 is defined by

$$T(B,y_0)=\left\{v\in Y\,|\,v=\lim\lambda_n(y_n-y_0),\lambda_n\geq 0,\ y_n\in B, y_n\to y_0, n\in N\right\}.$$

In general, a tangent cone is not closed. If the topology is induced by a norm, then a tangent cone is indeed closed. By $\overline{T}(B,y_0)$ we denote the closure of the cone $T(B,y_0)$.

Theorem

Let B be a nonempty subset of a real normed space (X, $\|.\|$). Then the tangent cone $T(B,y_0)$ is closed for each $y_0\in\overline{B}$.

Proof

Let $(h_n)_{n\in N}$ be any sequence in $T(B,y_0)$ with $\lim_{n\to\infty}h_n=h\in X$. For each tangent h_n there exist a net $(x_{n_i})_{i\in I_n}$ of elements in B and a net $(\lambda_{n_i})_{i\in I_n}$ of positive real numbers with $y_0=\lim_{i\in I_n}x_{n_i}$ and $h_n=\lim_{i\in I_n}\lambda_{n_i}(x_{n_i}-y_0)$.

Consequently, for each $n\in N$ there is an $i(n)\in I_n$ with $\|x_{n_i}-y_0\|\leq\frac{1}{n}$ for all $i\geq i(n)$ and

$\|\lambda_{n_i}(x_{n_i}-y_0)-h_n\|\leq\frac{1}{n}$ for all $i\geq i(n)$.

If we define $y_n=x_{n_{i(n)}}\in B$ for all $n\in N$ and $u_n=\lambda_{n_{i(n)}}>0$ for all $n\in N$, then we get $y_0=\lim_{n\to\infty}y_n$ and $\|u_n(y_n-y_0)-h\|\leq\frac{1}{n}+\|h_n-h\|$ for all $n\in N$ which implies $h=\lim_{n\to\infty}u_n(y_n-y_0)$.

So h belongs to the tangent cone $T(B,y_0)$.

Lemma

If $B\subset Y$ is a convex subset, then for any $y_0\in B$ we have $\overline{T}(B,y_0)=\overline{\text{cone}}(B-y_0)$.

Proof

Take any $y\in B$. Then we have

$$y_n=y_0+\frac{1}{n}(y-y_0)=\frac{1}{n}y+(1-\frac{1}{n})y_0\in B$$

for all $n \in N$. So, we get $y_0 = \lim_{n\to\infty} y_n$ and $y - y_0 = \lim_{n\to\infty} n(y_n - y_0)$. But this implies that $y - y_0$ belongs to the tangent cone $T(B, y_0)$, and therefore we obtain

$$B - y_0 \subset T(B, y_0).$$

Since $T(B, y_0)$ is a cone, it follows further that cone $(B - y_0) \subset T(B, y_0)$.

Conversely, take any $h \in T(B, y_0)$. Then there exist $y_n \in B$, $\lambda_n > 0$ and $n \in N$ such that $y_0 = \lim_{n\to\infty} y_n$ and $h = \lim_{n\to\infty} \lambda_n (y_n - y_0)$. The last equation implies $h \in \overline{\text{cone}}\,(B - y_0)$. Thus $T(B, y_0) \subset \overline{\text{cone}}\,(B - y_0)$. If the topology is induced by a norm, then $T(B, y_0)$ is closed by Theorem. Then $\overline{T}(B, y_0) = \overline{\text{cone}}(B - y_0)$.

C. S-Convex, Nearly S-Convex, Closure S-Convex

Let S be a convex cone of Y. A subset C of Y is said to be:

(i) S-convex if $C + S$ is convex;

(ii) nearly S-convex if $C + S$ is nearly convex;

(iii) closure S-convex if $\overline{C + S}$ is convex.

It is clear that if C is S-convex, then it is also nearly S-convex and consequently closure S-convex. The following examples show that the converse implication is not generally true.

A. Example

We consider

$$C = \{(y_1, y_2) \in R^2 \mid -y_1 < y_2 \le 0, 0 < y_1 < 1\} \cup \{(0,0), (1,-1)\}.$$

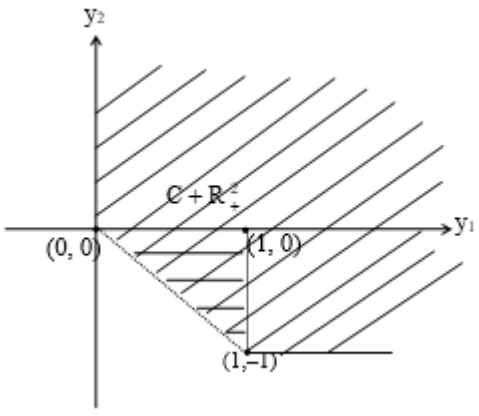

Figure 1

From Figure 1, we get C is closure R_+^2-convex, but it is not nearly R_+^2-convex.

B. Example

We consider $C_1 = C \cup \{(q, -q) \mid q \in Q \cap [0,1]\}$, where Q denotes the set of all rational numbers.

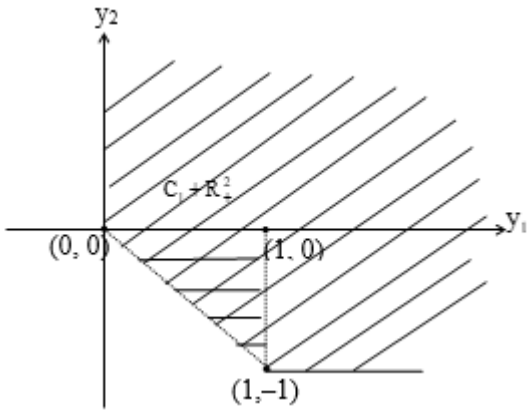

Figure 2

From Figure 2, we have C_1 is nearly R_+^2-convex, but it is not R_+^2-convex.

Lemma

Let S be a convex cone in Y with int $S \neq \emptyset$ and let $C \subset Y$. Then

$$\overline{C + S} = \overline{C + \text{int}\, S},$$

$$\text{int}\,\overline{C + S} = C + \text{int}\, S.$$

Proof

By Lemma, we have $\overline{C+S} = \overline{C+\overline{S}} = \overline{C+\overline{\text{int}\, S}} = \overline{C+\text{int}\, S}$.

Let $y \in \text{int}\,\overline{C + S}$. Then there exists a neighborhood U of zero such that $y - U \subset \overline{C + S}$. We choose some $s \in \text{int}\, S$ and a sufficiently small $\alpha > 0$ such that $\alpha s \in U$. Hence $y - \alpha s \in \overline{C + S}$. Consequently, we have $(y - \text{int}\, S) \cap (C + S) \neq \emptyset$.

Thus $y \in C + S + \text{int}\, S \subset C + \text{int}\, S$. The arbitrariness of y implies that $\text{int}\,\overline{C + S} \subset C + \text{int}\, S$.

Conversely, take any $y \in C + \text{int}\, S$. Then $y \in \overline{C + \text{int}\, S}$. Hence $y \in \overline{C + S}$. Therefore there exists a neighborhood U of zero such that $(y + U) \cap (C + S) \neq \emptyset$. Hence there exist $z \in y + U$ and $z \in C + S$. Let $z = y + u$ for every $u \in U$. So $y + u \in C + S$ and $y + U \subset C + S$. Hence $y + U \subset \overline{C + S}$. Therefore $y \in \text{int}\,\overline{C + S}$. Thus $C + \text{int}\, S \subset \text{int}\,\overline{C + S}$.

IV. Convexity of Set-Valued Mappings

In this section, we recall various types of convexity for set-valued mappings. Let X and Y be real Hausdorff topological vector spaces.

A. S-Convex, S-Quasiconvex, S-convexlike, and closure S-convexlike

Let $A \subset X$ be a convex set. A set-valued mapping $F: X \to Y$ is said to be:

(i) S-convex on A if, for all $x_1, x_2 \in A$, $y_1 \in F(x_1)$, $y_2 \in F(x_2)$ and $\lambda \in (0,1)$,
$$\lambda y_1 + (1-\lambda) y_2 \in F(\lambda x_1 + (1-\lambda)x_2) + S;$$

(ii) S-quasiconvex on A if, for all $x_1, x_2 \in A$, if $y \in F(x_1) + S$ and $y \in F(x_2) + S$, then
$$y \in F\left(\lambda x_1 + (1-\lambda) x_2\right) + S \text{ for all } \lambda \in (0,1);$$

(iii) S-convexlike on A if, for all $x_1, x_2 \in A$, $y_1 \in F(x_1)$, $y_2 \in F(x_2)$, and $\lambda \in (0,1)$,
$$\lambda y_1 + (1-\lambda) y_2 \in F(A) + S;$$

(iv) closure S-convexlike on A if, for all $x_1, x_2 \in A, y_1 \in F(x_1)$, $y_2 \in F(x_2)$, and $\lambda \in (0,1)$,
$$\lambda y_1 + (1-\lambda) y_2 \in \overline{F(A) + S}.$$

In Definition (iii) and (iv), the set A is not necessarily convex. In the sequel, when no confusion occurs, we omit S- in the above notions of convexity of set-valued mappings.

We shall give characterizations of some notions of convexity for set-valued mappings.

Proposition

(a) F is S-convex on A if and only if the epigraph of F,
$$\text{epi } F = \{(x, y) \in A \times Y \mid y \in F(x) + S\},$$
is a convex subset of $X \times Y$.

(b) F is convexlike [resp. closure convexlike] on A if and only if F(A) is S-convex [resp. closure S-convex].

Proof

(a)Take arbitrary elements $(x_1, y_1), (x_2, y_2) \in \text{epi } F$ and $\lambda \in [0,1]$. Because of the convexity of A we have
$$\lambda x_1 + (1-\lambda) x_2 \in A, \qquad (1)$$
and since F is S-convex, we obtain
$$\lambda y_1 + (1-\lambda) y_2 \in F(\lambda x_1 + (1-\lambda) x_2) + S. \qquad (2)$$
(1) and (2) imply $\lambda(x_1, y_1) + (1-\lambda)(x_2, y_2) \in \text{epi } F$. Consequently, epi F is a convex set. Conversely, now assume that epi F is a convex set. Let $x_1, x_2 \in A, y_1 \in F(x_1)$, $y_2 \in F(x_2)$ and $\lambda \in [0,1]$ be arbitrarily given. Because of the convexity of epi F we obtain $\lambda(x_1, y_1) + (1-\lambda)(x_2, y_2) \in \text{epi } F$ implying $\lambda y_1 + (1-\lambda) y_2 \in F(\lambda x_1 + (1-\lambda) x_2) + S$. Hence F is S-convex.

(b) Assume that F is convexlike [resp. closure convexlike] on A. Let $x_1, x_2 \in A$, $y_1 \in F(x_1)$, $y_2 \in F(x_2)$ and $\lambda \in [0,1]$ be arbitrarily given. Thus we get $y_1 \in F(x_1) \subset F(A) + S$ and $y_2 \in F(x_2) \subset F(A) + S$. Because of the convexlikeness of F, we get $\lambda y_1 + (1-\lambda) y_2 \in F(A) + S$. Therefore $F(A) + S$ is convex [resp. closure S-convex]. Conversely, assume that $F(A) + S$ is convex [resp. closure S-convex].

Take any $x_1, x_2 \in A$, $y_1 \in F(x_1)$, $y_2 \in F(x_2)$ and $\lambda \in (0,1)$. Therefore, $y_1 \in F(x_1) \subset F(A) + S$ and $y_2 \in F(x_2) \subset F(A) + S$.

By our assumption,
$$\lambda y_1 + (1-\lambda) y_2 \in F(A) + S.$$
Hence F is convexlike [resp. closure convex like] on A.

B. Example

Let $F: [-1,1] \to R^2$ be the set-valued mapping defined by
$$F(x) = \begin{cases} [-x, 0] \times \{0\} \text{ if } x \in [0,1]; \\ \{0\} \times [x, 0] \text{ if } x \in [-1, 0). \end{cases}$$
Take any $x_1, x_2 \in [-1,1]$ and $\lambda \in (0,1)$.

Case 1

If $x_1, x_2 \in [-1, 0)$, then $\lambda x_1 + (1-\lambda) x_2 \in [-1, 0)$ Take any $y \in F(x_1) + R_+^2$ and $y \in F(x_2) + R_+^2$ where $F(x_1) = \{0\} \times [x_1, 0]$ and $F(x_2) = \{0\} \times [x_2, 0]$.

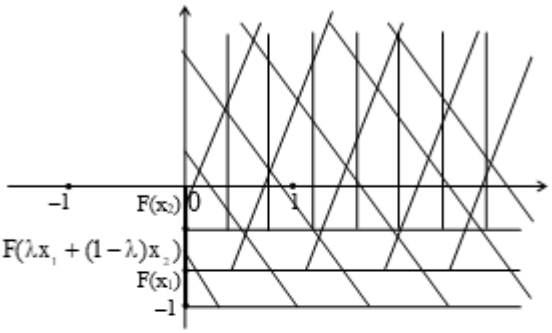

Figure 3

Where $F(x_2) + R_+^2$, $F(\lambda x_1 + (1-\lambda) x_2) + R_+^2$, $F(x_1) + R_+^2$

From Figure 3, we have
$F(x_2) + R_+^2 \subset F(\lambda x_1 + (1-\lambda) x_2) + R_+^2 \subset F(x_1) + R_+^2$. So $y \in F(\lambda x_1 + (1-\lambda) x_2) + R_+^2$. Therefore F is R_+^2-quasiconvex on $[-1, 0)$.

Case 2

If $x_1, x_2 \in [0,1]$, then $\lambda x_1 + (1-\lambda) x_2 \in [0,1]$. Take any $y \in F(x_1) + R_+^2$ and $y \in F(x_2) + R_+^2$ where $F(x_1) = [-x_1, 0] \times \{0\}$ and $F(x_2) = [-x_2, 0] \times \{0\}$.

From Figure 4, we have
$F(x_1) + R_+^2 \subset F(\lambda x_1 + (1-\lambda) x_2) + R_+^2 \subset F(x_2) + R_+^2$.
Thus $y \in F(\lambda x_1 + (1-\lambda) x_2) + R_+^2$. Hence F is $-R_+^2$ quasiconvex on $[0,1]$.

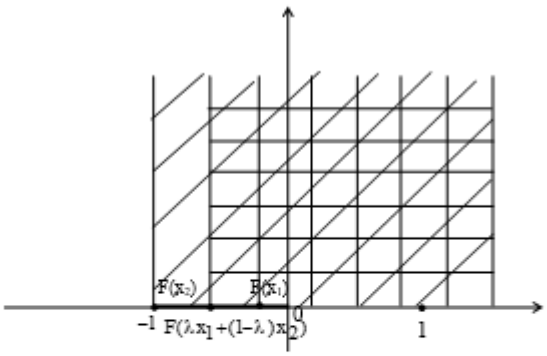

Figure 4

Where $R(x_2)+R_+^2$

$F(\lambda x_1+(1-\lambda)x_2)+R_+^2$

$F(x_1)+R_+^2$

Case 3

If $x_1\in[-1,0)$ and $x_2\in[0,1]$, then $\lambda x_1+(1-\lambda)x_2\in[-1,0)$ or $\lambda x_1+(1-\lambda)x_2\in[0,1]$. Take any $y\in F(x_1)+R_+^2$ and $y\in F(x_2)+R_+^2$.

Then $y\in(F(x_1)+R_+^2)\bigcap(F(x_2)+R_+^2)$.

From Figure 5, we get $y\in F(\lambda x_1+(1-\lambda)x_2)+R_+^2$ for $\lambda x_1+(1-\lambda)x_2\in[-1,0)$.

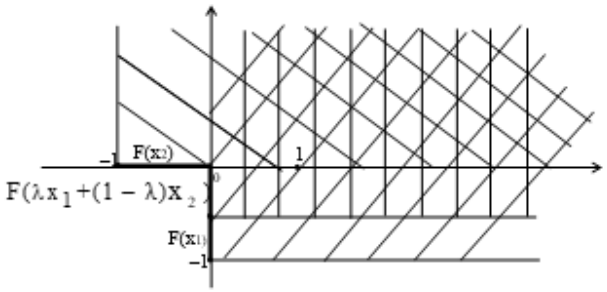

Figure 5

Where $F(x_2)+R_+^2$

$F(\lambda x_1+(1-\lambda)x_2)+R_+^2$

$F(x_1)+R_+^2$

From Figure 6, it is obvious that $y\in F(\lambda x_1+(1-\lambda)x_2)+R_+^2$ for $\lambda x_1+(1-\lambda)x_2\in[0,1]$. Therefore, F is R_+^2-quasiconvex.

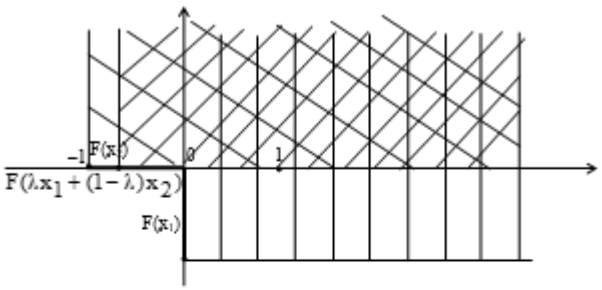

Figure 6

Where $F(x_2)+R_+^2$

$F(\lambda x_1+(1-\lambda)x_2)+R_+^2$

$F(x_1)+R_+^2$

Case 4

If $x_1\in[0,1]$ and $x_2\in[-1,0)$, then $\lambda x_1+(1-\lambda)x_2\in[-1,0)$ or $\lambda x_1+(1-\lambda)x_2\in[0,1]$. Take any $y\in F(x_1)+R_+^2$ and $y\in F(x_2)+R_+^2$.

Then $y\in\left(F(x_1)+R_+^2\right)\bigcap\left(F(x_2)+R_+^2\right)$.

From Figure 7, it is obvious that

$y\in F(\lambda x_1+(1-\lambda)x_2)+R_+^2$ for $\lambda x_1+(1-\lambda)x_2\in[-1,0)$.

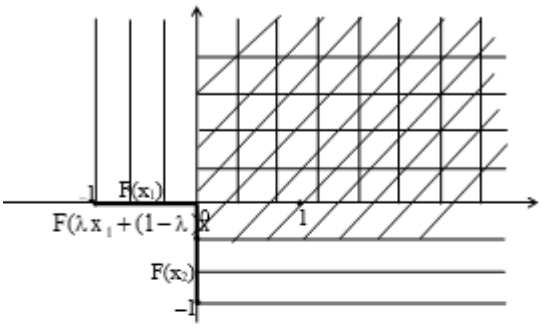

Figure 7

Where $F(x_2)+R_+^2$

$F(\lambda x_1+(1-\lambda)x_2)+R_+^2$

$F(x_1)+R_+^2$

From Figure 8, we get $y\in F(\lambda x_1+(1-\lambda)x_2)+R_+^2$ for $\lambda x_1+(1-\lambda)x_2\in[0,1]$. Thus F is R_+^2-quasiconvex. Hence for all cases F is R_+^2-quasiconvex on [–1, 1].

Observe that if Y is one-dimensional (i.e., F is real-valued), then each mapping $F: X \to Y$ is R_+-convexlike.

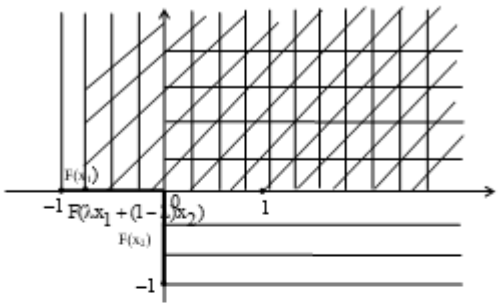

Figure 8

Where $\equiv F(x_2) + R_+^2$

$\equiv F(\lambda x_1 + (1-\lambda)x_2) + R_+^2$

$\equiv F(x_1) + R_+^2$

C. Example

Let $X = R^1, Y = R^2, A = [-1,1]$, and let $F: A \to R^2$ be the set-valued mapping defined by

$$F(x) = \begin{cases} \{-x\} \times [0,1] & \text{if } x \in [-1,0]; \\ \{x\} \times (-x, 0] & \text{if } x \in (0,1); \\ \{1\} \times [-1,0] & \text{if } x = 1. \end{cases}$$

Let $x_1 = -1, x_2 = 1$ and $\lambda = \frac{1}{2}$. Then $F(x_1) = F(-1) = \{1\} \times [0,1]$ and $F(x_2) = F(1) = \{1\} \times [-1,0]$. Take $y_1 = (1,0) \in F(x_1)$ and $y_2 = (1,-1) \in F(x_2)$. Therefore, $\lambda y_1 + (1-\lambda) y_2 = \frac{1}{2}(1,0) + \frac{1}{2}(1,-1) = (1, -\frac{1}{2})$.

Since $\lambda x_1 + (1-\lambda) x_2 = (-\frac{1}{2} + \frac{1}{2}) = 0$,

$$F(\lambda x_1 + (1-\lambda) x_2) = F(0) = \{0\} \times [0,1].$$

Thus $\lambda y_1 + (1-\lambda) y_2 \notin F(\lambda x_1 + (1-\lambda) x_2) + R_+^2$.

Therefore F is not convex on A. We have

$$F(A) + R_+^2 = \{(r_1, r_2) \in R^2 \mid r_2 \geq 0, r_1 = 0\} \cup \{(r_1, r_2) \in R^2 \mid r_2 > -r_1, 0 < r_1 < 1\} \cup \{(r_1, r_2) \in R^2 \mid r_2 \geq -1, r_1 \geq 1\}.$$

From Figure 9, we get $F(A) + R_+^2$ is not convex.

But $\overline{F(A) + R_+^2} = \{(r_1, r_2) \in R^2 \mid r_2 \geq -r_1, 0 \leq r_1 \leq 1\} \cup \{(r_1, r_2) \in R^2 \mid r_2 \geq -1, r_1 > 1\}$.

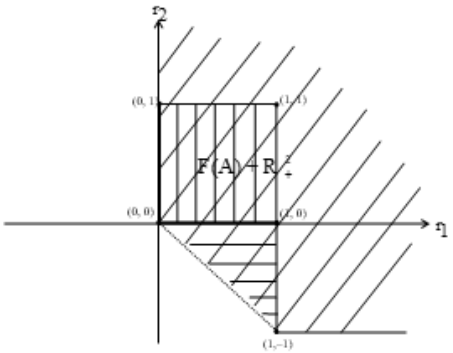

Figure 9.

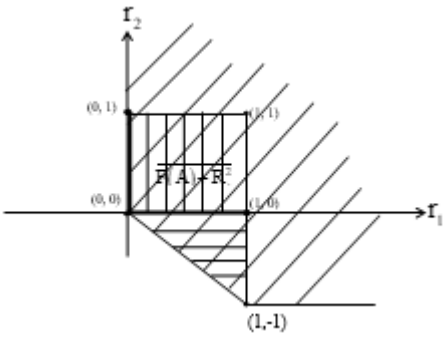

Figure 10.

From Figure 10, we have $\overline{F(A) + R_+^2}$ is convex. This means that F is closure convexlike on A and it is not convexlike on A.

V. Conclusion

We observed that if the set-valued mapping is not convex, it is not also convexlike but it is closure convexlike on a given interval. Moreover, Convexity of sets and set-valued mappings are used as an important role of vector optimization and some other fields involve set-valued constraints and set-valued objective mappings.

Acknowledgements

I would like greatly indebted to Dr Khin Maung Oo, Rector, Dr Win Soe and Dr Than Than Oo, Pro-rectors, University of Magway, for their permission. Thanks are due to Dr Myint Myint Khin, Professor and Head of Department of Mathematics, University of Magway, and Dr Khin San Wai, Professor, Department of Mathematics, University of Magway for their suggestions in preparing this paper.

References

[1] J. Horvath, "Topological Vector Spaces and Distributions", Volume I, Addison-Wesley Publishing Company, London, 1966.
[2] J. Jahn, "Mathematical Vector Optimization in Partially Ordered Linear Spaces", Verlag Peter Lang, Frankfurt, 1986.
[3] J. Jahn, "Vector Optimization: Theory, Applications, and Extensions", Spinger-Verlag, Berlin, 2004.
[4] W. Rudin, "Functional Analysis", McGraw-Hill, inc. New York, 1973.
[5] H. H. Schaefer, "Topological Vector Spaces", Spinger-Verlag, NewYork, 1971.
[6] W. Song, "Duality in Set-Valued Optimization, Dissertationes Mathematicae", House of the Warsaw University of Technology, 1998.

Article ID – JRA6006220

Linear Programming-based Crop Allocation and Cost Estimation System

Khin Lae Lae Phyo
Faculty of Computing
University of Computer Studies (Meiktila)
Meiktila, Myanmar
khinlaelaephyo@ucsmtla.edu.mm

Khin Myo Aye
Faculty of Computing
University of Computer Studies (Meiktila)
Meiktila, Myanmar
khinmyoaye@ucsmtla.edu.mm

Thein Than Thwin
Faculty of Computer Science
University of Computer Studies (Meiktila)
Meiktila, Myanmar
theinthanthwin@ucsmtla.edu.mm

***Abstract*—The crops are grown in Nyaung-U district three times a year. In the first season (from April to July), sesame or peanut or paddy is grown, paddy is planted in the second season (from July to January) and chick pea in the third season (from January to April). The farmers are traditionally planting without calculating the most profit. Thus, a decision support model for the peasant to estimate the crop allocation and cost. The data for the period April to July in 2019 are collected by interviewing the peasants. A prototype system is carried out with R statistical package using the library "lpSolve" and evaluation is conducted by comparing the simulated result cost and the result in real-world. The relative error of 2% shows that the proposed model is relevant for the peasants to use in their firm.**

***Keywords*—simplex method, linear programming, operation research, cost estimation**

I. Introduction

The peasants are the most important working forces in Myanmar because of being an agricultural country. To uplift the economy of Myanmar, the profit of such peasants has to be promoted effectively. Thus, choosing profitable crops and estimating the cost accordance with the market price become crucial. Unfortunately, peasants are still using the traditional way that cannot effectively estimate the cost and does not be suitable for market; and touch trouble with poverty. As a result, a decision support system that can suggest the appropriate crops and the certain estimation of the cost is essentially required.

In Nyaung-U district which is a central region of Myanmar, the seasonal crops including sesame, peanut and paddy are mainly grown. Such crops are planted within the same period between April and July. Unfortunately, one certain crop cannot be grown for all three seasons repeatedly because of soil degradation. However, the productivity rate of crops mostly depends on the quality of seeds and weather, the other resources such as dam and stream can be used as assistant. Thus, the appropriate plan for growing is an important factor of the peasants. Traditional way of growing doesn't describe which crops make most profit. By using linear programming model, the most appropriate growing plan, the most effective cost estimation for the crops which make most profit can be realized. Hence, it gives advice and recommendation to the farmers about the crops which make most profit next years.

The linear programming (LP) is one of the operation research models [1] and can be used in many real-world problems such as farming, marketing, distribution and policy decision making. Linear programming model becomes popular with the research of George B. Danzig in 1947 [2]. He tried to use LP model in planning, scheduling for uncertain condition dynamically. The authors of [3] also tried to use LP model to select the courses of action for allocation and transportation. Since LP can support the optimized decision, it is the best-studied solution method for farming. Thus, LP is mainly used to estimate the optimal result for crop planning in this work.

The rest of the paper is organized as follow. Section 2 described the theorical background that is required for understanding our work. The proposed methodology is presented in section 3. In section 4, the proposed model is explained. The result is discussed in section 5 and the paper is concluded in section 6.

II. Theorical Background and Related Works

Linear programming can support the best solution for the requirements which are represented in the form of linear relationships. However, it named linear programming, actually it is a mathematical optimization process [4]. LP can be used to represent the various types of problem in operations research in practice. Many types of specialized algorithms are based on some particular problems such as the flow of multi-commodity and the flow of network. Many other sub-concepts such as decomposition, and duality theory are also derived from such ideas. However, the LP technique is formerly used in microeconomics, many companies are currently using in important management including transportation, planning, production and various issues. Therefore, many management issues of the company and business organizations can be observed or evaluated their profit and investments using linear programming model. The form of business is timely changed in modern business world, the companies would try to get the profit in maximized amount and would try to spend minimized cost or resources. Thus, they characterize their problem in linear programming model. As a result, the LP model that can help the peasants to maximize their profit and to reduce the minimum cost is also proposed in this work.

Linear Programming being the most prominent operation research (OR) technique, it is designed for models with linear objective and constraint functions. Linear programming technique is applied to determine the optimum land allocation. And LP is used to determine the product mix for selling the medicated soap product in the manufacturing industry [5]. Linear programming approach is an effective tool to determine the optimal farm output by adopting optimized the cropping pattern in difference districts of Rajasthan[6]. It also applied to obtain the maximum productivity of maize in Sumbawa Regency [7]. And LP is also utilized to decide the product mix for the optimal profit with available resources in the Ethiopian apparel sector [8]. Heady[9] proposed the use of linear programming for determining optimum crop rotations on a farm. In this paper, we construct the LP model by using the agriculture data to determine the most profitable crop, then LP model will be solved by using R in Simplex algorithm. In this case, the objective function represents the profit per acre associated with the crops, while constraints related to the availability of resources such as seed, labour cost, fertilizer and general cost. The cost of growing, reaping and spraying contain in labour cost. The cost of using machines, livestock also include in the general cost.

A. Simplex Algorithm

The problem as linear equalities without an objective function was formulated by George B. Danzig in 1946. Simplex method can be developed into a linear objective function that needs to be maximized. The simplex algorithm constructs a feasible solution on polytope and traverse on each edger of that polytope to apexes with increasing values of the objective function to get the optimized solution. The simplex algorithm was proposed by George B. Danzig around 1947. The simplex algorithm is practical in practice and it is efficient. The simplex algorithm can also guarantee to obtain the global optimized solution, when particular precautions against cycling are taken. Thus, the simplex algorithm is mainly used in this work.

III. METHODOLOGY

To denote the various components of a Linear Programming model, the following notations are used.

Z = The objective function to be maximize

$x_j =$ Input variables

$c_j =$ Parameter of the objective function

$b_i =$ Maximum limit of the constraints

$a_{ij} =$ Coefficients of the functional constraint equations

In general, the mathematical model is

$$\text{Maximize} \quad Z = \sum_{j=1}^{n} c_j \, x_j$$

Subject to

$$\sum_{j=1}^{n} a_{ij} \, x_j \leq b_i \, , \qquad i = 1,2, \dots, m$$

$$x_j \geq 0 \, , \qquad j = 1,2, \dots, n$$

Standard form of LP model by using slack variables as x_{n+i} is

$$\text{Maximize} \quad Z = \sum_{j=1}^{n} c_j \, x_j$$

Subject to

$$\sum_{j=1}^{n} a_{ij} \, x_j + x_{n+i} = b_i \, , \qquad \text{i} = 1,2, \dots, \text{m}$$

$$x_j \geq 0 \, , \qquad \text{j} = 1,2, \dots, \text{n}$$

IV. THE PROPOSED MODEL

The peasants from Nyaung-U district collaborated in our work, thus, the data are collected with interactive interview that is performed for the period during April to July in 2019. Most of these peasants grow the crops including sesame, peanut and paddy as the first season crop in their traditional ways. According to the result of the interview, the main requirements of the peasants are successfully revealed. The resulted crucial requirement can be categorized into four categories including seed, labour, fertilizer and finance or cost. The gross profit of each peasants are also collected for the purpose of validation for our linear programming model.

Then, the main requirements (seed, labour, fertilizer and cost) are used as the constraints for the cultivating process in our model. The Table 1 demonstrate the detailed amount of resources used for one acre of each crop and maximum limit in our proposed model.

TABLE1. AMOUNT OF RESOURCES USED PER ACRE (FOR PROFIT)

Resources	Sesame/ acre (thousands of Kyats)	Peanut/ acre (thousands of Kyats)	Paddy/ acre (thousands of Kyats)	Availability (thousands of Kyats)
Seed	15	37.5	20	257.5
Labour cost	107.2	104	82.5	991.1
Fertilizer	20	60	91	603
General cost	69.2	68.1	45.3	617.8
Profit per acre	230.2	546.4	311.2	

In our model, the maximum profit in thousands of kyats is represented by the variable 'Z'. As the variable x_j represent each crop,

x_1 represents number of acres of sesame,

x_2 represents number of acres of peanut and

x_3 represents number of acres of paddy.

Then again, the variable b_j will be used to express the available maximum limit for each crop.

To maximize the profit, we have to define some constraints. Thus, the aforementioned collected requirements including seed, labour, fertilizer and cost are stated as the main constraints. As a result, the linear programming model is proposed as follows:

Maximize $Z = 230.2x_1 + 546.4x_2 + 311.2x_3$

Subject to

Seed: $15\,x_1 + 37.5\,x_2 + 20\,x_3 \leq 257.5$

Labor cost: $107.2\,x_1 + 104\,x_2 + 82.5\,x_3 \leq 991.1$

Fertilizer: $20\,x_1 + 60\,x_2 + 91\,x_3 \leq 603$

General cost: $69.2\,x_1 + 68.1\,x_2 + 45.3\,x_3 \leq 617.8$

$$x_j \geq 0, \quad j = 1,2,3$$

Then, the slack variables including x_4, x_5, x_6 and x_7 are introduced in our proposed model for the purpose of converting into the standard form. Consequently, the conditional sign less than or equal to ($\leq$) is turned to the conditional sign equal to (=). Thus, the whole proposed linear programming model becomes:

Maximize $Z = 230.2x_1 + 546.4x_2 + 311.2x_3$

Subject to

$$15\,x_1 + 37.5\,x_2 + 20\,x_3 + x_4 = 257.5$$

$$107.2\,x_1 + 104\,x_2 + 82.5\,x_3 + x_5 = 991.1$$

$$20\,x_1 + 60\,x_2 + 91\,x_3 + x_6 = 603$$

$$69.2\,x_1 + 68.1\,x_2 + 45.3\,x_3 + x_7 = 617.8$$

$$x_j \geq 0, \quad j = 1,2,3, \dots, 7$$

However, the resulted model can suggest the optimum for the maximum profit, the alternative model is also created with simplex algorithm to get the cost minimization model. In general, the mathematical model for minimize problem is

$$\text{Minimize} \quad Z = \sum_{j=1}^{n} c_j\,x_j$$

Subject to

$$\sum_{j=1}^{n} a_{ij}\,x_j \geq b_i\,, \qquad i = 1,2,\dots,m$$

$$x_j \geq 0\,, \qquad j = 1,2,\dots,n$$

To calculate the minimum cost, the same input variable including x_1, x_2 and x_3 are used along with the aforementioned constraints including seed, labour, fertilizer and cost. Then again, the variable b_j will be used to express the required amount for each crop. The Table 2 demonstrate the detailed amount of resources used for one acre of each crop and minimum limit in our proposed model.

A. Implementation

Finally, a prototype is created with the 'R' language with the statistical package 'lpSolve' for evaluation purpose. The prototype results for the maximum profit and the minimum cost are shown in Figure 1 and Figure 2 respectively.

TABLE2. AMOUNT OF RESOURCES USED PER ACRE (FOR COST)

Resources	Sesame/ acre (thousands of Kyats)	Peanut/ acre (thousands of Kyats)	Paddy/ acre (thousands of Kyats)	Requirements (Minimum) (thousands of Kyats)
Seed	15	37.5	20	255
Labour cost	107.2	104	82.5	985.1
Fertilizer	20	60	91	573
General cost	69.2	68.1	45.3	615.9
Cost per acre	211.4	269.6	238.8	

We get the minimization model as follow.

Minimize $Z = 211.4\,x_1 + 269.6x_2 + 238.8x_3$

Subject to

Seed: $15\,x_1 + 37.5\,x_2 + 20\,x_3 \geq 255$

Labour cost: $107.2\,x_1 + 104\,x_2 + 82.5\,x_3 \geq 985.1$

Fertilizer: $20\,x_1 + 60\,x_2 + 91\,x_3 \geq 573$

General cost: $69.2\,x_1 + 68.1\,x_2 + 45.3\,x_3 \geq 615.9$

$$x_j \geq 0, \quad j = 1,2,3$$

```
library(lpSolve)
> obj.fun<-c(230.2,546.4,311.2)
> constr<matrix(c(15,37.5,20,107.2,104,82.5,20,60,91,69.2,
  68.1,45.3),ncol=3,byrow=TRUE)
> constr.dir<-c("<=","<=","<=","<=")
> rhs<-c(257.5,991.1,603,617.8)
#now solving the model
> prod.sol<lp("max",obj.fun,constr,constr.dir,rhs,
  compute.sens=TRUE)
> prod.sol$solution
[1] 2.809494    3.914729    3.427762
> prod.sol
Success: the objective function is 3852.473
```

Fig. 1. The result of prototype for maximum profit

B. Validation

The proposed model is validated by using the simulated result from the implementation and the empirical result which is collected from the peasants in interview. To validate the proposed model, the absolute error which is the difference between the simulated value (x_0) from the prototype and the empirical value (x) are firstly calculated with the following formula

$$\Delta x = |x_0 - x|.$$

The simulated value from our prototype implementation is 2429 (thousands of kyats) and the

empirical cost is 2467.887603 (thousands of kyats). Thus, the absolute error is 38.887603 (thousands of kyats). However, the absolute error is inadequate due to the fact that it does not give any details regarding the importance of the error. Thus, the relative error which is the ratio of the absolute error of the estimated cost to the actual cost is calculated with the formula

Relative error = $(\Delta x)/x$.

The relative error can support an indication of how the output of our system is relative to the actual cost being considered.

$$\text{Relative error} = \frac{38.887603}{2467.887603} = 0.015767 \sim 0.02$$

The Relative error = 2%

Thus, we can say that the result of the proposed model coincide with the actual value.

```
library(lpSolve)
> obj.fun<-c(211.4,269.6,238.8)
> constr<matrix(c(15,37.5,20,107.2,104,82.5,20,60,91,69.2,
  68.1,45.3),ncol=3,byrow=TRUE)
> constr.dir<-c(">=",">=",">=",">=")
> rhs<-c(255,985.1,573,615.9)
#now solving the model
> prod.sl<-lp("min",obj.fun,constr,constr.dir,rhs,
compute.sens=TRUE)
> prod.sol$solution
[1] 3  4  3
> prod.sol
Success: the objective function is 2429
```

Fig. 2. The result of prototype for minimum cost

V. Result and Discussion

To development a crop allocation and cost estimation system for the peasant in Nyaung-U district, a linear programming model is development based on the data which is resulted from the interactive interview with such peasants in 2019. The crops are grown in the areas which received regularly water in Nyaung-U district, a central region of Myanmar. Then, a prototype system is developed with R language to get the simulated results as presented in the previous section. The main result of the prototype system shows that the optimum profit is 3852.473 (thousands of kyats). The resulted crop allocation plan shows that the suitable allocation for sesame, peanut and paddy are 2.809494 (~ 3 acres), 3.914729 (~4 acres) and 3.427762 (~3 acres) respectively. Then again, the prototype system also provide the minimum cost as 2429 (thousands of kyats) for that crop allocation plan. The empirical cost of the peasants is 2467.887603 (thousands of kyats). The proposed model is evaluated by comparing the simulated value with the empirical value that is extracted from the interview. The evaluation result shows that the absolute error is 38.887603 (thousands of kyats) with the relative error of 2%. Thus, the result of our model is nearly coincide with the actual value and it is usable for the peasants.

VI. Conclusion

A land allocation and cost estimation system is proposed based on simplex method of linear programming in this model. The proposed model is tested with the cultivation plan of the peasants in central Myanmar. The system suggested that the maximum profit of 3852.473 (thousands of kyats) can be got from the minimum cost of 2429 (thousands of kyats). The model is also validated with the real data. The model can produce the result which is nearly the same as the real result with the relative error of 2%. Thus, this work is useful in land allocation for the peasants. The peasants can use the proposed model to plan their crop using this method every year.

References

[1] F. S. Hiller and G. J., Lieberman, Introduction to Operation Research. McGraw- Hill Book Co. New York, 2004

[2] N. A. Sofi, A. Ahmed, M. Ahmad and B. A. Bhat, "Decision Making in Agriculture: A Linear Programming Approach ," International Journal of Modern Mathematical Sciences, 2015, 13(2), pp- 160-169

[3] W. B. Yahya, "Determination of Optimum Product Mix at Minimum Raw Material Cost, Using Linear programming, " Nigerian Journal of Pure and Applied Sciences, Vol.19, pp-1712-1721, 2004.

[4] G. B. Dantzig, "Linear Programming and Extension ," Princeton, University Press, Princeton,NJ. 1963

[5] B. Y. Waheed, K. G. Muhammed, O. I. Samuel, E. A. Adekunle, "Profit Maximization In A Product Mix Company Using Linear Programming," European Journal of Business and Management, ISSN 2222-1905,Vol 4, No.17, 2012.

[6] B. Mahak, R. Anil, "A Mathematical Approach to Optimize Crop Allocation – A Linear Programming Model," International Journal of Design & Nature and Ecodynamics, Vol. 15, No. 2, April, 2020, pp. 245-252

[7] T. Susilawati and Mikhratunnisa, "Optimization of corm production using the simplex method in Sumbawa Regency," International Seminar on Applied Mathematics and Mathematics Education, IOP Conf. Series: Journal of Physics, 2019.

[8] G. W. Woubante, "The Optimization Problem of Product Mix and Linear Programming Applications: Case Study in the Apparael Industry", Open Science Journal 2(2), 2017.

[9] E. Heady, "Simplified Presentation and logical aspects of Linear Programming Technique," Journal of farm economics, Vol 24, issue -5, pp -1035-1048, 1954.

Article ID – JRA6008520

Applying Graphical Method of Linear Programming in the Sector of Myanmar Agriculture

Nyunt Nyunt Wai
Engineering Mathematics Department
Technological University
Taunggyi, Myanmar
nyuntnyuntnyauntnyaunt@gmail.com

Thi Thi Swe
Engineering Mathematics Department
Technological University
Pakokku , Myanmar
dawthithiswae@gmail.com

Abstract **- Nowadays, there is no success without suitable decision making as individual, group, team and organization in social, economic and agriculture. Thus, the decision making plays an important role for development of social, economic and agriculture. A quantitative decision-making tool called linear programming model. In this paper, graphical method of linear programming and procedure is used to calculate the expense and maximize or minimize profits in the sector of Myanmar Agriculture (crop growing). A farmer growing firm' profit mainly depend on the cost cultivation and amount of labor. The graphical method of linear programming is applied to maximize or minimize profit of a farmer.**

Keywords**—Linear Programming, feasible region, maximize, minimize, constraints, decision variables, optimal solution.**

I. INTRODUCTION

Linear Programming is a branch of modern mathematics which can be applied to different various real –life situations – life circumstances. It is intensely utilized for a wide scope of issues from agriculture, economics, and industry, diet arranging, oil refining, education, vitality arranging, contamination control, transportation arranging and booking to innovative work and nearly in every utilitarian areas of management production, finance, marketing and personnel. Linear programming is an important area of mathematics called "optimization techniques". Linear programming techniques develop the quality of decisions. It is commonly used in manufacturing and the service industry. Linear programming consists of the main elements are constraints, decision variables, objective function and non-negativity constraints. Linear Programming models are using graphs of inequalities, which represent constraints, to produce a feasibility region . Constraints are used to limit the decision variables or unknowns to their permissible or feasible values. A linear programming is a mathematical program in which the objective function is a linear in the unknowns and constraints consists of linear equalities and inequalities. The various models to be discussed are

- Graphical Model (Use Algebra , Functions and Equations)
- Spatial Model (Use Vectors and Matrices)
- Logical Model (Use Statistics)
- Linear Programming Model (Use graphs and inequalities to identify feasibility region) .
- Algorithmic Model (Use Logical sequences, selection and repetition)

In this paper proposed linear programming in growing crops using graphical method with one example and other sample applications. That can be aimed to apply to get profit in growing crops and other apply areas are planning, trading, economic, transportation etc.

II. LINEAR PROGRAMMING CONCEPTS

A. Related Words

Juan WU, Xueqian GE [1], proposed linear programming model, the optimized investment decision-making of generation is simulated and analyzed. . Their investigated a reproduction model of the structure introduced limit with respect to the four force plants under the three diverse activity modes. Determined by the PC, the ideal introduced limit of the different limitations has got, which give a compelling technique for quantitative examination of for discerning enhanced plan Vishwa Nath Maurya, Ram Bilas Misra, Peter K Anderson, Kamlesh Kumar Shukla [2] benefit advancement of an Ethiopian compound organization situated in Adama (Ethiopia)[3] utilizing direct programming model. The benefits changed impressively inferable from emotional methodology. It was set up that the choices are attempted by experienced individuals without utilization of quantitative individuals and quantitative strategy. Livinus U Uko, Robert J Lutz, James A Weisel [4] explained a modified process-based on Linear Programming (LP) - that allots to workers the ideal loads that are perfect with their director relegated scores in every job. The linear programming model is intended to allot job .

B. History Of Linear Programming

It started in 1947 when G.B Dantzig structured the "simplex method" for comprehending linear programming details of U.S Air Force arranging issues. It before long turned out to be certain that an astonishing wide scope of clearly inconsequential underway administration could be expressed in linear programming terms and solved by the simplex method. Later, it was used to solve problems of management. Its algorithm can also be used to network flow problems. On Oct.14th, 1975, the Royal Sweden Academy of Science awarded the Nobel Prize in economic science to L.V. Kantorovich and T.C.Koopmans "for their contributions to the theory of optimum allocation of resources". The forward leap in searching for a hypothetically palatable calculation to take care of straight programming issues came in 1979 when L.G.Khachian distributed a portrayal of such a calculation.

III. THE LINEAR PROGRAMMING MODELS

Linear equations and linear inequalities are both referred to as linear constraints. The linear function that is to be maximized or minimized in an LP problem is called the objective function . A set of variables which satisfies the constraints of an LP problem is called a feasible solution. A feasible solution that maximizes or minimizes the objective functions is called an optimal solution.

$$
\begin{aligned}
&Z = c_1x_1 + c_2x_2 + c_3x_3 + \text{---------} + c_nx_n. \\
&a_{11}x_1 + a_{12}x_2 + a_{13}x_3 + \text{---------} + a_{1n}x_n = b_1 \\
&a_{21}x_1 + a_{22}x_2 + a_{23}x_3 + \text{---------} + a_{2n}x_n = b_2 \\
&a_{31}x_1 + a_{32}x_2 + a_{33}x_3 + \text{---------} + a_{3n}x_n = b_3 \\
&\text{----------} \\
&\text{----------} \\
&a_{m1}x_1 + a_{m2}x_2 + a_{m3}x_3 + \text{------} + a_{mn}x_n = b_m \\
&x_j \geq 0
\end{aligned}
\quad \Big\} \ (1)
$$

(1) is called a linear programming problem in standard form.

Let: Requirement of Maximization of the Linear Function

$$Z = c_1x_1 + c_2x_2 + c_3x_3 + \text{---------} + c_nx_n. \qquad (2)$$

Subject to constraints

$$
\begin{aligned}
&a_{11}x_1 + a_{12}x_2 + a_{13}x_3 + \text{---------} + a_{1n}x_n \leq b_1 \\
&a_{21}x_1 + a_{22}x_2 + a_{23}x_3 + \text{---------} + a_{2n}x_n \leq b_2 \\
&a_{31}x_1 + a_{32}x_2 + a_{33}x_3 + \text{---------} + a_{3n}x_n \leq b_3 \\
&\text{----------} \\
&\text{----------} \\
&a_{m1}x_1 + a_{m2}x_2 + a_{m3}x_3 + \text{------} + a_{mn}x_n \leq b_m \\
&x_j \geq 0. \quad j = 1,2,3,\dots,n
\end{aligned}
$$

(2) is objective function.

A. Some guidelines for model formulation

The linear programming model formulation process is an art that is learned with practice and experience ; the following general guidelines have been found helpful.

(1) Understand the problems thoroughly

(2) State the problems as concisely as possible, making verbal statements of the following

- The decision variables
- The objective function
- The constraints or limitations

(3) Using the decision variables as unknown.
e.g: $x_1 + x_2 \leq 100$

(4) Develop mathematical expressions that describe the objective and each of the constraints.
Add the non-negativity requirements ($x_j \geq 0$) for each of the decision variables.

B. The Sectors of Linear Programming Application

- Agricultural sector
- Diet sector
- Transportation sector
- Blending sector
- Trim sector
- Regional Planning sector
- Production Scheduling sector

C. Linear programming model formulation steps by graphical method

Step 1: Formulate the LP (Linear programming) model.
Step 2: Construct a graph and plot the constraint lines.
Step 3: Determine the valid side of each constraint line.
Step 4: Identify the feasible solution region.
Step 5: Plot the objective function on the graph.
Step 6: Find the optimum point.

IV. DATA PRESENTATION AND ANALYSIS FOR CROPS GROWING PROFITS

A Pa-Oh farmer owns 100 acres of land on which he can grow potatoes at a profit of 40000 Kyats per acre and corn at a profit of 120000 Kyats per acre. The costs of cultivation are 10000 Kyats per acre for potatoes and 20000 Kyats per acre for corn. The amount of labor required to seed one acre of potatoes is one-man day and one acre of corn is 4-man day. If his resources of money and labor are limited to 1100000 Kyats and 160-man days respectively how many acres of each crop should he grow in order to maximize profits? What are appropriate constraints and use graphical method of Linear Programming?

A. The data for this paper is collected by a Pa-Oh famer.

Total acres = 100 acres
Type of crops = 2 (Potatoes and corns)
Total limitation of cost cultivation = 1100000 Kyats

Total limitation of amount of labor = 160 man day

One acre of cost cultivation for potatoes = 10000 Kyats per acre
One acre of amount of labor for potatoes =1 man day per acre
One acre of cost cultivation for corn = 20000 Kyats per acre
One acre of amount of labor for corn = 4 man day per acre
The profit of potatoes = 40000 Kyats per acre
The profit of corn = 120000 Kyats per acre

TABLE I. TABLE OF CROP ALLOCATION DATA

Crops	*Cost cultivation*	*Amount of labor*
Potatoes	10000 Kyats per acre	1 man day per acre
Corn	20000 Kyats per acre	4 man day per acre
limitation	1100000 Kyats	160 man day

B. Model Formulation

Let the number of acres of potatoes = x_1
Let the number of acres of corn = x_2
Land : $x_1 + x_2 \leq 100$
The cost cultivation: $10000\,x_1 + 20000\,x_2 \leq 1100000$
Amount of labor : $x_1 + 4x_2 \leq 160$,
$x_1 \geq 0$ *and* $x_2 \geq 0$
Let Z denote the profit to be maximize.
The linear programming model for the above data is given by
Maximize Profit $Z = 40000\,x_1 + 120000x_2$
Let $x_1 + x_2 = 100$

Let $x_1 = 50 \Rightarrow x_2 = 50$ (50,50)
Let $x_1 = 0 \Rightarrow x_2 = 100$ (0,100)
Two points are (50,50) and(0,100)

$10000\,x_1 + 20000\,x_2 = 1100000$
Let $x_1 = 50 \Rightarrow x_2 = 30$ (50,30)
Let $x_1 = 110 \Rightarrow x_2 = 0$ (110,0)
Two points are (50,30) and(110,0)

$x_1 + 4\,x_2 = 160$
Let $x_1 = 40 \Rightarrow x_2 = 30$ (40,30)
Let $x_1 = 100 \Rightarrow x_2 = 15$ (100,15)
Two points are (40,30) and(100,15)

$x_1 + x_2 = 100$ (1)
$10000\,x_1 + 20000\,x_2 = 1100000$ (2)
$x_1 + 4x_2 = 160$ (3)
(1) and (2)
$x_2 = 10$
$x_1 = 90$

(2) and (3)
$x_2 = 25$
$x_1 = 60$

The intersection point of equation (1) and (2) is (90, 10).
The intersection point of equation (2) and (3) is (60, 25).

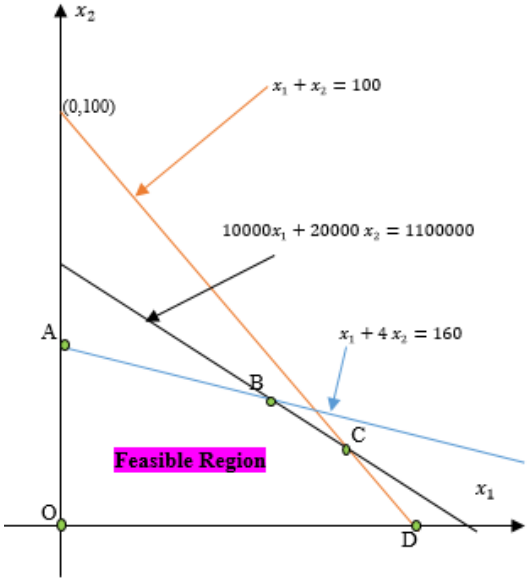

Fig 1. The graph of Crop allocation

A = (0, 40)
B = (60, 25)
C = (90,10)
D = (110,0)
O = (0,0)

TABLE II. TABLE OF FEASIBLE SOLUTIONS

Feasible Region corner points	$Z = 40000\,x_1 + 120000\,x_2$
O(0,0)	0
A(0,40)	4800000
B(60,25)	**5400000**
C(90,10)	4800000
D(110,0)	4400000

Max Z= 5400000 Kyats
x_1=60 and
x_2=25
The optimal solution = 5400000 Kyats at (60, 25).
The number of acres of potatoes = 60
The number of acres of corn =25
Maximize profit = 5400000 Kyats

C. Main results

The optimum result obtain from the graphical method , based on the data collected specified that the maximum profit of a Pa-Oh farmer is 5400000 Kyats and growing amount for potatoes is 60 acres , and growing amount for corns is 25 acres.

D. Other Cases

Linear programming models have other cases. These are three types other cases.

(1) infinite number of optimal solution (multiple optimal solution)
(2) no feasible solution
(3) Unbounded solution.

V. SOME APPLICATIONS

The data presentation and model formulation can be established in other sectors. Other sectors are showed in factory production, cloth production and pottery shop with three samples in the following.

Sample (1)

A factory manufacture two products X and Y. Each product is processed on two machines G and H. Type X requires 3 hours of processing time on G and 1 hour on H; type Y requires 2 hours of processing time on G and 2 hours on H. The available time is 30 hours and 22 hours for operations on G and H respectively. The product X and Y can be sold of the profit of 6000 Kyats and 8000 Kyats respectively. The numbers of product X and Y can be manufactured to maximize the profit.m. The data is collected by factory manufacture.

Type of products = 2 (X and Y)
Type of machines = 2 (G and H)
The available time for machine G = 30 hours
The available time for machine H = 22 hours
The required time for machine G in product X= 3 hours
The required time for machine H in product X= 1 hour
The required time for machine G in product Y= 2 hours
The required time for machine H in product Y= 2 hours
The profit for product X= 6000 Kyats
The profit for product Y= 8000 Kyats

Display constraint above sample 1 following:

TABLE III. TABLE OF PRODUCTION

Product	*Machine G*	*Machine H*	*Profits*
X	3 hours	1 hour	6000 Kyats
Y	2 hours	2 hours	8000 Kyats
Available time	30 hours	22 hours	

Model Formulation

Let x_1= the number of product X and
x_2 = the number of product Y.
Let Z denote the profit to be maximize

$$Z = 6000\, x_1 + 8000\, x_2$$

Subject to constraints

$$3x_1 + 2x_2 \le 30$$
$$x_1 + 2x_2 \le 22$$
$$x_1 \ge 0 \text{ and}$$
$$x_2 \ge 0,$$

Sample (2)

A cloth company is capable of manufacturing two types of clothing; shirt and blouses. The manufacture of each type of clothing also requires the amount of cloth and labor shown in table. The unit profit for shirt is 6000 Kyats and unit profit for blouse is 10000 Kyats. Each week, 160 square yard of cloth and 180 hours of labor are available. How many shirts and blouses should be manufactured to maximized weekly profits?

The number of shirts and blouses should be manufactured to maximized weekly profits that can be calculated by graphical method.

The data is collected by cloth manufacture
The unit profit for shirt = 6000 Kyats
The unit profit for blouse = 10000 Kyats
The available time for labor = 180 hours
The require amount of cloth = 160 square yard
Display constraint above problem2 following

TABLE IV. TABLE OF MANUFACTURING

Clothing (type)	Labor (hour)	Cloth (square yards)	Profits
shirt	2	2	6000 Kyats
blouse	4	3	10000 Kyats

.

Model Formulation

Let x_1 = the number of shirt and
x_2 = the number of blouses.
Let Z denote the profit to be maximize

$$Z= 6000\, x_1 + 10000\, x_2$$

Subject to constraint $2x_1 + 4x_2 \le 180$

$$2x_1 + 3x_2 \le 160$$

$x_1 \ge 0$ and $x_2 \ge 0$.

Sample (3)

Marry makes pottery by hand in her basement. She has 20 hours available each week to make bowls and vases. A bowl requires 3 hours of labor, and a vase requires 2 hours of labor. It requires 2 pounds of special clay to make a bowl and 5 pounds to produce a vase. She is able to acquire

35 pounds of clay per week. She sells her bowls for 50000 Kyats and her vases for 40000 Kyats. She wants to know how many of each item to make each week in order maximize her revenue.

The data is collected by Marry's pottery
Type of products = 2 (bowl and vases)
The available time for labor = 20 hours
The available time for weight of clay = 35 pounds
The required labor time for bowl= 3 hours
The required labor time for vase= 2 hours
The required weight of clay for bowl= 2 pounds
The required weight of clay for vase = 5 pounds
Display constraint above problem1 following:

TABLE V. TABLE OF PRODUCTION

Product	Labor time	weight of clay	Selling price
bowl	3 hours	2 pounds	50000 Kyats
vases	2 hours	5 pounds	40000 Kyats
Available time	20hours	35 pounds	

Model Formulation
Let x_1 = the number of bowls and
x_2 = the number of vases.
Let Z denote the maximize revenue.

$$Z= 50000x_1 + 40000x_2$$

Subject to constraint $3x_1 + 2x_2 \leq 20$ (time)

$2x_1 + 5x_2 \leq 35$ (pounds)

$x_1 \geq 0$ and $x_2 \geq 0$,

V. CONCLUSION

Linear programming is broadly utilized field of enhancement. Numerous pragmatics in activities examination can be communicated as linear programming issues. It has wide scope of down to earth business, trade, and agricultural applications and all the while has gotten so through a theoretical development. Numerous organizations can be created by applying this linear programming model. Linear programming can make problems solving developed to make decision for company managers. Most applications of linear programming can be searched in today's competitive economic environment.

ACKNOWLEDGMENT

Author Nyunt Nyunt Wai is thankful to Pa-Oh farmer U Khun Kyi Aung of Taunggyi, Shan State for giving approximate data for this research paper.

REFERENCES

[1] N. P. Akpan, & I. A. Iwok, "Application of Linear Programming for Optimal Use of Raw Materials in Bakery," International Journal of Mathematics and Statistics Invention (IJMSI) E-ISSN: 2321 – 4767 P-ISSN: 2321 – 4759, Volume 4 Issue 8 || October. 2016 ||PP-51-57.
[2] G. B. Dantzig, "Programming of interdependent activities: II Mathematical Model, Econometrica", 17 (3), pp. 200-211, 1949.
[3] D. B. George, "Linear Programming," Vol. 50, No. 1, January–February 2002, pp. 42-47.
[4] W. U. Juan, G. E. Xueqian, "Optimization Research of Generation Investment Based on Linear Programming Model," 1875-3892 © 2011 Published by Elsevier B.V. Selection and/or peer review under responsibility of ICAPIE Organization Committee.
[5] J. K. Shama, "Linear Programming Theory and Applications".
[6] W. A. Jame, "Dial a Forecast.", *Journal of Accountancy* December 2006, pp. 75-78.
[7] U. U. Livinus, L. J. Robert, W. A. James, "An Application of Linear Programming in Performance Evaluation", Academy of Educational Leadership Journal Volume 21, Issue 1, 2017.
[8] M. Zangiabadi, H. R. Maleki, "A Method for Solving Linear Programming Problems with Fuzzy Parameters": Asia Pacific Journal of Operational Research · August 2007.
[9] Vishwa Nath Maurya Ram Bilas Misra, Peter K Anderson, Kamlesh Kumar Shukla, "Profit Optimization Using Linear Programming Model: A Case Study of Ethiopian Chemical Company".

Article ID - JRA6001420

Structural and Dielectric Properties of $BaZrO_3$ Ceramic

Tun Soe
Engineering Physics Department
Mandalay Technological U*niversity*
Mandalay,Myanmar
drtunsoeygn99@gmail.com

Kyaw Myat Thu
Engineering Physics Department
Mandalay Technological U*niversity*
Mandalay,Myanmar
kyawmyatthu999@gmail.com

Nan Tha Zin
Engineering Physics Department
Mandalay Technological U*niversity*
Mandalay,Myanmar
drnanthazin@mtu.edu.mm

***Abstract*—High phase purity barium zirconate powders were synthesized from a solid-state reaction. Barium oxide (BaO) and zirconium dioxide (ZrO_2) were transferred to a steel vessel and ball milled for 5 hours. Reactive powders consisting of submicron particles and narrow particles size distribution was expected to be formed by heating a 1:1 molar mixture of BaO and ZrO_2 at 1100 ºC up to 3 hours. The sample was studied by X-ray diffraction (XRD). From these results, diffraction angle and interplaner spacing were studied on observed values and standard values conditions. And then crystallite size and lattice parameters were calculated. Morphological characteristics such as grain size and surface condition were determined from scanning electron microscopy (SEM). The dry powder mixture was pressed into pellets. An LCR GW INSTEK 821 meter was used for measuring the passive component primary parameters of inductance (L), capacitance (C), resistance (R) and impedance (Z). Dielectric properties of barium zirconate ($BaZrO_3$) ceramic were interpreted by means of capacitance-frequency, dielectric constant–frequency characteristics and dielectric loss - frequency.**

***Keywords*— barium zirconate, X-ray diffraction, scanning electron microscopy, dielectric properties and ceramic.**

I. INTRODUCTION

A. Properties of $BaZrO_3$

The alkaline-earth zirconates having the general chemical formula $MZrO_3$ (M = Ca, Sr and Ba) with perovskite structure have been projected as potential structural and electronic ceramics. In suitable doped forms they have been claimed to become ionic and/or electronic conductors [1, 2]. Among the perovskites with cubic structures, $BaZrO_3$ is a refractory ceramic material which is very promising due to its high melting point (2920 ºC) and low chemical reactivity with corrosive compounds; it is the sole ceramic material that does not follow phase transitions over the range from 1327 ºC down to -269 ºC. In addition, $BaZrO_3$ has excellent thermal stability and resistance due to a low coefficient of thermal expansion ($\alpha = 87\times 10^{-7}$/ ºC between 25 ºC and 1080 ºC) [2, 3].The complete structure of provskite is very simple and have a complete cubic symmetry in which atoms positions are as follows: A atom is located in the cube angles, B atom is located in the center, oxygen atom is located around B atom in the centers of sides of the cube. The crystal structure of $BaZrO_3$ was as shown in Fig 1 [5].

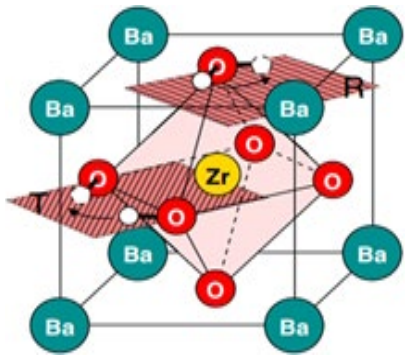

Fig 1. The crystal structure of $BaZrO_3$

B. Experimental Procedure

Firstly barium oxide (BaO) and zirconium dioxide (ZrO2) were mixed and ground by 1:1 molar ratio. The mixture powder was transferred into a steel vessel and ball-milled for 5 hours to reduce the particle grain size. The small sized powder was pre-sintered at 1100 ºC for 3 hours and crystalline BaZrO3 powder was formed. The crystalline powder was ground and mesh sieved to get uniform and lightest particles. After sieving, the crystalline BaZrO3 was evaluated by X-ray diffraction (XRD) and morphological characteristics were observed by Scanning Electron Microscopy (SEM). The dry powder was uniaxial pressed into pellet form. Ag-conductive layers were coated onto inner circles of BaZrO3 pellet while the outer circles were masked with a piece of tape. The Ag-layer of top surface was smaller than that of bottom surface of the pellet. The Cu-wire was soldered on both sides of Ag-conductive layers and ready to study the dielectric properties. After that it was calcined in air atmosphere at 1100 ºC for 3 hours. Crystal structure and phase identification of BaZrO3 ceramic was also studied by XRD. The surface morphological of BaZrO3 ceramic was examined by Scanning Electron Microscopy (SEM). Dielectric properties of BaZrO3 ceramic were interpreted by means of capacitance - frequency, dielectric constant - frequency characteristics

and dielectric loss - frequency. The procedure of BaZrO3 ceramic sample synthesis was described in Fig 2 to Fig 10.

Fig 2(a). Powders of BaO

Fig 2(b). Powder of ZrO_2

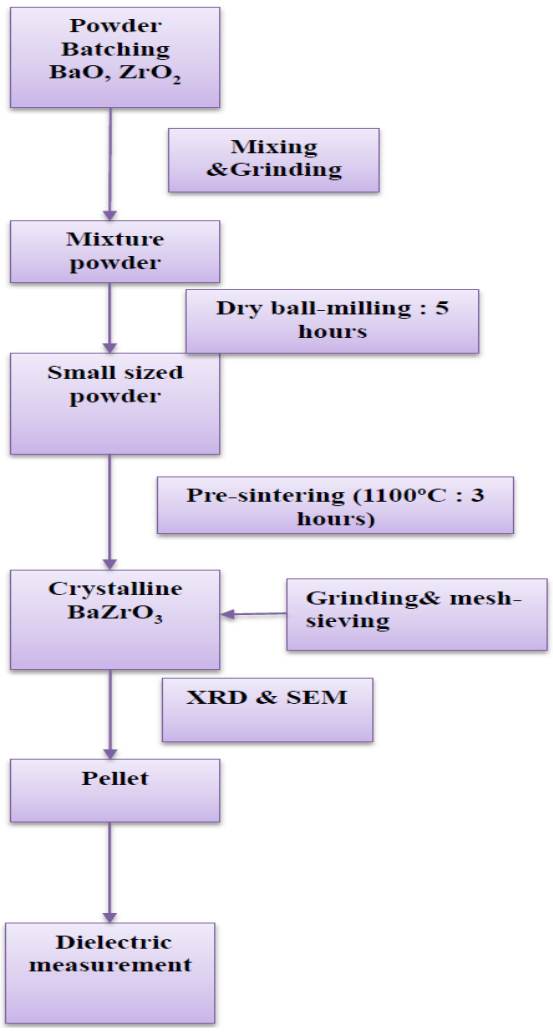

Fig 3. Flowchart of experimental procedure for $BaZrO_3$ ceramic

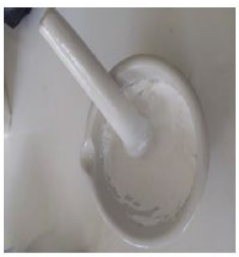

Fig 4. Mixing and grinding of $BaZrO_3$

Fig 5. On Mesh

Sieves

Fig 6. $BaZrO_3$ pellet

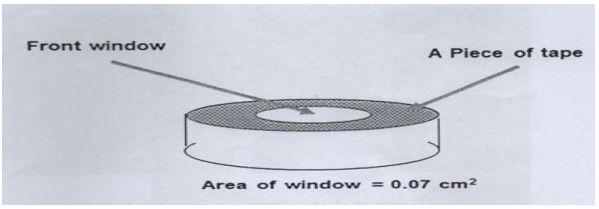

Fig 7. Masking the front side with a piece of tape

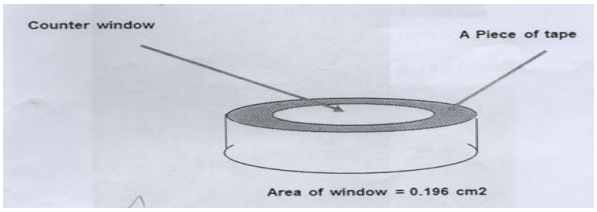

Fig 8. Masking the counter side with a piece of tape

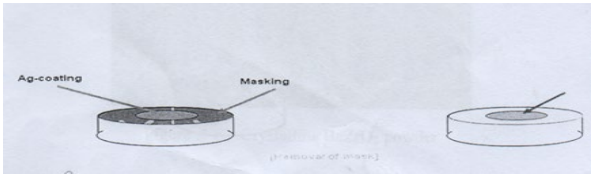

Fig 9. Front and back Ag-conductive layer formation

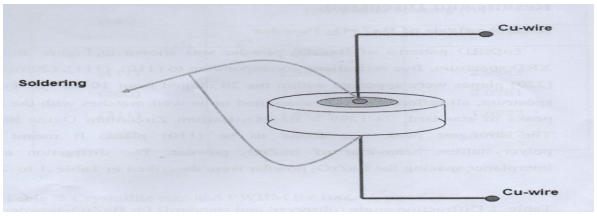

Fig 10. Cu-wire soldering with both conductive layers

II. Result and Discussion

A. XRD Analysis of BaZrO3 powder

The diffraction of X-rays by matter results from the combination of two different phenomena: (a) scattering by each individual atom, and (b) interference between the waves scattered by these between themselves. Bragg recognized a predictable relationship among several factors.

1. The distance between similar atomic planes in mineral (the interatomic spacing) which we call the d-spacing and measure in angstroms.
2. The angle of diffraction which we call the theta angle and measure in degree. For practical reasons

the diffractometer measures and angle twice that of the theta angle.

3. The wavelength of the incident X-radiation of Cu-K_a, symbolized by the Greek letter lambda and, in this thesis, equal to 1.54 angstroms. These factors are combined in Bragg's law:

$$n\lambda = 2d\sin\Theta$$

Where,

n = an integer,

λ = the wavelength of X-rays,

d = the lattice interatomic spacing and

Θ = the diffraction angle.

The XRD was used in this paper to identify the crystal structure in my sample after sintered at process temperature. The scanning of the 2Θ angle was started at 10˚, and ended at 70˚.The scanning rate was 0.5˚/min [6].This measurement was made in university research center of Yangon University. The powder X-ray Diffractometer (**RIGAKU, MULTIFLEX)** was described in Fig 11. XRD patterns of $BaZrO_3$ powder was shown in Fig 14. From the XRD spectrum, four reflections corresponding to (110), (200), (211) and (220) planes were appeared within the 2θ ranged from 10º to 70º. From XRD spectrum, all reflections were examined to be well-matches with the diffracted peaks of standard, 74-1299 > $BaZrO_3$ – Barium Zirconium Oxide library file. The strongest peak was found to be (110) plane. From these results, the sample was considered of barium zirconium oxide powder. The diffraction angle and interplaner spacing for $BaZrO_3$ powder were described in Table 1 and 2.

TABLE I. DIFFRACTION ANGLE (OBSERVED AND STANDARD) FOR $BaZrO_3$ POWDER

Planes (hkl)	Diffraction angle (Degree)	
	Observed	Standard
(110)	30.522	30.111
(200)	43.619	43.117
(211)	53.938	53.453
(220)	63.079	62.582

TABLE II. INTERPLANER SPACING (OBSERVED AND STANDARD) FOR BAZRO3 POWDER

Planes (hkl)	Interplaner Spacing (Å)	
	Observed	Standard
(110)	2.9264	2.965
(200)	2.0733	2.096
(211)	1.6985	1.712
(220)	1.4726	1.483

TABLE III. CRYSTALLITE SIZE AND FWHM FOR BAZRO3POWDER

Planes (hkl)	FWHM (rad)	Crystallite Size (nm)
(110)	0.275	29.91
(200)	0.311	27.61
(211)	0.396	22.49
(220)	0.478	19.54

The diameter of spherical shaped crystallite size could be identified as crystallite size, G, which calculated by Debye-Scherer equation

$$G = \frac{0.9 \times \lambda}{FWHM\ (rad) \times \cos\theta} \qquad (1)$$

Where,

G = crystallite size,

λ = wavelength to compute d-spacing

Θ = Bragg angle

The obtained calculated crystallite size values were summarized in Table 3 as compared to FWHM values. The lattice parameters were evaluated by cubic diffraction equation,

$$\frac{1}{d^2} = \frac{h^2 + k^2 + l^2}{a^2} \qquad (2)$$

Where,

d = interplaner spacing,

h, k, l = names of plane

a = lattice parameter

From the calculate values, the average crystallite size and average lattice parameter of BaZrO3 were 22.84 nm and 4.1941 respectively. The lattice parameters of BaZrO3 powder were described in Table 4. Diffraction angle, interplaner spacing and full wave half maximum values were obtained from data sheet of XRD result. From these data, crystallite size values and lattice parameter values were calculated by used of equation 1 and equation 2.

TABLE IV. LATTICE PARAMETERS FOR BAZRO3 POWDER

Planes (hkl)	Lattice Parameter(A)
(110)	4.1937
(200)	4.1925
(211)	4.1954
(220)	4.1948

Fig 11. The powder X-ray Diffractometer (**RIGAKU, MULTIFLEX)**

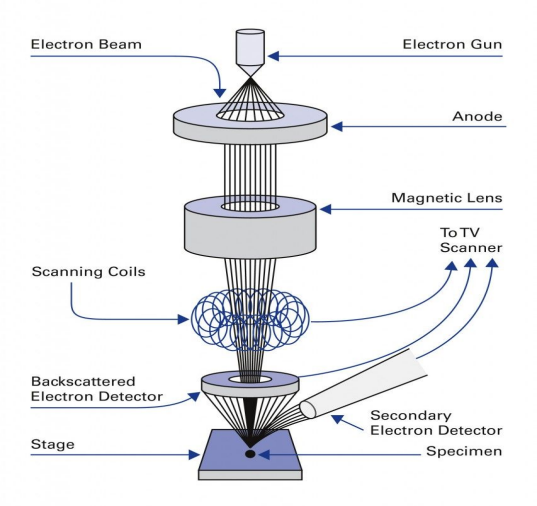

Fig 12. The principal feature of a scanning electron microscope

Fig 13. The LCR meter (GW INSTEK 821, USA)

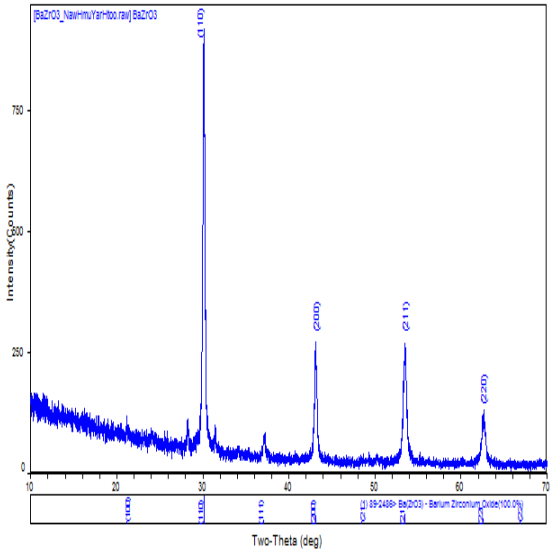

Fig 14. XRD Profile of BaZrO3 powder

B. SEM Analysis of BaZrO3 powder

SEM is probably the most widely used technique for surface analysis. A focus electron beam is scanned across its surface in synchronism with the spot of a display cathode ray tube. A detector monitors the intensity of a chosen secondary signal from the specimen (usually, secondary electrons are used), and the brightness of the spot on the display is determined by an amplified version of the detected signal. If the intensity of the emitted secondary signal changes across the specimen, then contrast will be seen in the image on the cathode ray tube. The resulting reflects the surface morphography of the specimen and can be readily interpreted because it contains light and shade in much the same way as everyday images which are families to our eye [7].In this work, the surface morphology as analyzed by using scanning electron microscope (JEOL, Model No. JSM-5610LV) with accelerating voltage 15kV and magnification 5000X.This measurement was made in physics department of West Yangon University. Fig 12 showed the principal feature of a scanning electron microscope. SEM microphotograph of BaZrO3 was shown in Fig 15. The magnification × 5000 BaZrO3 was surface carried out grain size. Irregular grains were appeared. The grain distribution was not uniform in this image and the grain feature could be identified. Agglomeration of grain was thicker and compact form in microstructure. The SEM image of BaZrO3 powder annealed at 1100 ºC revealed that the grain size was 1.33 µm. Thus, the growth of the BaZrO3 grain diameter was accelerated at higher annealing temperature. Fig 15 shows a representative scanning electron micrograph of the presently prepared (BaZrO3) ceramic sample and the grains size obtains from the figure of the order of micrometer.

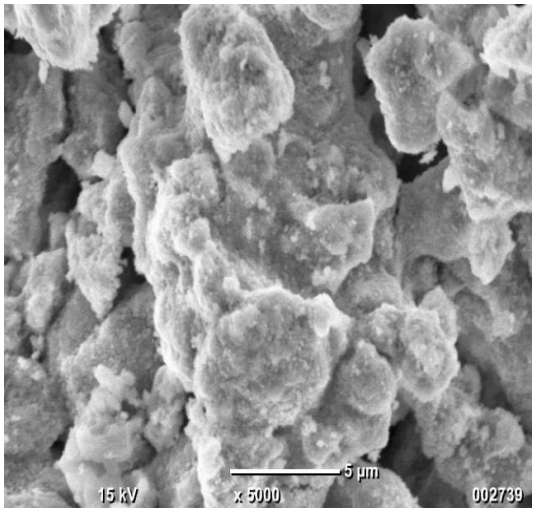

Fig 15. The SEM microphotograph of BaZrO3 powder

C. Dielectric behaviour of BaZrO3 ceramic

Fig 13 showed the Digital Impedance Analyzer (LCR meter; LCR GW INSTEAK 821 Quch Tech; 1730: Digibridge) of measuring change in capacitor and dielectric loss as a function of different frequencies. The dielectric constant was calculated by equation,

$$C = {}^{\varepsilon}o^{\varepsilon}r/d \qquad (3)$$

Where,

C is the capacitance, ε0 and εr is permittivity of the free space and relative permittivity the dielectric material respectively; A is the area of ceramic. These results were described in table 5. Graph of Capacitance and Frequency of BaZrO3 ceramic was shown in Fig 16. Graph of Dielectric constant and frequency of BaZrO3 ceramic was shown in Fig 17. Graph of Dielectric loss and frequency of BaZrO3 ceramic was shown in Fig 18.

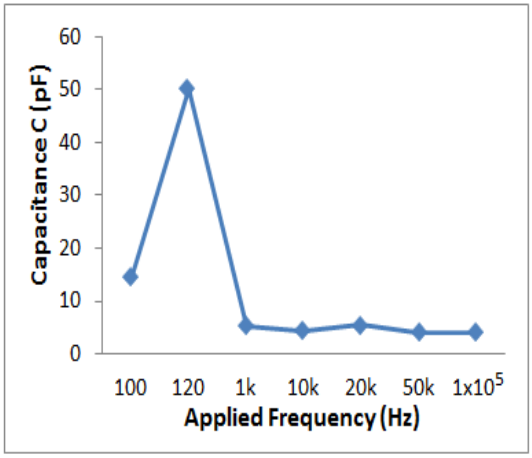

Fig 16. Graph of Capacitance and Frequency of $BaZrO_3$

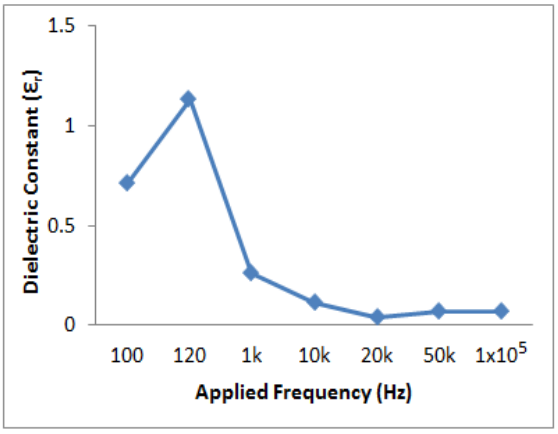

Fig 17. Graph of Dielectric constant and frequency of $BaZrO_3$

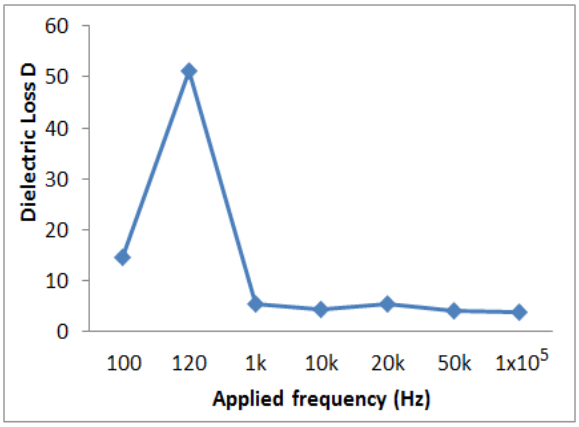

Fig 18. Graph of Dielectric loss and frequency of $BaZrO_3$

TABLE V. DIELECTRIC PROPERTIES OF BAZRO3 CERAMIC WITH DIFFERENT APPLIED FREQUENCY

Applied frequency (HZ)	Capacitance" C" (pF)	Dielectric constant "ε_r"	Dielectric loss" D"
100	14.30	0.71	14.54
120	50.20	1.13	51.06
1k	5.32	0.26	5.41
10k	4.44	0.11	4.52
20k	5.41	0.04	5.50
50k	3.98	0.07	4.05
$1x10^5$	3.88	0.07	3.95

III. CONCLUSION

The BaZrO3 powder was prepared using the conventional solid-state reaction method. Single phase BaZrO3 was identified by annealed powders. From the XRD spectra of powder and ceramic, four reflections corresponding to (110), (200), (211) and (220) planes were appeared within Bragg angle from 10º to 70º. The crystallite sizes were calculated to be 22.84 nm for powder. From SEM analysis the grain size of BaZrO3 powder was 1.33 µm. The frequency dependent dielectric parameters, such as capacitance, dielectric constant and dielectric loss for BaZrO3 ceramic have been investigated within the range of 100 Hz to 100 kHz.

From the dielectric analysis, the maximum capacitance and dielectric constant were observed at 120 Hz. The high values of dielectric constant at low frequency could be explained as the accumulation of charges at the grain boundaries and at the interfaces between the sample and the electrode. From the above reasons, the growth of BaZrO3 ceramic was suitable for cost effective ceramic preparation and BaZrO3 ceramic was quite promising candidate for ferroelectric memory device.

ACKNOWLEDGEMENTS

We would like to express our thanks to Dr Yin Mg Mg, Professor, Department of Physics, Yangon University, for his valuable supervision and guidance. We are greatly indebted of Dr Kyi Thar Myint, Retired Professor, Department of Physics, West Yangon University, for her valuable suggestions in this research work.

REFERENCES

[1] Ahmad Sazari et al Piscataway n J 08855 “Ferroelectric Ceramic: Processin, Properties and Applications”, Rutgers University of USA.
[2] Arrizumi A et al 1985 Japan J Apply Phys 247.
[3] MC Graw-Hill 2002 Concise Encyclopedia of Physics.
[4] Ross I M 1957 US Palent No 279-1760.
[5] S. Parida et al 2012 Structural rezinement, optical and microwave dielectric properties of $BaZrO_3$ Ceramics International 38 1294.
[6] lei Z 2006 “Cobaltferrite-Bariumtitannate So-helBifferroies” Ph. D Disseration, Department of Material Science and Engineering, University of MaryLand.
[7] Whittingham, M.S.et al.2003.Journal of Power Sources.

Article ID – JRA6002120

Investigation on Electrical Properties of Ni-Zn-Co Ferrites

Tin Myoe Min
Department of Physics
Myingyan University
Myanmar
tinmyoemin1@gmail.com

Aye Mya Phyu
Department of Physics
Defence Services Academy
Myanmar
ayemyaphyu.phyu5@gmail.com

Su Su Hlaing
Department of Physics
Myingyan University
Myanmar
susuhlaing2491@gmail.com

***Abstract*- Single phase soft ferrite nanocrystallites could be synthesized by various methods. Most of the methods start from preparation of powder or they are high temperature synthesis. Ferrite material having the compositional formula, $Ni_{0.35}Zn_{0.65-x}Co_xFe_2O_4$, (where x = 0.0, 0.1, 0.2 and 0.3) prepared by conventional ceramic technique. The substitution of cobalt (Co) in the $Ni_{0.35}Zn_{0.65-x}Co_xFe_2O_4$ ferrites produced appreciable changes in its electrical properties. Resistivity of the ferrite sample (x = 0.3) reached the maximum value of $9.39x10^7$ Ωcm at 303K. The activation energy varied from 0.404 eV to 0.432 eV. Curie temperature increased from 473K to 529K. Dielectric constant decreased to 18. The substitution of Co (x = 0.3) in the $Ni_{0.35}Zn_{0.65-x}Co_xFe_2O_4$ ferrites is the better than other compositions. All these changes are favorable for electrical applications. The synthesized $Ni_{0.35}Zn_{0.65-x}Co_xFe_2O_4$ would be useful in several technological applications such as soft magnets, low materials at high frequencies applications.**

***Keywords*: Ni-Zn-Co ferrite, ceramic technique, resistivity, activation energy, Curie temperature, drift mobility, dielectric constant**

I. INTRODUCTION

Spinel ferrites with the general formula AFe_2O_4 (A= Mn, Co, Ni, Mg, or Zn) are very important magnetic materials because of their interesting electrical properties with chemical and thermal stabilities [3,5]. Nickel zinc cobalt ferrite is one of the most important ferrites. It has a cubic structure of normal spinel-type and is a soft magnetic n-type semiconducting material, which finds a number of applications in heterogeneous catalysis, adsorption, and sensors and in magnetic technologies [7,8]. Recently, nanostructures of magnetic materials have received more and more attention due to their novel material properties that are significantly different from those of their bulk counterparts [6,9]. The ordered magnetic materials such as nanorods and nanowires have currently attracted a great interest due to their enhanced magnetic property [10].

II. MATERIALS AND METHOD

A. Sample Preparation

Ferrite material having the compositional formula, Ni0.35Zn0.65-xCoxFe2O4, where x values ranging from 0.0 to 0.3 in a step of 0.1 was prepared by the conventional ceramic technique. The starting materials used for the preparation of the samples are Fe2O3, NiO, ZnO and CoO in the form of powders. The qualitative compositions of samples were calculated in terms of weight percent according to the following chemical reaction [2].

$$NiO(0.35) + ZnO(0.65 - x) + CoO(x) + Fe_2O_3 \rightarrow Ni(0.35)\ Zn(0.65 - x)Co(x)\ Fe_2O_4$$

B. Stoichiometric Calculation and Powder Preparation

The appropriate weight percent of each oxide to be mixed for different compositions was calculated by the following formula.

$$\text{wt \% of oxide} = \frac{\text{molecular wt of oxide} \times \text{required wt of the sample}}{\text{sum of the molecular wt of the given composition}}$$

The required weight percent of each oxide materials, to be added for different composition, were weighted by using a digital balance. The care was taken to check the zero setting of the balance before weighing the powder on the balance. After properly weighing the materials, oxides of obtained compositions were crushed and mixed thoroughly for one and half hours in ethyl alcohol using agate mortar and pestle to get a homogeneous mixture.

C. Calcination and Grinding

After mixing and grinding, the mixtures were calcined to produce the desire compound by diffusion reaction. They were dried and calcined at 1000ºC for twelve hours followed by the furnace cooling in air atmosphere. The calcined materials were again mixed and crushed for one and half hours in ethyl alcohol to reduce it to small crystallites of uniform sizes [1].

D. Sintering and Shaping

The crushed powders were shaped into pellets and toroid forms with a hydraulic press to determine easily their electrical properties. For easier shaping, a few drops

of saturated solution of polyvinyl alcohol (PVA) is added into the powder mixtures as a binder. Under the pressure of 4x108Pa, the mixtures were shaped into pellets of 12.2mm in diameter and 3.3mm in thickness and toroid forms of 11.8mm in inner diameter, 22mm in outer diameter and thickness of about 3.6 mm. The shaped samples were finally sintered at 1100ºC for four hours in air followed by furnace cooling to obtain the equilibrium distribution of cations on A and B-sites [4].

The dimensions of the sintered samples are important for the calculation of electrical properties of these ferrites. So, they are measured accurately and calculated with geometrical relations. For a toroid, the effective cross-sectional area (A) is calculated by,

$$A = \frac{D_1 - D_2}{2} \times T \quad (1)$$

The mean magnetic path length (ℓ) is,

$$l = \frac{D_1 + D_2}{2} \times \pi \quad (2)$$

where, 'D1' and 'D2' are outer and inner diameters and 'T' is the thickness of the toroid. Then, the core volume can easily be calculated by multiplying 'A' and 'ℓ'.

For a pellet, the top or bottom surface area is,

$$A = \frac{\pi \times d^2}{4} \quad (3)$$

where, 'd' is the diameter of the circular area. The volume of the pellet can be calculated by multiplying 'A' with the thickness, 't' of this pellet [5]. The pellets and toroid forms of Ni0.35Zn0.65-x CoxFe2O4 samples are as shown in Figure 1.

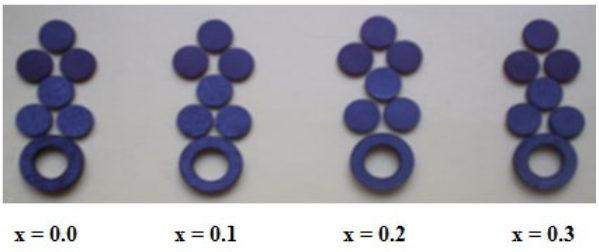

Fig 1. The pellets and toroid forms of $Ni_{0.35}Zn_{0.65-x}Co_xFe_2O_4$ samples

III. RESULTS AND DISCUSSION

A. Measurement of Electrical Resistivity

The electrical resistivity values of each ferrite sample, at different temperatures, were obtained by using equation,

$$\rho = \frac{RA}{l}. \quad (4)$$

The values of resistance in this equation were measured in experimental setup. These values were determined firstly at room temperature and then in the temperature range of 353K to 573K with intervals of 20K were obtained.

B. Resistivity Values at Room Temperature

Firstly, the cross-sectional area (A) and the thickness (l) of each sample were measured accurately. Then, the sample was placed in a sample holder that was immersed in an electrically heated steel chamber surrounded by asbestos. In the holder, the sample is sandwiched with two copper plates and filled with silver paste to get good conduct. Each copper plate was brought into contact with copper rod in the chamber as shown in Figure 2. The room temperature resistivities of all sintered samples were measured and have been plotted in Figure 3 as a function of Co content (x). The results are tabulated in Table 1. The research work was done on Universities' Research Center & Asia Research Center, University of Yangon, Myanmar.

It has been observed that resistivity shows an increasing trend at higher Co concentration. The resistivity value is smallest at x = 0.0 (2.78×107Ωcm) and is largest at x = 0.3 (9.39×107 Ωcm). This increasement may be due to the change in average grain size of the ferrites. The substitution process between Zn2+ ions with Co2+ ions can decrease in the mobility of charge carriers. Consequently, the resistivity values increase with increasing Co content.

This may also be due to the fact that Zn2+ ions prefer the occupation of tetrahedral A sites and Co ions prefer the occupation of octahedral B sites while Fe ions partially occupy both A and B sites. On increasing Co ion concentration (at B site), the Zn ion concentration (at A site) will be decreased. As a result, Fe ions migrate from B site to A site to substitute the reduction in Zn ion concentration (at A site). Hence, the number of ferrous and ferric ions at the B site (which is responsible for electrical conduction in ferrites) decreases and the resistivity increases on increasing Co ion substitution.

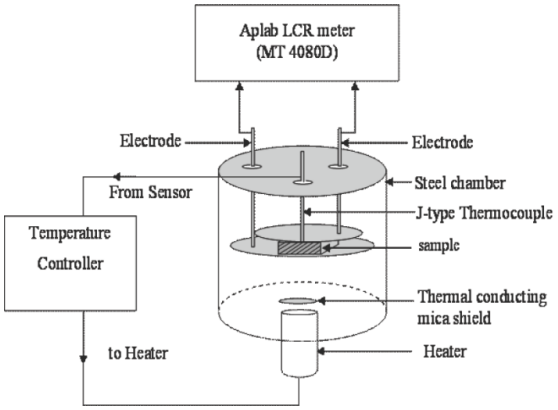

Fig 2. Schematic diagram for resistivity measurement of the sample

C. Variation of Resistivity with Temperature

The effect of temperature on the resistivity is presented in Figure 4 for all the studied samples. This figure clearly indicates that the electrical resistivity decreases as the temperature of the sample increases. This decrease in the resistivity is due to the semiconductive behavior of the studied samples which is controlled by Arrhenius relation equation.

$$\rho = \rho_\infty \exp(E_a / K_B T) \quad (5)$$

Where, 'ρ∞' is the resistivity extrapolated to T = ∞, 'T' is the absolute temperature, 'KB' is the Boltzmann constant and 'Ea' is the activation energy. The measured values are shown in Table 2.

TABLE I. RESISTIVITY AT 303K AND ACTIVATION ENERGY VALUES OF NI-ZN CO FERRITES

Co-contents (x)	Resistivity at 303K, ρ (×10^3 Ω cm)	Activation energy	
		E_r (eV)	E_p (eV)
0.0	2.78	0.404	0.412
0.1	4.73	0.417	0.425
0.2	7.43	0.427	0.433
0.3	9.39	0.432	0.441

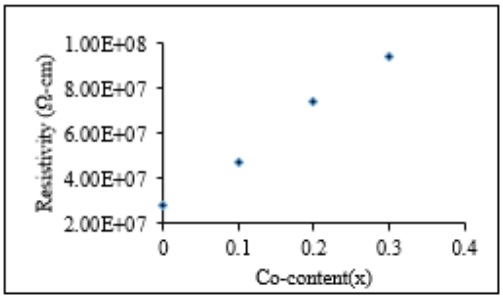

Fig 3. Resistivities of Ni0.35Zn0.65-xCoxFe2O4ferrite with different Co content (x) at 303K

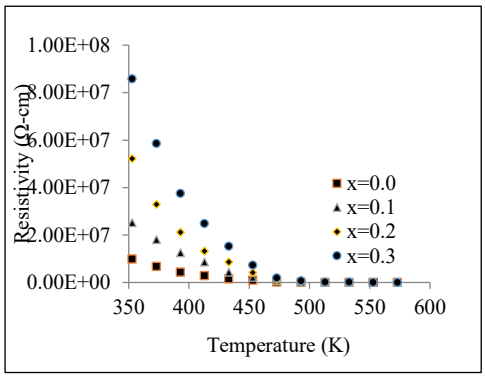

Fig 4. Temperature dependence on resistivity curves for Ni0.35Zn0.65-xCoxFe2O4 ferrite with different different Co content (x)

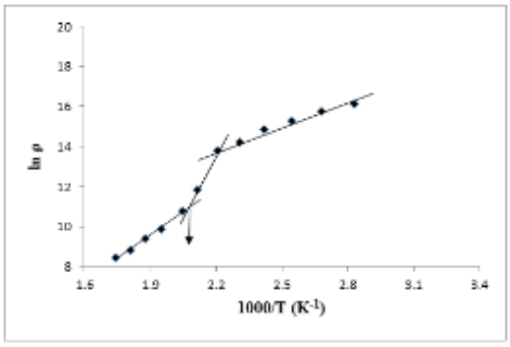

Fig 1. ln ρ Vs (1000/T) graph for Ni0.35Zn0.65Fe2O4 ferrite

TABLE II. TEMPERATURE DEPENDENCE ON RESISTIVITY FOR NI0.35 ZN0.65-XCOXFE2O4 FERRITE WITH DIFFERENT DIFFERENT CO CONTENT (X)

Temperature (K)	Resistivity (Ω-cm)			
	x = 0.0	x = 0.1	x = 0.2	x = 0.3
353	9.88E+06	2.53E+07	5.23E+07	8.59E+07
373	6.84E+06	1.81E+07	3.30E+07	5.86E+07
393	4.42E+06	1.26E+07	2.12E+07	3.75E+07
413	2.90E+06	8.70E+06	1.33E+07	2.48E+07
433	1.48E+06	4.31E+06	8.70E+06	1.53E+07
453	9.70E+05	2.22E+06	4.24E+06	7.36E+06
473	1.41E+05	8.73E+05	1.10E+06	1.93E+06
493	4.70E+04	2.43E+05	4.27E+05	6.57E+05
513	1.79E+04	7.48E+04	9.91E+04	2.26E+05
533	9.87E+03	2.23E+04	5.20E+04	1.14E+05
553	6.65E+03	1.25E+04	2.65E+04	6.25E+04
573	4.75E+03	8.25E+03	1.45E+04	3.25E+04

D. Determination of Activation Energy and Curie Temperature

To determine the activation energies of the samples, the dc resistivity data plotted as ln ρ Vs (1000/ T) graphs have been used. As shown in the Figure 5, 6, 7 and 8, the variation could be divided into three regions. The first one extends from room temperature up to about 353K where a kink is observed. This region is almost independent of Co concentration. The conduction phenomenon in this region is attributed to impurities. The second kink, at higher temperature, was observed that its value depends on Co concentration. By comparing the values of temperatures at this kink, Tρ, with Curie temperatures, TC, determined from gravity method in Table 3, one can attributed this kink to the magnetic transition from ferrimagnetic to paramagnetic state.

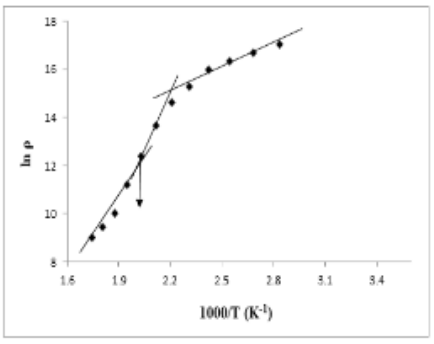

Fig 2. ln ρ Vs (1000/T) graph for Ni0.35Zn0.55Co0.1Fe2O4 ferrite

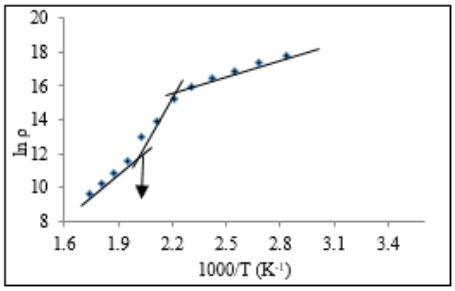

Fig 3. ln ρ Vs (1000/T) graph for Ni0.35Zn0.45Co0.2Fe2O4 ferrite

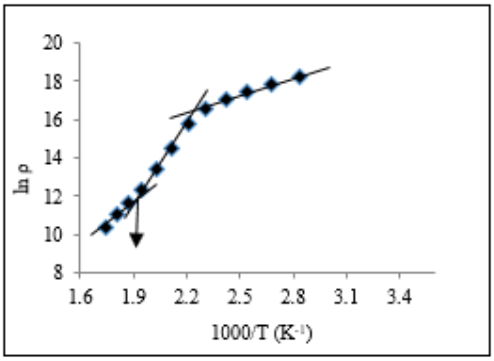

Fig 4. ln ρ Vs (1000/T) graph for Ni0.35Zn0.35Co0.3Fe2O4 ferrite

TABLE III. VARIATION OF TRANSITION TEMPERATURE AND CURIE TEMPERATURE WITH DIFFERENT CO CONCENTRATIONS

Co-concentrations (x)	Transition Temperature, T_p (K)	Curie Temperature, T_c (K)
0.0	470	473
0.1	492	495
0.2	503	507
0.3	525	529

The activation energies for the paramagnetic (Ep) and ferrimagnetic (Ef) regions were determined from the slopes of the lines on both sides of Tρ. These data are presented in Table 1. It is clear that 'Ep' is higher than 'Ef' because of the fact that the ferrimagnetic state is an ordered state, while, the paramagnetic state is a disordered state in which a charge carrier needs more activation energy to jump between adjacent sites. The values of both Ep and Ef increase as the Co concentration increased, as shown in Figure 9. It may be due to the increase in resistivity with the increase in Co concentration because activation energy behaves in the same way as that of electrical resistivity.

The Curie temperature increases continuously as the Co content increases, as shown in Figure 10. It can be caused by Co2+ ions behavior which prefers B sites for substitution content. The enter of Co2+ ions into the B sites shifts the same amount of Fe3+ ions into A sites instead of Zn2+ ions. Increase of the Fe3+ ions content in A site causes AB exchange interaction to be stronger and therefore it causes higher value of TC. The other reason is that the non-magnetic Zn ions have been replaced by the magnetic Co ions in the ferrite samples.

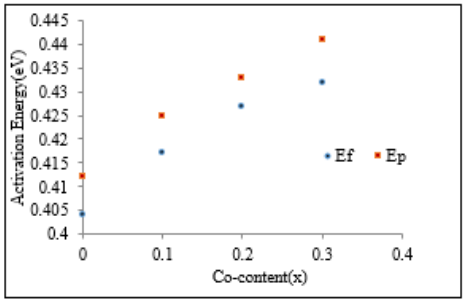

Fig 5. Variation of activation energies with different Co content (x) in Ni0.35Zn0.65-xCoxFe2O4

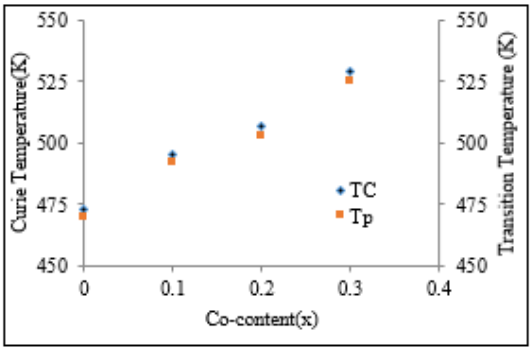

Fig 6. Variation of TC and Tρ with different Co concentration (x) in Ni0.35Zn0.65-xCoxFe2O4

E. Determination of Drift Mobility

The drift mobility (μd) values of all the ferrite samples have been calculated by using the following equation.

$$\mu_d = \frac{\sigma}{\eta e} \qquad (6)$$

Where, 'e' is the charge on an electron, 'σ' is the electrical conductivity and 'η' is the concentration of charge carriers. The variation of mobility is plotted against Co content in Figure 11 at 303K. The results are tabulated in Table 4. As shown in the table, the drift mobility decreases with increasing Co concentration. The value of mobility is greatest at x = 0.0 (10.4×10-12 cm2/Vs) and is smallest at x = 0.3 (2.97×10-12 cm2/Vs). It can also be seen that samples having higher resistivity have low mobility.

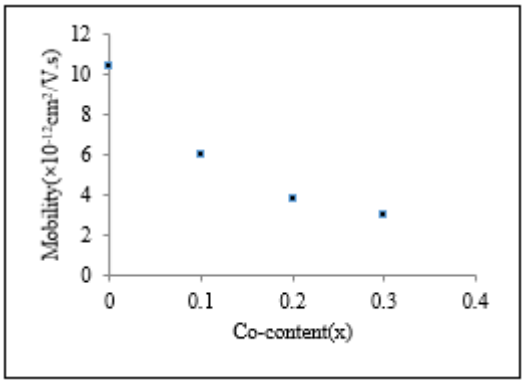

Fig 7. Drift mobility values as a function of Co content (x) at 303K in Ni0.35Zn0.65-xCoxFe2O4

TABLE IV. VARIATION OF DRIFT MOBILITY (MD) WITH DIFFERENT CO CONCENTRATIONS AT 303K

Co-concentrations (x)	Drift mobility, μd (×10⁻¹² cm²/Vs)
0.0	10.4
0.1	6
0.2	3.76
0.3	2.97

To examine the temperature dependence of mobility, a graph of mobility, μd (×10-12 cm2/Vs) and 1000/T (K-

1) is drawn in Figure 12. It is observed from the graph that, by increasing temperature, the resistivity decreases and thus the value of mobility also increases. It may be due to the hopping of charge carriers from one site to another as the temperature increases. The observed values are shown in Table 5.

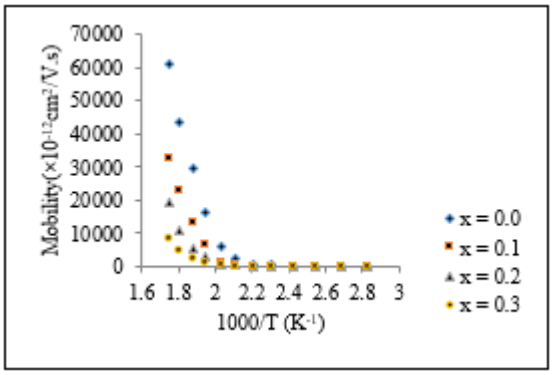

Fig 8. Drift mobility values as a function of temperature with Co content (x) in Ni0.35Zn0.65-xCoxFe2O4

F. Determination of Dielectric Constant

The variation in dielectric constant values (ε) of all the ferrite samples at a fixed frequency of 1 kHz have been obtained by using with the equation.

$$\varepsilon = \frac{Ct}{\varepsilon_0 A} \qquad (7)$$

Where, 'εo' is an electrical constant equal to 8.85 × 10-2 pF/cm, 'C' is the capacitance of the specimen in farads, 't' is the thickness of the specimen in cm and 'A' is the area of the specimen in sq-cm. The results show that the value of 'ε' can change with changing composition as well as with the temperature values.

G. Composition Dependence of Dielectric Constant

Dielectric constant in ferrites is contributed by several structural and microstructural factors. Compositional variation of dielectric constant of Ni- Zn-Co ferrites at 1 kHz frequency is shown in Figure 13. The results are tabulated in Table 6. It is observed that dielectric constant decreases with the increase in Co concentration.

The observed variation in dielectric constant may be understood on the basic of space charge polarization which is due to an inhomogeneous dielectric structure governed by the number of space charge carriers and the resistivity of the sample. The change in resistivity can obstruct the flow of space charge carriers and therefore impede the build-up of space charge polarization. Since the observed resistivity is increasing with Co2+ concentration in the present Ni-Zn Co ferrites, the dielectric constant is decreased with an increase in dopant concentration as a result of the space charge polarization.

H. Temperature Dependence of Dielectric Constant

The temperature dependence of dielectric constant at 1 kHz was studied in the temperature range from 303K to 573K for mixed Ni-Zn Co ferrites and the results were plotted in Figure 14. The results are shown in Table 7.

As can be seen from the Figure 14, the value of dielectric constant increases by increasing the temperature. This is the normal dielectric behavior for ferrites due to the increase in number of electric charge carriers and their drift mobilities. Since the resistivity of all ferrite samples decrease with increasing temperature, the drift mobility of the carriers increases. This increases the probability of electrons to reach the grain boundary in the bulk material. Consequently, polarization and dielectric constant increase. It is noted that Ni-Zn Co ferrite with higher Co content has smaller dielectric constant at a given temperature value. Variation of drift mobility with resistivity for Ni0.35Zn0.65-xCoxFe2O4 ferrite with different Co content is shown in Figure 15.

TABLE V. DRIFT MOBILITY VALUES AS A FUNCTION OF TEMPERATURE WITH CO CONTENT (X) IN NI0.35ZN0.65-XCOXFE2O4

Temperature (K)	Mobility (×10^{-12}cm^2/V. s)			
	x = 0.0	x = 0.1	x = 0.2	x = 0.3
353	29.3	11.2	5.37	3.24
373	42.4	15.7	8.51	4.75
393	65.5	22.5	13.2	7.43
413	99.9	32.6	21.1	11.2
433	196	65.9	32.3	18.2
453	299	128	66.2	37.8
473	2050	325	255	144
493	6160	1170	658	424
513	16200	6340	2830	1230
533	29400	13300	5400	2440
553	43600	22700	10600	4460
573	61000	32400	19400	8570

TABLE VI. VARIATION OF DIELECTRIC CONSTANT (E) WITH DIFFERENT CO CONTENTS AT 303K

Co-contents (x)	Dielectric Constant (ε)
0.0	94
0.1	49
0.2	31
0.3	18

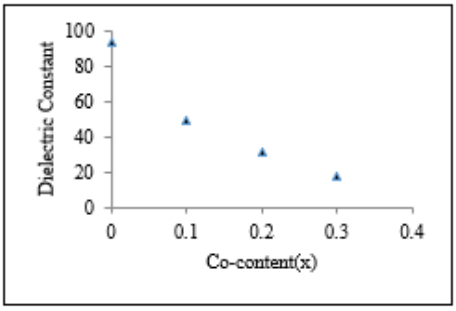

Fig 9 . The variation of dielectric constant at 1kHz with Co content (x) in Ni0.35Zn0.65-xCoxFe2O4 at 303K

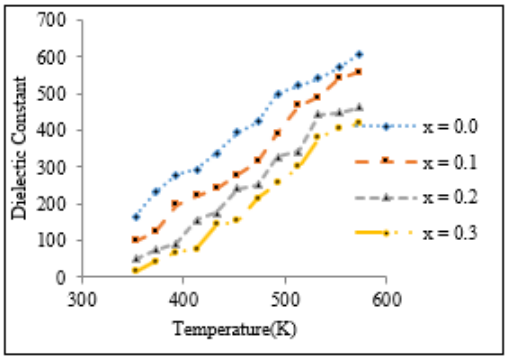

Fig 10. Dielectric constant values as a function of temperature with Co content (x) in Ni0.35Zn0.65-xCoxFe2O4

TABLE VII. DIELECTRIC CONSTANT VALUES AS A FUNCTION OF TEMPERATURE WITH CO CONTENT (X) IN NI0.35ZN0.65-XCOXFE2O4

Temperature (K)	Dielectric Constant			
	x = 0.0	x = 0.1	x = 0.2	x = 0.3
353	165.1136	99.47643	51.0330	15.9500
373	233.1110	123.3967	74.7939	42.9002
393	279.3249	197.9322	92.1089	66.5940
413	294.5063	222.7774	155.9282	76.1940
433	336.7974	241.0206	175.3196	143.4259
453	393.2492	278.2724	242.0093	152.7070
473	423.8671	315.0459	251.0033	215.9203
493	499.1363	391.7502	326.9103	256.7442
513	522.7376	467.2745	342.2193	300.7575
533	541.2359	489.7276	443.0034	379.2160
553	570.2592	540.5662	447.4685	406.0067
573	608.9462	558.7775	463.7343	419.0831

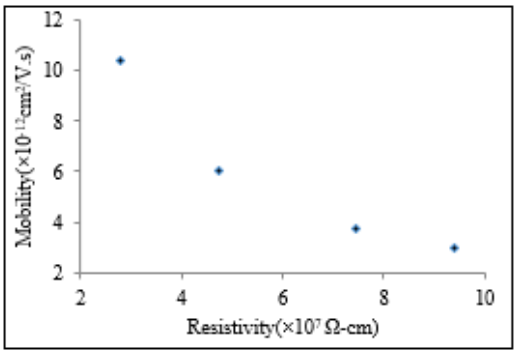

Fig 11. Variation of drift mobility with resistivity for Ni0.35Zn0.65-xCoxFe2O4 ferrite with different Co content

IV. CONCLUSION

Nickle-Zinc Cobalt ferrites (Ni0.35Zn0.65-xCoxFe2O4) with the composition (x = 0.0, 0.1, 0.2, 0.3) have been successfully prepared by using the conventional ceramic technique. The temperature dependence on resistivity measurement revealed an increase in resistivity upon increasing Co2+ dopant concentration in NiZn ferrite system. These are showed the increasing trend of grain size with increasing Co-contents. Activation energy in paramagnetic region is greater than in ferrimagnetic region which shows hopping conduction at higher temperature. The dielectric constant of each ferrite shows dopant concentration as well as temperature dependence. At higher temperature (i.e, at the Curie point), all samples lost their magnetic properties, abruptly. The values of Curie temperatures of the ferrites determined by the gravity method well agreed with the results from the temperature dependence on resistivity measurement.

ACKNOWLEDMENT

We would like to express our sincere thanks to Prof Dr Maung Maung, Principal, Myingyan University for his permission and encouragement to perform this research. We would like to thank Prof Dr Tin Tin Yee, Head of Department of Physics, Myingyan University for her valuable suggestions, comments and encouragements provided during the course of our research work.

REFERENCES

[1] Sattar A A et.al 2005 J Appl. Sci 5(1) 162
[2] Dann S E 2000 “Reaction and Characterization of Solids”, Bristol: Polestar Wheatons
[3] Lide D R 1995 “Hand book of Chemistry and Physics”, CRC: New York
[4] Sattar A A et.al 2007 J Mater Sci 42 149
[5] Goldman A 2006 “Modern Ferrite Technology”, Pittsburgh: Springer
[6] A. A Thant et al Journal of the Australian Ceramic Society 46 11
[7] Buschow K H, De Bore F R 2004 “Physics of Magnetism and Magnetic Materials”, New York: Kluwer Academic Publishers
[8] Kumar K V & Sreekanth T 2008 “Applied Physics”, New Delhi: S. Chand
[9] Aye Aye Thant, Pho Kaung, Srimala S, Itoh M, Othman R and Fauzi M N 2007 Proceeding of the PSU-UNS International Conference on Engineering Enviroment (ICEE), Songkhla, Thailand
[10] Santi Maensirl et al 2009 Nanoscale Res Lett 4 221.

Article ID – JRA6004620

Study of Two-Nucleon Bound State using CD-Bonn Potential

Thandar Kyi
Department of Physics
Meiktila University
Meiktila, Myanmar

Htun Htun Oo
Department of Physics
Meiktila University
Meiktila, Myanmar

Abstract: **The two-nucleon bound state is studied by using with CD-Bonn potential. Lippmann-Schwinger equation for two-body bound state system is solved by using Gauss-Legendre integration method. The binding energy of deuteron and corresponding wave function in momentum space are solved by using iterative method. Our result of the binding energy of the deuteron is 2.22312 MeV and the root mean square radius is 1.966fm.**

Keywords**: CD-Bonn potential, Lippmann-Schwinger equation, Gauss-Legendre integration method**

I. INTRODUCTION

In this research we will present the very simple and easiest way to handle numerical technique for the two-body problem. It is the simplest and one can understand the nucleon- nucleon interaction very well. Especially, we studied the structure of two-nucleon system, i.e., deuteron which consists of one proton and one neutron. Deuteron is the nucleus of deuterium and the name deuterium is derived from the Greek deuteros, meaning "second", to denote the two particles composing the nucleus [1]. Deuteron has a mass of 2.013553212745(40) u (equal to 1875.612 928(12) MeV) [2]. As the only two-nucleon bound state, its properties have continuously been viewed as important in nuclear theory as the hydrogen atom is in atomic theory.

Deuteron is an ideal system for studying the nucleon-nucleon interaction. To study this two-body bound system, the Lippmann-Schwinger equation is solved. In our two body Lippmann-Schwinger equation, CD-Bonn potential is used. The charge dependence (CD) predicted by the Bonn full model is reproduced accurately by the new potential, which is why we call the CD-Bonn potential [3]. But we will not discuss about this CD-Bonn potential in detail. We only emphasize the technique and how to handle this potential code. In this research, we studied the binding energy of deuteron with CD-Bonn potential by using the iterative method. We have also studied potential energy, kinetic energy and root mean square radius.

II. TWO-BODY BOUND SYSTEM

In studying the two-body system in momentum space we will start with time-independent Schrödinger equation.

$$\hat{H}|\psi\rangle = E\,|\psi\rangle \tag{1}$$

$$(\hat{H}_0 + \hat{V})|\psi\rangle = E\,|\psi\rangle \tag{2}$$

where, ψ is the wave function $\hat{H}_0$ is the kinetic energy operator and $\hat{V}$ is the potential energy operator. The kinetic energy operator has the property as

$$\hat{H}_0|p\rangle = \frac{\hat{p}^2}{2\mu}|p\rangle = \frac{p^2}{2\mu}|p\rangle \tag{3}$$

The solution of Schrödinger equation can be written as

$$|\psi\rangle = \frac{1}{E-\hat{H}_0}\,\hat{V}\,|\psi\rangle \tag{4}$$

This is the Lippmann-Schwinger equation in ket form and then we project it into momentum space as

$$\langle p\ell m|\psi\rangle = \left\langle p\ell m\left|\frac{1}{E-\hat{H}_0}\,\hat{V}\right|\psi\right\rangle \tag{5}$$

where, μ is reduced mass, p is the relative momentum between two particles, ℓ is the relative orbital angular momentum and m is the magnetic quantum number.

When operator $\hat{H}_0$ operates on, $\langle p\ell m|$ the above equation becomes

$$\langle p\ell m|\psi\rangle = \left\langle p\ell m\left|\frac{1}{E-\frac{p^2}{2\mu}}\,\hat{V}\right|\psi\right\rangle \tag{6}$$

After inserting the completeness relation,

$$\langle p\ell m|\psi\rangle = \frac{1}{E-\frac{p^2}{2\mu}}\sum_{\ell' m'}\int p'^2\,dp'\langle p\ell m|\,V\,|p'\ell' m'\rangle$$

$$\langle p'\ell' m'|\psi\rangle \tag{7}$$

For spherically symmetric potential, we can write as

$$\psi_\ell(p) = \frac{1}{E-\frac{p^2}{2\mu}}\sum_{\ell'}\int_0^\infty p'^2 dp'\,V_{\ell\ell'}(pp')\psi_{\ell'}(p') \tag{8}$$

This is known as the Lippmann-Schwinger equation for two particles in potential well.

In the above equation, $\psi_\ell(p)$ is the wave function for two-body system, p is momentum, μ is the reduced mass, $V_{\ell\ell'}(pp')$ is the potential matrix element and E is the total energy or binding energy of the two-body system.

Then, (8) is solved with FORTRAN. We need to transform this integral equation to discrete form to write a FORTRAN code then it is solved by using Gauss-Legendre integration method which is

$$\int f(x)dx = \sum_{i=1}^{n} f(x_i)w_i \quad (9)$$

where, x_i is gauss point and w_j is gauss weight.

In discrete form, the Lippmann-Schwinger equation becomes

$$\psi_\ell(p_i) = \frac{1}{E-\frac{p_i^2}{2\mu}} \sum_{\ell'} \sum_j p_j^2 w_j V_\ell(p_i, p_j) \psi_{\ell'}(p_j) \quad (10)$$

The above equation can be solved numerically by using the FORTRAN 90 code.

A. Evaluation of Energy by Iterative Method

The iterative method is applied to find the eigen value in our calculation. As a function of energy, the kernel of (10) is written as

$$K_{\ell,\ell',i,j}(E) = \frac{1}{E-\frac{p_i^2}{2\mu}} \sum_{\ell'} \sum_j p_j^2 w_j V_\ell(p_i, p_j) \quad (11)$$

For pure S-wave Using Eq. (11), Eq. (10) can be written in a compact form as

$$\psi(p_i) = K_{ij}(E)\psi(p_j) \quad (12)$$

Arbitrary value which is function of E is introduced as

$$\eta(E)\psi(p_i) = K_{ij}(E)\psi(p_j) \quad (13)$$

When $\eta(E)$ is equal to 1, one can see (12) and (13) are the same.

Therefore, our background idea is that we will find the energy E which can give $\eta(E)$ value 1. Suppose that E_1 is upper bound energy and E_2 is lower bound energy. We define the true energy $E = \frac{E_1+E_2}{2}$ which will be given to the kernel. We use the iterative method for that E and we pick up the η value. If the η value is less than 1, we let E to be E_1 or if the η value is greater than 1, we let E to be E_2 and iterate again. By repeating the above procedure, the gap between E_1 and E_2 becomes narrow and narrow and then the value of η approaches to 1. Finally, the value of energy, E corresponding to η value 1 is our desired binding energy, E.

B. Potential Matrix Elements in Momentum Space

The phenomenological potentials for two-body system are mostly represented in configuration space, r. So, we must have to transform these potentials from configuration space to momentum space, p.

The potential matrix elements can be written as

$$V_{\ell\ell'}(p, p') = \langle p\ell m|V|p'\ell' m'\rangle \quad (14)$$

The potential matrix elements in configuration space and momentum space are related as follows.

$$\langle p\ell m|V|p'\ell' m'\rangle = \int r^2 dr \int r'^2 dr' \sum_{\ell'' m''} \sum_{\ell''' m'''} \langle p\ell m|r\ell'' m''\rangle \langle r\ell'' m''|V|r'\ell''' m'''\rangle \langle r'\ell''' m'''|p'\ell' m'\rangle \quad (15)$$

where,

$$\langle p\ell m|r\ell' m'\rangle = \sqrt{\frac{2}{\pi}}\, j_\ell(pr) i^\ell \delta_{\ell\ell'} \delta_{mm'} \quad (16)$$

For the spherically symmetric potential and if the tensor force is ignored,

$$\langle r\ell m|V|r'\ell' m'\rangle = V_\ell(r) \frac{\delta(r-r')}{rr'} \delta_{\ell\ell'} \delta_{mm'}$$

Therefore, the transformed potential matrix element becomes

$$V_\ell(p, p') = \frac{2}{\pi} \int r^2 dr\, j_\ell(pr) i^{2\ell} j_\ell(p'r) V_\ell(r) \quad (17)$$

For the particular case $\ell = 0$,

$$V(p, p') = \frac{2}{\pi pp'} \int dr \left(\frac{e^{ipr} - e^{-ipr}}{2i}\right) \left(\frac{e^{ip'r} - e^{-ip'r}}{2i}\right) V(r) \quad (18)$$

Again, (18) can be rearranged and the result is

$$V(p, p') = \frac{1}{2\pi pp'} \int [e^{i(p+p')r} - e^{i(p-p')r} - e^{-i(p-p')r} + e^{-i(p+p')r}]\, V(r) dr \quad (19)$$

We define A = p + p' and B = p - p' and we get

$$V(p, p') = \frac{1}{2\pi pp'} \int_0^\infty [e^{iAr} - e^{iBr} - e^{-iBr} + e^{-iAr}]\, V(r) dr \quad (20)$$

This is the transformation of potential matrix elements from configuration or coordinate space to momentum space for S-wave.

C. Observable Quantities of Bound System

After solving (13) numerically, we will obtain the ground state energy and the corresponding wave function. The normalized wave function is

$$\psi_\ell^{nol}(p) = \frac{1}{\sqrt{\sum_\ell \int \psi_\ell^*(p)\psi_\ell(p)p^2 dp}}\, \psi_\ell^{un-nol}(p) \quad (21)$$

To check the quality of wave function, we will calculate kinetic energy, KE and potential energy, PE by using normalized wave function. The KE and PE for two-body couple channel is

$$KE = \frac{1}{2\mu} \int \psi_\ell^*(p)\psi_{\ell'}(p')p^4 dp \quad (22)$$

$$PE = \sum_{\ell\ell'} \int p^2\, dp \int p'^2 dp'\, \psi_\ell^*(p)\, V_{\ell\ell'}(p, p')\psi_{\ell'}(p') \quad (23)$$

For S-state ($\ell = 0$),

$$KE_S = \frac{1}{2\mu}\int \psi_0^*(p)\psi_{0'}(p')p^4dp \quad (24)$$

$$PE_S = \int p^2\,dp \int p'^2dp'\,\psi_0^*(p) V_{00}(p,p')\psi_0(p') \quad (25)$$

For D-state ($\ell = 2$),

$$KE_D = \frac{1}{2\mu}\int \psi_0^*(p)\psi_{0'}(p')p^4dp \quad (26)$$

$$PE_D = \int p^2\,dp \int p'^2dp'\,\psi_0^*(p) V_{00}(p,p')\psi_0(p') \quad (27)$$

For couple state of S and D,

$$PE_{SD} = \int p^2\,dp \int p'^2dp'\,\psi_0^*(p) V_{02}(p,p')\psi_2(p') \quad (28)$$

By adding kinetic energy, KE and potential energy, PE, we may obtain the binding energy, E as

$$E = KE_S + KE_D + PE_S + PE_D + 2PE_{SD} \quad (29)$$

To calculate the root mean square radius of two-body system, we will transform the wave function from momentum space to coordinate space.

The wave function in coordinate space is

$$\psi_{\ell m}(r) = \langle r\ell m|\psi\rangle \quad (30)$$

We insert the completeness relation and we get

$$\psi_{\ell m}(r) = \sum_{\ell' m'}\int p^2\,dp\,\langle r\ell m|p'\ell' m'\rangle \psi_{\ell' m'}(p) \quad (31)$$

Using the Eq. (16), the above equation becomes

$$\psi_{\ell m}(r) = \sqrt{\frac{2}{\pi}}\int p^2dp\, j_\ell(pr)i^{-\ell} \psi_{\ell' m'}(p) \quad (32)$$

Then, the wave function μ_ℓ can be defined as

$$u_\ell = r\psi_\ell(r) \quad (33)$$

For normalized wave function in coordinate space,

$$\sum_\ell \int \psi_\ell^*(r)\,\psi_\ell(r)r^2dr = 1 \quad (34)$$

$$\sum_\ell \int u_\ell^2(r)dr = 1 \quad (35)$$

$$\langle r^2\rangle = \sum_\ell \int u_\ell^2(r)r^2dr \quad (36)$$

From this equation we can calculate the root mean square radius of two-body system.

$$R_{rms} = \frac{1}{2}[\sum_\ell \int u_\ell^2(r)r^2dr]^{1/2} \quad (37)$$

III. RESULTS AND DISCUSSION

In this research, the binding energy of deuteron is studied with CD-Bonn potential, $V_{\ell\ell'}(pp')$.

Firstly, the binding energy of deuteron is studied by using the iterative method. To perform iterative method shown in Eq. (13), the wave function shown in (10) is used. In numerical calculation, the Lippmann Schwinger equation shown in (8) is solved by using Gauss-Legendre integration method to get (10). Therefore, we need to define the integral range in momentum space p of (8) in FORTRAN code as that the initial point is p_0, the midpoint is p_{mid}, the maximum point is p_{max}, and the number of grid points on integral range is Np. Firstly, we choose the input data set, p_0=0fm^{-1}, p_{mid}=10fm^{-1}, p_{max} =20fm^{-1} and Np=30. The precision of binding energy is studied by changing the number of grid points Np for the respective p_{max} as shown in Tables I, II, III, IV and IV.

It is found that the value of binding energy becomes converge at 2.22257 MeV starting from Np=54 for p_{max} =20fm^{-1} as shown in Table I. For p_{max} =30fm^{-1}, the value of binding energy becomes converge at 2.22303 MeV starting from Np=64 as shown in Table II. For p_{max} =40fm^{-1}, the value of binding energy becomes converge at 2.22310 MeV starting from Np=74 as shown in Table III. Finally, binding energy does not change although we increase the p_{max} from 50fm^{-1} to 60fm as shown in Tables IV and V. Our result of the converged binding energy of deuteron with iterative method is taken as 2.22312 MeV.

Secondly, the binding energy is calculated by using (29) adding the kinetic energy, KE and potential energy PE with normalized wave function shown in (21). To calculate the average kinetic energies and potential energies, we use the fined input data set for integral range in momentum space, p_0=0fm^{-1}, p_{mid}=25fm^{-1}, p_{max} =50fm^{-1} and Np=80. And the result obtained are shown in Table VI.

Now we can check it with the result obtained by iterative method. According to Table VI, the result is perfectly agreed with the result from iterative method. And therefore, our normalized numerical wave function is acceptable.

It is also found that the proton and neutron in the deuteron cannot bind with only S-wave or both S and D-wave. The coupling effect of S and D supports to bind the proton and neutron as a deuteron.

The values of S-state and D-state wave functions in momentum space, $\psi_0(p)$ and $\psi_2(p)$ are shown in Tables VII and VIII. The natures of S-state and D-state wave functions in momentum space, $\psi_0(p)$ and $\psi_2(p)$ are shown in Fig. 1 and Fig. 2.

Finally, we transformed our numerical wave function in momentum space to coordinate space. We had used this wave function in calculating root mean square radius shown in (37). We studied the precision of root mean square radius by changing the number of grid points Nx at x_{max}= 20 fm. The converged root mean square radius is 1.966 fm at Nx=90 and it does not change although we increase x_{max} to 30 fm as shown in Tables IX and X.

The values of S-state and D-state wave functions in coordinate space, $u_0(r)$ and $u_2(r)$ are shown in Tables XI and XII. The natures of S-state and D-state wave functions in coordinate space $u_0(r)$ and $u_2(r)$ are shown in Fig. 3 and Fig. 4.

TABLE I. THE CONVERGENCE OF BINDING ENERGY, E BY CHANGING THE NUMBER OF GRID POINTS NP FOR P_{MAX}= 20 FM^{-1}.

Np	p_{mid}(fm^{-1})	p_{max}(fm^{-1})	E(MeV)
30	10.00	20.00	2.22295
34	10.00	20.00	2.22186
38	10.00	20.00	2.22238
40	10.00	20.00	2.22253
44	10.00	20.00	2.22260
48	10.00	20.00	2.22258
50	10.00	20.00	2.22258
54	10.00	20.00	2.22257
58	10.00	20.00	2.22257
60	10.00	20.00	2.22257
64	10.00	20.00	2.22257
68	10.00	20.00	2.22257
70	10.00	20.00	2.22257

TABLE II. THE CONVERGENCE OF BINDING ENERGY, E BY CHANGING THE NUMBER OF GRID POINTS NP FOR PMAX= 30 FM-1.

Np	p_{mid}(fm^{-1})	p_{max}(fm^{-1})	E(MeV)
50	15.00	30.00	2.22302
54	15.00	30.00	2.22306
58	15.00	30.00	2.22305
60	15.00	30.00	2.22304
64	15.00	30.00	2.22303
68	15.00	30.00	2.22303
70	15.00	30.00	2.22303
74	15.00	30.00	2.22303
78	15.00	30.00	2.22303
80	15.00	30.00	2.22303

TABLE III. THE CONVERGENCE OF BINDING ENERGY, E BY CHANGING THE NUMBER OF GRID POINTS NP FOR PMAX= 40 FM-1.

Np	p_{mid}(fm^{-1})	p_{max}(fm^{-1})	E(MeV)
60	20.00	40.00	2.22313
64	20.00	40.00	2.22313
68	20.00	40.00	2.22311
70	20.00	40.00	2.22311
74	20.00	40.00	2.22310
78	20.00	40.00	2.22310
80	20.00	40.00	2.22310
84	20.00	40.00	2.22310
88	20.00	40.00	2.22310
90	20.00	40.00	2.22310

TABLE IV. THE CONVERGENCE OF BINDING ENERGY, E BY CHANGING THE NUMBER OF GRID POINTS NP FOR PMAX= 50 FM-1.

Np	p_{mid}(fm^{-1})	p_{max}(fm^{-1})	E(MeV)
70	25.00	50.00	2.22315
74	25.00	50.00	2.22314
78	25.00	50.00	2.22313
80	25.00	50.00	2.22312
84	25.00	50.00	2.22312
88	25.00	50.00	2.22312
90	25.00	50.00	2.22312

TABLE V. THE CONVERGENCE OF BINDING ENERGY, E BY CHANGING THE NUMBER OF GRID POINTS NP FOR PMAX= 60 FM-1.

Np	p_{mid}(fm^{-1})	p_{max}(fm^{-1})	E(MeV)
80	30.00	60.00	2.22315
84	30.00	60.00	2.22313
88	30.00	60.00	2.22313
90	30.00	60.00	2.22312
94	30.00	60.00	2.22312
98	30.00	60.00	2.22312
100	30.00	60.00	2.22312

TABLE VI. AVERAGE VALUES OF KE, PE AND E WITH CD-BONN POTENTIAL.

KE_S (MeV)	9.88888
KE_D (MeV)	5.71235
PE_S (MeV)	-4.76311
PE_D (MeV)	1.42071
PE_{SD} (MeV)	-7.24098
E (MeV) = KE_S+ KE_D+ PE_S + PE_D+2 PE_{SD}	-2.22312
E (MeV) from our iterative method	-2.22312

TABLE VII. THE VALUES OF S-STATE WAVE FUNCTION Ψ0(P) IN MOMENTUM SPACE.

p(fm^{-1})	$\Psi_0(p)$ [fm$^{-3/2}$]
0.0	12.77088
0.5	1.63569
1.0	0.35309
1.5	0.10395
2.0	0.01195
2.5	-0.00433

TABLE VIII. THE VALUES OF D-STATE WAVE FUNCTION Ψ2(P) IN MOMENTUM SPACE.

p(fm^{-1})	$\Psi_2(p)$ [$fm^{-3/2}$]
0.0	12.77088
1.0	1.63569
2.0	0.35309
3.0	0.10395
4.0	0.01195
5.0	-0.00433

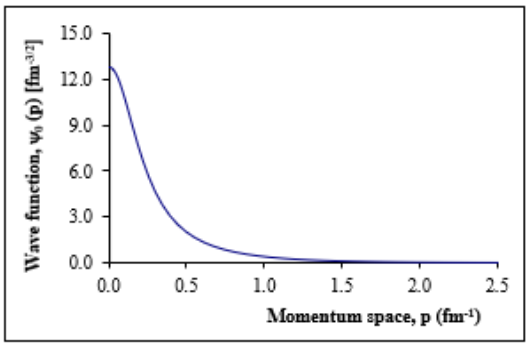

Fig 1. The S-state wave function of deuteron in momentum space.

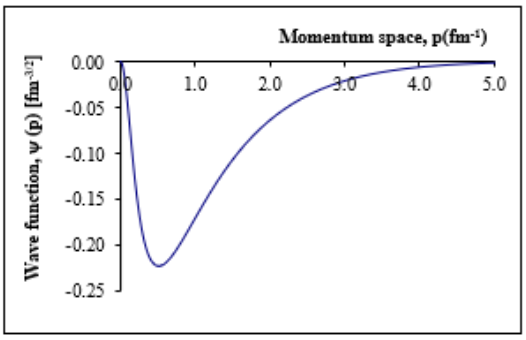

Fig 2. The D-state wave function of deuteron in momentum space.

TABLE IX. THE CONVERGENCE OF ROOT MEAN SQUARE RADIUS OF DEUTERON BY CHANGING THE NUMBER OF GRID POINTS NX FOR XMAX= 20 FM AT NP=150.

Nx	R_{rms}(fm)
60	1.971
70	1.967
80	1.968
90	1.966
100	1.966
110	1.966

TABLE X. THE CONVERGENCE OF ROOT MEAN SQUARE RADIUS OF DEUTERON BY CHANGING THE NUMBER OF GRID POINTS NX FOR XMAX= 30 FM AT NP=280.

Nx	R_{rms}(fm)
90	1.966
100	1.966
110	1.966
120	1.966
130	1.966
140	1.966
150	1.966

TABLE XI. THE VALUES OF S-STATE WAVE FUNCTION U0(R) IN COORDINATE SPACE.

r(fm)	$u_0(r)$ [$fm^{-1/2}$]
0.0	0.00004
2.5	0.47665
5.0	0.27888
7.5	0.15813
10.0	0.08843
12.5	0.04548
15.0	0.02638
17.5	0.02000
20.0	0.00841
22.5	0.00482
25.0	0.00250

TABLE XII. THE VALUES OF D-STATE WAVE FUNCTION U2(R) IN COORDINATE SPACE.

r(fm)	$u_2(r)$ [$fm^{-1/2}$]
0.0	0.00000
1.0	0.11629
3.0	0.09373
5.0	0.03900
7.0	0.01671
9.0	0.00837
11.0	0.00428
13.0	0.00273
15.0	0.00141

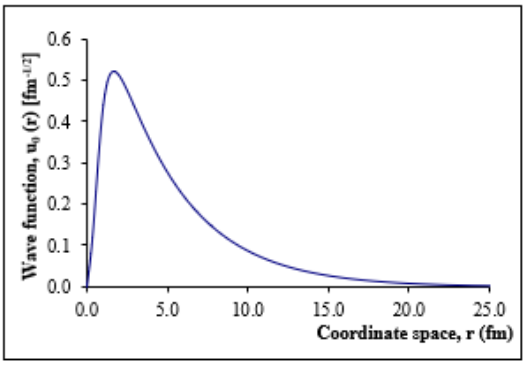

Fig 3. The S-state wave function of deuteron in coordinate space.

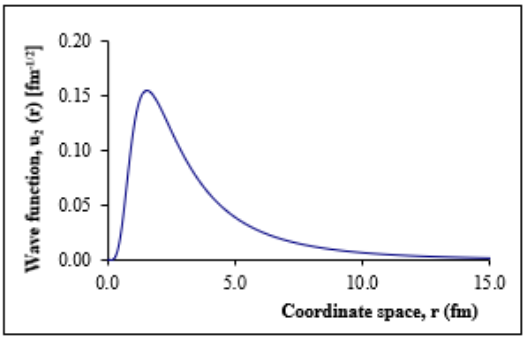

Fig 4. The D-state wave function of deuteron in coordinate space

IV. CONCLUSION

In this paper the two-nucleon bound state equation in momentum space has been presented. Then the transformation of potential from coordinate space to momentum space has been expressed. It is found that the coupling effect of S and D supports to bind the proton and neutron as a deuteron with the binding energy of -2.22312 MeV. The root means square radius of the deuteron in which the two nucleons can exist mostly is 1.966 fm.

ACKNOWLEDGEMENT

We are very grateful, first of all, to Professor Dr. Hla Hla Than, Head of Department of Physics, Meiktila University and Professor Dr. Daw Hla Win, Department of Physics, Meiktila University for their valuable advice and constant encouragement to do this research work.

We also convey special thanks to all teaching staff of Physics Department, Meiktila University.

REFERENCES

[1] O. Leary, Dan, "The deeds to deuterium". Nature Chemistry. 4 (3): 236, 2012.
[2] Physics.nist.gov. Retrieved on 2020-01-30.
[3] R. Machleidt, et al., Phys. Rev. C 63, 24001, 2001.

Article ID – JRA6006320

Effect of Temperature on Structural Feature, Microstructural Characteristics and Photovoltaic Properties of ZnO: Si Heterojunction Device

Kyay Mone Htun
Engineering Physics Department, Technological University (Magway),
Magway, Myanmar.
kyaymonehtun307@gmail.com

Cynthia Aye
Engineering Physics Department, Technological University(Magway),
Magway,Myanmar.
cynthiaaye0012@gmail.com

Sandar Aung
Department of Physics, University of Information Technology,
Yangon, Myanmar
sandaraung@uit.edu.mm

Pwint Yi Thein
Department of Physics, Nationalities Youth Resource Development Degree College,
Yangon, Myanmar.
susan74june@gmail.com

***Abstract*— ZnO films are deposited onto p - type Si (100) substrates via colloidal precursor solution route. Deposited ZnO films are sintered at 500ºC, 550ºC, 600ºC, 650ºC and 700ºC for each 1 hrs. X -rays diffraction studies are carried out to determine the phase assignment and structural feature of the prepared samples. Microstructural characteristics of the prepared samples are examined by using SEM technique. Photovoltaic properties of the prepared samples are characterized under illumination. From the short circuit current (I_{sc}) and open current voltage (V_{oc}) plots, photovoltaic parameter, such as efficiency (η) and fill factor (F_f) are estimated. In this paper simple, easy and less expensive, fabrication of second- generation solar cell is presented.**

***Keywords*—ZnO, Process Temperature, XRD, SEM, photovoltaics.**

I. INTRODUCTION

ZnO is one of the most important prospective short wavelength emitters owing to its large exciton binding energy (~ 60 meV) and a wide bandgap of 3.3 eV at room temperature. It also possesses unique physical and chemical properties, such as high chemical stability, high electrochemical coupling coefficient, broad range of absorption and high photostability, etc. The piezoelectric and pyroelectric properties of ZnO mean that it can be used as a sensor, converter, energy generator and photocatalyst. Because of its hardness, rigidity, and piezoelectric constant, it is an important material in ceramic industry, while its low toxicity, biocompatibility and biodegradability make it a material of interest in biomedicine and in pro - ecological system [1, 2].

In materials science, ZnO is classified as semiconductor in group II - VI, whose covalent is between ionic and covalent semiconductors. The crystal structures featured by ZnO are wurtzite, zinc blende and rock salt or Rochelle salt. Under ambient conditions, the wurtzite structure is the most thermodynamically stable phase. The zinc blende structure can be stabilized only by grown on cubic substrates, and the rock salt or Rochelle salt may be obtained only at high pressure (~10 GPa) synthesis. ZnO is also known as zincite in mineral form and very rare in nature [3].Schematic representation of a wurtzitic ZnO structure is displayed in Fig.1[4].

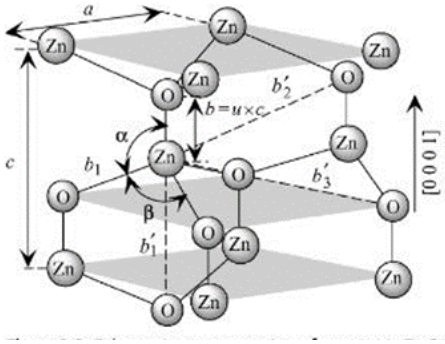

Fig.1 Schematic representation of a wurtzitic ZnO structure with lattice constants a in the basal plane and c in the basal direction, u parameter, which is expressed as the bond length or the nearest-neighbor distance b divided by c (0.375 in ideal crystal) α and β (109.47o in ideal crystal) bonds angles, and three types of second-nearest-neighbor distances b'1, b'2, and b'3.

Most of early studies on ZnO films were focused on effect of process temperature on structural, piezoelectric and optical properties of ZnO [5-7]. Influence of process temperature on structural feature, morphological characteristics and photovoltaic properties of ZnO : Si

heterojunction devices is subject of this investigation and examined in this research work.

II. Experimental Procedure

Zinc acetate Zn (CH3COO)2 and 2 - methoxyethanol (CH3OCH2CH2OH) are used as starting materials in this study. Two starting materials / solutions are mixed and put in the glass vessel and heat treated at 100oC with water - bath, known as indirect heat treatment for 2 hrs. During the heat treatment, the mixed solutions are stirred.

After that, ZnO precursor solutions are deposited on to p - type Si (100) with dimension (1 cm × 1 cm × 125 μm) and resistivity is 20 Ω cm. Before deposition, Si substrates are cleaned by using standard semiconductor cleaning process. Deposition procedures are carried out in clean chamber with spin coating technique. Firstly, wet films are dried at room temperature and sintered at 500oC, 550oC, 600oC, 650oC and 700oC for each 2 hrs. X - rays diffraction studies are carried out to examine the phase formation and structural feature of prepared samples by means of Rigaku Multiflux diffractometer with Cu Kα (λ = 1.5408 Å) monochromatic radiation. Prepared samples are scanned in the 2θ range from 10° to 70° with a scanned speed of 0.01°/sec.

Applied voltage and current are set to be 50 kV and 40 mA. X -rays diffraction spectra are recorded at room temperature. From the x - rays spectra, phase formation and structural feature, such as lattice constants, lattice distortion, unit cell volume, crystallite size and micro strain are investigated.

SEM technique is used to determine the microstructural characteristics of prepared samples by means of JEOL (JSM- 5610LV), and applied voltage and current are 15 kV and 68 μA. SEM images are recorded with 5000 magnification. SEM produces the images of prepared samples by scanning the surfaces of the sample with focused beam of electrons. The electrons interact with atoms in the prepared samples, producing various signals that contain information about the surface topography of the samples. The electrons beam is scanned in a raster scan pattern and position of the beam is combined with the intensity of the detective signal to produce an image. From the SEM images, grain growth situation, average grain size and presence of micro cracks are studied.

Photovoltaic properties of prepared samples are examined by using applied DC bias voltage in the range from – 1.5 V to + 2.5 V, with a step voltage, 0.1 V and delay time 1 minute, under illumination with sodium lamp source and lux meter (Extech - 401025). From the Isc vs. Voc plots, photovoltaic parameter, such as conversion efficiency (η) and fill factor (Ff) are evaluated.

III. Results And Discussion

X - rays diffraction spectra of ZnO films at different process temperatures are displayed in Fig.2. Peak search algorithm, known as Jade software is used to identify the unknown peaks in this study. Only diffraction peaks from polycrystalline, wurtzite, hexagonal - type ZnO structure with reference (66 - 3411 > JCPDS file) are observed. Further, all sharp diffraction peaks are found in all spectra. It is due to good crystallinity of prepared samples. From the x - rays diffraction spectra, lattice constants of the prepared samples are evaluated by using the following equation (1):

$$\frac{1}{d^2} = \frac{4}{3}\left(\frac{h^2+hk+k^2}{a^2}\right) + \frac{l^2}{c^2} \quad (1)$$

d = interplanar spacing

h, k, l = miller indices

a, c = lattice parameter

Interplanar spacing'd' values from (100) and (101) planes are substituted in equation (1) and, lattice parameters 'a' and 'c' are estimated. Unit cell volumes of hexagonal ZnO films samples are examined by using the equation (2):

$$V = \frac{\sqrt{3}}{4} a^2 \times 6 \times c \quad (2)$$

V = cell volume

Lattice constants, lattice distortion, and unit cell volume of prepared samples are listed in table (I).

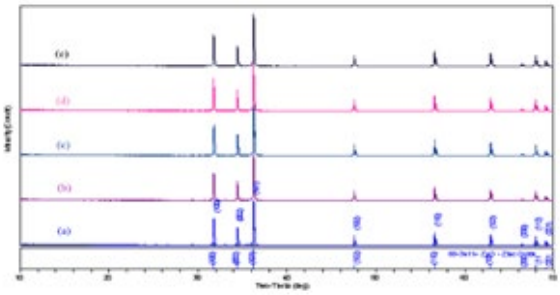

Fig.2 XRD Spectra of ZnO Films at (a) 500oC (b) 550oC (c)600oC (d) 650oC and (e) 700oC

TABLE.I List of lattice constants, lattice distortion and unit cell volume of prepared samples.

Temperature (°C)	'a(Å)'	'c(Å)'	Lattice distortion	Cell volume ($\times 10^{-30} m^3$)
500	3.241	5.289	1.632	143.890
550	3.243	5.279	1.628	143.796
600	3.247	5.258	1.619	143.665
650	3.249	5.225	1.608	142.852
700	3.251	5.172	1.591	141.577

Crystalline size and lattice micro strain of the prepared samples are estimated by using the following Debye - Scherrer equations (3) and (4), and listed in table (II).

$$D = \frac{0.9\lambda}{\beta \cos\theta} \quad (3)$$

$$\varepsilon = \frac{\beta}{4\tan\theta} \quad (4)$$

In these equations, β is full width at half of the peak maximum (FWHM), (101) plane and λ is the wavelength

of the using x-rays and θ is the peak position which is known as Bragg's angle.

Fig. 3 shows the variation of process temperature with lattice constants of prepared samples. It is obvious that, lattice constant " a " increases as process temperature increases, on the other hand, lattice constant " c " is lowered.

TABLE II. LIST OF CRYSTALLITE SIZE AND LATTICE MICRO STRAINOF PREPARED SAMPLES.

Temperature (ºC)	Crystallize size (nm)	Micro Strain ($\times 10^{-3}$)	FWHM of (101) plane (Rad) ($\times 10^{-3}$)
500	29.73	3.774	4.905
550	29.48	3.806	4.946
600	29.16	3.848	5.001
650	28.85	3.889	5.054
700	28.53	3.933	5.111

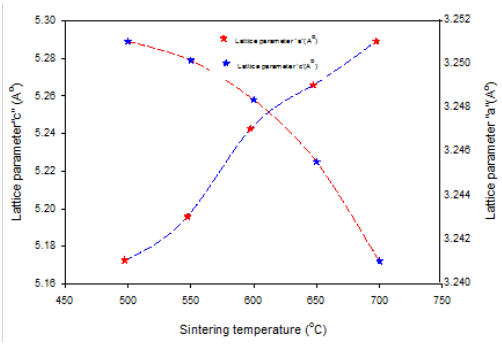

Fig. 3 The Variation of Process Temperature with Lattice Constants of Prepared Samples.

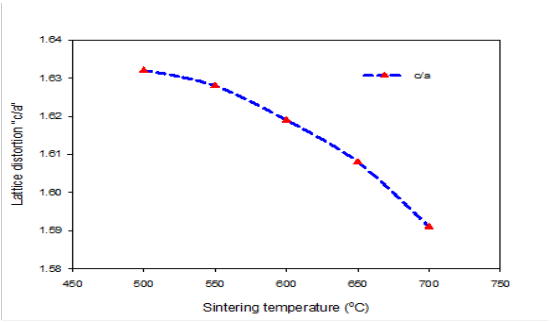

Fig.4 Influence of Process Temperature on Lattice Distortion of Prepared Samples.

Fig.4 illustrates the influence of process temperature with lattice distortion of prepared samples. It is found that, lattice distortion decreases when the process temperature is raised.

It is obtained that, unit cell volume decreases as the process temperature increases. In hexagonal wurtzite ZnO structure, lattice distortion c/a ~ 1.6. During the sintering process, that causes the appearance of micro strain in prepared samples. In addition, Si substrates induce micro strain in ZnO films, during the deposition and sintering processes. These facts indicate that, there are effect of process temperature on structural feature of prepared samples.

SEM images of the prepared samples at various process temperatures are depicted in Fig. 6.

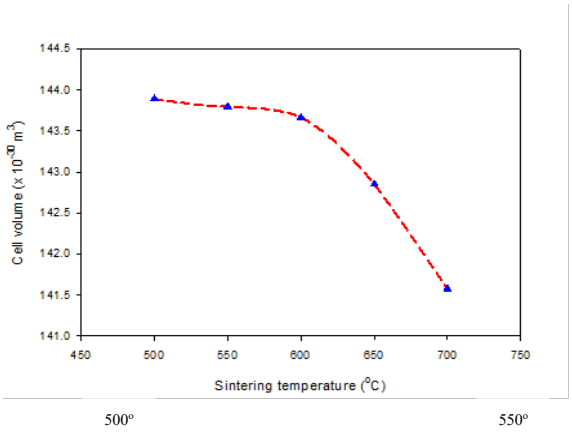

Fig.5 Effect of Process Temperature on Unit Cell Volume of Prepared Samples.

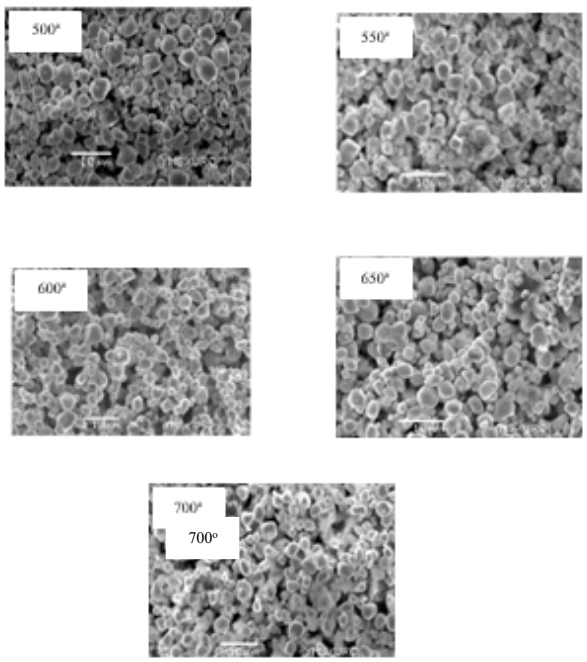

Fig 6. The SEM Images of ZnO: Si on p-Si at Various Temperatures.

Irregular micro grains are uniformly distributed in all images. Further, there are no micro cracks and no pin - hole arrangements in all images. Porosities are also found in all images. Average grain sizes of the prepared samples are estimated to be 4.6 µm, 5.2 µm, 4.16 µm, 3.32 µm and 2.8 µm at corresponding process temperatures 500oC, 550oC, 600oC, 650oC and 700oC respectively. There are small variation of average grain size with process temperature, as shown in Fig. 6.

Silver pastes are coated on both surfaces of ZnO films and Si substrates with area equals to 7.06 mm2. Current vs. voltage characteristics of prepared samples under

illumination (3k lux) at various process temperatures is shown in Fig. 7.

It is obvious that, negative current is formed at positive voltage in fourth quadrant of I - V circle, known as optoelectronic behavior. Open circuit voltage (Voc), known as the maximum voltage available from the solar cell and it occurs at zero current and short circuit current (Isc), which is known as the current through the solar cell when the voltage across the solar cell is zero, can be obtained by rotating the current axis with 180°. Isc vs. Voc plots are depicted in Fig. 8.

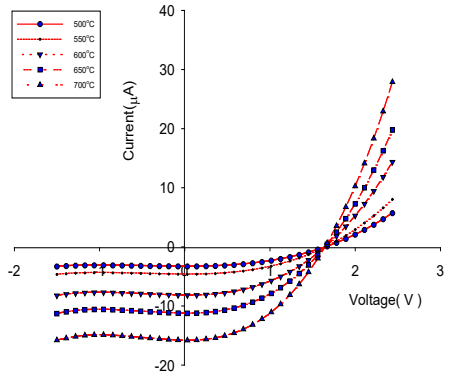

Fig. 7. Current vs. Voltage Characteristics of Prepared Samples under Illumination (3 k lux) at Various Process Temperatures.

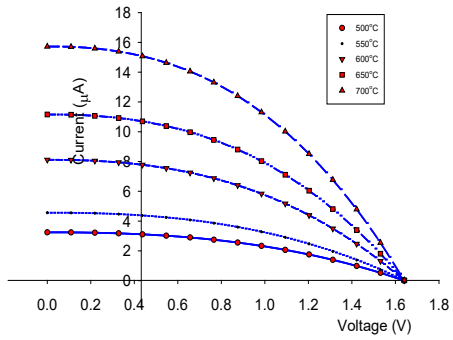

Fig.8. Isc vs. Voc plots of ZnO: Si Heterostructure at Various Process Temperatures.

From the Isc vs. Voc plots, important parameter of solar cell, such as efficiency (η) which converts the incident solar radiation into electricity and fill factor (Ff), which measures the quality of solar cell are estimated by using the following equations (5) and (6).

Efficiency is

$$\eta_{con} = \frac{P_{out}}{P_{in}} x100\% = \frac{I_m V_m}{P_{in}} x100\% \qquad (5)$$

The fill factor Ff can be obtained by the expression

$$F_f = \frac{I_m V_m}{I_{sc} V_{oc}} \qquad (6)$$

Photovoltaic parameters, such as open – circuit (Voc), short - circuit current (Isc), maximum voltage (Vm), maximum current (Im), voltage conversion efficiency (η) and fill factor (Ff) are evaluated and listed in tables (III) and (IV).

It is studied that, conversion efficiency decreases with increasing process temperature and fill factor varies with process temperature, as listed in table (IV).

TABLE III. LIST OF PHOTOVOLTAIC PARAMETERS, VOC , ISC, IM AND VM OF ZNO: SI.

Temperature (°C)	V_m(V)	I_m (μA)	V_{oc}(V)	I_{sc}(μA)
500	0.88	11.55	1.60	15.75
550	0.96	9.00	1.60	12.00
600	1.00	7.70	1.60	11.20
650	1.00	5.51	1.60	8.20
700	0.96	2.40	1.60	3.36

TABLE IV. LIST OF PHOTOVOLTAIC PARAMETERS, CONVERSION EFFICIENCY (η) AND FILL FACTOR (F_f).

Temperature (°C)	Conversion Efficiency (η)	Fill factor (F_f)
500	4.63	0.40
550	3.96	0.45
600	3.53	0.43
650	2.52	0.42
700	1.59	0.43

IV. CONCLUSION

ZnO films deposited on Si substrates via colloidal precursor solution route is studied in this research. Structural, microstructural and photovoltaic properties of ZnO: Si heterojunction devices are also examined. XRD results indicate that, there are polycrystalline, wurtzite, hexagonal - type ZnO structure. SEM images can be interpreted that, irregular micro grains are uniformly distributed. Further, there are neither micro cracks nor no pin - hole arrangements. Photovoltaic properties of prepared samples are acceptable and suitable for solar cell application.

ACKNOWLEDGEMENT

The authors would like to acknowledge the Universities Research Centre (URC), University of Yangon, for XRD examinations and SEM investigations. Thanks are also due to Dept. of Physics, Nationalities Youth Resource Development Degree College, Yangon, for photovoltaic characterizations. The authors also wish to express their sincere thanks to Rector, Technological University (Magway), for her encouragement and continuous interesting.

REFERENCES

[1] U. Ozgur et al., "A comprehensive review of ZnO materials and devices", J. of Appl. Phys., Vol 98, 041301, 2005.
[2] X. Lou, "Development of ZnO series ceramics semiconductor gas sensor", J. of Sens. and Trans. Tech., Vol 3, pp 1 – 5,1991.
[3] K. R. Agneszka and T. Jesionowski, "Zinc oxide - from synthesis to applications", Materials, Vol 7, pp 2833 – 2881, 2014.
[4] H Morkoc. and U Ozgur, " Zinc oxide:fundamentals, materials and device technology ", Wiley - VCH, Weinhein, Germany,2009,pp. 2-3, 2009.
[5] D. Tahir and K. H. Jae, "Effect of growth temperature on structural and electronic properties of ZnO thin film", Am. Inst. of Phys. Conf. Proc., Vol 1801, 020007, 2017.
[6] Mursai et al.,"Structural and optical properties of ZnO based films deposited by sol - gel coating method", J. of Phys. Conf. Ser., Vol 1116, 032020, 2018.
[7] W. Gao and Z. Li,"ZnO films produced by magnetron sputtering", Cera. Inter., Vol 30, issue 7, pp 1155 – 1159, 2004.

Article ID – JRA6009420

Study on Metal Ferroelectric Semiconductor Field Effect Transistor with Pb (Al,Ti)O_3 Gated Layer

Moe Min Min Aye
Department of Physics
University of Computer Studies
Loikaw, Myanmar
dr.moeminminaye2014@gmail.com

Thin Thin Kyu
Department of Physics
University of Yangon
Yangon, Myanmar
drthinthinkyu25@gmail.com

Saw Shine Ko
Department of Physics
Pathein University
Pathein, Myanmar
drsawshineko@gmail.com

***Abstract*—A study has been made on the behavior of Pb(Al, Ti)O_3, PAT gate material thin film grown by spin coating method. Reverse C-V characteristics exhibited a linear 1/C^2 versus V plot, from which a built-in voltage was about 0.8V. Drain characteristics of PAT FeFET were obtained at various annealing temperature with gate material. From the drain characteristic curves, the saturation voltage was found to range between 6.1–6.5V. The threshold voltage has been estimated by transfer characteristics with annealing temperature. The results show a potential application of Pb (Al, Ti)O_3 ferroelectric materials for oxide electronics.**

Keywords*— *Pb(Al, Ti)O_3, Drain characteristics, transfer characteristics, threshold voltage

I. INTRODUCTION

The ferroelectric field effect transistor is a type of transistor that depends on an applied electric field to guide the form and hence the electrical conductivity of a mode in a semiconductor material device [1]. A thin film transistor (TFT) is a special kind of field effect transistor made by depositing thin films for the metallic contacts, semiconductor active layer, and dielectric layer. The channel region of a TFT is a thin film that is deposited onto a substrate [2]. Lead titrate $PbTiO_3$ type ferroelectric thin films have also been required for application to many kinds of electric tools such as sensors, capacitors and microactuators [3]. Electronic device industries have recently been looking, to FeRAM (Ferroelectric Random Access Memory) as a talented non-volatile memory with superb high-throughput and energy-efficient quality. FeRAM operates on the principle that ferroelectric material, otherwise known as ferroelectrics, makes hysteresis in electric fields instead of polarization characteristics [4].

There has been an increased interest in ferroelectric field effect transistors FFET for memory cell applications lately because of their potential advantages over conventional FETs such as nonvolatile memory functionality, even after a power failure, and nondestructive readout properties The general idea of FFET transistors in which ferroelectric material is used as a gate insulator is not a new one as such a transistor was proposed [5]. On the other hand, in the metal ferroelectric semiconductor field effect transistor MFSFET-type cells, the ferroelectric capacitor is replaced by the gate ferroelectric capacitor of the FFET device. $PbTiO_3$ has been one of the extremely considered materials due to its individual combination of optical, electrical, and ferroelectric properties reported on research work on it. In this work Pb(Al, Ti)O_3, films were made with careful control of the annealing temperature[6]. In the present study, the reverse C-V characteristics drain, and transfer measurements have been used to characterize the film.

II. EXPERIMENTAL

To get the precursor solution, the raw materials of PbO, TiO2, and Al2O3 were chosen as starting materials. Firstly, these powder materials were weighed and mixed to get the chemical formula PbAlxTi1-xO3 (x = 5 mol %). Then, a few amount of acetone was added into the mixture and stirred with glass stirrer to be homogeneous. Primary ball-milling was carried out for 30 minutes. The homogeneous powder was sintered at 700ºC for 1hr in O2 atmosphere. The secondary ball-milling was performed to get crystalline powder. It was mixed with 2-methoxyethanol solvent to change into liquid phase and refluxed up to 100ºC for 30 min. After drying, it became precursor solution and ready to deposit onto desired substrate.

The p-type Si (100) orientations were chosen as starting substrates to get n-channel TFTs. They were cleaned with a dilute solution of HF: DIW (1:5), acetone and methyl alcohol to remove native contamination and dried at room temperature. SiO2's were thermally deposited on all p-Si (100) wafers. The middle zones of the insulating layers grown on Si wafers were covered with apiezon wax and their ends were etched with HF: DIW (1:3) to remove SiO2 layers totally. To fabricate source (S) and drain (D) regions, n-type phosphorus was deposited on these layers, annealed at 550ºC for 3hr. Thus phosphorus was allowed to enter Si by diffusion

mechanism. To form the gate (G) region, the precursor solutions were spin-coated onto middle zones of the substrates while S and D regions were masked with apiezon wax. To define the thin layers, cells were calcined at 500ºC, 550ºC, 600ºC, 650ºC, and 700ºC for 1hr. Cu electrodes were attached with S, G and D regions and back-side of the Si-wafer. In this paper was involved with the transfer characteristics of FeFET with PAT gate material. The schematic representation of preparation for PATFeFET was shown in Fig. 1. The research measurements were done at the Materials Science Lab, Department of Physics in University of Yangon.

III. Result and Discussion

1/C2-V characteristics of thin film transistor (TFT) short-channel cell were observed at applied frequency of 100kHz under biased voltage range from -4V to +5V by Digital Impedance analyzer (Quad Tech. 1730). To examine the TFT cell quality, 1/C2-V variation was essentially investigated and described at Fig. 2 (a-e). All measurements were performed at room temperature. From the 1/C2-V variation, it was amazed that 1/C2-V graph showed the linear relationship and therefore it was followed the standard Schottky relationship. The plot of 1/C2 as a function of V is a straight line whose intercept on the voltage axis gives Vbi and the slope can be used to determine the effective dopant concentration Ni. The slope of linear graph was enhanced with an increase in increasing ambient temperature. The electric field and potential distributions in the space- charge region of a Schottky barrier are obtained from the solution of a one dimensional Poission equation. The built-in-voltage of PAT gate layer at various annealing temperature was estimated from Fig. 2, such as 0.87V, 0.83V, 0.88V, 0.89V and 0.90V respectively.

When the substrate is grounded and a positive potential is applied at the PAT gate region, the positive charge on gate region induces and equal negative charge on the substrate part between the source and drain region. Thus, an electric filed is produced between the n+ regions. The direction of electric field is perpendicular to the plate of the diode. The negative charge in the p-Si (100) is arranged an inversion layer due to the electron of minority carrier. As the electric characteristic IDS-VDS variation are essentially measured at different gate to source voltages. Fig. 3 (a-e) indicated the electric characteristic of PAT FeFET at different ambient temperatures. As the positive voltage on the PAT gate electrode increases, the induce negative charge in the p-Si (100) substrate increases. Hence, the conductivity increases and current flow from source to drain through the induce channel. Thus, the drain to source current is enhanced at each gate to source voltage by increasing drain to source potential. It was obvious that the drain to source current is also enhance with an increase in gate to source potential. This fact implied that the fabricated FeFET with PAT gate material is said to be operated in E-Mode.

As the detail analysis of IDS-VDS characteristic, it is seemed that the drain to source current is not allowed to flow when the zero drain to source potential is applied at any gate voltage. These fact revealed that the normally-off nature of fabricated FeFET with PAT gate material.

From the drain characteristic, it is clear that to different states are produced. The drain current is linearly increased at low gate voltage until the saturated voltage. The saturated voltage of all transistors will found to be 6.5V, 6.4V, 6.3V, 6.2V and 6.1V for respective films.

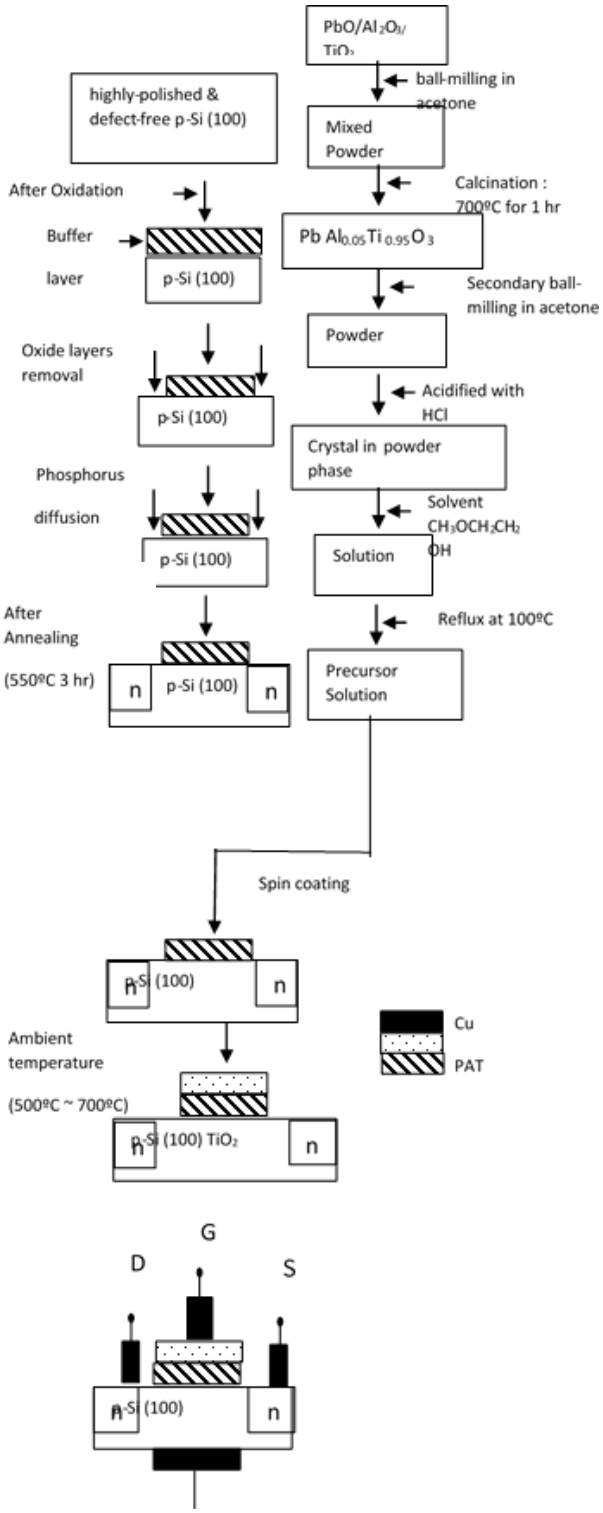

Fig. 1. Block diagram of FeFET with PATgate material

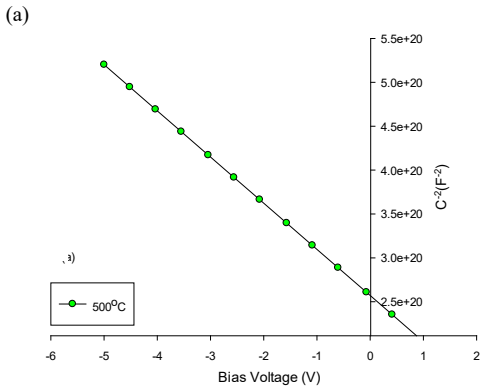

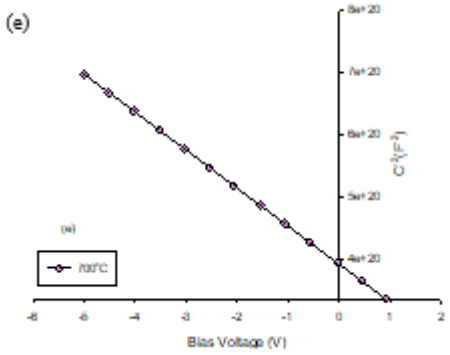

Fig. 2. $1/C^2$-V characteristics of PAT thin films at (a) 500°C (b) 550°C (c) 600°C (d) 650°C (e) 700°C

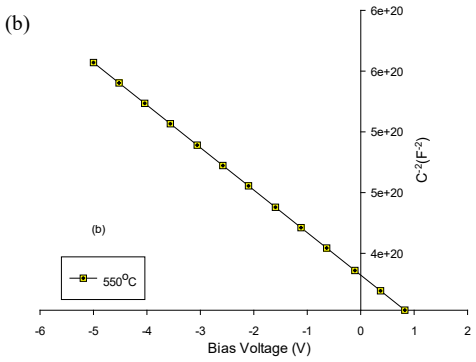

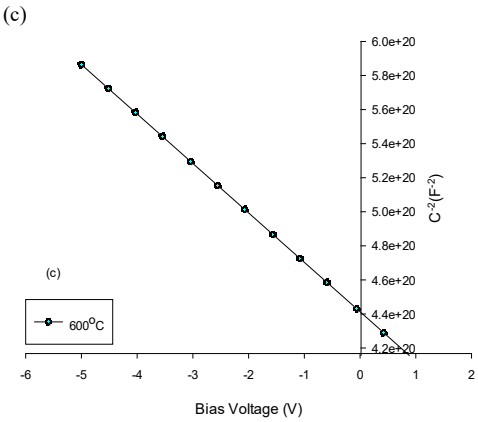

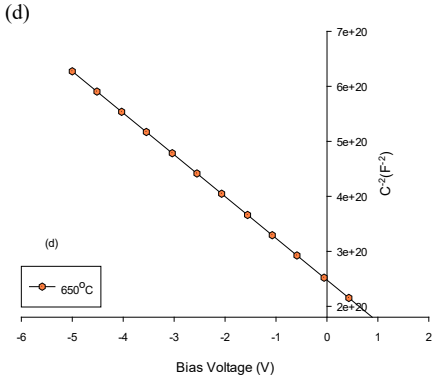

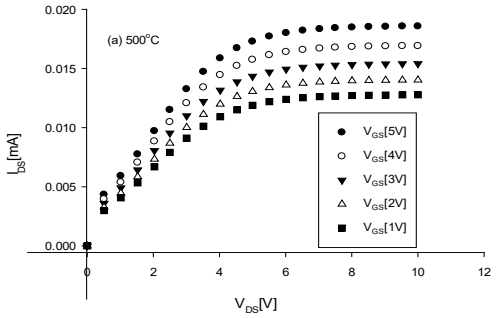

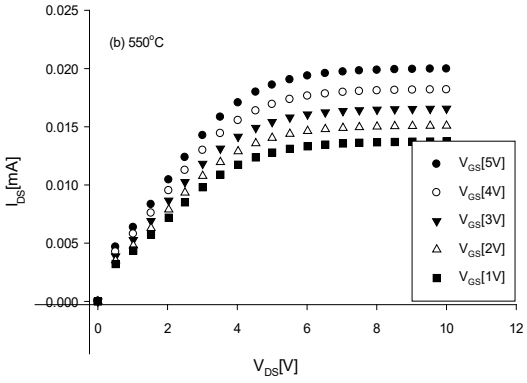

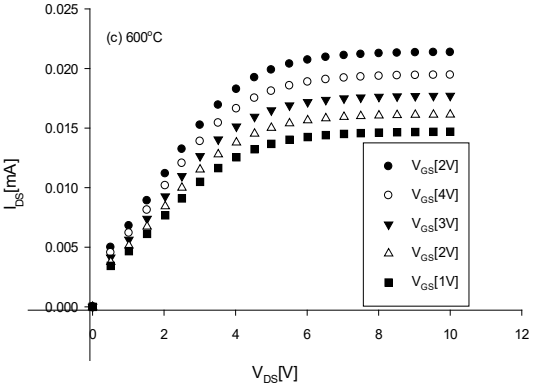

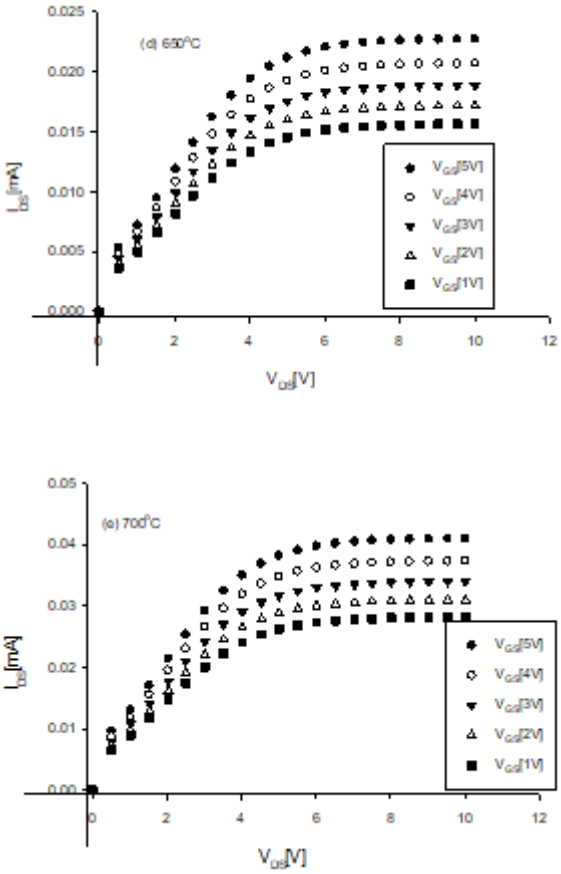

Fig. 3. Drain characteristic of PAT Short- Channel transistor at (a) 500°C (b) 550°C (c) 600°C (d) 650°C (e) 700°C

As the transfer characteristics, the drain to source current flow and gate to source voltage variation were measured at the saturation mode and shown in Fig. 4 (a-e). The drain current was exponentially enhanced with increasing gate to source voltage at the fixed drain voltage. At the low gate voltage region, I-V variation was formed and I-V2 variation was caused at high gate voltage region. Threshold voltages were estimated 4.22V, 4.33V, 4.11V, 3.7V and 3.6 V for respective cells.

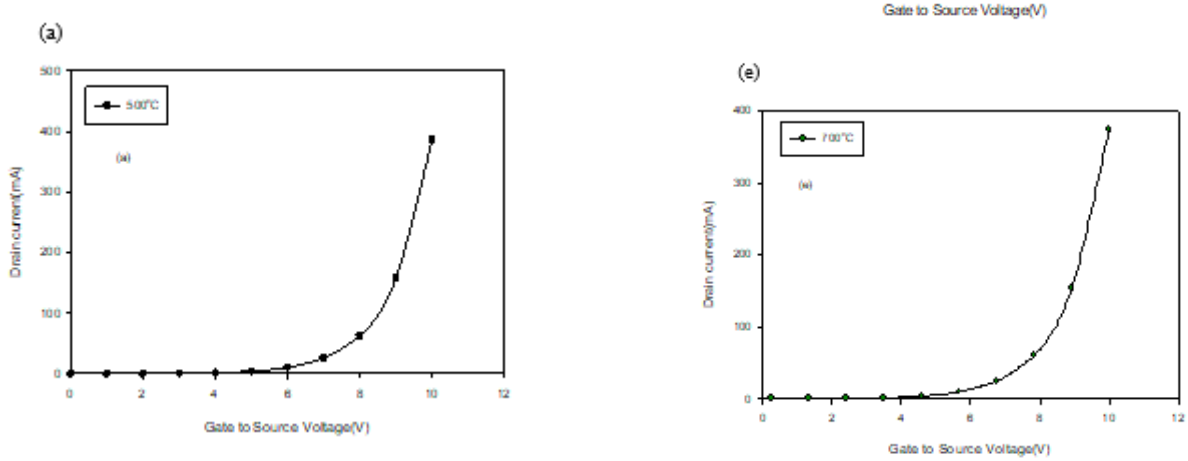

Fig. 4. Transfer characteristic of PAT FeFET at (a) 500°C (b) 550°C (c) 600°C (d) 650°C (e) 700°C

IV. CONCLUSION

PAT based ferroelectric gate material has been successfully fabricated on p-Si by spin coating. The reverse capacitance was measured based on voltage and the built-in voltage was estimated. FeFET is measured at various gate-to-source voltages. The saturation region of the PAT FeFET transistor is the filtered current ID. The drain current from the drain is the highest for the gate-source voltage VGS sent to the source of the FET transistor, so the saturation current flow maximizes the voltage. Saturation point is the active region of the ferroelectric FET. The saturation voltage of FeFET containing the PAT based ferroelectric gate material is around 6V. In this case, the transistor is in the ON state. The threshold voltage changes were studied by transfer characteristics. Studies have shown that it can be used as a single transistor (1T) of FeRAM (1T1C) structure.

ACKNOWLEDGMENT

I would like to give special thanks to Dr. Aung Myint Aye, Pro-Rector, University of Computer Studies (Loikaw), for his kind permission.

REFERENCES

[1] M. S. Tyagi, , "Introduction to Semiconductor Materials and Devices", John Wiley & Sons, new York, 2000.

[2] C. A. Vijendra and B. K. Govind, "Sol–gel Synthesis and Characterization of Lead Titanate Films", Cogent Chemistry, 2015.

[3] J. Zhai, X. Yao, M. Wu and L. Zhang, "Preparation and Microwave Characterization of $PbTiO_3$ Ceramic and Powder", Journal of Physics D Applied Physics, 2001.

[4] W. Jun, P. Xinchang, A. Mufit and L. Zhiqun, "Synthesis and Characterization of Perovskite $PbTiO_3$ Nanoparticles with Solution Processability", Journal of Materials Chemistry, 2010.

[5] A. Masanori, N. Kuniharu, I. Takashi, "Preparation of Al-doped $PbTiO_3$ Thin Films by Metalorganic Chemical Vapor Deposition and their Characterization", Japan Society of Applied Physics, 2000.

[6] Setter N. et al., "Ferroelectric Thin Films: Review of Mateials Properties and Aapplications", J. Appl. Phys., 2006.

Article ID – JRA6000520

Investigation of Some Heavy Metals in Soil Samples at Heinda Mining Area in Dawei Township, Tanintharyi Region, Myanmar

Kyi Phyu Lwin
Deptment of Engineering Chemistry
Technological University (Dawei)
Dawei, Myanmar
kyiphyulwin2@gmail.com

Thaw Dar San
Deptment of Engineering Chemistry
Technological University (Myeik)
Myeik, Myanmar
thawdarsan2020@gmail.com

Khin May Tint
Deptment of Chemistry
Pakokku University
Magway, Myanmar
khinmaytint36@gmail.com

***Abstract*— In this research, the contaminated soil samples (S_1, S_2, S_3, and S_4) were collected from four different localities: 150 m (site 1), 300 m (site 2), 450 m (site 3) and 600 m (site 4) distance far away from industrial Heinda mining areas in Dawei Township, Tanintharyi Region in February, 2020. Some physicochemical properties such as pH, moisture, texture, organic matter and humus of the collected soil samples were determined. The relative abundance of some elements present in soil samples were determined by EDXRF method. In addition, the concentrations of some heavy metals (Mn, Fe, Zn, Pb) contents in soil samples were analyzed by Atomic Absorption Spectrophotometer method. According to AAS method, 0.398 ppm, 0.393 ppm, 0.473 ppm and 0.886 ppm of Pb, 12.57ppm 13.85 ppm, 12.24 ppm and 13.64 ppm of Fe, 2.887 ppm, 3.392 ppm, 2.711 ppm and 4.009 ppm of Mn, and 2.403 ppm,2.565 ppm, 2.56 ppm, and 0.447 ppm of Zn were respectively found in the four soil samples: S_1, S_2, S_3, and S_4. pH of four soil samples were 5.14. 5.30, 5.35 and 5.46 respectively. Moisture contents of four soil samples were 7.73 %, 1.83 %, 0.93 % and 0.75 % respectively. Generally, it was found that pH of four soil samples were no significance difference. Sampling site 1 has highest moisture content because that site locates behind the stream. Soil types (texture) of four sampling soils were found to be silt loam for soil of site 1(S_1) and site 2(S_2) and sandy loam for soil of site 3 (S_3) and site 4 (S_4). The level of organic matter in soil samples were measured by rapid titration method of Walkley and Black. The contents of organic matter in soil samples were found to be 2.04 %, 1,28 %, 1.22 % and 0.87% respectively. Organic matter showed the highest levels at 150 m (site 1) distance from the industrial site of the Heinda mine, then overall a decreasing trend with increasing distances from the mining area. Organic matter is one of the main products of vehicular emission released to the atmosphere from both diesel and petrol operated vehicles. Elemental compositions in these soils were determined by EDXRF and heavy metals (Mn, Fe, Zn, Pb) were determined by AAS methods. Higher concentrations of heavy metals (Mn and Pb) in soil samples (S_4) were observed in sampling site 4 of Heinda mine area than that from other sampling sites. In addition, higher heavy metals concentration (Fe and Zn) in soil sample (S_2) were observed from sampling site 2 of that mine area. However, these values were found to be lower of WHO guideline value.**

***Keywords*—soil samples, Heinda mine area, Heavy metals, EDXRF, AAS, WHO**

I. INTRODUCTION

In this research paper, the rapid development of industry, the production and emission of the heavy metals have increased industrial wastes, toxic chemicals and heavy metals from the Smelters present environmental problems. Soil adjacent to the industrial area contains the highest concentration of the heavy metals. Thus, the purpose of this research is to study the distribution of heavy metals in soil of the Heinda mining area from Dawei Township, Tanintharyi Region. Thus, this research focused to investigate the content of heavy metals in soil. There are four sampling sites; site (1, 2, 3 and 4) for (150 m, 300 m, 450 m and 600 m) distance from the industrial sites of Heinda mine were investigated respectively. The physicochemical parameters in baized soil samples of Heinda mine were determined. Some heavy metals (Mn, Fe, Zn and Pb) from four sampling sites of Heinda mine were analyzed by AAS and EDXRF techniques.

Soil is defined as the upper layer of the earth or the loose surface materials of the earth in which plants prow. Soil is a natural body consisting of layer (soil horizons of mineral constitute of variable thicknesses. Soils are complex mixtures of minerals, water, air, organic matter, and countless organisms that are four major components of the soil. It forms at the surface of land - is the “skin of the earth”. Soil is capable of supporting plant life and is vital to lie on earth. The soil composition is shown in figure 1[1].

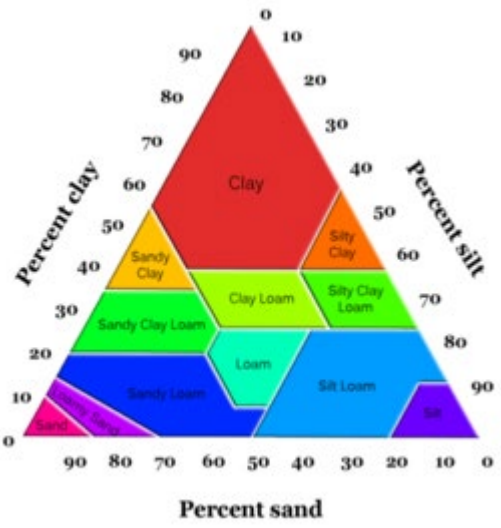

Fig. 1. Soil texture triangles

Aim

The main aim of the research work is to study some heavy metals (Mn. Fe, Zn, Pb) contamination and their physicochemical properties in soil samples collected from the Heinda mining area in Dawei Township, Tanintharyi Region.

Objectives

- To fulfill the aim of the research work, the following steps were carried outline this research work.
- To collect and prepare the selected soil samples from the Heinda mining area
- To assay some physicochemical properties such as (pH, Moisture, Texture)
- To identify and classify the nature of soil and elemental distribution of the contaminated soil
- To determine relative abundance of the element in soil samples by EDXRF method
- To investigate the concentration of heavy metals in soil samples by using Atomic Absorption Spectrophotometer (AAS)
- To assess the risk for human and livestock due to the heavy metal pollution

II. Materials and M ethods

Some of the instruments used in the experimental work.

- pH meter (INDEX (Model No.5), digital portable)
- balance (Mettles XT 220A) (Precise, Switzerland)
- Oven (Ambient 250 £20, Galen Kamp, England)
- AAS (Perkin Elmer Analyst 800) (Win Lab 32 software, Germany)
- EDXRF Energy Dispersive X-ray Florescence Spectrometer (Hindu EDX-700): Japan

A. Samples Collection

Soil samples were collected from four sampling sites of Heinda mining areas near Heinda village, in the month of February, 2020.The photomap and location sites are shown in Figures 2 and 3 and Table 1 respectively. Soil samples were taken about 20 cm depth from the surface of soil. The representative samples were taken systematically from 150 m 300 m, 450 m and 600 m distance of industrial Heinda mine in Dawei Township, Tanintharyi Region. The soil samples were dried in the shade before sieving Afterwards, gravel, roots, etc., were discarded. Then the collected soil samples were ground into fine powder and passed through a 0.2 mm sieve. The soil samples were stored in polyethylene bags and clearly labeled before measurements [2].

TABLE I. LOCATION OF FOUR SAMPLING SITES IN HEINDA MINING AREA OF DAWEI

Sampling Sites	Geolocations	
	Latitude	Longitude
Site-1	14^0 5′ 51.1″N	98^0 19′ 12.1″E
Site-2	14^0 5′ 52.1″N	98^0 19′ 07.1″E
Site-3	14^0 5′ 58.8″N	98^0 19′ 03.1″E
Site-4	14^0 5′ 57.2″N	98^0 19′ 58.1″E

Site 1- 150 m distance from the mining industrial site
Site 2- 300 m distance from the mining industrial site
She 3- 450 m distance from the mining industrial site
Site 4- 600 m distance from the mining industrial site

Fig.2 Maping of four sampling sites in Heinda mine area

(a)

(b)

(c)

(d)

Fig. 3. Location of four sampling sites in Heinda mine

B. Determination of Moisture Contents

The moisture contents of the mine soil samples were determined by oven- dried method.

Apparatus:An electric oven (Galen Kamp Co. England), porcelain crucibles, analytical balance and desiccators were used.

Procedure:An appropriate clan porcelain crucible was dried and then weighed. A 5.00 g of accurately weighed air-dried sampling soil was placed in the crucible. The crucible and contents were weighed. Then, it was heated in the oven at 105-110°C for 3 hours. Just after removal from the oven, it was allow cooling in a desiccator. The crucible and dried sample were weighed again. The process of heating, cooling and weighing were repeated until a constant weigh was obtained.

C. Determination of pH

pH of soil samples was determined by using pH meter

Apparatus: 100 mL beaker, 100 ml measuring cylinder, Metter balance XT 200A, pH meter (Index Model No5), conical flask.

Procedure: A 5.00 g of soil samples was placed in a 50 mL beaker and then, 50 ml of deionized water was added. The moisture was stirred vigorously for 5 minutes and let stand for 10 minutes. Before measuring the pH meter was calibrated to pH 4 and 7 using 0.1M HCl Then, the electrode of pH was placed in the slurry, swirl carefully and read the pH was measured with pH meter [4].

D. Determination of texture of collected soil samples

The texture of the soil samples were determined by pipette method.

Chemical: 10% of sodium pyrophosphate solution was used.

*Apparatus:*500 mL conical flask, 10 ml measuring cylinder, 1 L graduated cylinder, 25 mL Pipette, and porcelain basin were used.

Preparation of solutions: Sodium pyrophosphate solution (10%)

Procedure: A 50 g of soil sample was weighed and placed in a 500 mL conical flask. Then 125 ml of distilled water and 50 ml of 10% sodium pyrophosphate solution was added to disperse the soil colloids and healed for fifteen minutes and cooked down. After cooling the contents were transferred to a 1L graduated cylinder and the solution was make to the mark with distilled water and then keep overnight to allow the soil colloids to settle. Then, the contents were stirred for about four minutes. The solution from 9 cm depth was pipetted with 25 ml pipette and transferred to porcelain basin and then evaporated on a water bath. From the residue, the percentage of clay and sit were calculated [5].

E. Determination of organic carbon and humus in soil samples

Organic carbon and humus in soil samples were determined by Walker- Black method.

*Chemicals:*Phosphoric acid (85%), concentrated sulphuric acid (98% w/v Sp.gr- .84), sodium fluoride solid, standard potassium dichromate, ferrous ammonium sulphate and ferroin indicators, distilled water were used.

*Apparatus:*10 ml pipette, 50 ml burette, 500 ml conical flask, 100 ml volumetric flask, 100 ml measuring cylinder, analytical balance, magnetic stirrer were used.

*Preparation of solutions:*Ferrous ammonium sulphate was dissolved in 80 mL distilled water, added 2 mL of concentrated suphuric acid, cooked and dilated to 100 mL in a volumetric flask. A 4.9 g of potassium dichromate (dried at 105°C for 2 hours) was dissolved n distilled water and diluted to 100 mL in a volumetric flask. A 85 mL of

phosphoric acid was added with distilled water to a volume of 100 ml in a volumetric flask. A 0.15 g of o-phenanthrol line was dissolved in 10 mL of distilled water.

*Procedure:*A 0.5 g of air dried soil samples was weighed and paced in a 500 mL conical flask, 5 mL of 0.167 M potassium dichromate solution was added into the flask by means of a pipette and 10 mL of concentrated sulphuric acid was also added and swirl gently to mix. The mixture was kept for 30 minutes at room temperature and then it was diluted with 100 mL of distilled water. A 5 ml of 85% phosphoric acid and 0.2 g of sodium fluoride were added to the mixture and 5 drops of ferroin indicator was also added. The mixture was titrated with 0.5 M ferrous ammonium sulphate solution. The color of the solution at the beginning is yellow - orange to dark- green and then changes sharply to a wine red at the end point. The percentage of organic carbon and humus was calculated [6].

F. Elemental analysis of soil samples by EDXRF Technique

A sample 10g was weighted and pressed in a hydraulic press without any binder to obtain pellet. The obtain pellet was measured in the EDXRF spectrometer. The samples will send to Universities Research Center (URC), Yangon for element analysis by EDXRF.

G. Determination of Heavy Metal Conte nts (Mn, Fe, Zn, Pb) in Soil Samples by AAS method

Heavy metal contents in soil samples were determined by Atomic Absorption spectrometric (AAS) method.
Procedure: A 1 g of soil sample was accurately weighed and placed in 250 mL beaker and then treated with 10 ml aliquots of high purity concentrated nitric acid. The mixture was heated until dry on a sand bath and then cooked. This procedure was repeated with another 10 mL concentrated hydrochloric acid [7]. The digested soil samples were then warmed in 20 mL of 2 M hydrochloric acid to dissolve the metal salts. Extracts were filtered through what man No.40 filter paper and the volume were then adjusted to 40 ml with deionized water. The heavy metal concentrations in the above solutions were determined by Atomic Absorption Spectrophotometer [8].

III. Results and Discussions

A. Moisture Contents and pH values of Soil Samples

Moisture is usually determined by the drying to constant weight with the has in weight being considered as water. The moisture percent of four soil samples for 20 cm depth of 150 m, 300 m, 450 m and 600 m distance from the industrial sites of Heinda mine were determined respectively. Table 2 show the moisture contents of four soil samples from four mining sites of Heinda mine in Dawei Township. The moisture percent of four soil samples (S_1, S_2, S_3 and S_4) were found to be (7.73, 1.83, 0.93 and 0.75) % respectively.

In this research, the pH values of the soil samples for 20 cm depth of 150 m, 300 m, 450 m and 600 m distances from the industrial Heinda mining sites were determined respectively. pH values of four soil samples (S_1, S_2, S_3 and S_4.) 5.14, 5.30, 5.35 and 5.46 respectively are shown in Table 2. From the results, pH range falls into 5.1 to 5.5. It shows that all the mine soil samples S_1, S_2, S_3 and S_4 were strongly acid condition. The results of moisture and pH are shown in Figure 4. and Table 2.

B. Texture of Soil Samples

In this research, soil types of the collected soil samples from four sampling sites of the Heinda mine in Dawei Township were determined. The texture of four soil samples from four sampling sites of Heinda mine are shown in Table 3. According to the data, sand contents in soil samples (S_1, S_2, S_3 and S_4) were observed 35.00, 45.00, 79.00 and 63.45 percent respectively. Sit content in soil samples (S_1, S_2, S_3 and S_4.) were found to be the values of (43.00, 47.00, 14.00 and 32.75) percent respectively. Clay contents in four soil samples (S_1, S_2, S_3 and S_4) were abo observed (22.00, 8.00, 7.00 and 2.65) percent respectively. From the resultant data, soil texture of sample S_1 and S_2 are silt loam, soil sample S_3, and S_4 are sandy loam. These results are shown in Figure 5 and Table 3.

TEBLE II. MOISTURE AND PH VALUES OF THE SOIL SAMPLES FROM FOUR SITES OF HEINDA MINE AREA

Sites	Soil Samples	Moisture	pH
1	S_1	7.73	5.14
2	S_2	1.83	5.30
3	S_3	0.93	5.35
4	S_4	0.75	5.46

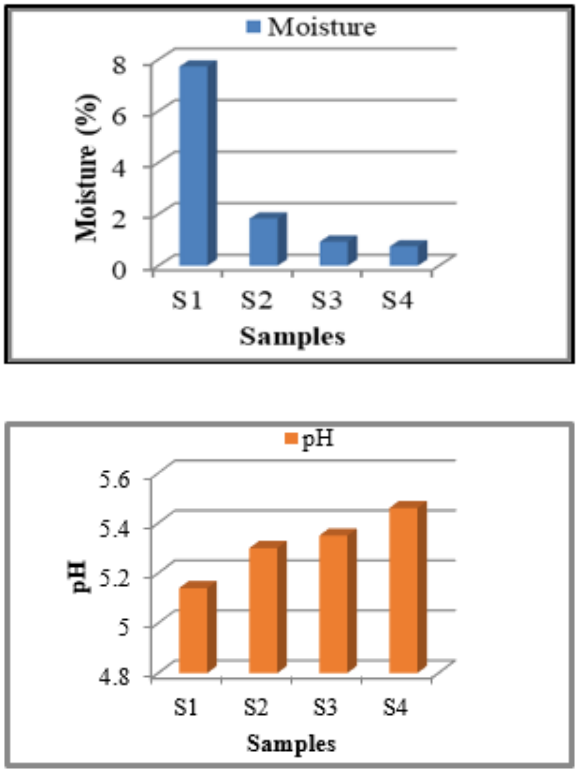

Fig. 4. Moisture and pH values of four soil samples

TABLE III. TEXTURE OF THE SOIL SAMPLES FROM FOUR SAMPLING SITES OF HEINDA MINING AREA

Sites	Sample Locations (Distance from mine)	Soil Samples	Sand (%)	Silt (%)	Clay (%)	Soil Type
1	150m	S_1	35.00	43.00	22.00	Silt loam
2	300m	S_2	45.00	47.00	8.00	Silt loam
3	450m	S_3	79.00	14.00	7.00	Sandy loam
4	600m	S_4	63.45	32.75	2.65	Sandy loam

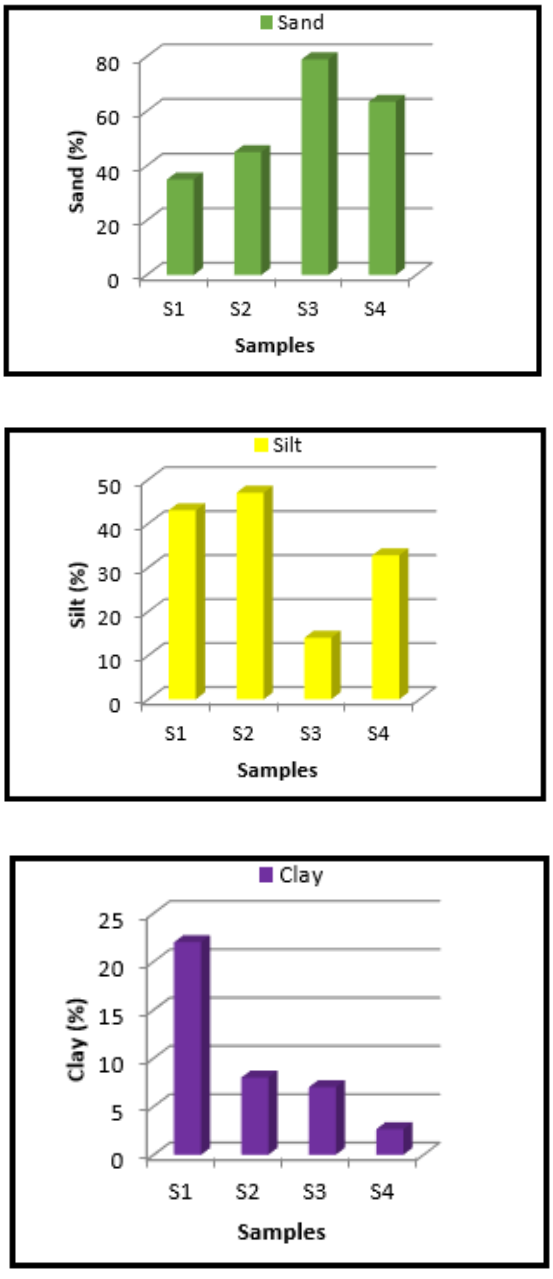

Fig 5. Texture of four soil samples

C. Organic matter and humus in soil samples

The organic matter and human were determined. Organic matter is especially important in providing soil samples. In this research, organic matters of soil samples (S_1, S_2, S_3 and S_4) were found to be the values of (2.04%, 1.28%. 1.22% and 0.87%) percent respectively.

The values of the humus percent were observed that (3.52%%, 2.21%, 2.10% and 1.50%) for four soil samples (S_1, S_2, S_3 and S_4) respectively. The organic matter (2.04%) and humus (3.52%) of sol sample S_1 from sampling site 1 has the highest of the others. The results were shown in Table 4 and Figure 6.

TEBLE IV. ORGANIC MATTER AND HUMUS FROM FOUR SAMPLING SITES OF PAGAYI MINING AREA

Sites	Sample Locations (Distance from Heinda mine)	Soil Samples	Organic matter (%)	Humus (%)
1	150m	S_1	2.04	3.52
2	300m	S_2	1.28	2.21
3	450m	S_3	1.22	2.10
4	600m	S_4	0.87	1.50

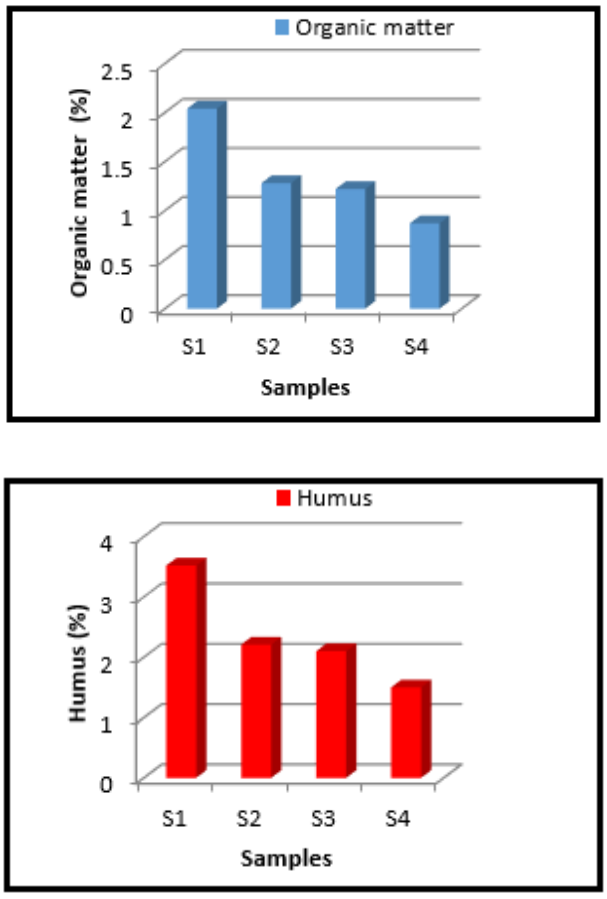

Fig. 6. Organic matter and humus of four soil samples

TABLE V. RELATIVE ABUNDANCE OF SOME HEAVY NETALS FROM FOUR SOIL SAMPLES IN HEINDA MINE AREA

Elements	Results of Relative Abundance (%)			
	S_1	S_2	S_3	S_4
Si	39.564	49.750	49.578	41.206
Fe	42.638	29.757	31.562	37.376
K	11.952	14.625	14.006	15.418
Ti	3.094	2.798	2.376	2.831
Mn	0.725	0.692	0.816	0.687
Sn	-	0.196	-	-
Zr	0.429	0.349	0.283	0.457
Rb	0.765	0.938	0.942	1.248
Pb	-	-	-	-
Zn	0.107	0.117	0.124	0.108
W	0.314	0.255	-	0.362
Cu	0.210	0.142	0.139	0.135
V	0.091	0.112	0.106	0.103
Y	0.077	0.083	0.067	-
As	-	0.084	-	-
Au	0.034	0.084	-	0.038

D. Semi Quantitative Analysis of Soil Samples by EDXRF Technique

In this research, semi quantitative analysis of soil samples was determined by g EDXRF technique. Figure 6 mention the EDXRF spectra of soil samples from four sampling sites of Heinda mine in Dawei Township. Table 5 shows the semi quantitative analysis of soil samples (S_1,S_2, S_3, and S_4) for 20 cm depth of 150m ,300 m, 450 m and 600 m distance far away from the industrial mine respectively. Three soil samples (S_2, S_3, and S_4) have the largest amount of silicon (Si). But sample (S_1) has the largest amount of iron (Fe). Small amount of K, Ti Mn, Zr, Rb, Zn, Cu and V were found in soil samples. Lead (Pb) was not detected in all soil Samples by EDXRF technique. Tungsten (W) and gold (Au) were found only in soil samples $S_1$and S_2 for sampling sites 1 and 2 of Heinda mine area.

E. Heavy Metal Contents of Soil Samples by Atomic Absorption Spectrophotometer

In the present work, atomic absorption spectrophotometer (Perkin-Elmer Analysis 800) was employed for the determination of the heavy metals in the collected soil samples. The soil samples from four sampling sites of industrial Heinda mine, Dawei Township were investigated. The contents of heavy metals (Mn, Fe, Zn, Pb) have been investigated. The results were reported in Table 6 and Figure 8.

From these determinations, the contents of heavy metals in soil sample S_1 were found to be 2.887 ppm of Mn, 12.57 ppm of Fe, 2.403 ppm of Zn and 0.398 ppm of Pb. The contents of heavy metals in soil sample S_2 was found to be the values of 3.392 ppm of Mn 13.85 ppm of Fe, 2.565 ppm of Zn and 0.393 ppm of Pb.

The contents of heavy metals in soil sample S_3 was found to be the values of 2.711 ppm of Mn, 12.24 ppm of Fe, 2.556 ppm of Zn and 0.471 ppm of Pb.

The contents of heavy metal in soil sample S_4 was found to be the vales of 4.009 ppm of Mn, 13.64 ppm of Fe, 0.447 ppm of Zn and 0.886 ppm of Pb.

For this observation, manganese (Mn) content in soil sample S_4 (600 m distance from industrial sites of Heinda mine) was the highest (4.009 ppm). If Mn content of soil is lower than 300ppm.

Iron (Fe) content in soil sample S_2 (300 m distance from industrial sites of Heinda mine) was the highest (13.85 ppm). Maximum allowable limit for iron is 100 ppm for soil. Although soil sample S_2 was the highest content, it does not exceed the maximum allowable limit for soil. Thus, the soil samples from these sampling sites were not said to be contaminated with iron.

Zinc (Zn) content in soil sample S_2 (300 m distance from industrial sites of Heinda mine) was the highest (2.565 ppm). However, zinc contents in soil sample S_2 and S_3 were not significant difference. Maximum allowable limit for zinc is 300 ppm for soil. It does not exceed the limit amount of heavy metal zinc for soil. Thus, the soil samples from these sampling sites were not said to be contaminated with zinc.

Lead (Pb) level content in soil sample S_4 (600 m distance from industrial zone of Heinda mine) was the highest (0.886 ppm). Maximum allowable limit of lead is 300 ppm for soil. In site 4, lead content was not exceeded the maximum allowable limit. Thus, the samples from these sampling sites were not said to be contaminated with lead.

According to results, soil sample S_2 has the highest vales of iron (13.85 ppm) and zinc (2.565 ppm), then soil sample S_4 has the highest values of manganese (4.009 ppm) and lead (0.886 ppm). Heavy metals contents are raised due to the mining industrial activity, metal smelting and accumulation of mining wastes [9]. However, heavy metals contents in all soil samples do not exceed the environment were not disturbed by the industrial works of Heinda mine [10].

TABLE VI. THE RESULTS OF HEAVY METALS CONTENTS FROM FOUR SOIL SAMPLES IN HEINDA MINE AREA

Sites	Soil Samples	Results of Heavy Metal Contents (ppm)			
		Mn	Fe	Zn	Pb
1	S_1	2.887	12.57	2.403	0.398
2	S_2	3.392	13.85	2.565	0.393
3	S_3	2.711	12.24	2.556	0.471
4	S_4	4.009	13.64	0.447	0.886
WHO permissible level (ppm)		300	100	300	300

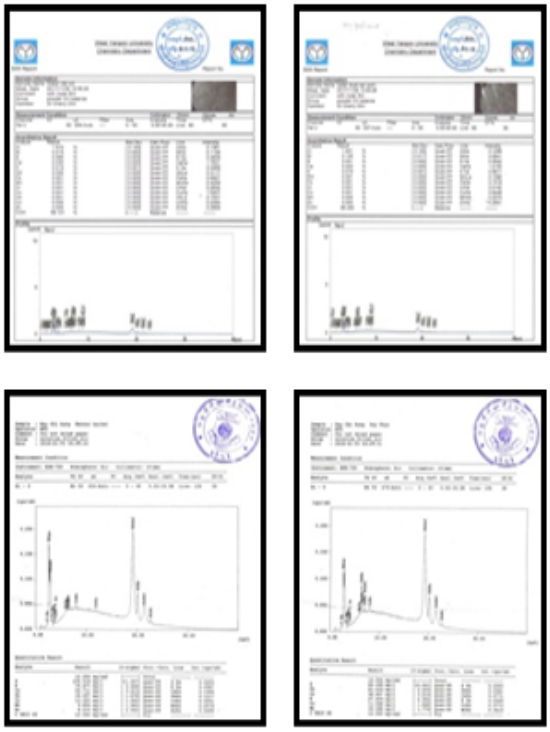

Fig.7. EDXRF spectrum of four soil samples from Heinda mine area

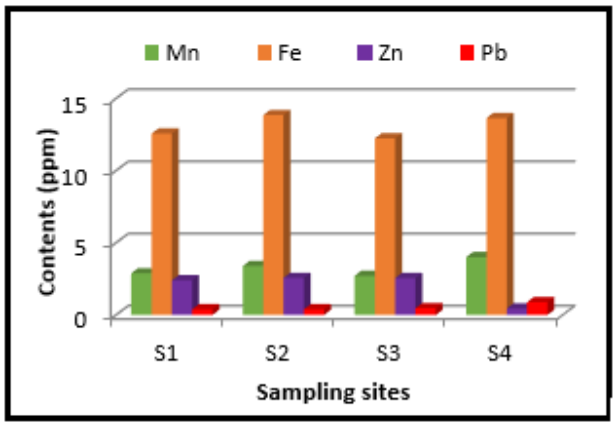

Fig.8. Heavy metals contents of four soil samples

IV. Conclusion

The present study concerns with the distribution of some heavy metals in surface soils of four sampling sites from Heinda mine in Dawei Township Tanintharyi Region. Soil samples were collected from 150 m, 300 m, 450 m and 600 m distances of Heinda mine's industrial zones. Physicochemical parameters such as pH, moisture, texture, organic matter, humus and heavy metals (Mn, Fe, Zn, Pb) were determined by conventional methods and modem instrumental techniques. The pH of the soil samples (S_1, S_2, S_3 and S_4) was found to be the values of 5.14, 5.30, 5.35 and 5.46 respectively. It shows that all soil samples from four sampling sites were in the acidic condition. The acidic condition may be due to the nature of the soil. The moisture percent of soil samples (S_1, S_2, S_3 and S_4) were found to be 7.73%, 1.83%, 0.93% and 0.75% respectively. It was found that the soil sample S, of site 1 for 150m distance from the industrial mining zone has the highest moisture percent 7.73%.The texture of the soil sample S_1, (site l) was found to be (35.00%, 43.00%, and 22.00%) for sand, silt and clay respectively. Soil type was slit loam due to the highest silt percent 43.00%. The soil sample S_2 (site 20 was found to be (45.00%, 47.00%, 8.00%) for sand, silt and clay respectively. Soil type was silt loam. Soil sample S_3, (site 3) and S_4 (site 4) were sandy loam. The sand, silt and clay percent of soil sample S_3 (site 3) were found to be (19.00%, 14.00%, 8.00%) respectively. The soil sample S_4 (site 4) was found to be (05.45%, 32.75%, 2.65%) for sand, silt and clay respectively. Organic matter and humus contents of the soil samples (S_1, S_2, S_3 and S_4) were found to be the vales of (2.04% and 3.52%) for S_1, (1.28% and 2.21%) for S_2, % and 2.109%) for S_3, and (0.87% and 1.50%) for S_4, respectively. It was found that he soil sample S_1, (site l) from the 150 m distance of industrial Heinda mine has the highest organic and humus, most probably due to dumping of waste from the workings of the mine. Heavy metal contents in soil samples were determined by Energy Dispersive X-ray Fluorescence (EDXRF) technique and Atomic Absorption Spectrophotometry (AAS) method. By the analysis of EDXRF, the soils were rich with silicon. Relative abundance of silicon (39.564, 49.750, 49.578 and 41.206) % for soil samples (S_1, S_2, S_3 and S_4) respectively. According to AAS methods, the contents of heavy meats were fund to be the values of Mn (2.887, 3.392, 2.711 and 4.009) ppm, Fe (12.57, 13.85. 12.24 and 13.64) ppm, Zn (2.403, 2.565, 2.556 and 0.447)ppm, Pb (0.398, 0.393, 0.47 and 0.886) ppm för soil samples (S_1, S_2, S_3 and S_4) respectively. The presents of heavy metal concentrations and other pollutants were detected with a maximum allowable limit of WHO guideline values. The content values of Mn, Fe, Zn and Pb were found to be lower values of WHO guideline vales. From these results, Mn contents in soil sample S_4 (site 4) of Heinda mine has the highest (4,009 ppm). Maximum allowable limit of Mn is 50 ppm for soil Mn content was found to be lower values of WHO guideline values. Fe content in soil sample S; (site 2) of Heinda mine has the highest (13.85 ppm). Fe content was found to be lower values of WHO guideline values (220 ppm). Zn content in soil sample S_2 (site 2) of Heinda mine has the highest (2.56S ppm). Maximum allowable limit of Zn s 300 ppm for soil. Zn content was found to be lower values of WHO guideline values. Pb content in soil sample S_4 (site 4) of Heinda mine has the highest (0.886 ppm). Pb content was found to be lower than the maximum allowable vales of (200 ppm). A few concluding remarks, S_2 (site 2) has the highest vales of Fe (5.3 ppm) and 2Zn (2.565 ppm), soil sample S_4 (site 4) has the highest vales of Mn 4.009 ppm) and Pb (0.886 ppm). However, these values were found to be lower values of WHO guideline values. From this research, sampling site 2 and 4 have the highest vales of some heavy metals, however these values were no significant risk for human and live stocks near to the Heinda village.

Acknowledgments

My deeply supervisor, Professor Dr Khin May Tint, Department of Chemistry, Pakokku University, her guidance, close supervision numerous invaluable suggestions, encouragement, comments and

administrative supervision and co-operation throughout this research work. I am very grateful to all my teachers of the Department of Engineering Chemistry, Myeik Technological University, for their kind understanding.

REFERENCES

[1] L. Alessio, M. Campagna, and R. Lucchini, "From lead to manganese through mercury: Mythology, science, and lessons for prevention," *Am. J. Ind. Med.*, vol. 50, no. 11, pp. 779–787, 2007.

[2] C. Aydinalp and S. Marinova, "Lead in Particulate Deposits and in Leaves of Roadside Plants," p. 4.

[3] W. F. Bennett, *Nutrient deficiencies & toxicities in crop plants*. APS Press, 1993.

[4] R. Ebinghaus, R. M. Tripathi, D. Wallschläger, and S. E. Lindberg, "Natural and Anthropogenic Mercury Sources and Their Impact on the Air-Surface Exchange of Mercury on Regional and Global Scales," in *Mercury Contaminated Sites*, R. Ebinghaus, R. R. Turner, L. D. Lacerda, O. Vasiliev, and W. Salomons, Eds. Berlin, Heidelberg: Springer Berlin Heidelberg, 1999, pp. 3–50.

[5] R. E. Speece, "Anaerobic biotechnology for industrial wastewater treatment," Sep. 23, 2008.

[6] R. M. Harrison and R. Perry, "The analysis of tetraalkyl lead compounds and their significance as urban air pollutants," *Atmospheric Environ. 1967*, vol. 11, no. 9, pp. 847–852, Jan. 1977.

[7] M. L. Jackson, "Soil Chemical Analysis - Advanced Course.," *Soil Chem. Anal. - Adv. Course*, no. Edition 2, 1969, Accessed: Sep. 08, 2020.

[8] L. H. P. Jones, C. R. Clement, and M. J. Hopper, "Lead uptake from solution by perennial ryegrass and its transport from roots to shoots," *Plant Soil*, vol. 38, no. 2, pp. 403–414, Apr. 1973.

[9] C. E. Millar, *Fundamentals of soil science*, 4th Edition. J. Wiley, 1965.

[10] W. H. Organization, *Guidelines for Drinking-water Quality*. World Health Organization, 1993.

Article ID – JRA6000720

A Study on Preliminary Phytochemical Investigation, Elemental Analysis and Antimicrobial Activity of Inflorescence of Mango

Ei Ei Khaing
Department of Chemistry
Hinthada University
eieikhaingchem@gmail.com

Aye Aye Aung
Department of Engineering Chemistry
Technological University (Hinthada)
thathninswe94@gmail.com

Ohn Mar Tin
Department of Chemistry
Hinthada University
ohnmartin209@gmail.com

***Abstract*— The inflorescence of *Mangifera indica* L. (Mango) used in folk medicine was chosen for present study. The gastrointestinal tract infection becomes one of the local health problems that many researchers innovate for finding anti-pathogenic substances from natural sources. The aim of the study is to find out phytochemicals, nutrient elements and antimicrobial activity of *Mangifera indica* L. inflorescence. At first, preliminary phytochemical tests have revealed that the absence of cyanogenic glycosides in the sample according to test tube method. As the nutrient elements, inflorescence sample contains relatively the highest content of K and Ca whereas minor components of S, P, Fe, Cu, Mn, Zn and Au according to Energy dispersive X-ray fluorescence (EDXRF) spectrum. By direct extraction method, four crude extracts of inflorescence sample were prepared by petroleum ether, ethyl acetate, 96 % ethanol and water solvent. The antimicrobial activity of four crude extracts was investigated against eight tested microorganisms by agar well diffusion method. It was found that all tested samples except petroleum ether extract showed antimicrobial activity against tested microorganisms with the range of zone diameter between 12~29 mm. From the results, it could be applied as the local health remedy to the local indigenous communities of our country. Since some elements were also found in inflorescence sample, it could be expected to become a potential food and drug source.**

Keywords*— *Mangifera indica* L., *inflorescence, phytochemicals, elements, antimicrobial activity

I. INTRODUCTION

In Myanmar, gastrointestinal (GI) problem is one of the major health problems. Therefore, the present research designated to explore the promising Myanmar medicinal plant in the use of traditional drug for food poisoning, typhoid and diarrhea related to GI problems. Mango tree (*Mangifera indica* L.) cv. Ma-chit-su with flowers and its inflorescence shown in Figure 1(a) and 1(b), family Anacardiaceae [1], Tha-yet in Myanmar name is well known for medicinal purposes and its delicious fruit [2]. In addition, mango inflorescence is used in diarrhea, nosebleeds, reducing cholesterol, controlling diabetes and in the treatment of acidity problems [3]. The plant is a shaded tree, 10 to 40 m in height [4]. Mango flowers are small (5-10 mm) in diameter, have a 10 part perianth consisting of four or five sepals and petals that are ovate [5]. It is widely distributed in Myanmar. This research can contribute to local indigenous medicine and may solve some problems related to pathogenic microorganisms. In the study, the sample collection, preliminary phytochemical investigation, elemental analysis, preparation of crude extracts, screening of antimicrobial activity from the inflorescence sample have been carried out.

(a) (b)

Fig 1. (a) *M. indica* L. (mango tree) cv. Ma-chit-su (b) *M. indicia* L. inflorescence

II. MATERIALS AND MRTHODS

The sample of *M. indica* L. (Mango) cv. Ma-chit-su inflorescence was collected from Hinthada University campus, Hinthada Township, Ayeyarwady Region in March, 2019. The plant was identified by plant taxonomists at Department of Botany, Hinthada University. The inflorescence sample was cleaned and dried at room temperature for two weeks. Then, the dried sample was powdered and stored in air- tight container to avoid moisture changes and other contamination.

A. Preliminary Phytochemical Tests of M. indica L. Inflorescence by Using Test Tube Method

Preliminary phytochemical investigation was carried out on powdered, dried sample of *M. indica* L. inflorescence.

B. Qualitative Elemental Analysis of M. indica L. Inflorescence by EDXRF Spectrometry

Qualitative elemental analysis of *M. indica* L. inflorescence was analyzed by Energy dispersive X-ray fluorescence spectrometer (Shimadzu's EDX-7000/8000) at Monywa University. The dried powder sample was fabricated into pellet by using pellet making machine. It can analyze the elements from sodium to uranium. The individual elements comprising in the sample re-emit their own characteristic X-rays. The X-rays are detected by using semiconductor detector [Si (Li)] which permits multi-element, simultaneous analysis.

C. Preparation of Crude Extracts of M. indica L. Inflorescence by Direct Extraction Method

The powdered sample of *M. indica* L. inflorescence (50 g) was extracted with (500 mL) petroleum ether (PE), ethyl acetate (EtOAc) and 96 % ethanol (EtOH) in separate conical flasks, respectively for at least three weeks and then filtered. Water extract of inflorescence sample was prepared by boiling 50 g of sample with 500 mL of distilled water for 6 h and filtered. The filtrates were evaporated by using rotary evaporator and desiccated and also weighed. Extractive values were described in terms of % in weight by weight on the powdered materials. The four crude extracts from *M. indica* L. inflorescence were applied to investigate antimicrobial activity.

D. Antimicrobial Activity of Crude Extracts of M. indica L. Inflorescence Against Eight Tested Microorganism by Agar Well Diffusion Method

For the examination of *in vitro* antimicrobial activity, agar well diffusion method was used because of its simplicity, speed of performance, economy and reproducibility [6]. In the antimicrobial activity, four crude extracts: PE, EtOAc, 96 % EtOH and H_2O extracts, were determined against eight microorganisms such as *Escherichia coli* AHU5436, *Bacillus subtilis* IFO90571, *Bacillus pumilus* IFO12092, *Candida albicans* NITE09542, *Pseudomonas fluorescens* IFO94307, *Staphylococcus aureus* AHU8465, *Agrobacterium tumefaciens* NITE09678 and *Malassezia furfur* AUV0255 by employing agar well diffusion method at Department of Chemistry, Hinthada University. These eight tested microorganisms were obtained from the source of NITE and Kyowa Hakko Co. Ltd., Pharmaceutical Research Development (PRD), Ministry of Technology and University of Yangon (UY). These microorganisms were cultured at Biotechnology and Development Center of Pathein University. The test procedure was as follows: the test samples (1 g each) were dissolved in 1 mL of appropriate soluble solvent, and introduced into sterile petridishes for testing eight cultured microbial strains. The test organisms were incubated in test broth medium containing glucose (0.5 g), yeast (0.3 g), peptone (0.2 g) and distilled water (100 mL) at 27°C for 24 h. Assay medium containing glucose (50.0 g), peptone (30.0 g), yeast (30.0 g), agar (14.0 g) and distilled water (1000 mL) were placed in a beaker and the contents were heated for 10 min. The assay medium was put into sterilized conical flask and plugged with cotton wool and then autoclaved at 121 °C for 15 min. After cooled down to 40 °C, 0.1 mL of suspended strain was inoculated to the assay medium with the help of a sterilized disposable pipette near the burner. About 20 mL of medium was poured into the sterilized petri-dishes and allowed to set the medium. Once solidified, the dishes were cooled for 2 h at room temperature. After solidification, the agar well was made with 8 mm sterile cork borer from each agar. After inoculums had been dried for 5 min, the wells were filled with test sample (0.2 mL extracts) to be tested. After 24-48 h incubation at 27 °C, the zones of inhibition diameter including 8 mm well were measured with digital calipers in millimeter. If clear zones (inhibitory zones) surrounding the agar well were found to be indicated that it would be the presence of bioactive metabolites which inhibit the growth of test organisms. The incubated petri-dish without test sample was taken as control and antibiotics; chloramphenicol was used as standard for this study.

III. RESULTS AND DISCUSSION

A. The Results of Preliminary Phytochemical Tests of M. indica L. Inflorescence

Phytochemical screening serves as an initial step to recover new sources of phytochemical and biologically active compounds. For the reasons, the phytochemical test was carried out on *M. indica* L. inflorescence and it was found that the inflorescence sample consists of alkaloids, α-amino acids, carbohydrates, flavonoids, glycosides, organic acids, phenolic compounds, reducing sugar, saponins, starch, steroids, tannins and terpenoids. However, cyanogenic glycosides (plant toxin), were not detected in it. Alkaloids possess the properties of antitumor, antiviral, antihypertensive, antidepressant, antimicrobial and anti-inflammatory activities. Flavonoids are used in antibacterial, anti-inflammatory, anti-allergies, anti-mutagenic, antiviral and antithrombotic activity. Glycosides are used as antibiotic, anticancer, antidiabetic, purgative, treatment of congestive heart failure and cardiac arrhythmia. Phenols are strong antioxidants and they are very useful in prevention and management of chronic diseases (cancer and cardio vascular diseases). Saponins stand for antiviral, antiviral, anti-inflammatory, anti-helminthic, anticancer and anti-cytotoxic activity. Steroids are used as anti-inflammatory, antitumor, anti-allergies, anti-asthma, anti-eczema, anti-arthritis. Tannins are also antiviral, antibacterial and antitumor properties. The uses of terpenoids include antimicrobial, antifungal, antiviral, anti-hyperglycemic, anti-inflammatory, antioxidant and anti-parasitic [7]. From the study, it could be denoted that the selected sample, *M. indica* L. inflorescence may be a good

source of herbal medicine. The results are described in TABLE I and Fig. 2.

TABLE I. RESULTS OF PHYTOCHEMICAL INVESTIGATION OF *M. indica L. INFLORESCENCE*

No.	Test	Ext.	Reagents used	Observation	Re-mark
1.	Alkaloids	1% HCl	Wagner's reagent	Reddish brown	+
			Dragendorff's reagent	Orange ppt	+
			Sodium picrate	Yellow ppt	+
			Mayer's reagent	White ppt	+
2.	α-amino acids	D/W	Ninhydrin reagent	Purple colour	+
3.	Carbohydrate	D/W	10 % α-naphthol & conc: H_2SO_4	Red ring	+
4.	Cyanogenic glycosides	D/W	Sodium picrate solution & conc: H_2SO_4	No brick red ppt	-
5.	Flavonoids	96 % EtOH	NaOH & dil. HCL	Yellow colour	+
6.	Glycosides	D/W	10 % lead acetate	White ppt	+
7.	Organic acids	D/W	Bromocresol green	Blue colour	+
8.	Phenolic compounds	D/W	5 % $FeCl_3$ & 1% $K_3Fe(CN)_6$	Deep blue colour	+
9.	Reducing sugars	D/W	Benedict's solution	Green colour	+
10.	Saponins	D/W	Distilled water	Marked Frothing	+
11.	Starch	D/W	Iodine solution	Red colour	+
12.	Steroids	$CHCl_3$	Acetic anhydride & conc: H_2SO_4	Reddish brown colour	+
13.	Tannins	96 % EtOH	1 % Gelatin	White ppt	+
14.	Terpenoids	96 % EtOH	Acetic anhydride & Conc. H_2SO_4	Pink colour	+

(+) = presence (-) = absence

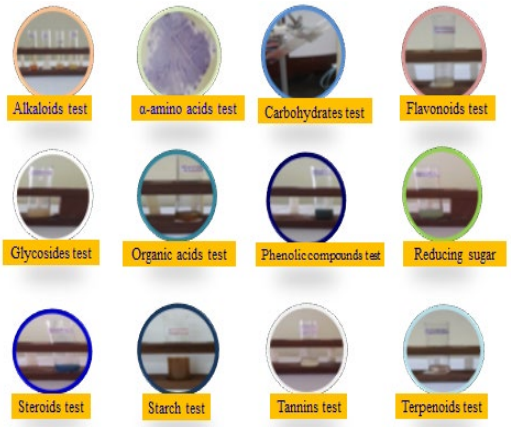

Fig 1. Preliminary phytochemical investigation of M. indicia L. inflorescence

B. The Results of Qualitative Elemental Analysis of M. indica L. Inflorescence by EDXRF

Under vacuum condition, EDXRF spectra of *M. indica* L. inflorescence sample was shown in Fig. 3 and TABLE II. In this study, two kinds of elements such as K and Ca were found to be relatively high whereas S, P, Fe, Cu, Mn, Zn and Au were minor components in the sample. In addition, potassium peak was also the most prominent and so it showed that potassium was the highest content in the inflorescence sample. According to the literature survey, potassium deficiency can cause nervous irritability, mental disorientation, low blood sugar, insomnia and coma. Calcium plays a very important role in bones, teeth, muscles system and heart functions. Phosphorus needs along with calcium to build strong healthy bone [8]. In fact, potassium (K), calcium (Ca), phosphorous (P) and sulphur (S) are important macro elements which are needed large amount in human body. Iron (Fe), copper (Cu), manganese (Mn), zinc (Zn) and Gold (Au) are micro elements required very small amount in human body. From this study, the macro elements were found to be the major components in selected inflorescence sample. From the result, it could be deduced that mango inflorescence may support in human health. In addition, the analysis of elemental content can determine physicochemical properties of the inflorescence sample, as well as retard the growth of bacteria.

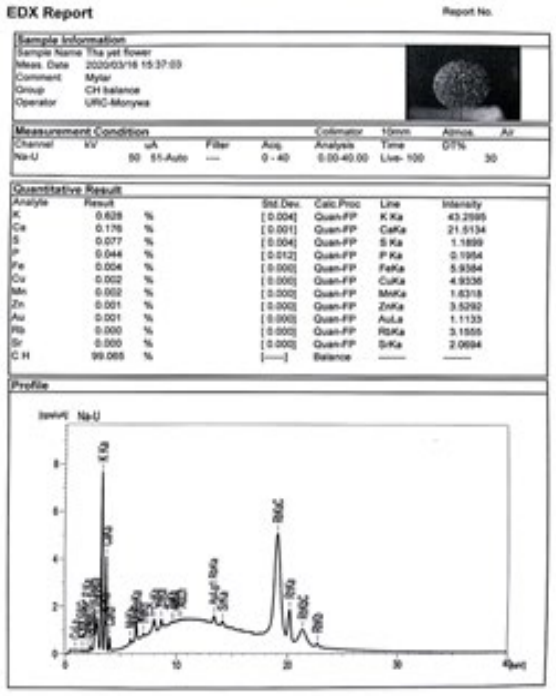

Fig 2. EDXRF spectrum of *M. indica* L. inflorescence

TABLE II. ELEMENTAL ANALYSIS OF M. *indica* L. INFLORESCENCE BY EDXRF

No.	Element	Relative Abundance (%)
1.	K	0.628
2.	Ca	0.176
3.	S	0.077
4.	P	0.044
5.	Fe	0.004
6.	Cu	0.002
7.	Mn	0.002
8.	Zn	0.001
9.	Au	0.001
10.	C/H	99.065

C. *Assessment of Four Crude Extracts from M. indica L. Inflorescence by Various Solvents*

The dried inflorescence powder collected from Hinthada University campus was extracted with various solvents and yielded petroleum ether extract (12.46 %), ethyl acetate extract (20.62 %), 96 % ethanol extract (27.30 %) and water extract (29.20 %). It was assumed that polyphenolic and flavonoid compounds may involve in higher yielded 96 % ethanol and water extracts. Thus, it could be denoted that *M. indica* L. inflorescence possesses medicinal properties.

D. *Investigation of Antimicrobial Activity of Four Crude Extracts from M. indica* L. *Inflorescence by using Agar Well Diffusion Method*

In traditional medicine system, many plants or herbs are claimed to have therapeutic efficacy without any scientific basis. As one of the aims of the present study, the antimicrobial activity was performed with particular reference to pathogenic microorganism potential to cause GI tract infection, diarrhea, septicemia, crown gall disease, food poisoning, dandruff, seborrheic dermatitis and abscess in skin, mouth, nose etc. In the present work, antimicrobial activity of four crude extracts from *M. indica* L. inflorescence were investigated on eight species of microorganisms by agar well diffusion method at Department of Chemistry, Hinthada University. Agar well diffusion method is based on the inhibition zone diameter in millimeter (mm) of the well. The larger the zone diameter is, the more activity on the tested microorganisms. In this study, the assay medium in absence of sample with culture microorganisms was utilized as control. The four crude extracts were tested with eight microorganisms such as *Escherichia coli* AHU5436, *Bacillus subtilis* IFO90571, *Bacillus pumilus* IFO12092, *Candida albicans* NITE09542, *Pseudomonas fluorescens* IFO94307, *Staphylococcus aureus* AHU8465, *Agrobacterium tumefaciens* NITE09678 and *Malassezia furfur* AUV0255. The measurable inhibition zone diameter of four crude extracts showed the degree of antimicrobial activity (Fig. 4 and TABLE III). From the results, it was observed that ethyl acetate, ethanol and water extracts of inflorescence sample exhibited against all tested microorganisms with the inhibition zone diameters between 12~19 mm, 20~29 mm and 13~24 mm respectively whereas petroleum ether extract has no activity. Out of these extracts, ethanol extract showed the most potent to the tested microorganisms. Nevertheless, ethyl acetate extract of inflorescence sample revealed the medium inhibition to eight microorganisms in comparison with the inhibition zone of standard chloramphenicol (15~30 mm). By finding results, *M. indica* L. inflorescence may be effectively used as active remedy for this treatment of their related diseases and fungal infection.

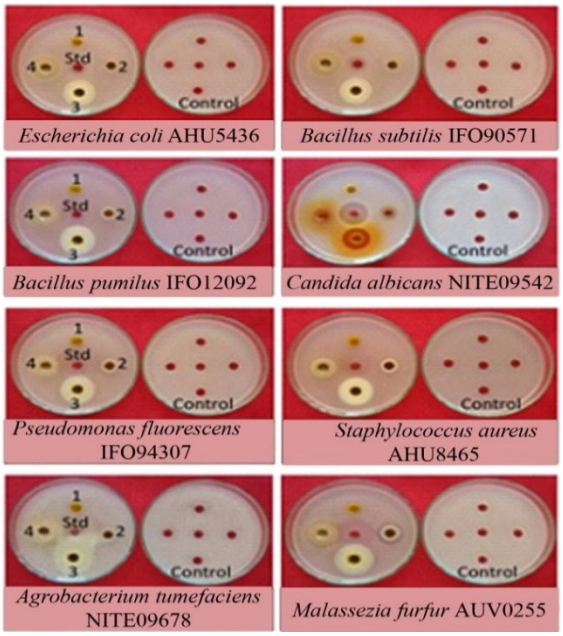

Counterclockwise Position

1. PE extract
2. EtOAc extract
3. EtOH extract
4. Water extract

Std. Chloramphenicol

Fig 3. Inhibition zone of four crude extracts from *M. indica* L. Inflorescence against eight microorganisms

TABLE III INHIBITION ZONE DIAMETERS OF FOUR CRUDE EXTRACTS FROM *M. indica* L. *INFLORESCENCE*

Microorganisms	Inhibition Zone Diameters (mm) of Test Samples				
	1[a]	*2*[b]	*3*[c]	*4*[d]	*Std.*[e]
Escherichia coli AHU5436	-	15	26	21	15
Bacillus subtilis IFO90571	-	18	26	21	15
Bacillus pumilus IFO12092	-	16	27	22	24
Candida albicans NITE09542	-	16	28	20	17
Pseudomonas fluorescens IFO94307	-	13	20	13	30
Staphylococcus aureus AHU8465	-	15	24	20	17
Agrobacterium tumefaciens NITE09678	-	12	26	20	18
*Malassezia AUV*0255	-	19	29	24	25

[a] petroleum ether extract, [b] ethyl acetate extract, [c] ethanol extract, [d] water extract, [e] chloramphenicol (std.)

agar well diameter = 8 mm, - = no activity
10 mm ~ 14 mm (+), 15 mm ~ 19 mm (+ +) 20 mm above (+ + +)

IV. CONCLUSION

The preliminary phytochemical tests on *M. indica* L. cv. Ma-chit-su inflorescence (mango inflorescence) revealed the absence of plant toxin, cyanogenic glycosides in the inflorescence sample. From EDXRF spectrum, mango inflorescence sample was found that it contains macro elements as well as some micro elements needed for human health. By using direct extraction method, four crude extracts were prepared from mango inflorescence using PE, EtOAc, 96 % EtOH and water as their solvent polarity. Screening of antimicrobial activity of four crude extracts from mango inflorescence sample was also investigated by employing agar well diffusion method against eight species of microorganisms. It was observed that ethanol extract of mango inflorescence exhibited the most potent inhibition zone diameters between 20~29 mm against all tested microorganisms whereas petroleum ether extract didn't show activity. Based on the finding of present study it is concluded that mango inflorescence possesses antimicrobial activity. In addition, it may be recommended that polar extract (ethanol extract) of mango inflorescence may be used as main materials for the traditional medicine formulation for the treatment against GI tract infection, diarrhea, septicemia, crown gall disease, food poisoning, dandruff, seborrheic dermatitis and abscess in skin, mouth, nose etc. The result of this study is an encouragement for further work that will lead to the isolation of active principles as well as elucidation of the structure and investigation of other bioactivities from mango inflorescence.

ACKNOWLEDGMENT

We would like to express our heartfelt gratitude to Dr Nilar Myint (Rector) and Dr Mar Lar, Pro-Rector, Hinthada University, for their giving the permission to report this research paper. We also convey special gratitude to Professor Dr Thi Thi Aye, Department of Chemistry, Hinthada University for her enthusiastic reading and faculty members of our Department. We deeply thanks to responsible and honorable persons of Journal of Research & Applications (JRA), UCSMTLA, 2020.

REFERENCES

[1] T. Okuda, "Systematics and health effects of chemically distinct tannins in medicinal plants," *Phytochemistry*, vol. 66, no. 17, pp. 2012–2031, Sep. 2005.

[2] T. Yeshitela, P. Robbertse, and P. Stassen, "The impact of panicle and shoot pruning on inflorescence and yield related developments in some mango cultivars," 2003.

[3] L.A., Ouma, J., Ambuko, S., Shibairo and W. O., Owino, "Comparison of quality attributes of mango fruits produced from two contrasting agro-ecological zones of Kenya," 2014.

[4] L.J., Ambuko, "The plight of smallholder mango farmers in Kenya during the peak season – Hortfresh Journal." Hortfresh Journal, pp. 356-360, 2016.

[5] S. Maloba, J. Ambuko, M. Hutchinson, and W. Owino, "Off-Season Flower Induction in Mango Fruits Using Ethephon and Potassium Nitrate," *J. Agric. Sci.*, vol. 9, no. 9, Art. No-9, Aug. 2017.

[6] K., Ando, "Sampling, Isolation, Cultivation and Preservation of Microorganisms", Biological Resource Center, National Institute of Technology and Evaluation (NITE), Japan, 2004.

[7] P. P. Brahmkshatriya and P. S. Brahmkshatriya, "Terpenes: Chemistry, Biological Role, and Therapeutic Applications," in *Natural Products: Phytochemistry, Botany and Metabolism of Alkaloids, Phenolics and Terpenes*, K. G. Ramawat and J.-M. Mérillon, Eds. Berlin, Heidelberg: Springer, 2013, pp. 2665–2691.

[8] WHO, *Quality Control Methods for Medicinal Plant Materials,* Revised, Geneva, 2005.

Article ID – JRA6001120

Determination of Vitamin-C Content and Antioxidant Activity of fruit of *Adansonia digitata* Linn. (Met-lin-gyin)

Pa Pa San
Department of Chemistry
Yadanabon University, Myanmar
papasan1771@gmail.com

***Abstract*— Fruits are generally acceptable as good source of nutrient and supplement for food in a world faced with problem of food scarcity. In this research work, among the rich source of vitamin-C, Baobab fruit (Met-lin-gyin) was selected for chemical analysis. Firstly, phytochemical screening for the Baobab fruit was performed. According to phytochemical screening, alkaloid, flavonoid, glycoside, phenolic, polyphenol, saponin, terpene, tannin, reducing sugar and protein were found to be present in Baobab fruit. The determination of ascorbic acid content in Baobab fruit sample solution by a redox titration method. Ash content, moisture content of Baobab fruit were determined by conventional procedures. The mineral contents of Baobab fruit were measured by Energy Dispersive X-ray Fluorescence (EDXRF) method. Moreover, antioxidant activities of Baobab fruit evaluated on the basis of their scavenging activity of the stable 1,1-diphenyl 2-picrylhydrazyl (DPPH) free radical.**

Keywords*— Met-lin-gyin fruit, vitamin C content, EDXRF, DPPH

I. INTRODUCTION

Vitamin is a powerful antioxidant and extremely important in human nutrition. Vitamin C has been shown to be related to low blood pressure, enhanced immunity against many tropical diseases, lower incidence of cataract development and lower incidence of coronary disease. The daily recommended intake for healthy adults is 65 mg [1].

As a result of its high natural vitamin C content, baobab fruit pulp has a well-documented antioxidant capability. The antioxidant capacity of baobab fruit pulp was investigated using the photochemiluminescence (PLC) assay, comparing the antioxidant properties of the fruit pulp to the antixodant properties of several other fruits including kiwi, orange, apple and strawberry. The high vitamin C and antioxidant content of the fruit pulp may have a role to play in the extension of shelf-life for foods and beverages, as well as cosmetics. The food/beverage industry could introduce baobab fruit pulp into foods in order to act as a preserving ingredient by preventing oxidation of lipids on the food. This plant is commonly found in Africa and many parts of Myanmar. Baobab pulp fruit is rich in carbohydrates (glucose, fructose), protein, calcium, iron and phosphours. It also provides large amount of ascorbic acid vitamin C [3].

A. Vitamin C

Ascorbic acid is one form of vitamin C. L-ascorbic acid (vitamin C) is an essential nutrient for health maintenance.

Ascorbic acid is a naturally occurring organic compound with antioxidant properties. It is a white solid, but impure samples can appear yellowish. It dissolves well in water to give mildly acidic solution [3].

Vitamin C or ascorbic acid can be obtained from fruits or vegetables. Vitamin C also acts as an antioxidants, scavenging potential harmful molecules called free radicals. Although not firmly established by clinic trails, this antioxidant capacity may help boast immue function, protect against cancer, cataracts, agerelated macular degeneration of the retina and other chronic disease. Vitamin C intake may be particular helpful to smokers, as they are more likely to suffer from oxidatative stress and cell damage that can deplete vitamin C.

In human, vitamin C is essential to a healthy diet as well as being a highly effective antioxidant. It is a water soluble antioxidant that plays a vital role in protecting the body from infection and disease. The baobab fruit was found to have the highest content of vitamin C at 280 to 300 mg/100 g, out of all fruits investigated. This compared to a vitamin C content of 46 mg/100 g in orange, a well-documented source of vitamin C. Baobab fruit pulp was found to have interesting antioxidant properties in particular the Integral Antioxidant Capacity (IAC) value of baobab fruit pulp was higher than that of orange pulp [2].

Ascorbic acid acts as a free radical scavenger and its reaction are faster, compared to other scavenging molecules such as polyphenols. Met-lin gyin fruit can be eaten as a good natural source of antioxidants which help

to prevent the dangers of free radicals which can cause cancer and other undesirable health detriments [3].

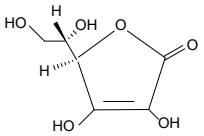
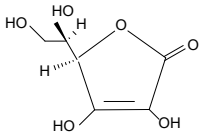

L-Ascorbic acid	D-Ascorbic Acid
Molecular formula	– $C_6H_8O_6$
Molecular mass	– 176.12 g mol^{-1}
Appearance	– white or lightyellow solid
Solubility in water	– 330 g/L

Ascorbic acid was originally called L-hexuronia acid. The new name for L-hexuronic acid is derived from sorbutus (seurvy), the disease caused by a deficiency of vitamin C. Chemically, there exists a D-ascorbic acid which does not occur in nature. It may be synthesized artificially. It has identical antioxidant properties to L-ascorbic acid, yet has far less vitamin C activity [2].

The aim of the present research work is to determine the ascorbic acid content in Baobab fruit (Met-lin-gyin) by using Iodometric titration and antioxidant activity of Baobab fruit were carried out.

B. Botanical Description of Adansonia digitata Linn.

Fig. 1. The plant, flower and fruit of *Adansonia digitata* Linn.

(Met-lin-gyin)

Family	:	Malvaceae
Subfamily	:	Bambacaceae
Botanical name	:	*Adansonia digitata* Linn.
Myanmar name	:	Met-lin-gyin
English name	:	Baobab
Part used	:	Fruits
Medicinal uses	:	antidiabetic, antitumor active, hepatiprotective, obesity

The fruit pulp used as eye drop to cure-measles. Leaves useful in treatment of liver and kidney, diarrhoea. Powder roots given for malaria treatment [8].

II. Material and Method

A. Sample Collection and Preparation

The sample Met-lin-gyin was collected from Pyin-Oo-Lwin Township, Mandalay Region. Sample of fruits (Met-lin-gyin) was washed and cut into small pieces. The sample (100 g) and distilled water were cursed to paste like state for approximately two minutes using a blender. The homogenized sample was then made up to 100 mL in a volumetric flask and then filter the sample.

B. Determination of Phytochemical Test of Met-lin-gyin (Baobab fruit) [6] [9]

Fig. 2. Phytochemical Screening of Fruit of Met-lin-gyin

C. Preparation of Vitamin C Standard Solution

0.250 g ascorbic acid was dissolved in the beaker with 250 mL distilled water. The solution was transferred into 250 mL volumetric flask and diluted to the mark with distilled water [10].

D. Standardization of the Iodine Solution with the Standard Vitamin C Solution

25 mL of vitamin C solution was pipette into 125 mL conical flask. Ten drops of 1 % starch solution were added and then titrated against iodine solution until blue-black colour was observed.

Procedure

25 mL of sample solution was taken in a conical flask. 10 drops of 1 % starch solution were added and then titrated with standard iodine solution until dark-

green colour appeared. Then the amount of ascorbic acid contents were calculated [10].

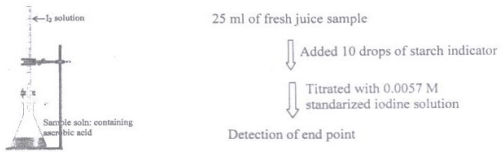

Fig. 3. Flow chart for Determination of Ascorbic Acid Content

E. Standardization of the Iodine Solution with the Standard Ascorbic Acid Solution [10]

Concentration of Ascorbic Acid

1000 mL_____176g_____1M

250 mL _____0.25g_____?

$$1\times \frac{1000' \ 0.25}{250' \ 175}$$

$$= \frac{1.00}{176} = 0.0057 \text{ M}$$

I_2 solution 25 mL × concentration of I_2 solution = ascorbic acid 25 mL × 0.0057 M

Concentration of I_2 solution = 25× 0.0057 mmol of ascorbic acid

$$= 25 \times 0.0057 \text{ mmol of } I_2$$

$$= \frac{25' \ 0.0057}{25}$$

$$= 0.0057 \text{ M}$$

F. Determination of Ash, Content, Moisture Content, Mineral Content, Antioxidant Activity of Baobab Fruit (Met-lin-gyin)

The moisture content, ash content of Baobab fruit was determined by AOAC method [10].

The elemental composition of Baobab fruit was measured by applying Energy Dispersive X-ray Fluorescence (EDXRF) [XEPOF EDXRF Spectrometer].

The antioxidant activity of Baobab fruit was determined by 1, 1-diphenyl-2- Picrylhydrazyl (DPPH) radical Scavenging assay method by using Spectrophotometer [5].

G. Determination of Ascorbic Acid Content in Pulp of Baobab Fruit (Met-lin-gyin)

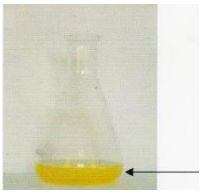

original colour

End point

Procedure

25 mL of the fresh juice sample of Met-lin-gyin fruit (pulp) was titrated with 0.0057 M iodine solution to reach the end point. Once all the ascorbic acid has been oxidized, a slight excess of added iodine forms a dark complex with starch indicator giving a colour. This is the titration end point.

The amount of ascorbic acid content in pulp of Baobab fruit (Met-lin-gyin) 19 cm3 was obtained [10].

III. Results and Discussion

The amount of vitamin C in a sample was determined by redox titration. This method determines the vitamin C concentration in a solution by a redox titration using iodine solution. Ascorbic acid is an essential antioxidant needed by the human body. As the iodine is added during the titration, the ascorbic acid is oxidized to dehydroascorbic acid, while the iodine is reduced to the iodide ions.

Due to the reaction, the iodine formed is immediately reduced to iodide as long as there is any ascorbic acid present. Once all the ascorbic acid has been oxidized, the excess iodine is free to react with the starch indicator, forming the deep color starch iodine complex. This is the endpoint of the titration.

A. Preliminary Phytochemical Test of Met-lin-gyin Samples

TABLE I. THE RESULTS OF PHYTOCHEMICAL TEST FOR THE CRUDE EXTRACT OF MET-LIN-GYIN SAMPLES

No.	Constituents	Reagent used	Observation	Result
1.	Alkaloid	(1) Wagner's reagent (2) Dragendroffs solution	brown ppt orange ppt	+ +
2	Glycoside	H_2O, 10 % Lead acetate	white ppt	+
3	Reducing sugar	H_2O, Benedicts solution	Brick-red ppt	+
4	Phenolic	H_2O, 10 % $FeCl_3$	Greenish blue color	+
5	Saponin	EtOH, conc:H_2SO_4 shake	Froth like comb	+
6	Flavonoid	EtOH, conc:HCl, Mg turing, Δ	Brown red color solution	+
7	Terpene	Pet-ether, Acetic anhydride, $CHCl_3$, conc:H_2SO_4	Red purple colour solution	+
8	Lipophilic	H2O, 0.5M KOH	Deep colour solution	+
9	Polyphenol	EtOH, 1% $FeCl_3$, 1% $K_3[Fe(CN)_6]$	Blue green color solution	+
10	Tannin	10% $FeCl_3$ + dil H_2SO_4	Yellowish brown ppt.	+
11	Protein	NaOH solution and NaOH solution	violet colour solution	+

According to this table, the fruits of Met-lin-gyin consists of glycoside, polyphenol, phenolic, reducing sugar, flavonoid, terpene, saponin, alkaloid, protein, tannins, respectively.

B. Determination of Moisture Content

$$\text{Moisture (\%)} = \frac{A - B}{A} \cdot 100$$

A = before drying, sample weights in gram

B = after drying , sample weights in gram

No.	Sample	Moisture (g)	Moisture %
1.	5 g	4.498	89.96
2.	5 g	4.498	89.96
3.	5 g	4.498	89.96

The moisture content was found to be 89.96 %.

C. Determination of Ash Content

The ash content was calculated by using the following relation.

$$\text{Percent ash content} = \frac{\text{weight of residue}}{\text{weight of sample}} \times 100$$

No.	Sample	Moisture (g)	Moisture %
1.	1 g	0.0446	4.46
2.	1 g	0.0450	4.50
3.	1 g	0.0453	4.53

The ash content was found to be 4.5 %.

TABLE II. DETERMINATION OF MINERAL CONTENTS IN BAOBAB FRUIT (MET-LIN-GYIN)

No.	Element	Measuring value (%)
1.	Potassium	0.8869
2.	Calcium	0.5692
3.	Silicon	0.4154
4.	Chlorine	0.1469
5.	Aluminum	0.0945
6.	Phosphorus	0.05580
7.	Titanium	0.01159
8.	Sulfur	0.01151

According to above table, the pulp of Baobab fruit was found to have the relatively high amount of potassium (0.8869 %) and a fair amount of calcium (0.5692 %), silicon (0.4154 %) and chlorine (0.1469 %) respectively.

D. Determination of Ascorbic Acid Content in Pulp of Baobab Fruit (Met-lin-gyin)

TABLE III. TITRATION OF 25 ML FRESH JUICE SAMPLE OF MET-LIN-GYIN FRUIT (PULP) WITH 0.0057 M IODINE SOLUTION

Indicator-starch

No.	Initial volume(cm^3)	Final volume(cm^3)	Used volume (cm^3)
Rough	0	20	20
1	0	19	19
2	0	19	19
3	0	18	18

E. Titration of Met-lin-gyin (Pulp) Sample Juice with I2 Solution

Sample juice 25mL = I_2 19mL × 0.0057M
= 0.1083 mmol of I_2
= 0.1083 mmol of ascorbic acidin sample
= 0.1083×10^{-3} mol × 176 g mol^{-1}
= 0.0 1906 g ascorbic acid

sample juice 25 mL _____ascorbic acid 0.01906 g
sample juice 250 mL_____

$$\frac{250' \ 0.01906}{25}$$

= 0.1906g
= 0.1906×10^3 mg
= 190 mg

∴Content of ascorbic acid = 190 mg/100 g

F. Determination of Antioxidant Activity of Met-lin-gyin (Baobab) Fruit

Antioxidant activities of samples were expressed as percentage of DPPH radical inhibition and IC50 value (□g/mL). IC50 values of the samples were calculated from the concentration Vs percent inhibition curve. Values of ascorbic acid and Met-lin-gyin fruit in percentage ranged from 48.25 to 60.82 and from 46.75 to 50.76 respectively. The results of antioxidant activity using DPPH method in Met-lin-gyin fruit using ascorbic acid as a positive control are shown in Table IV and V.

TABLE IV. ABSORBANCE VALUES AND % INHIBITION OF STANDARD ASCORBIC ACID

Ascorbic Acid	Std. 1	Std. 2	Std. 3	Std. 4	Std.5
Concentration of(□g/mL)	0.25	0.5	1	2	4
Absorbance	0.3459	0.3422	0.3257	0.2915	0.2619
Inhibition (%)	48.25	48.80	51.27	56.39	60.82

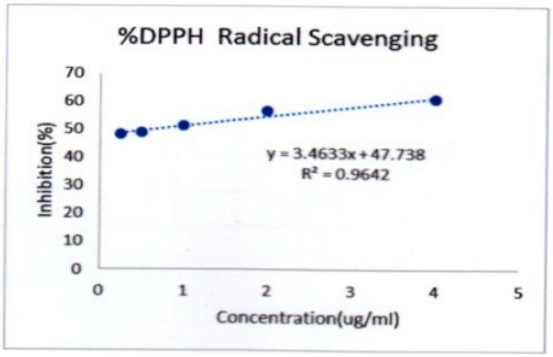

Fig. 4. Plot of % inhibition Vs concentration of standard ascorbic acid

TABLE V. ABSORBANCE VALUES AND % INHIBITION OF MET-LIN-GYIN FRUIT SAMPLES POWDER

Met-lin-gyin Powder	Test 1	Test 2	Test 3	Test 4	Test 5
Concentration (μg/mL)	15.62	31.25	62.5	125	250
Absorbance	0.3359	0.3499	0.3462	0.3352	0.3291
Inhibition (%)	46.75	47.65	48.21	49.85	50.76

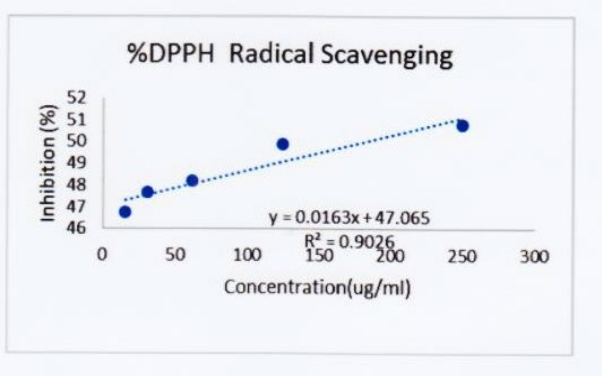

Fig. 5. Plot of % inhibition Vs concentration of Met-lin-gyin fruit powder

TABLE VI. IC50 VALUES OF STANDARD ASCORBIC ACID AND FINELY MET-LIN-GYIN FRUIT POWDER

Test samples	**IC_{50} values (µg/mL)**
Ascorbic Acid	0.65
Finely Met-lin-gyin fruit powder	18.06

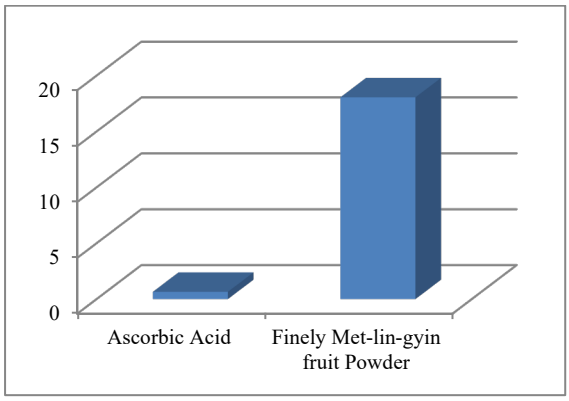

Fig. 6. C_{50} values of standard ascorbic acid and finely Met-lin-gyin fruit powder

IV. CONCLUSION

Vitamin C requirements for wound repair, normal heating processes, and trauma are based upon its role in collagen synthesis and fiber cross-linking. Stimulation all the immune system by vitamin C account for it use in the prevention and treatment of infections. In this research was Baobab (Adansonia digitata Linn.), a tree plant belonging to the Malvaceae family is widespread throughout the hot, drier regions of tropical and which may live for hundreds of years. Baobab fruit crude extract gives positive test for glycoside, protein, polyphenol, phenolic, reducing sugar, flavonoid, terpene, saponin, alkaloid and tannins respectively. The moisture and ash content of Baobab fruit sample was found to be 89.96 % and 4.5 %. The mineral content of Baobab fruit contains Ca, K, Al, Si, P, S, Cl, and Ti. And also, the ascorbic acid content in Baoba fruit was 190 □g/100g. IC50 value was 18.06 □g/ml compare to that of standard ascorbic acid which was 0.65 □g/mL. Baobab fruit (Met-lin-gyin) contains large amount of vitamin C. Ascorbic acid (vitamin C) increases the absorption of iron from the intestines and improves iron nutrition. It also acts an antioxidant activity and essential nutrient for health maintained.

ACKNOWLEDGMENT

We would like to express our deep gratitude and sincere thanks to Prorector Dr Si Si Khin and Dr Tint Moe Thu Zar, Yadanabon University, for their encouragement and permission for this research work. We also wish to express our profound gratitude to Dr Hlaing Hlaing Myat, Professor and Head of Chemistry Department, Yadanabon University, for her help to measure the experimental data.

REFERENCES

[1] www./ en.wikipedia.org/ wiki/ Adansonia. Digitata.
[2] www.crps forthefurter.org/ publication/ Monographs/ Baobab monograph.pdf.
[3] www.Africa Journal of Food Science Vol.5 (16) pp. 833-844.
[4] B. Aparna,"A Textbook of Practical Plant Chemistry", first Edition, 5. Chaud and Company Ltd, 2000.
[5] W. Williams, M. E. cuvelier and C. Berset, "Use of a Free Radical Method to Evaluate Antioxidant Activity" LWT-Food Sci Technol, 28, 25-30, 1995.
[6] J. B. Harborne, "Phytochemical Methods: A Guide to Modern Techniques of Plant Analysis", Chapman and Hall Ltd. USA, 1993.
[7] Stipulae Johnvanhulst. Com/ DocS/ PDF/ Hepatoprotective Influence of Adansonia Digitata Pulp. Pdf.
[8] San Khin, "Some medicinal and useful plants, both Indigenous and Exotic of Burma", 1st Edition, 1970.
[9] Tin Wa, Maung. Phytochemistry Screening: Method and Procedure Phytochemical Bulletin of Botanical Society of America. Inc. 5 (3): 4.10, 1992.
[10] Al. Vogel, "A Text Book of Quantitative Inorganic Analysis", 3rd Edition, Longman Group Limited, 1971.

Article ID – JRA6001520

Study on Water Quality Analysis in Some Areas of Upper Myanmar

Nyein Thida
Department of Physics
University of Yangon, Myanmar
nyein151270@gmail.com

Shwe Sin Oo
Department of Physics
Panglong University, Myanmar
77floralshwesin@gmail.com

Myo Min Thein
Department of Physics
Maubin University, Myanmar
mminntheinn@gmail.com

***Abstract*—The objective of the research paper was to measure some physicochemical parameters and elemental concentration of three water samples from different water sources at Chin State and Magway Division in upper Myanmar. And then, water quality indices for measured parameters were calculated to assess the quality of water in these areas. Some physicochemical parameters of collected water samples were examined at ALARM Ecological Laboratory situated in Kamayut Township, Yangon and elemental analysis were done at the university research center (URC), University of Yangon. Due to the study results, dissolved oxygen for water sample-2 is 7.7 mg/L and it was higher than the allowed value "5" set by the Indian Council of Medicine Research (ICMR). The rest of the obtained physicochemical parameters were well below the standard values of drinking water guidelines (WHO). For metals concentration, the amounts of lead (Pb) for all samples were higher than the permissible values of WHO, guidelines and iron content for all samples was nearly closed to the standards of water quality guidelines. The value of WQI for sample-1 was 65.513, for sample-2 was 55.341 and sample-3 was 58.698. All sample water sources were poor quality ratings according to calculated WQIs. So, three water sources are not suitable for not only domestic usage but also drinking purpose without treatment.**

Keywords*—*water quality, physicochemical parameters, elemental concentration, water quality index.

I. INTRODUCTION

Water is a crucial environmental factor for all lives all over the world. Through the world, ocean water is 97% and freshwater is only 3%. Good quality of drinking water is an essential requirement for good health and thus, we have healthy, happy lives and a good standard of living. But in most countries, water sources are being contaminated due to human activities, urbanization, increase in industries and growth of population. So, water sources in most places are continuously deteriorated. Similarly, in our country, the quality of drinking water gets worst to deforestation, mining condition and gold production. And hence, water sources in our country are under threat and necessary to analyze water quality continuously and build up the monitoring system for water management. Therefore, physicochemical parameters and some concentration of elements were determined and then the obtained results were compared with guidelines for drinking water standards set by WHO. Finally, water quality indices for all water samples were calculated to determine the quality of water in this study area.

II. EXPERIMENT

A. Study area

Three sampling sites were selected in one place of Chin State and two places of Magway Division in Upper Myanmar.

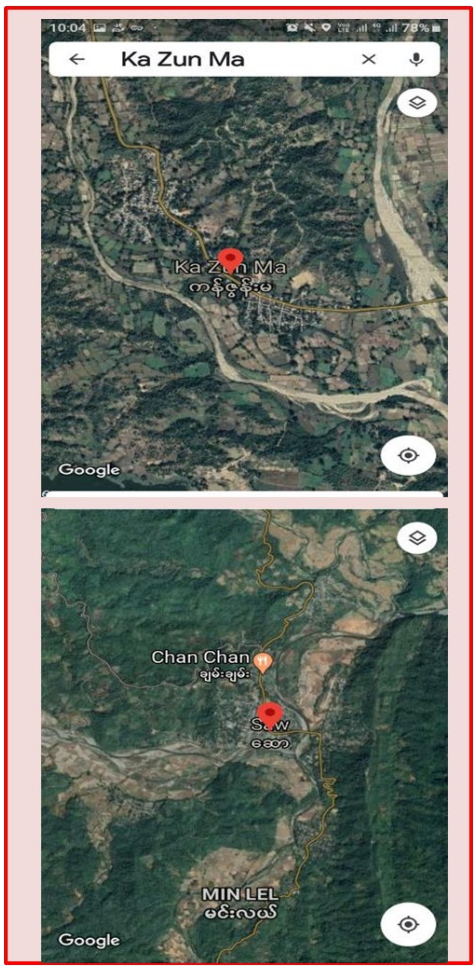

Fig 1. Map of Study Area

Water samples were collected from each site to assess it for a period of "February 2020". One water sample was collected round about 9:30 am on the 21st of February and two samples were collected at 11:15 am on 22nd of February using dry and clean plastic bottles.

Water samples were taken from three different sources and all water sources are used as domestic usage.

Sample 1(surface water): Kanpetlet township, Mindat District, Chin State. (20º 12' 1" N 94º 1' 0" E)

Sample 2(surface water): Saw township, Gangaw District, Magway Division. (21º 13' N 94º 12' E)

Sample 3(surface water): Kanzunma village, Seikphyu township, Pakokku District, Magway Division. (21º 01' N 94º 24' 39" E)

B. Experiment apparatus

The selection of suitable sample container is also of utmost importance for the analysis of water. Normally, plastic or glass may be preferred for containing and storing of sample water. Before using, sampling plastic (polyethylene) should be washed and rinsed first with tap water and then these bottles were dried under room temperature. After that, they were carried to the sampling area. Two water samples were collected from different sources in two townships at Magway Division and one sample was collected from a township at Chin State. Samples were collected in prepared, clean and dry plastic bottles that were fitted with covers and then these bottles were put in a box that cannot be entered any effects like sunlight. After that, all water samples were brought into laboratory for the measurement of various parameters.

Fig 2. Collected water sample bottles.

C. Analysis of Water Sampling

In this study, analyzed parameters were distinguished into two parts: (i) physicochemical parameters such as pH and (ii) chemical characteristics of water parameters like of arsenic. To determine physicochemical parameters, all water samples were brought to ALARM Ecological Laboratory. HANNA HI 98129, 98130 testers with electrode method was used to measure pH and EC. Lovibond Spectro Direct was used to measure turbidity, alkalinity and hardness. TDS meter was used to find value of TDS. Electrochemical Probe method was used Dissolved Oxygen measurement. To measure chemical characteristics of water parameters, sample water bottles were sent to the university research centre (URC) at the University of Yangon and high-performance PinAAcle™ 900H S/N PHCS16091301 Atomic Absorption Spectroscopy AAS was used to analysis.

D. Data

TABLE I. PHYSICOCHEMICAL PROPERTIES OF WATER SAMPLES FROM STUDY AREA IN UPPER MYANMAR. [1] [2] [3]

Sr No	Parameters	Standard Values S_i WHO (2011)	Measured results		
			Chin State		Mgway Division
			Sample-1	Sample-2	Sample-3
1	pH	6.5-8.5	7.4	7.2	7.3
2	Turbidity	< 5	< 5	< 5	< 5
3	TDS	500	392	11	133
4	Conductivity	2500	700	20	200
5	Hardness	200	160	91	113
6	Dissolved Oxygen	5(ICMR)	4.32	7.7	6.4
7	Alkalinity	120 (WPCSR)	211	113	148

All parameters' values are expressed in mg/L except pH, turbidity (NTU), electrical conductivity (µS cm-1).

WPCSR (Water Pollution Control Statement of Regulation Turkish) ICMR = Indian Council for Medical Research

According to the above table (1), pH values of all water samples range from 7.2 to 7.4. Three sources deviate slightly from neutral water pH of 7 but these values are within the standard value of WHO guidelines. Similarly, turbidity of water is valid for standard value due to the results getting from the laboratory.

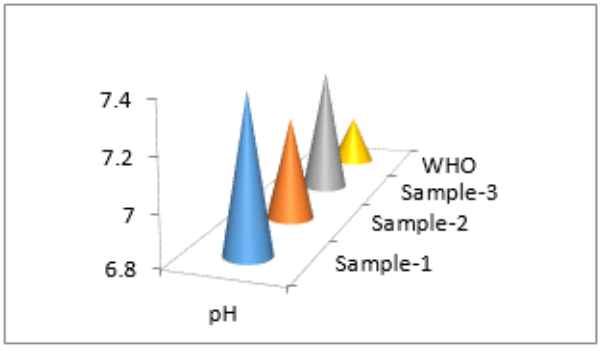

Fig 3. The results of pH for all water samples.

Total dissolved solids (TDS) means the amount of dissolved minerals. TDS meter by electrode method was used to analyze. From the values of TDS, the least TDS value is 11 mg/L and the most is 392 mg/L respectively.

Reported values of TDS are well below the WHO standard. The permissible limit for TDS is 500 mg/L. The result data means that the concentration of dissolved mineral is not a dangerous condition for water users because it is under the permissible limit.

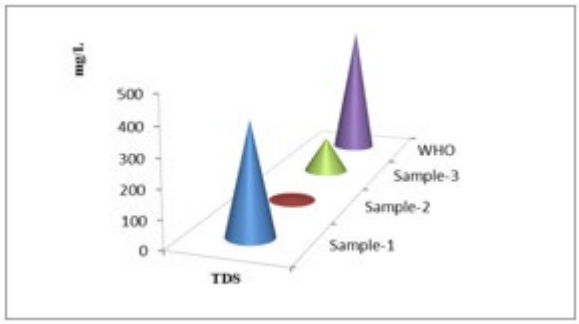

Fig 4. Comparison of TDS with WHO standard.

The measured conductivities of water are presented in table (1). The maximum value is 700 µS/cm and the minimum is 20 µS/cm. The standard value for conductivity is 2500 µS/cm. Conductivity means the amount of dissolved ionic components in different kinds of water. The result gives that the water from Saw Township, Magway Division has little solute dissolution.

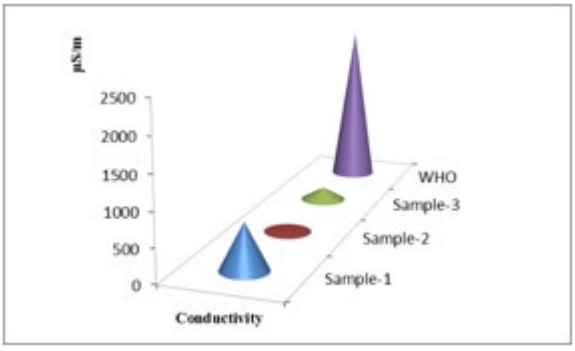

Fig 5. The measured results of conductivity.

The value of hardness for water from Saw Township is 160 mg/L, water from Kanpetlet Township is 91 mg/L and water from Kazunma village is 113 mg/L. The measured values are very far below the drinking water quality guidelines set by WHO. In general, the observed values for alkalinity are within the Water Pollution Control Statement of Regulation Turkish (WPCSR).[3]

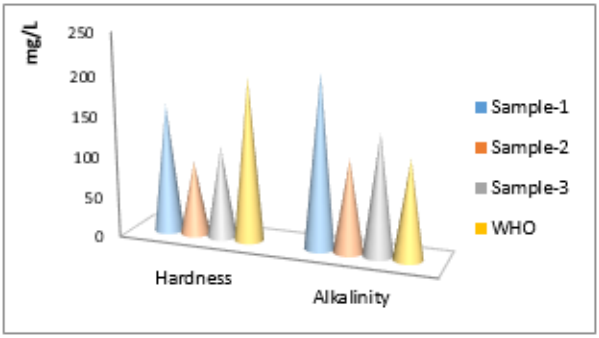

Fig 6. Hardness and alkalinity values for all water sources.

In studying the results of dissolved oxygen for all water samples, dissolved oxygen for water sample-2 is 7.7 mg/L and it is higher than the allowed value "5" set by Indian Council for Medical Research (ICMR). The rest of the two samples are under the limitation of ICMR.

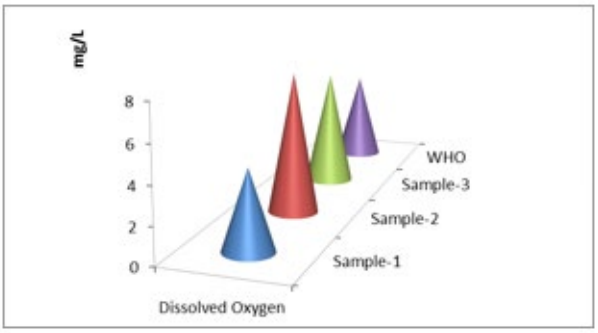

Fig 7. The amount of dissolved oxygen in three water samples compared with WHO standard.

TABLE II. THE ACHIEVED RESULTS OF HEAVY METALS FOR THREE WATER SAMPLES COLLECTED FROM A STUDY AREA. [1] [4]

Sr No	Parameters	Standard Values S_i WHO (2011)	Measured results		
			Chin State		Magway Division
			Sample-1	Sample-2	Sample-3
1	Arsenic	0.01	0.00093	ND	0.00015
2	Cadmium	0.003	0.00003	0.00002	0.00003
3	Lead	0.01	0.035	0.030	0.032
4	Copper	2	0.030	0.049	0.038
5	Cromium	0.05	ND	ND	ND
6	Iron	1	0.954	0.964	0.959
7	Zinc	5	0.164	0.164	0.165
8	Magnesium	30	1.279	0.230	2.136
9	Calcium	100	32.860	0.941	35.300
10	Potassium	100	ND	ND	0.040

All parameters were measured in mg/L.

In this paper, elemental concentration was divided into two parts such as heavy metal (As, Cd, Pb) and dissolved metals (Cu, Cr, Fe, Zn, Mg, Ca and K). The amount of arsenic (As) in sample-2 was not detected using AAS method and also arsenic concentrations for the rest of the samples are lower than the WHO standard. This is a very lucky condition for the people in this area. Similarly, cadmium contents in water samples were very lower than the permissible values limited by WHO. But lead concentrations in all water sites were greater than the value of the WHO permissible limit. For all water samples, the concentration of chromium is not detected and concentration of potassium for sample-1 and 2 are not detected. Among 10 parameters, iron concentrations for three samples are closed to the allowed limits of the WHO. The other measured values are well below the standard values set by the WHO.

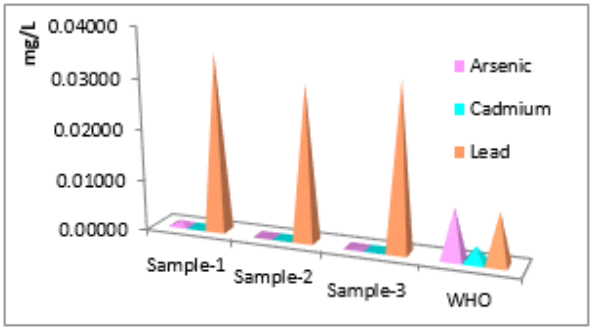

Fig 8. Concentration of arsenic, cadmium and lead for all water sources.

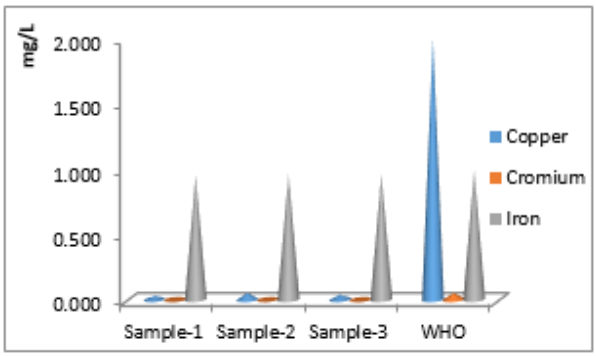

Fig 9. Concentration of copper, chromium and iron for all water sources.

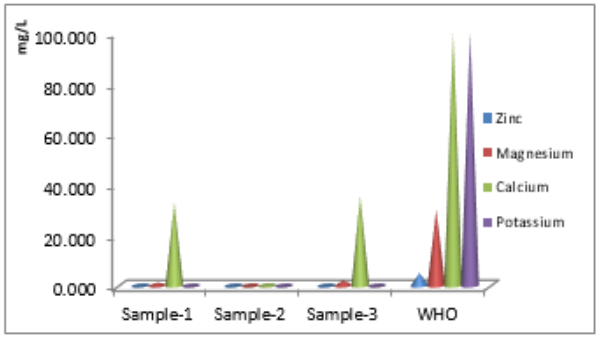

Fig 10. Concentration of zinc, magnesium, calcium and potassium for all water sources.

III. ANALYSIS

A. Water quality index (WQI)

The index is among the most effective and efficient method to communicate the information on water quality trends to the policymakers and decision makers in water quality monitoring. WQI shows a useful representation of the overall quality of water for the healthy use of public. For the evaluation of WQI, various parameters namely pH, electrical conductivity (EC), hardness, turbidity, total dissolved solid (TDS), alkalinity, cadmium, lead, copper, zinc, potassium, sodium and calcium were analyzed to assess.

For computation of the values of water quality index, the following steps must be used. (Horton 1965). [5]

(i) First Step

In the first step, each of thirteen parameters has been computed as a weight (wi) according to its relative equation used in the overall quality of water for drinking uses. [Mufid al-hadithi,2012]

$$W_i = \frac{Relative\ constant}{Standard\ values\ of\ i^{th}\ parameters}$$

(ii) Second Step

In the second step, the relative weight (Wi) is calculated using a weighted arithmetic method. [Brown et al., 1972, Horton, 1965]

$$W_i = \frac{w_i}{\sum_{i=1}^{n} w_i}$$

In above equation, Wi is the relative weight, w_i is the weight of each parameter and "n" is numbers of measured parameters.

(iii) Third Step

In the third step, a quality rating scale (Qi) for ith water quality parameter was computed the following equation.

$$Q_i = 100 \times [\frac{C_i}{S_i}]$$

In above equation, C_i is the concentration of each parameter in each water sample (measured data) and S_i is the drinking water standards by WHO. In table-2, the measured values of thirteen parameters for three water samples and standard permissible values according to WHO were described.

(iv) Fourth Step

Before calculating WQI values, the value of SI is first computed for each parameter to assess the quality of surface water in this region. To determine SI, the following equation was used.

$$SI_i = W_i \times Q_i$$

where, SIi is sub index of ith parameter and Qi is the quality rating based on the concentration of ith parameter.

Finally, calculation of WQI, a single number for all water quality, was made using a weighted arithmetic method in the following step.

$$WQI = \sum SI_i$$

Calculated water quality index of water samples is usually distinguished into five categories shown in table-3.

TABLE III. WATER QUALITY RATING AND WQI VALUES. [7]

WQI value	Rate of Water Quality
0-25	Excellent
26-50	Good

51-75	**Poor**
76-100	**Very Poor**
Above 100	**Unfit for Drinking Purpose**

B. Results of Water Quality Index (WQI)

TABLE IV. THE CALCULATED VALUES OF WATER QUALITY INDICES FOR THREE WATER SAMPLES.

Sr No	Parameters	Calculated results					
		Chin State		Mgway Division	Chin State		Mgway Division
		Sample-1 q_i	Sample-2 q_i	Sample-3 q_i	Sample-1 wi qi	Sample-2 wi qi	Sample-3 wi qi
1	pH	26.67	13.33	20	0.00564688	0.00282238	0.00423463
2	Turbidity	-	-	-	-	-	-
3	TDS	78.4	2.2	26.6	0.00028231	7.9219E-06	9.5783E-05
4	Conductivity	28	0.8	8	2.0165E-05	5.7614E-07	5.7614E-06
5	Hardness	80	45.5	56.5	0.00072018	0.0004096	0.00050862
6	Dissolved Oxygen	107.083	71.875	85.417	0.03855929	0.02588132	0.03075763
7	Alkalinity	175.83	94.16	123.33	0.00262754	0.00140709	0.001843
8	Arsenic	9.3	-	1.5	1.67440866	-	0.27006591
9	Cadmium	1	0.667	1	0.60014647	0.4002977	0.60014647
10	Lead	350	304	320	63.0153795	54.7333582	57.6140613
11	Copper	1.5	2.45	1.9	0.00135033	0.00220554	0.00171042
12	Cromium	-	-	-	-	-	-
13	Iron	95.4	96.4	95.9	0.17176192	0.17356236	0.17266214
14	Zinc	3.28	3.25	3.3	0.00118109	0.00117029	0.00118829
15	Magnesium	4.263	0.767	7.12	0.00025584	4.6031E-05	0.0004273
16	Calcium	32.86	0.941	35.3	0.00059162	1.6942E-05	0.00063556
17	Potassium	-	-	0.04	-	-	7.2018E-07
				WQIs	65.5129318	55.341186	58.6983435

To get WQIs for three samples, four steps mentioned in the above section were used in this calculation. By noting table-4, three kinds of WQIs of water samples were higher, and they were within the rate of poor water quality by table-3. Except concentration of lead, all other parameters and calculated data were very low. Higher concentration of lead can cause greater values of WQIs for all water samples and in addition it made poor quality water sources. Therefore, water samples in this study area were not safe for drinking purpose.

IV. CONCLUSION

Physicochemical parameters such as pH, turbidity, TDS, conductivity, hardness, dissolved oxygen and alkalinity and chemical parameters (As, Cd, Pb, Cu, Cr, Fe, Zn, Mg, Ca and K) of three water samples were studied in this paper. From the point of physicochemical parameters, only one parameter, dissolved oxygen of water sample-2, is greater than the drinking water standard set by ICMR. But it is not very distinct in calculation of WQIs. In addition, one chemical parameter, lead, was dissolved in larger amount than the allowed values in all samples. Larger content of lead (Pb) can cause greater value of WQI and so on poor quality of water. The molarities of potassium for sample-1 and 2 were very much less than the detective limits and it was not good for the health of the residents because potassium is one of the essential trace elements for human health. In short, all water samples studied in this paper were not safe for drinking water but it can be used for other purposes.

ACKNOWLEDGEMENT

I would like to thank Dr Khin Khin Win, Professor and Head, Department of Physics, University of Yangon, for her kind permission and encouragement to carry out this work. I also would like to express my gratitude to all Professors at Department of Physics, University of Yangon, for their kind and encouragement to undertake this research paper.

REFERENCES

[1] World Health Organization, Ed., *Guidelines for drinking-water quality*, 4th ed. Geneva: World Health Organization, 2011.
[2] "Hard water," *Wikipedia*. Sep. 12, 2020, Accessed: Sep. 16, 2020.
[3] R. K. Horton, 'An Index Number System for Rating Water Quality,' Journal of the Water Pollution Control Federation, Vol. 37, No. 3, 1965, pp. 300-306.
[4] Cadmium (EHC 134, 1992).
[5] "AJER." http://www.ajer.org/v5(10).html (accessed Sep. 16, 2020).

Article ID – JRA6001720

Study on Effect of Additional Fe Ions on Structural Features and Optical Bandgaps of TiO_2 Anatase

SapaiAung
Department of Engineering Physics
Technological University
Taunggyi, Myanmar
sapaiaung099@gmail.com

Sandar Aung
Department of Physics
University of Information Technology
Yangon, Myanmar
sandaraung@uit.edu.mm

Moe Moe Aye
Department of Engineering Physics
Technological University
Taunggyi, Myanmar
moemoeayetg@gmail.com

Pwint Yi Thein
Department of Physics
Nationalities Youth Resource Development Degree College
Yangon, Myanmar
susan74june@gmail.com

***Abstract*— Additional Fe ions substituted metal oxide material TiO_2 anatase is studied by means of its structural features and optical bandgaps. Analar grade TiO_2 anatase and Fe_3O_4 are used as starting materials in this research work. Fe substituted TiO_2 anatase structures are prepared by conventional solid state sintering. TiO_2 and Fe_3O_4 are mixed by the stoichiometric equation: (1 - x) TiO_2 + (x) Fe_3O_4, where x = 0, 1 mol%, 2 mol%, 3 mol%, 4 mol% and 5 mol% respectively. Mixing, grinding and sintering processes, known as standard ceramic preparation procedure, are performed to obtain the homogeneous TiO_2: Fe structures. X - ray diffraction studies are carried out to examine the phase formation and structural features of the TiO_2: Fe structures. Then, lattice constants, lattice distortion, unit cell volume, crystallize size and lattice micro strain of TiO_2: Fe structures are examined. XRD results indicate that, there are no significant changes of tetragonal TiO_2 anatase structure after Fe substitution, due to incorporation of Fe ions with the crystal lattice of TiO_2. Optical bandgaps of TiO_2: Fe structures are investigated by UV - Vis spectrophotometric method. It is observed that, optical bandgap is lowered by increase of Fe ions content in TiO_2 anatase. TiO_2: Fe structures are potential candidates for photocatalytic and hydrogen production applications, due to reducing its bandgap and it is also expected to increase the efficiency of absorbing visible light**.

Keywords*— *TiO_2 anatase, Fe ions, structural features, bandgap.

I. Introduction

Titanium dioxide TiO_2 is a well multifunctional metal oxide material because of its wide range of applications and benign properties such as high photocatalytic activity, high thermal and chemical stability, and nontoxicity. The wide range of use of TiO_2 is due to its unique electronic and structural properties. TiO_2 exists in three main crystallographic forms: anatase, rutile and brookite. One of three forms, anatase is found to be able to decompose water molecules to hydrogens and oxygens under ultraviolet (UV) irradiation. Many organic pollutants such as dyes can be degraded by TiO_2. To use TiO_2 as a photocatalyst, it is necessary to induce them by light irradiation with energy level higher than their bandgap energy. However due to high bandgap of TiO_2 (> 3 eV), its optical applications is limited to UV region of electromagnetic spectrum. Doping opens up the possibility of changing the electronic properties of TiO_2, altering their composition and optical properties. Much effort has been made by incorporating doping with metal ions, such as nickel, chromium, iron, vanadium, and zinc [1] [2] [3] [4] [5].

Iron metal ions have been considered as suitable candidate for doping owing to the facts that, ionic radius of both Fe^{3+} (0.64 Å) and Ti^{4+} (0.68 Å) is similar size. Therefore, it can be easily incorporated with the crystal lattice of TiO_2 [6] [7] [8]. One of the advantages of inclusion of Fe into TiO_2 lattice is its potential application in photo-catalysis and hydrogen production due to reducing the energy gap of TiO_2 and increasing the efficiency of absorbing visible light [9]. Additional Fe ions substituted TiO_2 anatase structures are examined by means of its structural features and optical bandgaps in this research work.

II. Experimental Procedure

A. Preparation

Analar grade TiO2 anatase and Fe3O4 are chosen and used as starting materials. TiO2 anatase and Fe3O4 are weighted and mixed by the desired composition, (1- x) TiO2 + (x) Fe3O4, where x = 0, 1 mol%, 2 mol%, 3 mol%,

4 mol% and 5 mol%. The mixtures are grinded by using ball - milling process for each 3 hrs. Then, the mixtures are conventional sintered at 500oC for each 3 hrs. After first sintering process, the mixtures are grinded again by ball - milling process for each 3 hrs. Furthermore, the mixtures are conventional sintered at 700oC for each 3 hrs.

B. Characterization

X - ray diffraction studies are carried out to investigate the phase formation and structural features of TiO2: Fe by means of Rigaku Multiflux with Cu Kα (λ = 1.5418Å) monochromatic radiation. The TiO2 : Fe specimens are scanned from 2 θ (θ = Bragg angle) in the range from 10° to 70° with a step size of 0.01°/ sec. X - rays spectra are recorded at room temperature and applied voltage and current of XRD machine are set to be 50 kV and 40 mA. From the x - rays spectra, lattice constants, lattice distortion, unit cell volume, crystallite size and lattice micro strain are studied. Optical properties of TiO2: Fe specimens are examined by using UV - Vis spectrophotometer (UV 1800 Shimadzu) in the wavelength from 190 nm to 700 nm with 1.0 nm resolution and wavelength accuracy is ± 0.01 nm. UV 1800 consists of deuterium: tungsten halogen lamp source and UV probe software is attached. From the UV absorption spectra, optical bandgaps of TiO2: Fe specimens are evaluated.

III. Results And Discussion

A. X - Rays Diffraction Spectra of TiO_2

Fe specimens are shown in Fig. 1. Peak search and identify algorithm, known as Jade software is used in this study. Only diffraction peaks from single phase, tetragonal, polycrystalline TiO2 anatase (71 - 1169 > JCPDF) reference, are observed. In addition, (101) peak is the most intense peak and a little shift of (101) peak is found in all spectra. Covalent radius of Fe (132 pm) is relatively smaller than covalent radius of Ti (160 pm). These results indicate that additional Fe ions are incorporated into Ti site. Furthermore, sharp peaks are examined in all spectra, due to better crystallinity of TiO2: Fe specimens. From the x - rays spectra, lattice constants of TiO2: Fe specimens are calculated by using the following equation (1):

$$\frac{1}{d^2} = \frac{h^2+k^2}{a^2} + \frac{l^2}{c^2} \quad (1)$$

d = interplanar spacing

h , k , l = miller indices

a, c = lattice parameters

Unit cell volumes of the TiO_2: Fe specimens are determined by using the following equation (2):

$$\text{Unit cell volume} = a \times a \times c \quad (2)$$

where a, c = lattice parameters

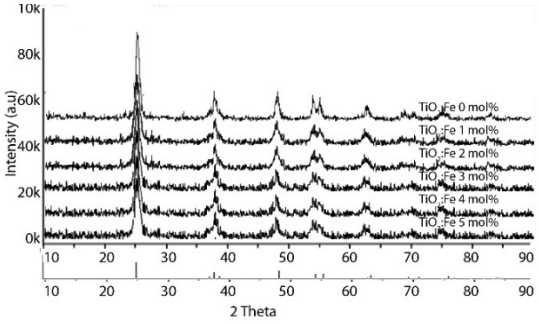

Fig. 1. XRD spectra of: (a) TiO_2: Fe (0 mol%) specimen (b) TiO_2: Fe (1 mol%) specimen ,(c) TiO_2: Fe (2 mol%) specimen (d) TiO_2: Fe (3 mol%) specimen ,(e) TiO_2: Fe (4 mol%) specimen (f) TiO_2: Fe (5 mol%) specimen

Lattice constants, lattice distortion and unit cell volume of TiO_2: Fe specimens are listed in table (1).

TABLE I. LIST OF LATTICE CONSTANTS, LATTICE DISTORTION AND UNIT CELL VOLUME OF TiO_2 : FE SPECIMEN

Fe Concentration (%)	Lattice Parameter "a(Å)"	Lattice Parameter "c(Å)"	Lattice distortion	Cell volume ($x10^{26}m^3$)
0	3.765	9.510	2.526	134.833
1	3.766	9.508	2.524	134.883
2	3.769	9.507	2.522	135.064
3	3.770	9.506	2.521	135.145
4	3.733	9.504	2.518	135.344
5	3.778	9.502	2.525	135.633

B. Crystallite Size and Lattice Micro Strain of TiO_2

Fe specimens are examined by using the Debye - Scherrer equations (3) and (4):

$$D = \frac{0.9\,\lambda}{\beta cos\theta} \quad (3)$$

$$\varepsilon = \frac{\beta}{4tan\theta} \quad (4)$$

In these equations, β is full width at half of the most intense peak maximum (FWHM) and λ is the wavelength of the using X-ray and θ is the peak position which is known as Bragg's angle. Crystallite size and lattice micro strain of TiO_2: Fe specimens are listed in Table II.

TABLE II. LIST OF CRYSTALLITE SIZE AND LATTICE MICRO STRAIN OF TIO2 FE SPECIMENS.

Fe Concentration (mol%)	Crystallize Size (nm)	Micro Strain (με)
0	29.34	3.673x10-3
1	29.16	3.816x10-3
2	28.85	3.407x10-3
3	28.71	3.425x10-3
4	28.56	3.451x10-3
5	28.34	3.486x10-3

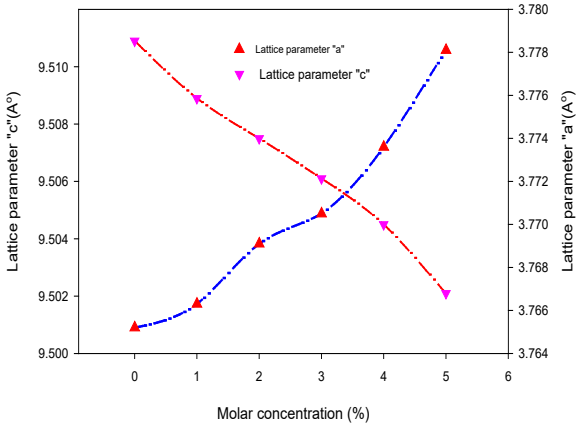

Fig. 2. Influence of Fe content on lattice constants of TiO_2 specimens.

Fig.2 shows the influence of Fe content on lattice constants of TiO_2 specimens. It is observed that lattice constant "a" increases as Fe content increases, while lattice constant "c" is lowered.

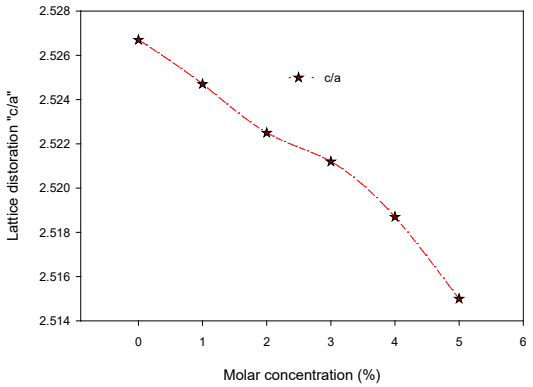

Fig.3. Variation of Fe content with lattice distortion of TiO2 specimen.

Fig.3. depicts the variation of Fe content with lattice distortion of TiO_2 specimen. It is found that lattice distortion (c/a) decreases as Fe content increases in TiO_2 specimens.

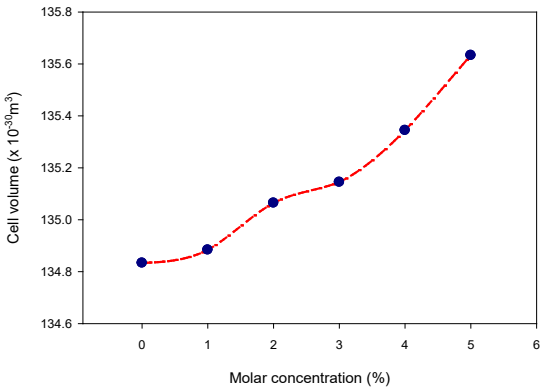

Fig.4. Effect of Fe content on unit cell volume of TiO_2 specimen.

Fig.4 illustrates the effect of Fe content on unit cell volume of TiO_2 specimen. It is obvious that, unit cell volume slightly increases when Fe content is raised. In TiO_2 anatase, lattice distortion (c/a) is ~ 2.5 and that causes the micro strain during the sintering process. In addition, additional Fe ions create the dislocations, vacancies and defects in host TiO_2. These results can be interpreted as variation of Fe content on structural features of TiO_2 is observed. There are no considerable changes of tetragonal TiO_2 anatase structure after Fe addition, due to additional Fe ions are diluted into host TiO_2 anatase structure. Optical absorption spectra of TiO_2: Fe specimens are depicted in Fig. 5.

The optical bandgap measurement consists of the excitations of electrons from valence band to conduction band using photons of selected frequencies. The process does not change the number of carriers involved. The optical bandgap is the energy difference between the top of the valence band bottom of the conduction band. Electrons are generally able to jump from one band to another as long as a specific minimum amount of energy for the transition, the bandgap energy, is provided.

From the absorption spectra, bandgaps of TiO_2: Fe specimens are examined by using the following equation (5), and listed in Table III.

$$E_g = \frac{hc}{\lambda} \tag{5}$$

where h = Planck 's constant

c = speed of light

and λ = wavelength, peak value from absorption spectrum, in nm

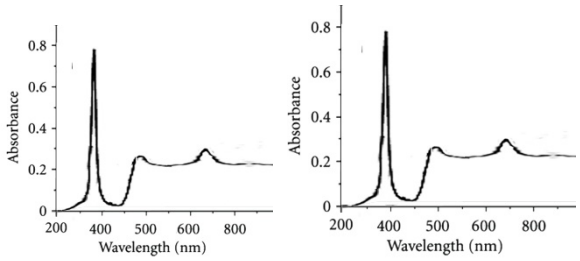

(a) Fe (0 mol%) (b) Fe (1 mol%)

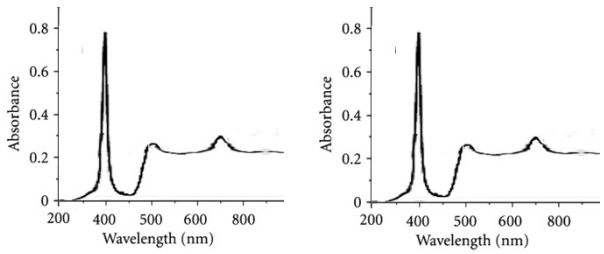

(c) Fe (2 mol%) (d) Fe (3 mol%)

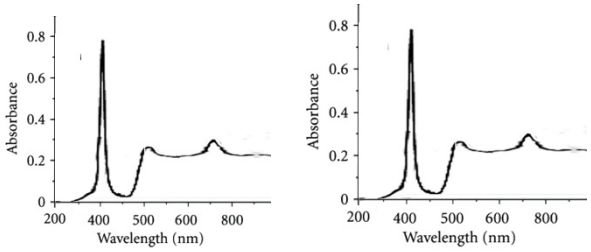

(e) Fe (4 mol%) (f) Fe (5 mol%)

Fig.5. UV-Vis absorption spectra of TiO_2:Fe specimens

TABLE III. LIST OF OPTICAL BANDGAPS OF TIO2: FE SPECIMENS.

Fe Concentration (mol %)	Peak value from absorption spectrum (nm)	Energy gap (eV)
0	376.37	3.28
1	382.19	3.23
2	386.99	3.19
3	391.90	3.15
4	396.94	3.11
5	403.43	3.06

It is studied that; optical bandgap decreases as Fe content increased in TiO_2 anatase. Decreasing energy bandgap and TiO_2: Fe specimens contributes to low recombination rate of the photo-generated electron-hole pairs, and leads to higher photocatalytic activity.

IV. CONCLUSION

Additional Fe ions substituted TiO_2 anatase is studied by means of its structural features and optical bandgaps. Fe substituted TiO_2 anatase specimens are prepared by conventional sintering and standard ceramic preparation procedure. XRD results reveal that there are no significant changes of tetragonal TiO_2 anatase structure after Fe addition. It is believed that additional Fe ions are incorporated into Ti site in host TiO_2 anatase structure. It is also found that optical bandgap decreases as additional Fe content increases. It is expected that, decreasing optical bandgap in TiO_2: Fe means the increase the efficiency in absorbing visible light for photocatalytic activity.

ACKNOWLEDGMENT

The authors would like to acknowledge the Universities ' Research Center (U R C), University of Yangon for XRD examinations and AMTT Co. for UV - Vis spectroscopy investigations.

REFERENCES

[1] M. Humayun, F. Raziq, A. Khan, and W. Luo, "Modification strategies of TiO2 for potential applications in photocatalysis: a critical review," *Green Chemistry Letters and Reviews*, vol. 11, no. 2, pp. 86–102, Apr. 2018.

[2] F, Han, V S R Kmbalar, M Srinivasan, D Rajaratham and R Naidu "Tailored Titanium Dioxide Photocatalysts for the Degradation of Organic Dyes in Wastewater Treatment: A Review".

[3] S. Yadav and G. Jaiswar, "Review on Undoped/Doped TiO2 Nanomaterial; Synthesis and Photocatalytic and Antimicrobial Activity," *Journal of the Chinese Chemical Society*, vol. 64, no. 1, pp. 103–116, 2017.

[4] A Zeleska, "Doped-TiO2: a review".

[5] O. Ola and M. M. Maroto-Valer, "Review of material design and reactor engineering on TiO2 photocatalysis for CO2 reduction," *Journal of Photochemistry and Photobiology C: Photochemistry Reviews*, vol. 24, pp. 16–42, Sep. 2015.

[6] Y. Yang, Y. Yu, J. Wang, W. Zheng, and Y. Cao, "Doping and transformation mechanisms of Fe3+ ions in Fe-doped TiO2," *CrystEngComm*, vol. 19, no. 7, pp. 1100–1105, Feb. 2017.

[7] M. Ghorbanpour and A. Feizi, "Iron-doped TiO2 Catalysts with Photocatalytic Activity," *Journal of Water and Environmental Nanotechnology*, vol. 4, no. 1, pp. 60–66, Jan. 2019.

[8] J. O. Carneiro *et al.*, "Iron-doped photocatalytic TiO2 sputtered coatings on plastics for self-cleaning applications," *Materials Science and Engineering: B*, vol. 138, no. 2, pp. 144–150, Mar. 2007.

[9] S B Eadi, S W Jeong and H W Jeon, "A novel preparation of iron-doped TiO2 nanoparticles with enhanced photocatalytic activity ".

Article ID – JRA6001920

Preparation of Chitosan/Glutaraldehyde/Silver Particle Composite Beads Using Biowaste Materials by Green Synthesis

Than Than Moe
Department of Chemistry
MSc Student
Meiktila University, Myanmar
thanthanmoe 22222@gmail.com

Zin Mar Aung
Department of Chemistry
Associate Professor
Meiktila University, Myanmar
zinmaraung181273@gmail.com

Khaing Su Wai
Department of Chemistry
Assistant Lecturer
Meiktila University, Myanmar
khaingsuwai.mtla@gmail.com

***Abstract*— This research has been focused on the preparation of chitosan/glutaraldehyde/silver particle composite beads (CS/glu/PPAgNPs) via synthesized value - added chitosan from waste shrimp shells and silver particle solution using biowaste materials especially pineapple fruit peels by green synthesis method for reducing of environmental pollution. The brown colour of synthesized pineapple peel silver nanoparticles solution (PPAgNPs) were confirmed by ultraviolet (UV) – Visible spectrophotometer and crystallite size of synthesized PPAgNPs were determined by X-ray diffractometer (XRD). Prepared chitosan and CS/glu/PPAgNPs composite bead were determined by Fourier Transform Infrared Radiation (FT IR) analysis and physicochemical properties viz. pH, moisture content, density and then solubility of prepared beads were also studied. The antimicrobial activity of prepared chitosan and CS/glu/PPAgNPs composite bead were also determined by agar well diffusion method. Synthesized CS/glu/PPAgNPs beads 0.3 g were used to remove 79.9756 % of 25 mgL^{-1} initial concentration of methylene blue (MB) dye in solution. The quality grade prepared CS/glu/AgNPs beads can be applied for water purification.**

Keywords*—Chitosan, Pineapple peels, Silver nanoparticles, Antimicrobial agents, Methylene blue dye

I. INTRODUCTION

In the present, all over the world have been challenged to environmental pollutions. Biowaste materials are caused for one of the factors for environmental pollutions. Many researches are interesting and focusing the nanotechnology highlights the possibility of green chemistry pathways to produce technologically important nanomaterials. Nanocomposite materials are very essential in the century because most of the fields have been applying in various kinds of patterns. It is one of the most widely used products in practice.

Chitosan is a non-toxic, biodegradable polymer of high molecular weight and very much similar to cellulose, a plant fiber. Chitosan is one of the world's most plentiful biopolymers produced from chitin using fungal species and exoskeleton of sea creatures such as crayfish, lobster, prawn, crab and shrimp. Use of chitosan as an ideal absorbent for dye removal has received much attention by researchers because of its relatively low cost and extraordinary absorption capability for dye removal [1].

Normally, biowastes comes from organic waste products from indoors and outdoors. The kitchen waste is mainly composed of organic matter collected in the kitchen. The fruits peels are especially easily available, efficient, affordable, eco-friendly, natural and also rich in bioactive compound. These bioactive compounds can be used as antioxidants and antimicrobial agents [2]. Pineapple peels contained phenolic compound, ferulic acid, vitamin A and vitamin C as antioxidants [3]. These compounds are mainly supported as reducing agent in the synthesis of silver nanoparticles for the reduction of silver ion to silver.

Metal nanoparticles which have a high specific surface area and a high fraction of surface atom have been studied extensively [4]. Smaller the size of the particles greater will be the aspect ratio i.e., greater surface area compared to their volume. This increased surface area of the smaller nanoparticles enhances the reactivity of the nanoparticles with the surrounding molecules. Silver nanoparticles are mainly synthesized by physical and chemical approaches, which are economically expensive and involve in chemical toxic. The biological synthetic approach for silver nanoparticles is advantageous over physicochemical method because it is simple, cost effective, environmental-friendly, and easy to scale up for mass production. Biowastes are commonly composed of different types of phytochemical compound which participate in the reduction of Ag^{+} to Ag^{0} and stabilization of silver nanoparticle by acting as a capping agent [5]. Green synthesis procedures have several merits such as, simple, inexpensive, good stability of nanoparticles, less time consumption, non-toxic byproducts and large-scale synthesis [6].

Silver nanoparticles are clusters of silver atoms in the size range of 1-100 nm [5]. Among all metal nanoparticles, AgNPs have great importance due to their application in

various fields such as nanomedicine, antimicrobial agent, in ground water purification [7].

In this research, prepared chitosan(CS) from shrimp shell and synthesized silver nanoparticle solution using waste ripe fruit pineapple peel (PPAgNPs) were mixed and glutaraldehyde (glu) was added as cross – linked agent to form CS/glu/PPAgNPs gel leading to CS/glu/PPAgNPs beads by green synthesis. Prepared chitosan and silver nanoparticle solution were determined by appropriate method. Prepared CS/glu/PPAgNPs beads were applied as antimicrobial agents as well as adsorbents which are removal of methylene blue (MB) dyes that is one of used in textile industry.

II. EXPERIMENTAL

A. Materials

In the research, prepared chitosan from biowaste material of shrimp shells and pineapple peels from pineapple fruits for using in the synthesis of silver nanoparticles were collected from Local Market in Meiktila Township, Mandalay Region in Myanmar. Chemical reagents of sodium hydroxide, hydrochloric acid and silver nitrate used were purchased from British Drug House (BDH) Co. Ltd.

B. Preparation of Chitosan from Shrimp Shells

For the preparation of chitosan, raw materials of shrimp shells were demineralized with 5 % hydrochloric acid at room temperature for about five days. After demineralization, deproteinization of that sample with 5 % sodium hydroxide was carried out for four days and finally, deacetylation process that convert chitin to chitosan were performed with 65 % sodium hydroxide for about seven days. Resulting chitosan was determined with physicochemical parameters such as pH by pH meter and moisture content by oven drying method. After the preparation of chitosan, calculation of yield percent was carried out and that prepared chitosan was determined by FT IR analysis.

Fig. 1. Raw shrimp shells

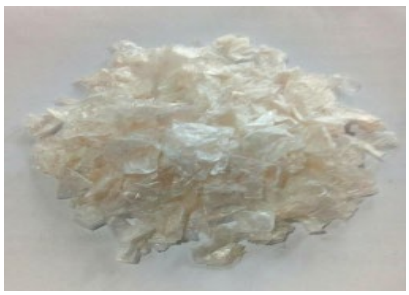

Fig. 2. Photograph of prepared chitosan

C. Synthesis of Silver Nanoparticles Using Pineapple Peel Extract

In the synthesis of silver nanoparticles, pineapple peels extract solution was firstly performed by 1:4 weight by volume ratio of pineapple peel pieces and deionized water. Then 3:10 volume by volume ratio of pineapple peels extract solution and 0.003 M silver nitrate solution were mixed with magnetic stirrer to obtain brown colour of silver nanoparticles PPAgNPs solutions for reduction of Ag+ ions at room temperature. Confirmation of the existence of synthesized silver nanoparticles solution were determined by UV-Visible (UVmini-1240, Shimadzu) spectrophotometer.

The resulting PPAgNPs solutions were carried out by centrifuging, decanting and drying to get PPAgNPs powder for the measurement of the X-ray diffractometer (Rigaku-D-max 2200, Japan) as shown in Fig. 3 (d).

Fig. 3. Photographs of (a) pineapple peel (b) pineapple peel water extract (c) pineapple peel silver nanoparticles solution (PPAgNPs) and (d) PPAgNPs powder

D. Preparation of CS/glu/PPAgNPs Composite Beads

Chitosan 2 g was dissolved in a mixture of 2 % acetic acid solution and 100 mL of prepared PPAgNPs solution with constant stirring at room temperature for 6 hrs and then 5 drops of 2 % glutaraldehyde as cross- linked agent was added in the mixture. Then, the solution was dropped into 2 M NaOH solution with thin nozzle (0.5 mm diameter). The chitosan-based silver nanoparticle solution drops were coagulated in the NaOH to get spherical beads. The beads were dried at room temperature and collected in air tight container.

Prepared beads were determined by physicochemical parameters such as pH, moisture content, density and solubility in water, acid as well as alkali. Furthermore, the functional group of prepared beads were determined by FT IR analysis.

Fig. 4. Photographs of (a) chitosan based silver nanosolution drops coagulated in NaOH solution and (b) dried CS/glu/PPAgNPs composite beads

E. Application of CS/glu/PPAgNPs Composite Beads

Prepared CS/glu/PPAgNPs composite beads were applied as antimicrobial agents and as adsorbent for removal of dye.

The antimicrobial activities of synthesized beads were measured by agar-well diffusion method. Nutrient agar was boiled and 20-25 mL of the medium was poured into the test tube and plugged with cotton wool and autoclaved at 100 ˚C for 45 minute in an autoclave. After that, the flask was cooled down to 30-35 ˚C and poured into sterilized petridish and 0.02 mL of spore suspension was also added into the dishes. The agar was allowed to set for 2 hrs after the 8 mm plate agar disc was made with the help of sterilized cork borne. Then, about 0.1 mL of sample was introduced into the agar-disc and incubated at 37 ˚C for 24 hrs. The inhibition zone (clear zone) which appeared around the agar-disc indicated the presence of antibacterial activity. The resulting data are presented in Fig. 9 and TABLE III.

Alternatively, application of prepared CS/glu/PPAgNPs composite beads were used in adsorption process by dosage method.

In the research, stock solution and serial dilution were performed and measurement of absorbance were carried out by using spectrophotometer. The results are shown in the TABLE IV and the calibration curve that plotting the absorbance against with the concentration of MB was performed. That calibration curve is presented in Figure 10. Adsorption process of prepared CS/glu/PPAgNPs composite beads were performed by the batch experiments in six set of conical flasks where 10 mL of methylene blue with initial concentration of 25 mgL-1 were placed in each flasks. Various weight of CS/glu/PPAgNPs composite beads sample (0.05, 0.10, 0.15, 0.20, 0.25 and 0.30) g were added to separate flasks and kept in a shaker of 150 rpm for 15 minute at 30 °C. The concentrations of methylene blue solution in the supernatant solutions before and after adsorption were determined by using spectrophotometer at its maximum wavelength of 665 nm. The photograph of separated flasks for adsorption processes are shown in Fig 5. The efficiency of adsorption of methylene blue on CS/glu/PPAgNPs beads can be calculated by using the equation (1) and the resulting data are presented in TABLE V.

$$\text{Adsorption (\%)} = \frac{(C_0 - C_e)}{C_0} \times 100 \qquad (1)$$

where, C0 is initial concentration of adsorbate (MB) solution (mgL-1) and Ce is equilibrium concentration of adsorbate (MB) solution (mgL-1).

The adsorptive behavior of homogeneous surfaces CS/glu/PPAgNPs bead by monolayer chemisorptions was demonstrated by Langmuir isotherm model. Langmuir isotherm for adsorption of methylene blue dye on CS/glu/PPAgNPs beads are shown in Fig. 12 and the resultant data from calculation according to equation (2) are presented in TABLE VI. At equilibrium, the methylene blue concentration retained in the adsorbent phase, qe (mgg-1), was calculated by equation

$$q_e = \frac{(C_0 - C_e)\,V}{W} \qquad (2)$$

where, qe is the amount of adsorbate adsorbed per unit weight of adsorbent (mgg-1), C0 is initial concentration of adsorbate solution (mgL-1), Ce is equilibrium concentration of adsorbate solution (mgL-1), V is volume of the solution (L) and W is mass of adsorbents (g).

Fig. 5. Photographs of adsorption of MB on various concentration of CS/glu/PPAgNPs composite beads

III. RESULTS AND DISCUSSION

A. Preparation and Physicochemical Properties of Chitosan

Chitosan from shrimp shell was obtained by demineralization, deproteinization and deacetylation processes. Yield percent of chitosan 13.27 % was obtained from raw shrimp sample. It was observed that physicochemical properties of prepared chitosan have the value of pH 6.7 and 8.84 % of moisture content.

B. Green Synthesis and Confirmation of Silver Nanoparticles Using Pineapple Peels

Extraction of fruits peels were performed by 1:4 (w/v) ratio of peels and deionized water. The photograph of pineapple peels extract solution is presented in Fig. 3(b). Silver nanoparticles solutions were carried out by using silver nitrate solution and peel extracts as reducing agents as shown in Fig. 3 (c).

According to UV- visible analysis, it was revealed that the surface plamon resonance band of prepared silver nanoparticle solution is appeared at nearly 442 nm as shown in Fig.6. That the maximum wavelength is confirmed the brown colour of silver nanoparticle solution in the range between 400- 480 nm.

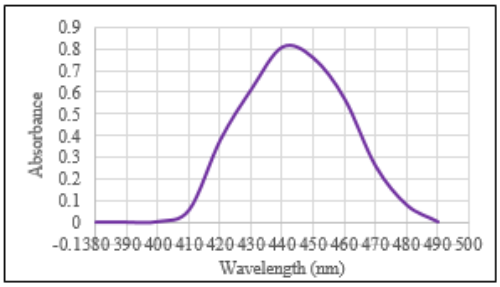

Fig. 6. Plot of absorbance V_s wavelength of pineapple peel extract silver nanoparticles solution (PPAgNPs)

The XRD pattern of synthesized silver nanoparticle is presented in Fig.7 and TABLE I. From the results, average crystallite size of prepared silver nanoparticles is 18.672 nm by calculation of the following Debye Scherrer's formula and the miller indices of (111), (200) and (220) were appeared at 2-θ value of 38.864°, 44.341° and 64.134° respectively. The arrangement of the crystalline structure is faced centered cubic.

Debye Scherrer's formula is

$$t = \frac{0.9\lambda}{\beta \cos\theta}$$

where, t is crystallite size in nm or (A°), λ is wavelength (A°) or nm, θ is diffraction angle of the peak under consideration at FWHM (°), β is observed FWHM (in radians) and FWHM is full-width at half-maximum respectively.

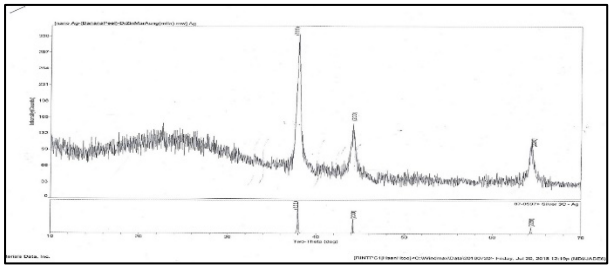

Fig. 7. XRD pattern for PPAgNPs powder

TABLE I. CRYSTALLITE SIZE OF SYNTHESIZED PPAGNPS POWDER

No	Miller Indice (h k l)	FWHM (deg.)	2-Theta (deg.)	Crystallite Size (nm)
1	(111)	0.451	38.864	18.735
2	(200)	0.507	44.341	16.972
3	(220)	0.463	64.134	20.309
Average crystallite size				18.672

C. Preparation and Physicochemical Properties of CS/glu/PPAgNPs Composite Beads

CS/glu/PPAgNPs beads containing 2 g of chitosan, 2 % acetic acid, 5 drops of 2 % glutaraldehyde and 100 mL of synthesized PPAgNPs solution were fabricated by green synthesis. Physicochemical parameters viz. pH, moisture content percent, density (gmL-1) and solubility percent of water, acid and alkali of fabricated CS/glu/PPAgNPs beads are shown in TABLE II. It was shown that the prepared beads are resistance to acid and basic condition.

D. FT IR Analysis of Prepared Chitosan and CS/glu/PPAgNPs Composite Beads

The FT IR spectra of chitosan and CS/glu/ PPAgNPs composite beads are presented in Fig. 8(a) and Fig. 8 (b). In the Fig. 8 (a) and Fig.8 (b), broad bands at 3427.51 cm-1 and 3425.58 cm-1 are assigned for stretching vibration of O-H and N-H in the polysaccharide moieties and the peak at 2926.01 cm-1 and 2924.09 cm-1 are due to the stretching vibration of the aliphatic C-H bonds. The peak at 1654.92 cm-1 is showed that the C-O stretching vibration in the amide bond in chitosan. The shifted peak at 1593.2 cm-1 is presented a significant decrease of transmittance in this band region and the peak at 1740 cm-1 is appeared in CS/glu/ PPAgNPs. It was indicated that the silver particles are bound to the functional groups of chitosan [8]. The new band at about 1740 cm-1 corresponds to the carbonyl stretching vibrations in ketone, aldehydes and carboxylic acid. The peak at 1382.96 cm-1 shows stretching vibration of CN in chitosan. In the spectrum of CS/glu/PPAgNPs bead, that CN stretching vibration is disappeared due to deformation of the bond.

TABLE II. PHYSICOCHEMICAL PROPERTIES OF CS/GLU/PPAGNPS BEADS

Parameters	CS/glu/PPAgNPs beads
pH	8.000
Moisture content (%)	0.2433
Density(gmL^{-1})	1.7140
Solubility in deionized water	Insoluble
Solubility in 2 % acetic acid	Insoluble
Solubility in 2 % NaOH solution	Insoluble

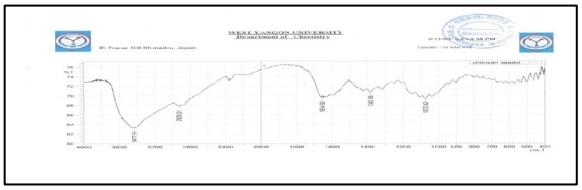

(a)

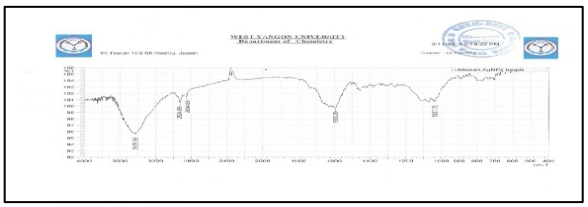

(b)

Fig. 8. FT IR spectra of prepared (a) chitosan and (b) CS/glu/PPAgNPs composite bead

E. Application of Fabricated CS/glu/PPAgNPs Beads For Antimicrobial Activity

According to antimicrobial measurement, it was displayed that only chitosan sample is moderately inhibited on Bacillus subtilis, Staphylococcus aureus and

Bacillus pumilus but poorly inhibited on Pseudomona fluorescens, Candida albican and Escherichia coli.

After the fabrication of CS/glu/PPAgNPs composite beads, they are strongly inhibited on all of six microorganisms such as Bacillus subtilis, Staphylococcus aureus, Pseudomona fluorescens, Bacillus pumilus, Candida albican and Escherichia coli. This is because of the electrostatic interaction between negatively charged cell membrane of microorganism and positively charged of silver ions of CS/glu/PPAgNPs composite bead responsible for antimicrobial activity.

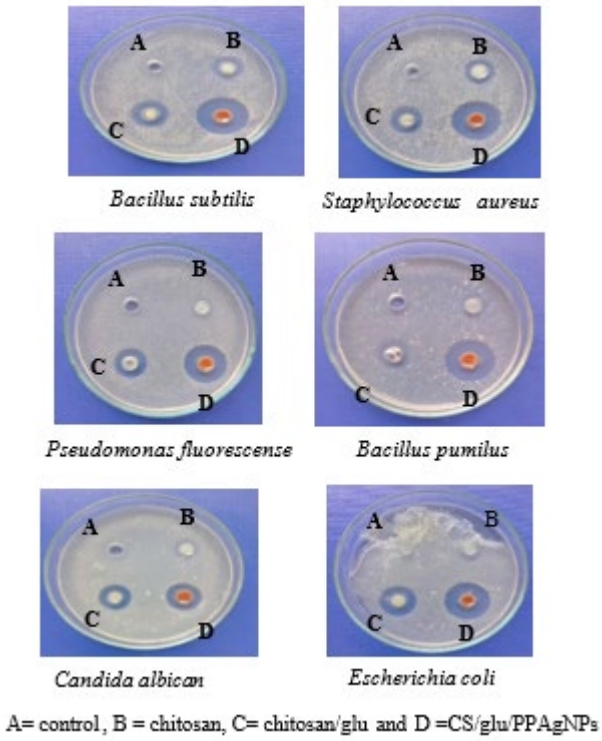

Fig. 9. Antimicrobial activities of prepared chitosan and CS/glu/PPAgNPs on different microorganisms

TABLE III. ANTIMICROBIAL ACTIVITY OF PREPARED CS/GLU/PPAGNPS COMPOSITE

Microorganisms	Inhibition zone (mm)		
	B	*C*	*D*
Bacillus subtilis	19.26 (++)	22.43 (+++)	34.06 (+++)
Staphylococcus aureus	19.78 (++)	18.45 (++)	35.78 (+++)
Pseudomona fluorescens	13.22 (+)	17.89 (++)	30.07 (+++)
Bacillus pumilus	16.99 (++)	18.16 (++)	30.17 (+++)
Candida albican	12.66 (+)	16.87 (++)	22.16 (+++)
Escherichia coli	12.18 (+)	21.14 (+++)	26.56 (+++)

Agar well – 8 mm
8 mm ~ 14 mm (+)
15 mm ~ 19 mm (++)
20 mm and above (+++)
B = chitosan *C* = chitosan/glu *D* =CS/glu/PPAgNPs

F. Application of Fabricated CS/glu/PPAgNPs Beads For Removal of Methylene Blue dye

TABLE IV. DATA FOR CALIBRATION CURVE OF METHYLENE BLUE DYE (λmax= 665 nm)

Concentration(mg/L)	Absorbance
3.125	0.102
6.250	0.226
12.500	0.338
25.000	0.467
50.000	0.659
100.000	1.257
200.000	2.735

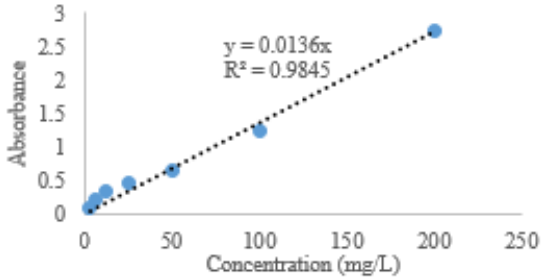

Fig. 10. Calibration curve of absorbance against methylene blue dye concentration (λ_{max} = 665 nm)

TABLE V. EFFECT OF ADSORBENT DOSAGE OF CS/GLU/PPAGNPS BEADS BY USING METHYLENE BLUE DYE

CS/glu/PPAgNPs dose (g)	Adsorption (%)
0.05	18.2960
0.10	34.1764
0.15	47.7648
0.20	59.1180
0.25	73.7760
0.30	79.9756

(Initial concentration = 25 mgL^{-1}, pH = 8)

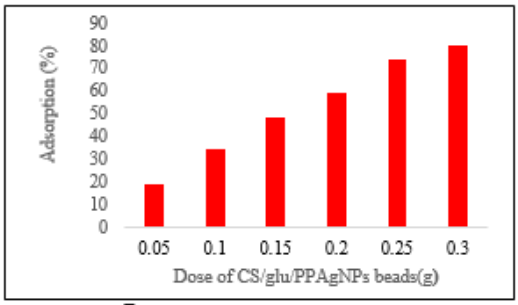

Temperature = at room temperature,
Initial concentration = 25 mgL^{-1}, pH = 8,

Fig. 11. Effect of adsorbent dosage of CS/glu/PPAgNPs beads by using methylene blue dye

TABLE VI. DATA FOR ADSORPTION OF MB ON CS/GLU/PPAGNPS BEADS FOR LANGMUIR MODELING

Sample	Dose(g)	C_e(mgL^{-1})	q_e(mgg^{-1})	C_e/q_e(gL^{-1})
A	0.05	20.4260	0.9148	22.3280
B	0.10	16.4559	0.8544	19.2600
C	0.15	13.0588	0.7960	16.4055
D	0.20	10.2205	0.7389	13.8320
E	0.25	6.5560	0.7378	8.8858
F	0.30	5.0061	0.6665	7.5110

C_0, initial dye concentration = 25 mgL^{-1}, Volume of solution = 10 mL

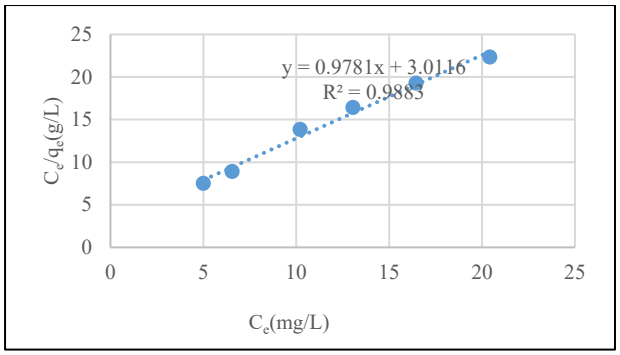

Fig. 12. Langmuir isotherm for adsorption of methylene blue by CS/glu/PPAgNPs beads at room temperature (dosage method)

Alternatively, prepared CS/glu/PPAgNPs beads were used as adsorbent for removal of methylene blue (MB) dye. In the experiment, dosage of prepared CS/glu/PPAgNPs beads increases with increasing adsorption percent within 0.05 to 0.30 g of beads. It was exhibited that 0.30 g of beads can be removed 79.9756 % of initial concentration 25 mgL-1 of MB dye in solution at 30 ºC in the limiting of shaking time within 15 min by using calibration curve and equation (1).

The Langmuir model is used to demonstrate the adsorptive behavior of homogeneous surfaces by monolayer chemisorptions, with no sideways interaction between adsorbate species with different layers of adsorbent surfaces.

From the Langmuir isotherm, it was found that the correlation coefficient R2 value is 0.9883 in depicting this model on equilibrium data. This value indicated that the adsorption data seen to fit Langmuir isotherm. The fact that Langmuir isotherm fit the experimental data very well confirms the monolayer coverage of MB dye onto CS/glu/PPAgNPs bead, qm is 1.0224 mgg-1 according to slope, 1/qm in Fig. 12 and also the homogeneous distribution of active sites on the adsorbent, since the Langmuir equation assumes that the surface is homogeneous. It was observed that the value of the Langmuir constant related to the affinity of the binding sites and energy of adsorption, b is 0.3248 Lmg-1 from the formula 1/qmb.

The essential features of the Langmuir isotherm can be expressed in term of a dimensionless constant called separation factor, RL. The value of RL was determined by calculation from the formula

$$R_L = \frac{1}{1 + bC_0} \quad (3)$$

where, C0 is initial dye concentration (mgL-1), b is the Langmuir constant related to the affinity of the binding sites and energy of adsorption (Lmg-1).

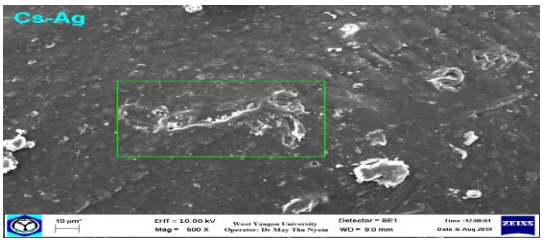

Fig. 13. SEM photomicrograph of fabricated CS/glu/PPAgNPs composite bead before adsorption by methylene blue dye

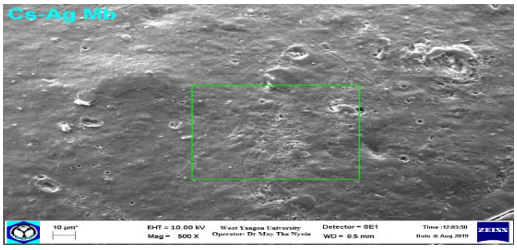

Fig. 14. SEM photomicrograph of fabricated CS/glu/PPAgNPs composite bead after adsorption by methylene blue dye

The shape of the isotherms depend on the value of RL. The shape of isotherm is unfavourable if RL>1, linear if RL=1, favourable if 0<RL <1 and irreversible if RL=0 [9]. According to the experimental results, the value of RL for MB dye on beads is 0.1096 that indicates that the adsorption process is favorable.

Surface morphology of CS/glu/PPAgNPs composite bead before and after adsorption is shown in Fig. 13 and Fig. 14. According to SEM photomicrograph, it was observed that surface morphology of CS/glu/PPAgNPs composite bead before adsorption of MB dye has rough and porosity. But smooth surface of CS/glu/PPAgNPs composite bead after adsorption of MB dye was appeared due to MB dye adsorbed on the pore of CS/glu/PPAgNPs composite bead. Therefore, homogeneous surface of CS/glu/PPAgNPs composite bead after adsorption of MB dye was occurred.

IV. CONCLUSION

According to the results, the quality grade prepared CS/glu/PPAgNPs composite beads were performed by using the waste materials shrimp shells and pineapple peels. The prepared CS/glu/PPAgNPs composite beads have the antimicrobial activity and the removal of dyes. Therefore, the valuable compatibility CS/glu/PPAgNPs composite beads are used as adsorbents in water purification.

This research is cost effective, eco-friendly and innovative preparation of beads lead to more effective applications for green approach to environment.

ACKNOWLEDGEMENT

We feel million thanks to committee chair person, Rector Dr. Mie Mie Khin, for permission of JRA publication.

We would like to express our profound gratitude to Professor, Dr Ni Ni Aung, Head of the Department of Chemistry and Dr Ni Ni Sein, Professor, Meiktila University, for their invaluable guidance, providing all of the departmental facilities and constant encouragement.

REFERENCES

[1] M. T. Vakili., M. Rafatullah, M. H. Ibrahim and A. Z. Abdullah. "Preparation of Chitosan Beads for the Adsorption of Reactive Blue 4 from Aqueous Solutions. *Iranica Journal of Energy and Environment*, vol. 7(2), pp.124-128, 2016.

[2] J. Balavijayalakshmi and V. Ramalakshimi. "Carica Papaya Peel Mediated Synthesis of Silver Nanoparticles and Its Antibacterial Activity against Human Pathogens". *Journal of Applied Research and Technology,* vol. 15(5), pp. 413-512, 2017.

[3] V. Saraswaty *et al. "*Pineapple Peel Wastes as a Potential Source of Antioxidant Compounds". IOP Conference Series: Earth and Environmental Science, 2017.

[4] O. S. Aysha. "Biosynthesis of Silver Nanoparticles Using *Citrus limon* Linn. Peel Extract and Its Antibacterial Property against Selected Urinary Tract Pathogen". . *Journal of Biological and Scientific Opinion*, vol.2 (3), 2014.

[5] S. Phongtongpasuka, S. Poadanga and N. Yongvanichb. "Environmental-Friendly Method for Synthesis of Silver Nanoparticles
From Dragon Fruit Peel Extract and Their Antibacterial Activities". *Energy Procedia*, vol. 89, pp.239, 2016

[6] S. R. Senthilkumar and T. Sivakumar. "Green Tea (Camellia Sinensis) Mediated Synthesis of Zinc Oxide (ZnO) Nanoparticles and Studies on Their Antimicrobial Activities". *International Journal of Pharmacy and Pharmaceutical Sciences,* vol. 6(6), 2014.

[7] P. Paralikar. "Biogenic Synthesis of Silver Nanoparticles Using Leaves Extract of *Epiphyllum Oxypetalum* and Its Antibacterial Activity". *Austin Journal of Biotechnology & Bioengineering,* vol. 1(7), 2014.

[8] N. Saifuddin, , C. Y. Nian, L. W. Zhan and K. X. Ning. "Chitosan-Silver Nanoparticles Composite as Point-of-use Drinking Water Filtration System for Household to Remove Pesticides in Water". *Asian Journal of Biochemistry*, vol.6(2), pp.142-159, 2011

[9] B. Meroufel., O. Benali, M. Benyahia, Y. Benmoussa and M. A. Zenasni, "Adsorption Removal of Anionic Dye from Aqueous Solution by Algerian Kaolin: Characteristics, Isotherm, Kinetic and Thermodynamic Studies", *J. Mater. Environ*. *Sci*, vol. 4(3), pp. 482-491, 2013.

Article ID – JRA6002720

Effect of Prepared Organic Composite Fertilizer on Soil Fertility

Win Win Khaing
Department of Chemistry
Mandalay University of Distance Education
Mandalay, Myanmar
winwinkhaing.mumdy@gmail.com

Ring Lali
Department of Chemistry
Banmaw University
Banmaw , Myanmar
catherinelilaliz…1@gmail.com

Myint Myint Khaing
Department of Chemistry
Mandalay University of Distance Education
Mandalay, Myanmar
myintmyintk591@gmail.com

***Abstract*— The present work is an attempt to increase the soil fertility by applying organic composite fertilizer in agricultural sites. The organic composite fertilizer was prepared by the use of agricultural wastes such as sesame stalk biomass and farmstead wastes from cattle-pen by anaerobic digestion process. Three different weight ratios of agricultural wastes to farmstead wastes (1:1, 1:2, 2:1) were created. The total waste mixture 250 kg was anaerobically digested for each condition. The physicochemical properties of the prepared fertilizers such as pH, moisture, plant nutrients of potassium, nitrogen, phosphorus and organic carbon were determined by chemical and instrumental methods. The mineral composition of one of the prepared organic fertilizers was examined by (Energy Dispersive X-ray Fluorescence) EDXRF spectrometer. The prepared fertilizers were utilized for local organic farming. The soil fertility of the selected farm before cultivation was determined. Then, the soil fertility due to residual effect of using organic fertilizer was determined.**

Keywords—Agricultural waste, Anaerobic, EDXRF, Farmstead waste, Nutrient

I. INTRODUCTION

As Myanmar is an agricultural country, the agricultural sector is the backbone of its economy. There is no doubt that any fertilizer, organic or inorganic, natural or synthetic, supplies the nutrients for plant growth and optimum yield. But the use of chemical fertilizers contributes largely to the deterioration of the environment and to reduce soil fertility [1]. Therefore it is necessary to substitute with organic fertilizers in agriculture.

In general, organic fertilizers are natural materials derived from agricultural wastes, animal excreta, human excreta, vegetable matter and household waste. Organic fertilizer releases nutrients over an extended period of time. They act much like the slow –release fertilizers. Natural fertilizers provide the nutrients needed for the plant growth. The essential nutrients for plant growth are nitrogen, phosphorus and potassium. There are also many other chemicals needed by plants in small quantities such as copper, manganese, iron, sulphur and others [2].

Using natural fertilizer helps the soil to have a good structure to hold water and air because it also provides organic matters called humus to the soil. One of the best natural fertilizers is manure because it feeds the soil with humus and plant nutrients. The lost plant nutrients can be replaced by fertilizers. Continued use of organic fertilizers results in increased soil organic matter, reduced erosion, better water in filtration and aeration, higher soil biological activity as the materials decompose in soil, and increased yields after the year of application (residual effect). Proper handling of organic fertilizers enhanced their quality and effectiveness [3].

Soil is very important because it can produce food for human beings and animals. There are different types of soil, each of which has different effects on the plants that grow from them. The formation of a soil is influenced by organisms, climate, topography, parent material and time [4]. A good soil for growing agricultural plants has about 45% minerals, 5% organic matter, 25% air and 25% water. All crop plants need the same kinds of elements in addition to water and air, but plants differ in the relative amount of their requirements of these essentials. But some elements are toxic to plants such as celenium, arsenic, fluorine, aluminium and nickel [5].

Today, scientists, farmers and other professional consider the characteristics of the agricultural soil and how to maintain its fertility. The aim of this research is to prepare eco-friendly organic composite fertilizer using biomass and to utilize potentially in agriculture.

II. EXPERIMENT

A. Sample Collection and Preparation

In the present study, sesame stalk biomass was collected from the farm after pitting sesame seeds on the harvest time. The botanical name of sesame is Sesamum indicum L. It belongs to Pedaliaceae family [6]. They were chopped into pieces. Farmstead wastes were collected from cattle-pen at Kabyu village Kyaukpadaung Township, Mandalay Region. The raw materials which were collected on September 2015 were mixed for a series of preparation of organic fertilizers. Three different ratios of collected materials were created. The weights

ratios of sesame stalk wastes to farmstead waste were (1:1), condition 1 (S-1), (1:2) condition 2 (S-2), (2:1) condition 3 (S-3). The mixture totally 250 kg was prepared for anaerobically digestion for each condition.

B. Determination of Physicochemical Properties of the Prepared Samples

Physicochemical properties of the prepared raw sample mixture such as pH, total solid and volatile solid were determined by instrumental, analytical and titrimetric methods [7]. The results are described in table 1.

C. Preparation Organic Composite Fertilizers

A series of preparation of organic fertilizers were carried out by anaerobic treatment for each condition [8]. The production processes for all selected conditions were carried out simultaneously. The mixed raw materials for each condition were packed with plastic sheet and were allowed to anaerobically digest in the burrow for three months. After completely digestion of composite fertilizers, they were allowed to dry in air. The liquid which leak out during digestion process from each condition was collected and reused by spraying to the respective fertilizers. Three different organic fertilizers labeled as POF-1, POF-2, and POF-3 were obtained. The yield percentages of prepared fertilizers were calculated based upon the total weight of used materials. The yield percentages are described in Table (1) and the fertilizer preparation processes are described in Fig 1, 2, 3 and 4.

Fig.1 Sesame stalk wastes and farmstead waste

Fig.2.Preparation of raw mixture for anaerobic digestion

D. Determination of Physical Properties and Nutritive Values of Prepared Organic Fertilizers

The physical properties such as pH and moisture of the prepared fertilizers were directly measured by pH meter and by heating oven at 105°C respectively. The total nitrogen content was determined by Kjeldahl method using the chemicals such as 0.05M concentrated sulphuric acid, 0.1 M hydrochloric acid, 2g copper II sulphate crystal, potassium sulphate, sodium hydroxide, boric acid and methyl red indicator. Total Potassium content was determined by UV-Visible Spectrophotometer [9]. The phosphorus and organic carbon content of the prepared fertilizers were determined at Ministry of Agriculture and Irrigation, Department of Agriculture (Land Use) Mandalay. The results are described in table 2.

Fig.3.Preparation of organic fertilizers by anaerobic digestion

Fig.4. Prepared organic fertilizers POF-1, POF-2, and POF - 3

E. Determination of Mineral Compositions of Prepared Fertilizers by EDXRF Method

Relative abundance of the minerals presents in prepared fertilizers (POF-2) was determined by EDXRF spectrometer. X-ray spectroscopy permits simultaneous analysis of light elements to heavy elements. The results are described in table 3.

F. Determination of Nutritive Values of the Soil before and after Plantation

To test the residual effect of organic fertilizers on the soil, the soil sample was technically collected from the farm before growing (2015, April) and after harvest (2016, September) at Kyaukpadaung Township. The collecting area was limited around about 100 square feet. The nutritive values such as nitrogen, phosphorus, potassium and organic carbon content of the collected soil were determined at Ministry of Agriculture and Irrigation, Department of Agriculture (Land Use) Mandalay. The results are listed in table 4.

III. RESULTS AND DISCUSSION

A. Relation between physicochemical Properties of the wastes and Yield of Fertilizer

The pH values of all sample mixtures are slightly acidic. The performance of the reactors was evaluated by estimating destruction of total solid and volatile solid. Total solid means the weight of sample left after drying the sample at 105°C for a minimum of two hours compared with the total weight of the sample before drying. The total solid concentration of the sample influences the pH and effectiveness of the microorganisms in the decomposition process. When the total solid percentage of the waste mixture in an anaerobic continuous digestion process increases, the yield of fertilizer also increases. Therefore, the yield of fertilizer is totally affected by total solid digested. In this research, POF-2 which is given by condition 2 gives the highest yield. Volatile solid is the weight loss of the sample weighted before and after burning the sample at 550°C for at least five hours. The final ash left is the mineral content in the sample.

TABLE I. PHYSICOCHEMICAL PROPERTIES OF RAW MIXTURE AND YIELD % OF PREPARED FERTILIZERS

sample	pH	Total solid (%)	Volatile solid (%)	Fertilizer Yield%
S-1	6.2	85.50	34.00	45
S-2	6.9	89.95	40.00	50
S-3	5.2	86.80	28.42	42

B. Physicochemical Properties and Nutritive Values of Prepared Organic Fertilizers

TABLE II. PHYSICOCHEMICAL PROPERTIES AND NUTRIENT VALUES OF PREPARED FERTILIZERS

POF	pH	M (%)	N (%)	P (%)	K (%)	OC (%)
1	7.55	8.5	1.95	1.92	2.09	5.00
2	7.25	8.1	1.25	1.50	2.03	5.50
3	7.9	8.5	1.01	1.20	1.88	4.25

POF = Prepared Organic Fertilizer,
M = Moisture
N = Nitrogen
P = Phosphorus
K = Potassium
OC = Organic Carbon

As shown in table 2, although the pH of each raw mixture is slightly acidic, the pH of each prepared fertilizer is nearly neutral. The prepared organic fertilizers are rich in essential macronutrients such as nitrogen, phosphorus, potassium and organic carbons. Among them, potassium content is relatively much rich than nitrogen and phosphorus content. Therefore, the prepared fertilizers are suitable for growing any kind of crops but the most suitable for growing seed-bearing crops science potassium is essential for fruiting and seed formation [10].

C. Mineral Composition of Prepared Fertilizers

From EDXRF information, it was observed that the prepared fertilizers were composed of minerals which are essential for plant growth. Potassium is relatively abundant among them. Moreover, it can be clearly seen that the toxic minerals such as lead, mercury and arsenic, nickel are not present in the prepared fertilizers. The results are shown in the following table 3 and EDXRF spectrum of POF-2 which was given the highest yield is described in figure 5.

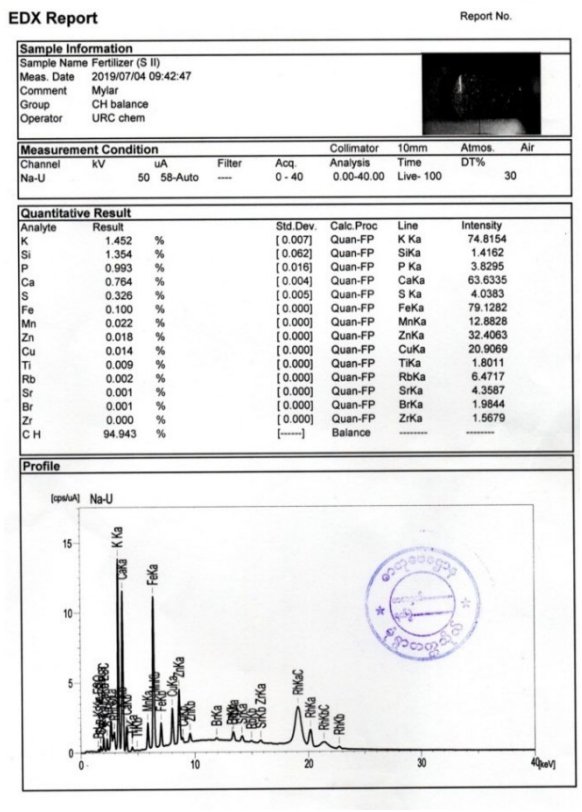

Fig 5. EDXRF spectrum of POF-2

D. Utilization of Prepared Fertilizers in Plantation

The prepared organic composite fertilizers were utilized for plantation in order to mainly determine the residual effect of them to the growing soil. This means that how the prepared organic fertilizer can maintain or increase to the soil fertility. So, the prepared organic fertilizers were mixed because the amount of nutrients contained are not identical but in similar. About 30kg of prepared fertilizers were utilized for the plantation of sesame in particular farm around about 100 square feet as described in experiment section, 2.6. This is because the

prepared organic fertilizers (POF-1, POF-2, POF-3) are relatively rich in potassium contents than the other two such as nitrogen and phosphorus. Although all the plants require essential nutrients (N, P, K) for plant growth, good amount of potassium is required for seed bearing plants in fruiting and seed formation. Therefore, the prepared organic fertilizers were utilized for sesame plantation.

TABLE III. MINERAL COMPOSITION OF POF-2

No	Elements	Relative abundance (%)
1	Potassium	1.452
2	Silicon	1.354
3	Phosphorus	0.993
4	Calcium	0.764
5	Sulphur	0.326
6	Iron	0.100
7	Manganese	0.022
8	Zinc	0.018
9	Copper	0.014
10	Titanium	0.009

E. Nutritive values of the Soil before and after Plantation

According to the resultant data of nutritive values of the particular soil before and after plantation, the nutritive values especially the organic carbon content increases on the tested soil. This is due to residual effect of organic fertilizers. According to the literature, the organic carbon content in agricultural soil should have 5%. Therefore, using organic fertilizers in agricultural sites causes not only supply the nutrients to the plants but also increases organic carbon content and nutrients. The results are described in table 4.

TABLE IV. NUTRITIVE VALUES OF THE SOIL BEFORE AND AFTER GROWING

Soil nutrition	Before growing	After growing
Nitrogen (%)	0.55	0.92
Phosphorus (%)	0.32	0.50
Potassium (%)	0.19	0.25
Organic carbon (%)	3.10	5.80

IV. CONCLUSION

According to experimental results, it was observed that the weight ratios of sesame stalk biomass to farmstead waste (1:2) gave the highest yield of composite fertilizers. In this study, prepared organic fertilizers are rich in essential nutritive values such as nitrogen, phosphorus, potassium and organic carbon although the content of these values is different form each other. However, the potassium content in each prepared organic fertilizer is relatively more than the other nutrients. Therefore, the prepared fertilizers are more suitable for growing seed-bearing plants such as beans, sesame and peas. As shown in table 4, it can be said that the prepared organic fertilizers can increase the soil fertility due to residual effect. The prepared organic fertilizers have great potential for application in agriculture. Therefore, this study proves that environmental contamination due to applying chemical fertilizers in agriculture can be reduced as well as can promote agricultural sites by replacing with eco-friendly organic fertilizers.

ACKNOWLEDMENT

We would like to express our gratitude to responsible and honorable persons of Journal of Research & Applications (JRA), UCSMTLA for giving a chance to submit research paper.

REFERENCES

[1] Manum A, Torii S, "Journal of Advanced Agricultural Technology" pp. 94-99, 2014.
[2] P. Kalpana, G. Sai Bramari and L. Anitha, "Asian Journal of Plant Science and Research, vol (3), 49-57, 2011.
[3] P. Bartoleshi, A. Guido, "How to make and use compost, pp.379-436, 2011.
[4] Thompson and Toen "Soils and Soilfertillity". 3rd Edition, (MC GRAW HILL Publication in the agriculture science) 1973
[5] P. R. Hesse, "A Textbook of Soil Chemical Analysis," John Murrary. London, 1971.
[6] Ah Shin Naganthein, 1976. "Pon Pya Say Abidan". III. 3rd Edition, Mingalar printing, press, Rangoon
[7] Fruit and vegetable waste utilization, Science Tech Entrepreneur January, 2007.
[8] J. Mata Alvarez, F. Cecchi, P. llabres and P. Pavan, "Anerobicdigestion of the Barcelona central food market organic wastes: plant design and feasibility study", Bioresour Technol, 42, 33, 1992
[9] Va. Arlington, AOAC, 15th ed, USA : "Official Methods of Analysis of Association of Official Analytical Chemists", 1990.
[10] Royl. Donahue, "An Introduction to Soils and Plant Growth", 2nd Edition,1968.

Article ID – JRA6003720

Preparation of Bioplastic from Straws and Seeds of *Artocarpus heterophyllus* Lam. (Pain-Nae)

Moe Tin Khaing
Department of Chemistry,
Yadanabon University, Myanmar
moetin.khaing@gmail.com

Than Than Myint
Department of Engineering Chemistry,
Technology University (Kyaukse),
drthanthanmyint.mandalay@gmail.com

Aye Aye Khaing
Department of Chemistry
Mandalay Universit
ayeayek280@gmail.com

***Abstract*—The aim of this research is to prepare bio-plastic films using straws and seeds powder of *Artocarpus heterophyllus* Lam. (Pain-Nae) reinforced with yam starch, polyvenyl alcohol (PVA) as water repellent and biologically degradable polymer, glycerol and cotton seeds oil-polyol as plasticizers and zinc oxide (ZnO) as nanofiller by casting method. Firstly, straws and seeds samples of *Artocarpus heterophyllus* Lam. were made as dried powder. Antimicrobial properties of the crude extracts of these dried powder samples were tested in four solvents systems such as ethanol (EtOH), ethyl acetate (EtOAc), n- hexane and acetone($R_2C=O$) by using Agar Well Diffusion Method using seven selected microorganisms in order to check the quality of food packaging materials. And also the antioxidant activities of straws and seeds powder extracts were determined by DPPH Assay Method. Starch compounds were isolated from fresh straws and seeds powder samples and Fourier Transform Infrared (FTIR) spectroscopic measurements were performed on these starch compounds. Characteristic absorption bands of FT IR spectra of two starch compounds and their related functional groups were also assigned. Bio-plastic films were prepared by using the waste products of Pain-Nae blending with their respective constituents in the ratios, a, b, c and d. Screening Electron Microscopic (SEM) measurement and determination of some physical and mechanical properties of prepared bio-plastic films were carried out by their respective standard methods. This research could contribute to green bio-plastic field of applied chemistry with crop-based ecofriendly bio-plastic films.**

***Keywords*— bio-plastic films, microorganisms, extract, physical and mechanical**

I. INTRODUCTION

Nowadays plastic has been chosen as the packaging material due to its safe and robust (waterproof, light, and heat) capacity and cheap price [1]. Synthetic plastic is produced from non-renewable resources and therefore most plastics are petroleum-based [5]. According to European Bio-plastics, bio-plastic can be defined when the plastic is bio-based and biodegradable, or it has both capacities [6]. The jackfruit has many important medicinal uses like antioxidant, anti-inflammatory, anticancer, and antifungal and antimicrobial activity, respectively [7]. Edible films can be produced from

waste jackfruit straw as a raw material and the bio-plastic edible films of jackfruit straw can be degraded easily [2]. Jackfruit straws are the waste of food industries which can cause the environmental threat and so the solution for the negative effects of jackfruit straw waste has been tried to convert it as bio-based film combination with starch [1]. Jackfruit seeds contain 8-15% of the total weight of the fruit and have a carbohydrate content of 36.7 grams per 100 grams and the starch content is about 94.5% [4]. Among the biodegradable polymers, starch is the most valuable one due to its abilities such as readiness, biodegradability, renewability and reasonable cost [3]. Bio-plastic or organic plastic is mostly compost of polymer materials from natural sources of vegetable oil, sugarcane, corn, potato and pea starch and from microbe such as yeast while synthetic plastics are from petroleum. Out of biodegradable polymers, starch has been regarded as one of the most potential due to its readiness, biodegradability, low-cost and renewability [3]. Edible films can help to prevent and protect the effects of some physical, chemical and biological deterioration and Starch, carbohydrates, and natural fibers can be used in the edible films production. Straws and seeds of jackfruit have been tried to apply as a raw material of edible films all over the world and its chemical constituents are glucose, fiber, sucrose, starch, and cellulose. In Myanmar, there have many kinds of species and they are widely used as food and traditional medicine. And therefore, the main aim of this research is to produce starch from fresh samples and bio-plastic films from powdered samples of straws and seeds of *Artocarpus heterophyllus* Lam. (Pain-Nae) from Myitkyina area, Myanmar varying four ratios of their constituents.

A. Botanical Description

Family	Moraceae
Genus	*Artocarpus*
Species	*heterophyllus*
Botanical name	*Artocarpus heterophyllus* Lam.

English name Jackfruit
Myanmar name Pain-Nae
Parts -used Straws and seeds

Fig. 1. The Habit, fruit, straws and seeds of Artocarpus *heterophyllus* Lam.

II. Materials and Methods

A. Materials

Commercial grade chemical reagents and solvents were used in this research work. Cotton seeds oil-based polyol used in this research as plasticizer was synthesized in the laboratory of Faculty of Science, University of Malaysia.

B. Sample Collection and Preparation

The fruits of Artocarpus heterophyllus Lam. (Pain-Nae) were collected from Siterpur, Myitkyina, Myanmar. The fruits were peeled and straws and seeds were separated for further analysis.

C. Preparation of Straws and Seeds Powder

Fresh straws (100) g and seeds (100) g of Artocarpus heterophyllus Lam. were cut and dried in the oven at 60°C for 2 days. Then they were cooled in the desiccator and grounded into dried powder.

Fig.2. Straws and straws powder

Fig.3. Seeds and seeds powder

D. Antimicrobial Activity Test

Agar Well Diffusion method [10] was used to observe anti-microbe activity of straws and seeds of Artocarpus heterophyllus Lam. with the application of seven selected microorganisms on four solvent extracts and examined at the Department of Chemistry, Meikhtila University.

E. Determination of Antioxidant Activity

Ethanol extract of straws and seeds of Artocarpus heterophyllus Lam. was used to determine their antioxidant activity at Department of Chemistry, University of Mandalay by using by DPPH free radical scavenging assay method [11].

F. Preparation of Starch from Fresh Samples

Fruits of Artocarpus heterophyllus Lam. were washed with water and peeled and got the fresh straws after removing arils, bulbs and seeds. Fresh straws sample 100 g and 250 mL of distilled water were blended to get homogeneous slurry. Then the mixture was filtered and the resulting fitrate was allowed to stand for 24 hours. The residue containing starch was washed with water and it was allowed to stand for 24 hours. After allowing for precipitation the resulting sediment was wet starch and it was dried in the oven at 60°C to get dried starch from fresh straws. To get the starch of fresh seeds, same procedure was utilized as shown above in the preparation of starch from fresh straws.

G. FT IR Spectroscopic Characterization

FT IR spectra of straws and seeds starch were measured at the Department of Chemistry, University of Myitkyina. The resulting FT IR spectral data were shown in results and discussion, Figures 13 and 14.

H. Preparation of Bioplastic Flims Based on Straws and Seeds-Powder

In the ratio (a), straws or seeds powder 1 g, Yam starch 1 g, PVA 1 g were placed ino a glass beaker and they were made as solution by adding water until to reach the 50 mL mark of the beaker. The glass beaker containing mixture solution was placed onto a magnetic stirring hotplate with 200 rpm and 70°C. The mixture solutin was heated on constant heting temperature 70°C and stirred 200 rpm for 2 h. After 2 h, the megnetic stirror was turned off. Glass beaker cotaining a mixed solution of bioplastic was cooled beofre printing. Then the solutin was poured into a glass petridish. Bioplstic solution was dried in the room temperature for 24 h. After drying, bioplastic was removed from the petridish mold and then stored in a desiccator. Bioplastic films were obtained and they were used for further analysis.

In the ratio (b), straws or seeds 1 g, starch 1 g and PVA 1 g and glycerol 2 mL were applied. For the ratio (c), straws or seeds 1 g, starch 1 g and PVA 1 g and polyol which was obtained from the synthesis of commercial cotton-seeds oil 2 mL and in the ratio (d)) straws or seeds 1 g, starch 1 g and PVA 1 g and ZnO 1 g were utilized respectively. Then they all were made as solution by mixing with water until to reach 50 mL mark.